OVULE DEVELOPMENT AND ZYGOTE FORMATION

in

Brassica campestris L. cv.Candle

by

Michael J.Sumner

A thesis

submitted in partial fulfillment

of the requirements for the degree of

Doctor of Philosophy in the Department of Botany

The University of Manitoba

December, 1986

ISBN 0-315-37150-1

OVULE DEVELOPMENT AND ZYGOTE FORMATION IN *Brassica campestris* L. cv. Candle

by

MICHAEL J. SUMNER

A thesis submitted to the Faculty of Graduate Studies of the University of Manitoba in partial fulfillment of the requirements of the degree of

DOCTOR OF PHILOSOPHY

TABLE OF CONTENTS

LIST OF FIGURES

Page

Page

Page

Page

Page

Page

Page

LIST OF ABBREVIATIONS

A	-Antipodal
Ab	-Abaxial
ABB	-Aniline blue black
Ad	-Adaxial
CC	-Central cell
CH	-Chalazal
CN	-Chalazal nucellus
CV	-Crystal violet
CW	-Cell wall
D	-Dictyosome
Dmi	-Double membrane-bound inclusion
DNA	-Deoxyribonucleic acid
E	-Egg
ER	-Endoplasmic reticulum
Fa	-Filiform apparatus
II	-Inner integument
L	-Lipid
N	-Nucleus
Nu	-Nucellus
M	-Mitochondrion
Mb	-Microbody
Mgw	-Megagametophyte wall
Mt	-Microtubule
OsFeCN	-Osmium ferricyanide
P	-Plastid
PAS	-Periodic acid-Schiffs reaction
PA-TCH-SP	-Periodic acid-Thiocarbohydrazide-silver proteinate (Thiery test)
Pm	-Plasma membrane
PN	-Polar Nucleus
PP	-Primary parietal
RNA	-Ribonucleic acid
RER	-Rough endoplasmic reticulum
S	-Synergid
SER	-Smooth endoplasmic reticulum
Sh	-Synergid hook
St	-Starch
Thiery Test	-PA-TCH-SP
UA/Pb	-Uranyl acetate-lead citrate
UV	-Ultra violet
V	-Vacuole
Wp	-Wall projections

ACKNOWLEDGEMENTS

I wish to gratefully acknowledge the constructive criticism and review of the manuscript by my supervisor, Dr. L. Van Caeseele. I would also like to thank the other members of the advisory committee, Dr. P.K. Isaac, Dr. I. Morrison, Dr. D. Punter, and Dr. W. Remphrey, for their suggestions and valuable assistance.

I wish to thank all of my colleagues from the department of Botany for their support and help over the duration of the thesis. I am particularly indebted to Dr. A. Olchowecki for the reproduction of the colour plates and to Mr. G. Burgess for the many hours spent in the dark room reproducing the black and white plates. To them both, a very special thank you.

I wish to thank Ms. Rosalie Gillespie who gave freely of her time in teaching me the basic techniques of electron microscopy. A special acknowledgement to Dr. A. Hopkin for his friendship, encouragement, and countless hours of discussion over the past four years.

I wish also to thank Dr. J. Reid for providing me with the opportunity to achieve my goal.

Finally, I wish to acknowledge my wife, Marie, for her patience, help, and understanding. Thank you.

ABSTRACT

A study was made of ovule development in Brassica campestris cv. Candle (canola-rapeseed), from the initiation of the ovule to the mature megagametopyte, using techniques of light, fluorescence, and electron microscopy and histochemistry. The ovule of B. campestris is bitegmic, campylotropous, and exhibits the Polygonum-type of megagametophyte development.

The inner integument is dermal in origin from a series of wedge-shaped intials. The outer integument is derived from both dermal and subdermal initials that originate proximal to the inner integument.

The megasporocyte cell arises from an archesporial or primary sporogenous cell. During mid-prophase of meiosis I, there is a reduction in megasporocyte ribosomes. The megasporocyte plastids and mitochondria exhibit a chalazal polarity. Nuclear vacuoles with internal membrane-bound inclusions are present.

The products of meiosis are a triad or tetrad of megaspores. Expansion of the megagametophyte is micropylar and correlates with the formation of a large central vacuole and a marked increase in dictyosome activity. The cells of the young megagametophyte, the egg, two synergids, three antipodals, and a binucleate central cell, show a similar composition and distribution of organelles.

The mature central cell is devoid of the large central vacuole characteristic of the coenocytic and early cellular stages of megagametophyte development. Cell wall projections, of the transfer cell type, extend from the mid-region of the central cell to the region of the egg apparatus. The wall projections are Thiery-positive

as are the contents of dictyosome vesicles, which appear to contribute to central cell wall projection formation. The polar nuclei are partially fused, prior to fertilization, united by polar bridges and ER interconnections. A network of central cell ER extends from the wall projections to the egg apparatus.

The antipodal cells are ephemeral cells that degenerate shortly after anthesis. The antipodals do not increase in size following their formation and the cells exhibit a limited number of mitochondria, plastids, and dictyosomes. The cell walls of the antipodals are Thiery and calcofluor-positive.

The micropylar and chalazal cell walls of the mature egg apparatus and the micropylar synergid filiform apparatus are Thiery and PAS-positive. The filiform apparatus and the micropylar walls of the egg apparatus are calcofluor-postive. The egg is a polarized cell with a large micropylar vacuole and a chalazal polar nucleus with perinuclear plastids and mitochondria. The synergids appear to be metabolically active cells with long parallel arrays of RER, plastids with starch, and an abundance of mitochondria and dictyosomes. The dictyosomes release vesicles with Thiery-positive contents that appear to contribute to the formation of the filiform apparatus.

The degeneration of one of the synergids is independent of pollination. The pollen tube penetrates the degenerate synergid by way of the filiform apparatus and discharges its contents. The zygote exhibits a marked shrinkage, following fertiliztion, and the large micropylar vacuole of the egg disappears. Cell walls in the chalazal regions of the zygote become calcofluor-positive. The ovule, 72 h after anthesis, does not appear to be receptive to a pollen tube. The

egg and central cells appear healthy and similar to the egg and central cells at anthesis. At this time of development, both synergids have degenerated. The degeneration of the persistent synergid, and the lack of fertility of of the megagametophyte at this period of development, suggests that the persistent synergid may be important in attracting the pollen tube to the egg apparatus.

INTRODUCTION

Canola varieties of Brassica campestris and Brassica napus represent Canada's second largest agricultural cash crop. Despite the economic importance of this oil seed crop there have been relatively few studies on the development of the ovule or seed in any of the Brassica species. To date all embryological studies on Brassica have been restricted to light microscope studies that have utilized coagulative fixatives, paraffin embedding techniques, and outline or camera lucida drawings in the presentation of results (Rathore and Singh 1968, Sulbha 1957, Ahuja and Bhaduri 1956, Pearson 1933, and Thompson 1933). The present study represents the first study of ovule development in Brassica utilizing the improved modern techniques of light and electron microscopy and only the second such study within the family Cruciferae. Patricia Schulz and William Jensen have published a number of papers over the last 18 years on various aspects of ovule development in Capsella bursa-pastoris. The literature on Capsella as it pertains to the present study has been included in the general literature review. To summarize, the studies on Capsella include the megasporocyte (Schulz and Jensen 1981), megasporogenesis (Schulz and Jensen 1986), the antipodals (Schulz and Jensen 1971), the mature central cell (Schulz and Jensen 1973), the central cell after fertilization (Schulz and Jensen 1974), the synergids (Schulz and Jensen 1968a), and the egg and zygote (Schulz and Jensen 1968b).

The present study attempts to provide an integrated approach to the study of ovule development. The major objectives were to investigate:

1. the morphological and cytological changes in the ovule from its inception to maturity using recent techniques for light and electron microscopy.

2. the chemical nature of the filiform apparatus and the cell walls of the antipodals, egg, and synergids using fluorescence, light and electron microscope histochemical techniques.

3. the time interval between pollination and fertilization and to map the course of the pollen tube into the ovule.

4. the fate of the mature ovule that remains unfertilized for some time after anthesis and to determine the approximate stage where the ovule becomes incapable of fertilization.

LITERATURE REVIEW

The initial impetus for the study of plant embryology was the discovery of the pollen tube by Amici in 1824 and his observation that pollen tubes grew from the stigma to the ovule. In the ensuing years there was considerable controversy instigated by Schleiden's theory that the embryo within the ovule arose from the tip of the pollen tube. In 1849, Hofmeister published a comprehensive survey of 38 angiosperm species and proposed that the embryo arose from a preexisting cell within the ovule and did not arise from the pollen tube. In 1884, Strasburger showed that the pollen tube discharged its contents into what is now termed the megagametophyte and he described for the first time the process of syngamy in angiosperms. In the late 1890's Nawaschin and Guignard, in separate publications, showed that both sperm were involved in the reproductive process and demonstrated for the first time the process of double fertilization. Hofmeister, Strasburger, Nawaschin, and Guignard made meticulous observations on living material and were the true pioneers of present day embryology. The advent of paraffin microtomy, at the turn of the century, made the preparation and sectioning of material easier and less time consuming. As a result, the embryological literature grew exponentially and the period of comparative embryology with distinctive systematic overtones was born. Unfortunately, the preparation of material for paraffin microtomy included the widespread use of acid fixatives that preserved the nucleus but coagulated and altered the cytoplasm of the cell. In addition, the detailed illustrations of the ovule and contents of the megagametophyte were often replaced by outline diagrams. On the

positive side, the voluminous literature resulted in our present understanding of the embryological diversity of the angiosperms giving modern workers a baseline from which to begin to understand the cytology of the various types of ovules, megagametophytes, and microgametophytes of the angiosperms. The reviews of Maheshwari (1950, 1963) and Davis (1966) provide excellent overviews and at times detailed summaries of the early embryological literature.

The advent of electron microscopy marked the beginning of the "modern" era of structural botany. In the field of ovule development the pioneers of the mid-1960's were J.E. van der Pluijm, P.R. Bell, B. Rodkiewicz, and W.A Jensen. The early use of potassium permanganate fixatives destroyed much of the cytosol but did give an accurate map of organelle distribution within plant cells. The use of aldehyde and osmium tetroxide fixatives, though not artifact-free, provided a more accurate representation of what was happening in the living cell. Methacrylate and epoxy resins resulted in the production of ultrathin sections for electron microscopy and thin sections for light microscopy that greatly enhanced the resolution of both systems. This review of the literature will concentrate on the modern era of structural botany as it pertains to pre-fertilization and post-fertilization ovule development in angiosperms. The study of the angiosperm megagametophyte using the improved techniques for light and electron microscopy has been reviewed by Kapil and Bhatnagar (1981) and a recent monograph on the embryology of the angiosperms (Johri 1984) covers a large portion of the literature prior to 1981.

The onset of meiosis in the megasporocyte cell results in a number of cytoplasmic and nuclear alterations in the cell. Nuclear

vacuoles, resulting from the dilation of the nuclear envelope have been reported to occur in a number of vascular plants Zea (Russell 1979), Pteridium, Dryopteris, Marsilea, Pinus, and Lycopersicon (Scheffield et al. 1979), Gasteria (Willemse and De Boer-De Jeu 1981), and Capsella (Schulz and Jensen 1981). Within this expanded nuclear envelope there are frequent membrane-bound electron-opaque deposits that are considered to be of nuclear origin. The fate of these deposits is unknown but Dickinson and Heslop-Harrison (1977) feel the deposits represent remnants of the nuclear diploid phase that are being eliminated during the transition to the gametophyte phase. During this transition phase there is similar elimination of a large portion of the cytoplasmic ribosome population of the megasporocyte cell during prophase of meiosis (Newcomb 1973a, Dickinson and Potter 1978, Russell 1979, Schulz and Jensen 1981, Medina et al. 1981). There are two theories as to the mechanism of elimination of the ribosome population. Dickinson and Heslop-Harrison (1977) propose that some of the ribosomes survive meiosis by being encapsulated and protected by cytoplasmic membrane-bound inclusions. The remaining unencapsulated cytoplasmic ribosomes are eliminated by digestive enzymes. Schulz and Jensen (1981, 1986) report that, in Capsella, ribosomes and a large number of organelles are encapsulated in membrane-bound autophagic vacuoles and thus eliminated from the cell cytoplasm. These autophagic vacuoles are active throughout meiosis and into the early stages of megagametogenesis. Russell (1979) reported the occurrence of similar autophagic activites in the ovule of Zea that extended from the megasporocyte to the 4-nucleate stage of megagametophyte development. In a number of angiosperm species, the ribosome population of the

functional megaspore increases at the completion of meiosis (Newcomb 1973a, Dickinson and Potter 1978, Russell 1979, Medina et al. 1981, and Schulz and Jensen 1986).

In some monosporic angiosperms there have been reports of a distinct polarity in the megasporocyte cell. In Gasteria (Willemse and Bednara 1979), Zea (Russell 1979), and Glycine (Kennel and Horner 1985) there is a distinct chalazal polarity of organelles during prophase of meiosis I, suggesting the future acquisition of the majority of megasporocyte organelles by the functional megaspore. However, in Zea (Russell 1979), this polarity of organelles does not appear to be carried into the tetrad stage. Schulz and Jensen (1986) report the elimination of regions of cytoplasm and organelles in all four cells of the tetrad by the action of autophagic vacuoles. Early studies on megasporogenesis postulated the total elimination of plastids and mitochondria during meiosis (Bell and Muhlethaler 1964, Israel and Sagawa 1964, Bell et al. 1966, Woodcock and Bell 1968) and their "de novo" synthesis from outpockets of the nuclear envelope.

An aniline blue-positive substance, believed to be the beta 1-3 glucan, callose, commonly has been found associated with the cell walls of the megasporocyte, dyad, and tetrad of species that exhibit the monosporic Polygonum-type of megasporogenesis (Russell 1979; Schulz and Jensen 1981, 1986; Kennel and Horner 1985). In these species, at the tetrad stage, the chalazal functional megaspore is typically free of callose deposits. In the monosporic Oenothera-type, where the three chalazal megaspores degenerate and the micropylar megaspore forms the megagametophyte, the distribution of callose is similar to the Polygonum-type except it is the micropylar functional

megaspore that is free of callose desposits (Rodkiewicz 1970, Jalouzot 1978). In the tetrasporic type, where the entire original megasporocyte cell functions in megagametophyte development, there are no deposits of callose during meiosis (Kapil and Bhatnagar 1981). The supposed function of callose is to isolate the diploid phase of the life cycle from the haploid and to allow the autonomous development of the gametophyte generation (Heslop-Harrison and McKenzie 1967).

The functional megaspore is the first cell of the megagametophyte generation. In the majority of angiosperm ovules the formation of the coenocytic megagametophyte involves three mitotic divisions within the enlarging functional megaspore producing an 8-nucleate megagametophyte. The functional megaspore of Crepis becomes highly vacuolate prior to the first division of the nucleus (Godineau 1973), while in Pisum the formation of the large central vacuole of the megagametophyte begins at the 2-nucleate stage by the apparent coalescence of smaller vacuoles (Medina 1980). The vacuole forms between the two nuclei and establishes a chalazal and micropylar polarity in the embryo sac. The expansion of the megagametophyte is acropetal in Oryzopis (Maze et al. 1970) and corresponds with an increase in size of the central vacuole. In Gasteria the maximum number of organelles in the megagametophyte is attained at the functional megaspore stage, prior to the first free nuclear division in the megagametophyte (Willemse and Franssen-Verheijen 1978). In contrast, Godineau (1973) reports a progressive increase in the numbers of organelles in Crepis over the course of megagametogenesis. In Zea, Russell (1979) reports an increase in organelles up to the 4-nucleate stage of development followed by the elimination of

mitochondria and chloroplasts due to the autophagic activity of megagametophyte vacuoles that comprise what Russell termed the "lytic complex". In Helianthus (Newcomb 1973a), Allium, and Impatiens (from Willemse and van Went 1984) there is an increase in lipid bodies and plastid starch during the coenocytic phase of megagametophyte development. In Gasteria starch and lipids are present during the early stages of megagametogenesis but disappear prior to the cellularization of the megagametophyte (Willemse and Franssen-Verheijen 1978). In the majority of angiosperms the mature megagametophyte consists of seven cells. There are three antipodal cells at the chalazal end of the megagametophyte and an egg and two synergids (egg apparatus) at the micropylar end of the megagametophyte that are separated from the antipodals by the largest cell of the megagametophyte, the binucleate central cell.

The method of wall formation in the angiosperm megagametophyte is somewhat controversial. There are two basic theories dealing with the mechanism of cell wall formation during this phase of the angiosperm life cycle. One theory envisions the encapsulation of the synergid, antipodal, and egg nuclei and cytoplasms by what is termed free wall formation. According to the theory, free wall formation occurs independently of karyokinesis and does not involve microtubules. The cell walls are initiated at the wall of the megagametophyte as pegs of wall material that expand centripetally into the megagametophyte cytoplasm. The formation of cell walls around the egg apparatus and antipodals by free wall formation has never been demonstrated. Most of the literature in support of the free wall theory is derived from studies on endosperm formation in Helianthus (Newcomb 1973b),

Stellaria (Newcomb and Fowke 1973), Haemanthus (Newcomb 1978), and Triticum (Morrison and O'Brien 1976). Fineran et al. (1982) have challenged the free wall theory and provide convincing evidence that the initial endosperm cell walls in Triticum involve typical phragmoplasts and that these cell walls are derived from centifugally growing cell plates. Cass et al. (1985), in a study on cell wall formation in the megagametophyte of Hordeum, have provided the first ultrastructural evidence for the formation of cell walls around the antipodal and egg apparatus nuclei in the angiosperm megagametophyte. Cell wall formation in the megagametophyte of Hordeum was shown to involve elongated cell plates associated with clusters of microtubules. Cass et al. (1986) suggest that the four nuclei at the micropylar end of the megagametophyte of Hordeum are separated by two cell plates. A vertical cell plate separates the sister synergid nuclei and an initially horizontal cell plate separates the egg and polar nuclei. The horizontal cell plate expands centrifugally with one edge contacting the megagametophyte wall while the opposing edge branches. One branch grows in a micropylar direction and separates the egg nucleus from the two synergid nuclei. Chalazal growth of the vertical wall between the synergids eventually contacts and fuses with the horizontal plate. The horizontal plate forms the chalazal wall of all three cells.

Willemse and van Went (1984) report that cell walls are absent in the chalazal half of the egg apparatus in the majority of angiosperms that have been surveyed. Exceptions, in which the egg apparatus is encased entirely by a PAS-positive wall, have been reported in Capsella (Schulz and Jensen 1968a, 1968b), Epidendrum

(Cocucci and Jensen 1969a), Papaver (Olson and Cass 1981), Ornithogalum (Tilton 1981), and Scilla (Bhandari and Sachdeva 1983). Folsom and Peterson (1984) have shown the chalazal walls of the synergids and egg of Glycine to be Thiery-positive. The antipodal cell walls of Capsella (Schulz and Jensen 1971), Papaver (Olson and Cass 1981), and Scilla (Bhandari and Sachdeva 1983) are PAS-positive.

In Papaver (Olson and Cass 1981), Scilla (Bhandari and Sachdeva 1983), and in Aconitum (Bohdanowicz and Turala-Szybowska 1985), the antipodal cells enlarge following anthesis and develop wall projections of the transfer cell type (Gunning and Pate 1969). These persistent antipodals are rich in plastids, mitochondria, and dictyosomes and appear to play a role in the transport of nutrients into the megagametophyte following fertilization. Commonly, in grasses, the three antipodal cells undergo a series of mitotic divisions to form a chalazal aggregation of antipodal tissue. In Zea (Diboll and Larson 1966) and in Hordeum (Cass et al. 1986) the antipodal cells adjacent to chalazal nucellus develop wall ingrowths and in Zea all the antipodal cells possess a cytoplasm that appears to be synthetically active. Wall ingrowths have also been shown to occur in angiosperms that possess ephemeral, but synthetically active, antipodal cells (Newcomb 1973a, Wilms 1981a). The antipodal cells of Capsella are also ephemeral but contain few organelles and appear to be synthetically inactive (Schulz and Jensen 1971).

In most angiosperms, the mature central cell is a highly vacuolate binucleate cell containing two polar nuclei and a thin layer of parietal cytoplasm adjacent to the egg apparatus, antipodals, and lateral walls of the megagametophyte (Willemse and van Went 1984). In

Petunia the cytoplasm of the central cell contains few mitochondria, dictyosomes, and ER (Went 1970c). Central cell plastids are large and contain starch. Unlike Petunia the central cell of the majority of angiosperms appears to be a metabolically active cell that is rich in organelles. In Gossypium (Jensen 1965b, Schulz and Jensen 1977), Epidendrum (Cocucci and Jensen 1969a), Helianthus (Newcomb 1973a), Capsella (Schulz and Jensen 1973), Plumbago (Cass and Karas 1974), Stipa (Maze and Lin 1975), and Spinacia (Wilms 1981a) the central cell contains abundant proplastids, mitochondria, ER, and dictyosomes. In Capsella the cytoplasm of the central cell has a similar rich composition of organelles, however, the plastids are well developed chloroplasts and the authors consider the central cell to be autotrophic.

Wall projections have been reported to occur in the unfertilized central cell of Linum (Vasart and Vasart 1966), Helianthus (Newcomb and Steeves 1971, Newcomb 1973a), Stellaria (Newcomb and Fowke 1973), Euphorbia (Gori 1977), and Glycine (Folsom and Peterson 1984). In Capsella wall projections are absent from the central cell prior to fertilization (Schulz and Jensen 1973), but develop on the lateral walls of the central cell, on the central cell side wall of the suspensor (Schulz and Jensen 1974), and on the extreme chalazal walls of the central cell following fertilization. Tilton et al. (1984), report the formation of wall projections in the micropylar region of the central cell of Glycine following fertilization. These wall projections are thought to function as transfer cells by increasing the membrane surface area for the active transport of solutes into the megagametophyte (Newcomb and Steeves 1971).

The two polar nuclei, following completion of the third mitotic division, are located at opposite poles of the megagametophyte. In the majority of angiosperms the two polar nuclei migrate to the micropylar-central region of the megagametiophyte where nuclear fusion occurs. The fusion of the polar nuclei within the central cell of Gossypium involves the initial contact and subsequent fusion of the outer nuclear envelopes followed by the contact and fusion of the inner membranes of the nuclear envelope, in localized areas between the two polar nuclei (Jensen 1964). The resulting regions of fusion between the two nuclei produce narrow nuclear bridges of continuous nucleoplasm. Subsequent reports have confirmed the presence of nuclear bridges between partially fused polar nuclei in Capsella (Schulz and Jensen 1973), Petunia (Went 1970b), Stipa (Maze and Lin 1975), Spinacia (Wilms 1981b) and Glycine (Folsom and Peterson 1984). In Capsella (Schulz and Jensen 1973) and Helianthus (Newcomb 1973a), the polar nuclei completely merge forming a single fusion nucleus prior to double fertilization.

In the majority of angiosperms, the mature egg has been shown to be a polarized cell. The micropylar region of the cell typically contains a large vacuole with the nucleus and the majority of organelles in the cytologically inactive chalazal cytoplasm (Willemse and van Went 1984). In Gossypium (Jensen 1965b) and Papaver (Olson and Cass 1981), the polarity of the egg is reversed with the majority of the egg cytoplasm, including the nucleus, in the micropylar region of the cell while the chalazal region is occupied by a large vacuole. In Stipa (Maze and Lin 1975), there is no consistent and characteristic distribution of mature egg organelles and vacuoles. The mature egg is

considered by most authors to be a metabolically inactive cell, e.g. in Gossypium (Jensen 1965b), Capsella (Schulz and Jensen 1968b), Petunia (Went 1970c), Nicotiana (Mogensen and Suthar 1979) and Spinacia (Wilms 1981a). The egg cell typically contains perinuclear plastids and mitochondria. The plastids often contain starch (Jensen 1965b, Schulz and Jensen 1968b, Went 1970c, Newcomb 1973a, Maze and Lin 1975, Mogensen and Suthar 1979, Wilms 1981a). The ER is short stranded, the dictyosomes are typically few in number and the lack of vesicle activity indicates a low rate of synthetic activity (Maze and Lin 1975). In Nicotiana (Mogensen and Suthar 1979) and Epidendrum (Cocucci and Jensen 1969a) the mature egg is reported to be completely free of dictyosomes. Newcomb (1973a) reports a lack of active dicyosomes and ER in the egg of Helianthus but considers the large egg nucleolus, numerous ribosomes, plastids, and mitochondria indicative of a metabolically active cell. Extensive profiles of ER in Glycine suggested to Folsom and Peterson (1984) that the egg of soybean was also a metabolically active cell.

In all angiosperms studied to date, the mature synergids have been shown to exhibit a cytoplasm that suggests a metabolically active cell. The synergids are typically rich in mitochondria, plastids, ER, and dictyosomes, though the distribution of these organelles varies in different species (for a review see Willemse and van Went 1984). In addition, a micropylar filiform apparatus is a characteristic feature of the synergid. The filiform apparatus in angiosperm synergids varies from a simple vase-shaped micropylar thickening of the common synergid wall as seen in Petunia (Went 1970a), Helianthus (Newcomb 1973a), and Nicotiana (Mogensen and Suthar 1979) to a highly digitate elaboration

of cell wall material as seen in Gossypium (Jensen 1965a), Zea (Diboll and Larson 1966), Capsella (Schulz and Jensen 1968a), Hordeum (Cass and Jensen 1970), Stipa (Maze and Lin 1975), Spinacia (Wilms 1981a), Scilla (Bhandari and Sachdeva 1983) and Glycine (Folsom and Peterson 1984). Synergids of the digitate type, which increase the plasma membrane surface area are considered transfer cells (Gunning and Pate 1969). Jensen (1965a) was the first to suggest an absorption function for the synergid based on the presence of a filiform apparatus, numerous mitochondria in the immediate vicinity of the filiform apparatus, an elaborate network of ER that would function as an internal transport system and numerous active dicytosomes. A similar absorption function has been attributed to the synergids of Capsella (Schulz and Jensen 1968a), Stipa (Maze and Lin 1975), Spinacia (Wilms 1981a), and Glycine (Folsom and Peterson 1984). The absence of an extended area of plasma membrane in the filiform apparatuses of Helianthus (Newcomb 1973a), Quercus (Mogensen 1972) and Petunia (Went 1970a) suggested to these authors that these cells do not function as transfer cells. In Plumbago, where synergids are lacking, the mature egg cell has been shown to possess a digitate filiform apparatus (Cass 1972). The cytoplasm of the mature egg cell of Plumbago contains active dictyosomes and numerous mitochondria in the vicinity of the filiform apparatus (both synergid-like characteristics).

The filiform apparatus in the majority of angiosperms has been shown to be PAS-positive in Gossypium (Jensen 1965a), Zea (Diboll and Larson 1966), Capsella (Schulz and Jensen 1968a), Hordeum (Cass and Jensen 1970), Paspalum (Chao 1971), Plumbago (Cass 1972), Proboscidea (Mogensen 1978a), Nicotiana (Mogensen and Suthar 1979), Papaver (Olson

and Cass 1981), Spinacia (Wilms 1981a), and Scilla Bhandari and Sachdeva 1983). Chao (1971) suggested that the PAS-positive material in the filiform apparatus of Paspalum was hemicellulose derived from the breakdown of synergid starch (Yu and Chao 1979). Jensen (1965a) identified pectins and suggested the probable presence of cellulose and hemicellulose as the major chemical components of the filiform apparatus of Gossypium.

Another proposed function of the synergids is the attraction of the pollen tube. Went (1970a) considered the primary function of the synergid of Petunia was the secretion of a chemotropic substance into the micropyle for the attraction of the pollen tube. A chemotropic function for the synergids has also been suggested in Helianthus (Newcomb 1973a), Spinacia (Wilms 1981a), Agave (Tilton and Mogensen 1979), and Ornithogalum (Tilton 1981). Chao (1971, 1977) identified a PAS-positive substance in the micropyle of Paspalum and suggested that the substance may function in guiding the pollen tube to the megagametophyte. Calcium appears to be involved in the tip growth of the pollen tube and has frequently been accorded a chemotropic function. Mascarenhas and Machlis (1964) found an increasing gradient of calcium ions from the stigma to the placenta and provided evidence that calcium was involved in chemotropism in Antirrhinum. However, calcium alone has proven to be chemotropically inactive in a number of angiosperms (Rosen 1971).

In all species of angiosperms that have been studied using the modern techniques of light and electron microscopy, the pollen tube has been shown to enter one of the synergids by way of the filiform apparatus (Willemse and van Went 1984). In a number of angiosperms the

pollen tube enters one of the synergids that has degenerated prior to arrival of the pollen tube. Degeneration of one of the synergids prior to the arrival of the pollen tube but after germination of the pollen tube on the stigma, has been shown to occur in Gossypium (Jensen and Fisher 1968), Quercus (Mogensen 1972), Stipa (Maze and Lin 1975), Proboscidea (Mogensen 1978b), Nicotiana (Mogensen and Suthar 1979), Spinacia (Wilms 1981b). Cass and Jensen (1970) also report the degeneration of one of the synergids of Hordeum irrespective of whether pollination has occurred or not. Jensen et al. (1977) found that in cultured ovules of Gossypium the early degeneration of one of the synergids and the persistence of the other synergid was independent of pollination suggesting that one of the synergids is preprogrammed for eventual degeneration. In Capsella (Schulz and Jensen 1968a), Petunia (Went 1970b), Papaver (Olson and Cass 1981), and perhaps Helianthus (Newcomb 1973b) both synergids remain intact until one is penetrated by the pollen tube.

The pollen tube discharges its contents into the degenerate synergid. The transfer of the two sperms from the degenerate synergid to the egg and central cell has not been observed in angiosperms (Went and Willemse 1984), though Russell (1983) has proposed a mechanism, substantiated by electron micrographs, for the transfer of sperm cells to the egg and central cell of Plumbago. In Plumbago the pollen tube penetrates the filiform apparatus of the egg, continues growing chalazally through the PAS-positive wall, between the egg and central cell plasma membranes, and discharges the vegetative nucleus and two sperm cells into the chalazal wall region between the egg and central cell. According to Russell, the prior dispersion of the egg-central

cell wall material permits the direct apposition of sperm, egg, and central cell plasma membranes which subsequently fuse. The dissolution of the fusion membranes results in the transmission of one sperm nucleus and its associated mitochondria and chloroplasts into the egg cell and the other sperm nucleus and its associated mitochondria into the central cell. Russell provides convincing morphological evidence for the transmission of sperm organelles that may contribute to male cytoplasmic inheritance.

At the ultrastructural level, the process of double fertilization has been observed by Jensen and Fisher (1967) in Gossypium, Went (1970b) in Petunia and by Wilms (1981b) in Spinacia. Nuclear fusion appears to be similar to that described by Jensen (1964) for the fusion of the polar nuclei and results in the formation of localized nuclear bridges between the nuclei of the sperm and egg and between the second sperm nucleus and the polar nuclei. The nuclear bridges enlarge and there is complete fusion of the nuclear membranes.

Zygote formation in Gossypium (Jensen 1968), Hibiscus (Ashley 1972), and Nicotiana (Mogensen and Suthar 1979) is characterized by a distinct shrinkage of the zygote cell. The zygotes of Epidendrum (Cocucci and Jensen 1969b), Hordeum (Norstog 1972), and Quercus (Singh and Mogensen 1975) do not exhibit a decrease in size following fertilization. In Capsella the micropylar vacuole, characteristic of the egg, decreases in size but soon expands until it is larger than the egg vacuole (Schulz and Jensen 1968b). Schulz and Jensen do not report a shrinkage of the zygote in Capsella. In Capsella the tip of the zygote elongates and there is an increase in plastid starch, lipids, polysomes, and dictyosomes. The dictoysomes are active in the

micropylar and chalazal regions of the zygote and appear to be involved in cell wall synthesis. The electron-opaque deposits between the chalazal wall of the egg and central cell disappear following fertilization in Capsella. Mogensen and Suthar (1979) report that, as in the egg, dictyosomes are absent from the zygote of Nicotiana. They speculate that ER, adjacent to the zygote plasma membrane, may be responsible for the formation of the PAS-positive cell wall. In Gossypium (Jensen 1968) and in Epidendrum (Cocucci and Jensen 1969b), as in Capsella, there is a marked increase in helical polysomes following fertilization. With the exception of Petunia (Went 1970b), angiosperm zygotes seem to increase in metabolic activity following fertilization. Similarly the central cell exhibits an increase in apparent metabolic activity following triple fusion, with an increase in dictyosomes, ER, mitochondria and plastids. In Gossypium, the ER becomes arranged into long parallel cisternae (Schulz and Jensen 1977). In the central cell of Capsella there is a similar increase in cytoplasmic organelles and a decline in chloroplast starch and cytoplasmic lipid by the second division of the endosperm nucleus (Schulz and Jensen 1974). Wall projections, that were absent from the central cell of Capsella prior to fertilization, form on the lateral micropylar and chalazal walls of the central cell and on the central cell side of the embryo suspensor.

MATERIALS AND METHODS

I. Plant material.

In order to achieve several of the objectives of this study, as outlined in the introduction, it was necessary to control when and if pollination was to occur. Potential problems associated with self-pollination were minimized by selecting Brassica campestris, a sporophytic self-incompatible species (Hinata and Nishio 1980), for the study.

Plants of Brassica campestris L. cv.Candle (canola-rapeseed) were grown in a plant growth cabinet (Controlled Environments Ltd.,model E 15) under Sylvania Lifeline cool white fluorescent tubes at a light intensity of 200 uE.m-2s.-1. During the initial four week period, from the young seedling stage through to the mature rosette leaf stage, a shortday 8 h photoperiod (day temperature, 22°C; night temperature, 18°C) was maintained to prevent precocious flower formation. At the end of the four week period, the photoperiod was increased to 16 h to induce bolting and inflorescence development (Orr 1978).

II. Selection and collection of ovules for fixation.

To obtain the early stages of ovule development (ovule primordium to the two-nucleate megagametophyte), pistils were excised from flowers and the ovary dissected into 0.5 mm. segments. At the early stages of development, the majority of the ovules were oriented with their longitudinal axis perpendicular to the longitudinal axis of the pistil. The longitudinal axes of older ovules was parallel to the longitudinal axis of the pistil but the precise orientation of the ovule within the ovary was unpredictable. To permit accurate specimen orientation prior to sectioning, ovules beyond the two-nucleate

megagametophyte stage were dissected from the pistil. Older pistils were excised from flowers and the ovules removed from the ovary loculus using a fine-tipped glass microprobe. The ovary wall was dissected and the proximal end of the ovule funiculus excised from the placenta of the ovary. Pistil segments and intact ovules were immediately immersed in buffered fixative.

The external morphology of the mature ovule shortly after fertilization is identical to the mature unfertilized ovule at anthesis. Prior to sectioning, potentially fertilized ovules were distinguished from unfertilized ovules using a procedure modified from that of Olson and Cass (1981) to visualize pollen tubes that have penetrated the ovule micropyle. Ovules were removed from pollinated pistils using the microprobe technique described previously and transferred to dwell slides containing 0.05% aniline blue (C.I.42755, Polysciences) in 0.025 M phosphate buffer (pH 6.8), and viewed with a Nikon Optiphot compound microscope equipped with an epifluorescence attachment and a 50W high pressure mercury vapor lamp. The fluorochrome in aniline blue binds to callose, a beta 1-3 glucan, located within the pollen tube cell wall, and fluoresces when examined with UV or blue light. Ovules with pollen tubes in the micropyles were separated from those ovules without and each immediately immersed in buffered fixative.

III. Light microscopy

Brightfield and phase contrast light microscope observations were made using a Nikon Optiphot compound microscope. Differential interference contrast light microscope observations were made using a Leitz Ortholux compound microscope. Photographic images were recorded

on 35 mm Plus-X 125 ASA film or 35 mm Ektachrome 160 ASA tungsten corrected professional film. Photographic negatives were projected using a Simmon-Omega (model automega D3) point source photographic enlarger and the photomicrographs recorded on Ilford multigrade II medium grade paper.

(A) Fixation, infiltration and embedding.

Ovules and pistil segments were fixed in 3 % glutaraldehyde in 0.025 M phosphate or cacodylate buffer (pH 6.8) for two h at room temperature, followed by 24 h at 4°C in the same fixative, then either post-fixed for 4 h in 2% osmium tetroxide in 0.025 M phosphate or cacodylate buffer (pH 6.8) or processed further without osmium tetroxide fixation. The tissues were dehydrated in a graded ethanol series (20 min each), followed by successive changes of ethanol:propylene oxide (3:1; 1:1; 1:3; for 30 min each) and three changes of 100% propylene oxide (30 min each). The tissues were infiltrated with a mixture of propylene oxide and Spurr's low viscosity epoxy resin (Spurr 1969)(3:1; 1:1; for 2 h each; 1:3 for 48 h), followed by daily changes of 100% fresh Spurr's resin for 7 days. There was constant tissue rotation during all stages of dehydration and infiltration. Following infiltration, the specimens were embedded in 100% Spurr's resin in shallow 44 mm diameter aluminum pans and polymerized at 70°C under partial vacuum for 16 h.

Mature ovules at anthesis were also fixed in glutaraldehyde, dehydrated in a graded ethanol series and embedded in glycol methacrylate (O'Brien and McCully 1981). The glycol methacrylate material was polymerized at 60°C under partial vacuum for 16 h. The chamber of the vacuum oven was flushed with nitrogen to provide the

oxygen reduced environment necessary for glycol methacrylate polymerization.

(B) Staining glycol methacrylate embedded material.

Cubes of resin containing ovules were cut from polymerized flats of glycol methacrylate, the desired orientation determined, and the cubes of resin containing the ovule glued to blank epoxy beem capsules using fast curing epoxy adhesive. Sections (1-2um) were cut, using dry glass knives, on a Sorvall Porter Blum JB4 microtome and transferred to gelatin-coated slides (Jensen 1962) using fine forceps (Feder and O'Brien 1968). Following staining, all sections were mounted in 70% aqueous sucrose.

(i) Toluidine blue O (Feder and O'Brien 1968).

Sections were stained with 0.05% Toluidine blue O (C.I.52040, Fisher) in 0.05 M benzoate buffer at pH 4.4. Toluidine blue is a cationic metachromatic dye which will stain certain chemical components of tissues a colour different from that of the dye in solution (O'Brien and McCully 1981). Toluidine blue generally binds to macromolecules containing large numbers of polyanionic binding sites (e.g. carboxyl, sulphate, and phosphate groups). The colour shift is from blue to red with the strongest metachromatic reaction (i.e. reddest) being for polymers containing sulfated groups; polymers containing carboxyl groups exhibit a slightly weaker reaction (i.e.pink); and polymers containing phosphate groups exhibit the weakest metachromatic reaction (purple). Sulfated polysaccarides (e.g. fucoidan) and carboxylated polysaccarides (e.g.pectic acids, alginic acids) will stain red to dark pink, RNA will stain purple, and DNA

will stain blue. By what is termed negative metachromasia, lignin and some polyphenols stain green (O'Brien et al. 1964).

(ii) Alcian blue 8GX (McCully 1970).

Sections were stained in 0.1% acidified aqueous solutions of the cationic dye alcian blue 8GX (C.I.74240, Polysciences) to localize carboxylated polysaccharides. The dye was either dissolved in 0.5 N HCl, giving a staining solution of pH 0.5 or in 3% acetic acid giving a staining solution of pH 2.5. At pH 2.5 the carboxyl groups of carboxylated polysaccharides are ionized and stain orthochromatic blue in the presence of the cationic dye. At pH 0.5 (below the pK of the carboxyl group) carboxylated polysaccharides are unstained.

(C) Staining epoxy embedded material

To facilitate a correlative light microscope and transmission electron microscope study, the majority of the light micrographs were obtained from glutaraldehyde-osmium tetroxide fixed - Spurr's epoxy resin embedded material. Cubes of resin containing ovules and pistil segments were cut from polymerized flats of Spurr's resin, the correct orientation determined and the cubes of resin and tissue glued to blank epoxy beem capsules with fast curing epoxy adhesive. Sections (0.75-1.0 um) were cut, using a Sorvall Porter Blum JB4 microtome and glass knives fitted with a boat. Serial sections were obtained using the technique of Fisher (1968). Tacki-wax (Central Scientific) was applied to the upper and lower block faces. As successive sections were cut, a serial ribbon of adhering sections was formed on the water film of the knife boat. The ribbon was picked up with a glass microprobe and transferred to a gelatin coated slide (Jensen 1962).

All sections, unless otherwise stated, were mounted in 70% aqueous sucrose.

Unlike glycol methacrylate, a water permeable plastic, the epoxy plastics are relatively water impermeable. Traditional staining techniques developed for fresh, paraffin-embedded, and glycol methacrylate-embedded tissue rely heavily on dyes dissolved in water or aqueous buffers. The majority of these staining techniques have proven to be ineffectual when applied to epoxy-embedded plant tissue. Limited success has been achieved using cationic dyes (eg. toluidine blue, methylene blue, azure II) at high pH (O'Brien and McCully 1981). These staining procedures were found to be unsatisfactory for general survey work since contrast between various cell components is poor.

(i) Crystal violet

Superior contrast was obtained by staining epoxy sections, on a warming tray at 85°C, with 2% ethanolic crystal violet (C.I.42555, Fisher) in 0.05 M ammonium oxalate buffer at pH 6.7 (Gerhardt et al. 1981) for 0.5-1.0 min. The sections were rinsed in warm running water for 5 min. Crystal violet, used under these conditions, possesses the same metachromatic properties described previously for toluidine blue O. The use of crystal violet to stain plant tissues embedded in epoxy resins has not been previously reported, though it is commonly used in bacteriology as part of the Gram staining procedure and in animal histology to metachromatically stain amyloid.

(ii) Aniline blue black (Fisher 1968)

Aniline blue black, an anionic dye, was used to localize protein. Sections were stained in 1% aniline blue black (C.I.20470, Polyscience) in 7% acetic acid for 15 min at 60°C. The sections were

briefly rinsed in 7% acetic acid to remove excess stain then mounted in glycerol containing 5% acetic acid. The cytosol of healthy cells stained light blue while that of degenerating cells, presumably rich in hydrolytic proteins, stained dark blue. Mitochondria, plastids, and regions of nuclei stained light to dark blue.

(iii) Periodic acid Schiff reaction (PAS) (Jensen 1962)

The PAS reaction was used to localize insoluble carbohydrates. The mechanism of this two-step histochemical procedure is well documented (Hale 1957). Periodic acid (PA) oxidizes vicinal 1,2 glycol groups (hydroxyl groups at the 2nd and 3rd carbon) in carbohydrates to aldehydes, which react with the Schiff's reagent to produce a magenta color at the reaction site. Glucans with 1-4 linkages, such as pectic compounds, hemicellulose, starch, and the oligosaccharide side chains of glycoproteins, are PAS-positive. Cellulose, as it occurs in cell walls, is reported to be PAS-negative, due perhaps to steric hindrance of available vicinal glycol groups (O'Brien and McCully 1981). Compounds will be PAS-negative where the hydroxyl groups are not attached to vicinal carbon atoms or where one of the vicinal carbons is involved in linkages (Beta 1-3 glucans, e.g. callose). Certain compounds, other than carbohydrates, will also exhibit a PAS-positive reaction. These include the amino acids serine, threonine, and hydroxylysine, which have vicinal hydroxy-amino groups that can be oxidized to dialdehydes. Certain lipids will also react positively (Roland 1978). Lignin will combine with Schiff's reagent and give a positive reaction without prior periodic acid oxidation (O'Brien and McCully 1981).

Sections were immersed in 0.5% 2,4 dinitrophenyl hydrazine in 15% acetic acid for 15 min to block endogenous aldehydes. Following a 10 min rinse in running water the sections were oxidized in 1% aqueous periodic acid for 30 min, rinsed in running water for 10 min, then placed in Schiff's reagent (Fisher) for 40 min. The sections were briefly bleached in 3 successive baths of 0.5% aqueous sodium metabisulphate (2 min each) and rinsed in running water for 10 min. The sections were either examined directly or counter stained with crystal violet or aniline blue black.

IV. Fluorescence microscopy.

Fluorescence microscope observations were made using a Nikon Optiphot compound microscope fitted with an episcopic fluorecscence attachment, and a 50W high pressure mercury lamp. For illumination with ultra violet light (UV) a UV excitation filter (330-380nm), dichroic mirror DM400 and a barrier filter transmitting above 420nm were used. For illumination with blue light a blue excitation filter (410-485nm), dichroic mirror DM505 and a barrier filter transmitting above 515 nm was used. Photographic images were recorded on 35 mm Plus-X 125 ASA film or 35 mm Ektachrome 160 ASA tungsten-corrected professional film.

Both fresh and epoxy-embedded tissue was used. Prior to staining Spurr's epoxy-embedded material with fluorochromes, the resin was removed from the sections using a modification of the procedure of Lane and Europa (1965). Sections mounted on gelatin-coated slides were immersed in a saturated solution of potassium hydroxide in 95% ethanol for two min, rinsed in 3 changes of 95% ethanol, followed by five min in running water. The resin was removed to facilitate access of the

fluorochrome to the tissue and to eliminate the problem of background autofluorescence caused by the resin.

(A) Calcofluor (Fulcher and Wong 1980)

Sections from material fixed in glutaraldehyde - osmium tetroxide were immersed in 1% periodic acid or 10% hydrogen peroxide for 30 min to bleach osmium from the tissues. Sections were stained in 0.01% aqueous Calcofluor white M2R (Polysciences) for 5 min, rinsed in running water, mounted in 70% sucrose, and viewed under UV light. Calcofluor has been used as a general stain for plant cell walls (Hughes and McCully 1975) and in the study of the site of cellulose synthesis and microfibril assembly (Schnepf et al. 1982). Calcofluor has some specificity for mixed linkage B-glucans (Wood and Fulcher 1978) and it has been shown to bind to cellulose and chitin fibrils (Herth and Schnepf 1980).

(B) Aniline blue (O'Brien and McCully 1981)

Fresh tissue of pollinated stigmas, styles, and ovules, and bleached sections of glutaraldehyde - osmium tetroxide-fixed, epoxy-embedded ovules (with the resin removed) were stained for five min in 0.05% aniline blue (C.I.42755, Polysciences) in 0.01 M phosphate buffer at pH 8.5, mounted in the buffered stain and illuminated with either UV or blue light. The fluorochrome in aniline blue is thought to be specific for the B 1-3 glucan, callose (Jensen 1962), though Smith and McCully (1978) question the absolute specificity, suggesting it may also bind to other cell wall polysaccharides. They have shown that aniline blue specificity for callose is enhanced by prior treatment of the tissues with toluidine

blue O (to block carboxylated polysaccharides) and the PAS procedure (to block polysaccharides with vicinal glycol groups).

(C) Cellulase Extraction

The Spurr's epoxy resin was removed from sections of mature ovules using a modification of the procedure of Lane and Europa (1965). The sections were immersed in a 5 mg/mL solution of cellulase (Sigma, practical grade) in 0.05 M phosphate buffer ph 5.5 at room temperature (Hickey and Coffey 1978). The sections were then stained with Calcofluor and viewed with fluorescence optics under UV light.

V. Transmission electron microscopy (TEM).

All electron microscope observations were carried out on either an AEI 801S or an AEI 6B electron microscope operating at an accelerating voltage of 60 kv. Electron images were recorded on Kodak Electron Image 8.3 X 8.4 cm sheet film. The electron image negatives were projected using a Simmon-Omega (model automega D3) point source photographic enlarger and the photomicrographs recorded on Ilford multigrade II medium grade paper.

(A) Conventional fixation and staining

The methods of fixation, dehydration, infiltration, embedding, and orientation of ovules and pistil segments for TEM were as described in section III.A. for light microscopy.

Ultrathin sections (.06-.08 um) were cut with a Dupont diamond knife using a Reichert OM-U2 ultramicrotome. Sections were collected on uncoated copper or nickel 75/300 mesh grids and stained for 25 min with a saturated solution of uranyl acetate (UA) in 50% methanol (O'Brien and McCully 1981) followed by 10 min in lead citrate (Reynolds 1963) under a constant flow of nitrogen gas.

(B) Periodic acid - thiocarbohydrazide - silver proteinate (PA-TCH-SP) (Thiery, 1967)

The PA-TCH-SP procedure, used to localize insoluble carbohydrates, is a modification of the PAS procedure. Periodic acid (PA) is used to selectively oxidize vicinal glycol or glycol-amino groups to aldehydes. The aldehydes are then condensed with thiocarbohydrazide (TCH) to produce thiocarbohydrazones which are strong reducing agents (Roland 1978). Subsequent staining with silver proteinate (SP) results in the deposition of reduced silver over the reaction site. Compounds that are PA-TCH-SP positive or negative correspond to those descibed previously for the PAS reaction. The control most commonly used in this study was the substitution of water for periodic acid. Additional controls were the blockage of aldehydes with aqueous 0.1% sodium borohydride and the omission of TCH or SP from the staining procedure (Roland 1978).

Ultrathin sections of ovules, fixed in glutaraldehyde - osmium tetroxide, were collected on 75/300 mesh nickel grids. Grids were floated section-face down on 1% aqueous periodic acid for 30 min in a high humidity chamber, followed by three changes of 10 min each in distilled water. Grids were transferred to 0.2% thiocarbohydrazide (TCH) in 20% aqueous acetic acid for 2,5,10 and 24 h (5 h proved to be optimum), followed by successives rinses of 10%, 5%, and 1% aqueous acetic acid (20 min each) and three rinses of distilled water (30 min each). The grids were then immersed in 1% aqueous silver proteinate for 30 min in the dark followed by 3 successive rinses of 1 h each in distilled water.

(C). Osmium tetroxide and potassium ferricyanide (OsFeCN) (Hepler 1981).

The OsFeCN post-fixation procedure was used to stain the endoplasmic reticulum (ER) and nuclear envelope. The initial use of this procedure in plant ultrastructure was by Hepler (1980) in a study of the distribution of ER in dividing cells of barley. Animal cytologists had used the technique to contrast the sarcoplasmic reticulum of muscle cells (Forbes et al. 1977) and a modification of the procedure (without calcium) had been used previously to stain glycogen (Bruijn and Breejen 1975). The chemical basis of the staining reaction is unknown; however, White et al. (1979) suggested that metal-containing proteins on membranes chelate the cyano-bridged osmium-iron complexes resulting in the deposition of these electron-opaque complexes on the membrane sites.

The removal of calcium chloride from the fixatives or the addition of phosphate buffer, which would precipitate the calcium, abolishes the selective staining of the ER and nuclear envelope (Hepler 1981). Hepler also noted that only a portion of the ER of onion and lettuce roots and barley leaves was selectively stained by the procedure. He suggested that the distance from the fixation front may be a reason for the abscence of a positive staining reaction. The OsFeCN procedure did not ubiquitously stain the ER of the integument, nucellus, or megagametophyte of Brassica. Distance from the fixation front was not a factor, since stained and unstained ER were both found in regions closest to and furthest away from the fixation front. Frequently, in contiguous cells, with equal access to the stain, the ER of one cell was stained positively, while the ER of the adjacent cell was

unstained. In certain synergid cells of the megagametophye, some of the ER within the one cell, would stain positively while the ER in other regions of the cell remained unstained. Clearly, access to the tissue is not the reason why some of the ER is unstained. There must be a difference in the chemical content of the stained and unstained ER at the time of fixation; however, until the mechanism of staining is understood, the value of the OsFeCN method will be to discern the distribution of ER in the cell.

Ovules were fixed in 3% gluteraldehyde in 0.025 M cacodylate buffer (pH 6.8) with 5 mM calcium chloride for 2 h at room temperature followed by 24 h at 4°C in the same fixative. Following a wash in 0.025 M caycodylate buffer (pH 6.8) with 5 mM calcium chloride, the ovules were post-fixed in a mixture of 2% osmium tetroxide and 0.8% potassium ferricyanide in 0.025 M cacodylate buffer with 5 mM calcium chloride for 4 h at room temperature.The methods of dehydration, infiltation, embedding, orientation, sectioning,and staining were the conventional TEM methods described previously. Some sections were examined without additional uranyl acetate-lead citrate staining.

OBSERVATIONS

I. YOUNG OVULE

(A) Ovule and replum initiation

Ovule primordia of Brassica campestris are trizonate. The protodermal layer (zone 1) and subdermal layer (zone 2) of the ovule primordium divide anticlinally, while zone 3, consisting of all tissues inside the second primordial layer, is characterized by periclinal, anticlinal and oblique divisions (Figs. 1, 2.). At the time of ovule initiation two replum primordia, located between the ovule primordia and extending the length of the ovary, are initiated (Fig. 1). The dermal tissues of the two opposing replum primordia are tightly appressed. Prior to the onset of megasporogenesis in the ovule, the central region of the replum is composed of small thin-walled cells (Fig. 4) and the two replum primordia can no longer be distinguished as separate entities. By the 4-nucleate stage of megagametophyte development, these central cells of the replum develop thick, PAS-positive, unlignified cell walls (Fig. 26). Between this central zone of collenchyma and the lateral vascular bundle of the ovary wall, is a region of enlarged, starch-containing parenchyma cells with prominent intercellular spaces. The replum divides the ovary into two loculi, each containing 10-12 ovules at maturity.

(B) Inner integument initiation and development

The ovule, prior to the onset of megasporogenesis, consists of a nucellus, chalaza and funiculus derived from zones 1,2 and 3 of the ovule primordium (Fig. 2). These three regions of the ovule which form a continuous tissue are more easily distinguished as separate entities following integument initiation and development (Fig. 18). The ovule

of Brassica campestris is bitegmic. The inner integument is entirely dermal in origin. It is derived from a collar of protodermal initials circumjacent to the base of the nucellus. The individual wedge-shaped initials, located four to five cells proximal to the nucellar apex, is the product of an oblique division of a protoderm cell of zone 1 (Figs. 2, 5, 7, 8). The inner integument initials originated on the adaxial side of the ovule adjacent to the replum (Fig. 2). The production of initials continues around the circumference of the ovule toward the abaxial side adjacent to the ovary wall (Figs. 2, 5). Bifacial divisions of the distal wedge-shaped apical initials (Fig. 8) produce the two layered inner integument (Figs. 8, 18), though intercalary anticlinal divisions may also be involved in the acropetal growth of the integument during the early stages of development. By the functional megaspore stage of megagametophyte development the distal tip of the inner integument is even with the apex of the nucellus (Fig. 18) and by the early 2-nucleate stage the nucellus is completely enveloped by the inner integument. The inner integument component of the micropyle, distal to the apex of nucellus, is also formed by the early 2-nucleate stage of development (Fig. 21). The proximal regions of the inner integument adjacent to the chalazal nucellus become three to four layered as a result of periclinal divisions of the innermost layer of the integument over the course of ovule develpoment (Figs. 26, 34, 52, 53). The more distal regions of the inner integument, lateral to the 2-nucleate and older megagametophytes, and the micropylar region of the inner integument remain, for the most part, two to three layered. The proximal region of the inner integument is five to seven layered by the mature ovule

stage of development and the innermost layers, adjacent to the chalazal nucellus, exhibit a marked radial expansion (Fig. 53). This, in conjunction with the lack of radial cell expansion in the lateral and micropylar regions of the inner integument, results in a mature ovule with a distinct swollen chalazal region and a narrow micropylar neck. During the course of ovule development, the periclinal division and radial expansion of cells in the proximal region of the inner integument between the raphe and the chalazal nucellus, a region termed the basal body (Bouman 1984), contributes to the characteristic curved chalazal nucellus of the campylotropous ovule (Figs. 26, 34, 52, 53). The inner integument basal body continues to enlarge following anthesis (Figs. 104, 134) .

(C) Outer integument initiation and development

The outer integument is derived from initials in zones 1 and 2 of the ovule primordium. The protodermal initials of the outer integument originate on the adaxial side of the ovule immediately proximal to the protodermal inner integument initial (Fig. 2). There is a slight radial expansion of the incipient outer integument protodermal initials which subsequently divide in an anticlinal plane concurrently with periclinal divisions in the contiguous subdermal zone 2 (Figs. 3, 5, 7). As with inner integument, the initiation of the outer integument continues around the base of the nucellus toward the abaxial side of the ovule (Fig. 5). The adaxial side of the outer integument, including the region contiguous with the raphe, exhibits the greatest growth of all integumentary tissues, and coupled with the arrested growth of the outer integument on the abaxial side, produces an asymmetric curvature in the ovule (Fig 18). This, coupled with the

greater growth of the funiculus on the abaxial side, results in a sigmoid ovule (Figs. 18, 26). The acropetal growth of the outer integument, on the adaxial side of the ovule, results in this portion of the outer integument enveloping both the adaxial inner integument and the nucellus by the functional megaspore stage (Fig. 18) and contacting the abaxial side of the inner integument by the 4-nucleate stage of megagametophyte development (Fig. 26). This forms the outer integument component of the micropyle (Figs. 26, 34). The abaxial side of the outer integument includes a small ridge of anticlinally derived protodermal cells immediately distal to the funiculus, a file of protodermal and a few subdermal derivatives between the inner integument and the raphe (Figs. 18, 34). The greater growth on the adaxial side of the outer integument results in the characteristic inverted campylotropous ovule with the micropyle directed toward the funiculus (Figs. 26, 34). The proximal regions of the adaxial outer integument are for the most part three layered during early ovule development (Fig. 34), but become four layered at maturity by periclinal division of the middle layer (Fig. 53). The distal region of the adaxial side of the outer integument, near the micropyle, is composed of two to three layers of large vacuolated parenchyma cells. The raphe constitutes a zone of tissue between the chalazal nucellus of the ovule and the funiculus (Figs. 18, 26, 34, 52, 53). A single vascular trace of xylem and phloem elements runs from the ovary wall through the funiculus and terminates in the distal portion of the raphe at the base of the chalazal nucellus (Fig. 54). This region of the nucellus contains starch and, unlike the more distal region of

chalazal nucellus, does not degenerate following anthesis, but remains intact and forms the chalazal proliferating tissue (Figs. 104, 134).

(D) Archesporial and primary sporogenous cells

The nucellus, derived from zones 1,2, and 3 of the ovule primordium, is a dome of parenchyma tissue distal to the point of insertion of the inner integument (Figs. 2, 3, 5, 7). During the period of integument initiation, the anticlinally derived nucellar cells of zone 2 are more or less isodiametric (Fig. 2). One or two cells from this zone immediately hypodermal to the nucellar apex enlarge and develop prominent nuclei (Fig. 4, 5). This group of cells constitutes the multicellular archesporium. Generally, one of these cells functions as the archesporial cell (Fig. 5) which divides periclinally into a small primary parietal cell and a larger obovate primary sporogenous cell (Fig. 3). Both the primary parietal cell and primary sporogenous cell are intensely stained by cationic dyes. The primary sporogenous cell differentiates into the megasporocyte cell.

Cytologically, the most distinctive feature of both the archesporial cell and the primary sporogenous cell is the large (6um) nucleus with prominent basiophilic nucleoli (Figs. 3, 5). The nucleolus is granular and regions of basiophilic heterochromatin (Fig. 3, 5) are located in the peripheral regions of the homogeneous nucleoplasm adjacent to the inner membrane of the nuclear envelope (Fig. 6). OsFeCN staining reveals a nuclear envelope with distinct nuclear pores and a small amount of short stranded ER distributed throughout the cell. In the extreme chalazal region of the cell an ER-derived electron-opaque microbody is present. Plastids are mainly perinuclear and exhibit electron-opaque regions within the stroma that

are presumed to be starch. The thylakoid lamellae of the plastid are poorly developed. In this respect they are similar to the plastids found in the other adjacent cells of the nucellus. In addition to starch, there are additional energy reserves present in all cells of the nucellus in the form of lipid. The spherical mitochondria of the primary sporogenous cell are similar to the mitochondria of adjacent nucellar cells. They range in size from 1-2 um and possess poorly developed cristae (Figs. 6, 10). Dictyosomes are present in all nucellar tissues and appear to be relatively inactive by virtue of the lack of vesicle production. The cytoplasm of the primary sporogenous cell in Figure 6 is vacuolate and slightly less electron-opaque than the surrounding nucellar cells. This reduction in electron-opacity is due to a lower population of ribosomes in the primary sporogenous cell perhaps reflecting its incipient differentiation into a megasporocyte cell.

(E) Megasporocyte

The megasporocyte typically develops from the primary sporogenous cell (Figs. 8, 9), though development directly from the archesporial cell does occur (Fig. 7). The megasporocyte at mid-prophase of meiosis I exhibits a very distinct morphology. At the level of the light microscope, the nucleus exhibits prominent nucleoli, synaptonemal chromosomal complexes and a non-basiophilic nucleoplasm (Fig. 7). The cytoplasm is noticeably less basiophilic than that of the adjacent nucellar cells and there appears to be an even distribution of organelles that are visible at the level of the light microscope.

At the ultrastuctural level, the mid-prophase nucleus is composed of regions of condensed chromatin distributed through an

electron-transparent nucleoplasm (Fig. 9) and a synaptonemal chromosomal complex is adjacent to a region of dilated nuclear envelope (Fig. 12). Within this region of dilated nuclear envelope are electron-opaque, membrane-bound inclusions. Because of a reduced ribosome population, the cytoplasm of the megasporocyte is more electron-transparent than the adjacent nucellar tissue (Figs. 9 ,11, 12). In contrast to the primary sporogenous cell, there is a lack of starch deposits in megasporocyte plastids. Similarly, the amount of stored starch, though still present in the plastids of the nucellar epidermis (Fig. 9), is less than the amount in nucellar cells at the primary sporogenous cell stage of development (Fig. 6). The number of dictyosomes found in the megasporocyte is greater than in the primary sporogenous cell and the presence of vesicles at the maturing face suggests a degree of metabolic activity (Fig. 12). Strands of ER are longer and more abundant in the megasporocyte as are the numbers of lipid bodies. Occasional plasmodesmata interconnect the cytoplasms of the megasporocyte and the chalazal nucellus. There are scattered deposits of electron-transparent material in the cell wall of the megasporocyte (Fig. 9). As in the primary sporogenous cell, megasporocyte mitochondrial structure is relatively simple with an absence of well defined cristae; however, the size of the organelle is reduced (0.5 um X 1.0 um), the shape is rod-like rather than spherical (Fig. 11) and the matrix is often electron-opaque (Figs. 9, 12). The megasporocyte contains unit membranes that entirely enclose parts of the cytoplasm (Figs. 9, 12). These inclusions are a distinctive feature of the megasporocyte and are classified as double membrane-bound inclusions if two unit membranes are present and as

multiple membrane-bound inclusions if more than two unit membranes are involved (Dickinson and Heslop-Harrison 1977). Figure 11 illustrates a multiple membrane-bound inclusion composed of four unit membranes enclosing a region of megasporocyte ribosomes. The large chalazal and micropylar vacuoles of the primary sporogenous cell (Figs. 3, 6) are lacking in the megasporocyte (Figs. 9, 12).

(F) Products of Meiosis

The first meiotic division of the megasporocyte results in the production of the two daughter cells that are approximately equal in size. Often the micropylar dyad cell degenerates prior to the onset of meiosis II (Fig. 13) resulting in a triad of meiotic cells at the completion of meiosis (Fig. 14). The triad is composed of the degenerate micropylar dyad cell and two megaspores derived from the second meiotic division of the chalazal dyad cell. The megaspore at the chalazal end of the triad, the functional megaspore, is slightly larger than its micropylar sister cell. A convex cell wall separates the two cells and the nuclei of both chalazal megaspores, unlike the nucleus of the chalazal dyad cell (see Fig. 13), exhibit prominent nucleoli. The transverse wall separating the two chalazal megaspores and the transverse wall between the middle megaspore and the micropylar dyad cell fluoresce when stained with aniline blue and viewed with epifluorescence optics under UV light (Fig. 15). The hypodermal nucellar cells adjacent to the triad enlarge during the meiotic process (Fig. 14). This region of hypodermal nucellar tissue persists intact through the late functional megaspore (Fig. 16) and early 2-nucleate (Fig. 21) stages of megagametophyte development.

(G) Functional Megaspore

The functional megaspore enlarges and assumes an obdeltoid shape (Fig. 16, 17). The prominent nucleolus is retained by the older functional megaspore (Fig. 17) and remains a characteristic feature of haploid megagametophyte nuclei through the course of megagametogenesis (Figs. 21, 28, 34, 43). The population of ribosomes is greater than in the megasporocyte but there is a reduced number of plastids in the functional megaspore (Fig. 17) as compared to the prophase megasporocyte (Figs. 12). The functional megaspore plastid is relatively undifferentiated with an electron-transparent, starch-free stroma and poorly developed thylakoid lamellae (Fig. 17). The mitochondria are small (0.5 - 1.0 um) and spherical with an electron-transparent matrix and poorly developed cristae. The mitochondria of the adjacent nucellar epidermis are larger and appear similar to those found in the nucellus at the primary sporogenous (Fig. 6) and megasporocyte (Fig. 9) stages of development. Membrane-bound inclusions, characteristic of the megasporocyte are not present in the functional megaspore (Fig. 17). The numbers of lipid bodies are reduced while the ER and dictyosome profiles are similar to those of the megasporocyte. A vacuole containing membranous and non-membranous cellular inclusions is present in the micropylar region of the cell.

(H) Two-nucleate Megagametophyte

A mitotic division in the functional megaspore produces the 2-nucleate megagametophyte. Figure 21 illustrates a young 2-nucleate megagametophyte that exhibits the same obdeltoid shape as the older functional megaspore in figure 16. The young megagametophyte contains

two centrally located juxtaposed nuclei and numerous, small parietally located vacuoles (Fig. 21). Micropylar to the megagametophyte are two of three non-functional megaspores (the third megaspore is out of the plane of section) and the enlarged hypodermal nucellar cells. The cytoplasm of the non-functional megaspores has degenerated, shows plasmolysis and stains intensely with cationic dyes.

Plastids are perinuclear, contain no starch deposits and are associated with both nuclei (Fig. 22). The number of plastids is greater than at the early megaspore stage and there is evidence of plastid replication. Mitochondria are distributed throughout the cell and are similar to those found in the functional megaspore, but more numerous. Small vacuoles are present in the extreme micropylar and chalazal regions of the cell. The mid-internuclear region is relatively free of organelles and contains numerous microtubules oriented parallel to the long axis of the cell (Fig. 23). Random dictyosome vesicles are associated with these microtubules.

The appearance of an enlarged central vacuole coincides with the micropylar growth of the 2-nucleate megagametophyte (Fig. 20). The enlarging megagametophyte fills the space once occupied by the hypodermal layer of nucellar cells and the degenerate megaspores. The micropylar nucellar epidermis is intact. The intensely stained, cresent shaped region of degenerate tissue, lateral to the mid-region of the megagametophyte, represents remnants of the degenerate megaspores and the lateral, hypodermal nucellar cells. These crescent-shaped regions are retained through megagametogenesis (Fig. 25) and are still present with the mature megagametophyte (Fig. 55), though the basiophilic contents are no longer present. Prior to the

initial expansion of the megagametophyte during the late 2-nucleate stage, the nucellus is completely enveloped by the inner and outer integuments (Fig. 21).

Figure 24 represents a 2-nucleate megagametophyte that is cytologically similar to the 2-nucleate megagametophytes in Figures 21 and 22 except for a greater number of lipid bodies and the presence of a small central vacuole between the two nuclei. However, the position of the young 2-nucleate megagametophyte at the extreme micropylar apex of the nucellus, immediately hypodermal to the nucellar epidermis, is not typical for this stage of development. Serial sectioning shows that the usual two or three remnant cells of meiosis, micropylar to the megagametophyte (Fig. 21), are not present. Further, the remainder of the ovule was atypical for this stage of megagametophyte development and resembled an older ovule at the 4-nucleate stage, in terms of size and integument morphology (Fig. 19). The hypodermal position of the young megagmetophyte, prior to its expansion, and the lack of meiotic products suggests that these plants may be diplosporous. If certain individuals within a population of Brassica campestris are in fact diplosporous, it is not known whether the diploid megagametophytes reach functional maturity. These ovule-types will be the subject of a future investigation.

(I) Four-nucleate Megagametophyte

A second free nuclear division produces the 4-nucleate megagametophyte. Figure 26 is an overview of the ovule at this stage of development. The sigmoid ovule is oriented with its longitudinal axis perpendicular to the long axis of the ovary. At about this stage of development the ovule turns and becomes re-oriented within the

loculus of the ovary, such that the long axis of the ovule is now parallel to the long axis of the ovary, with the micropyle directed toward the stigma and the style (Fig.111). The ovule (Ov), in the adjacent loculus of the ovary in figure 26 represents a cross-sectional view of the inner and outer integuments due to the re-orientation of the ovule within the ovary. There is continued micropylar expansion of the megagametophyte at the expense of the micropylar and lateral nucellar epidermis such that the megagametophyte in these regions comes in direct contact with the epidermis of the inner integument (Fig. 25). The outer tangential wall of the inner integument possesses a relatively thick, osmiophilic electron-opaque cuticle. Thin anticlinal walls of the lateral inner integument epidermis suggest the occurrence of anticlinal cell divisions within this tissue concurrent with the expansion of the megagametophyte. The inner integument cells adjacent to the micropylar region of the megagametophyte possess thick cell walls characteristic of non-dividing cells. During the 4-nucleate stage of development large amounts of starch accumulate within amyloplasts, primarily in the cells of the inner integument lateral and micropylar to the megagametophyte (Fig. 25). The starch grains are PAS-positive (Fig. 26). The presence of amyloplasts in these regions of the inner integument and later in the corresponding regions of the outer integument continues through megagametogenesis (Figs.38, 43, 52) and is a distinctive feature of the mature ovule at anthesis (Figs. 53 , 55, 104). Beginning at the 4-nucleate stage of development, cells of the inner integument epidermis, adjacent to the micropylar portion of the megagametophyte, divide periclinally to produce two sister cells

of equal size (Figs. 28, 29). The inner derivative, adjacent to the megagametophyte, exhibits an more electron-opaque cytoplasm. By the early cellular stages of megagametophyte development, the number of periclinal divisions of the inner integument epidermis, adjacent to the egg apparatus, has increased and many of the inner derivatives show signs of degeneration (Fig. 43).

The early 4-nucleate megagametophyte contains pairs of sister nuclei in close juxtaposition at both the micropylar (Fig. 27) and chalazal ends of the megagametophyte separated by a large central vacuole (Fig. 25). Smaller vacuoles were distributed throughout the cytoplasm around the nuclei(Fig. 27). There was no evidence of internuclear microtubules. The cytoplasm of the micropylar and chalazal ends of the 4-nucleate megagametophyte is similar. Plastids are more numerous but morphologically similar and in the same perinuclear location (Fig.27) as those found in the 2-nucleate megagametophyte (Fig. 22). Replication of mitochondria is evident (Fig. 27) and the morphology of the organelle is now similar to the mitochondria of the adjacent inner integument cells. OsFeCN staining reveals numerous short strands of ER distributed throughout the cytoplasm with connections to the nuclear envelope (Fig. 27). Dictyosomes, active in vesicle production, are mainly located in the peripheral regions, adjacent to the megagametophyte wall.

At the chalazal end of the older 4-nucleate megagametophyte, the sister nuclei become separated by a large vacuole (Fig. 28). Lipid bodies are more prevalent in both the micropylar (Fig. 29) and chalazal (Fig. 28) ends of the megagametophyte. There is a significant increase in the number of dictyosomes in the micropylar (Fig. 31),

chalazal (Fig. 33) and lateral (Fig. 30) cytoplasm of the older 4-nucleate megagametophyte. Some of dictyosome vesicles appear to be fusing with the wall of the megagametophyte and helical polysomes are present in the parietal cytoplasm, between the megagametophyte wall and the central vacuole (Fig. 30). At the 4-nucleate stage of development, irregularly shaped, membrane-bound vesicles containing tubular inclusions are often seen in close proximity to the megagametophyte wall (Fig. 32). Serial sections show the plasma membrane of the megagametophyte wall to be continuous with the bounding membrane of the vesicle containing the tubular inclusions (Fig. 33). Plasmodesmata are occasionally found interconnecting the chalazal regions of the megagametophyte with the nucellus (Fig. 32).

(J) Eight-nucleate Megagametophyte

A third mitotic division produces the 8-nucleate megagametophyte, ultimately composed of three antipodal cells, a central cell containing two polar nuclei, and an egg apparatus consisting of two synergids and an egg. Figures 34, 35, 36, 37 represent non-adjacent serial sections through the youngest 8-nucleate megagametophyte observed in this study. Three small (5um x 6um) elliptical antipodal nuclei occupy the chalazal end of the megagametophyte. Two of the antipodal nuclei are in close juxtaposition and occupy the extreme chalazal end of the megagametophyte (Fig. 34). The third antipodal nucleus is in a slightly more micropylar position (Fig. 35). The spherical nuclei of the egg apparatus are located in the extreme micropylar end of the megagametophyte and are slightly larger (8 um) than the antipodal nuclei. The two synergid nuclei (Figs. 34, 37) are in juxtaposition, although, due to the plane of sectioning, this fact

is not evident in either micrograph. The egg (Fig. 36) is slightly chalazal and lateral to the synergids and contains perinuclear plastids. The two polar nuclei are the largest nuclei (9 um) in the megagametophyte. Both polar nuclei are situated on the same side of the megagametophyte central cell, one near the antipodals (Fig. 34), the other near the egg apparatus (Fig. 35). The nuclei are separated by a distance of approximately 20 um. The majority of the central cell is occupied by vacuole.

When stained with crystal violet (Figs. 34, 35, 36, 37) or crystal violet-PAS (Fig. 38) and viewed with conventional brightfield optics it is difficult to determine if the antipodals and egg apparatus of the young 8-nucleate megagametophyte are free-nuclear or cellular. A faint boundary appears to separate one of the synergids from the egg and central cell in figure 36. However, the megagametophyte from an adjacent section, showing the other synergid, two of the antipodals, and the polars (Fig. 38), appears to be free-nuclear. When this section was viewed with differential interference contrast optics (Fig. 39), a definite partitioning of the antipodal and egg apparatus cytoplasms is evident, suggesting the presence of a cell wall. A common wall separates the juxtaposed antipodal nuclei and a convexly curved wall separates the antipodals from the central cell. The antipodals at this early stage of development are approximately 15 um long. The cell wall separating the synergid from the central cell is convexly curved and extends from the lateral to the central to micropylar end of the megagametophyte. The point of attachment of the common synergid-central cell wall to the

lateral edge of the megagametophyte is approximately 20 um from the extreme micropylar end of the synergid cell.

In an older megagametophyte the common cell walls of the synergid-central cell, egg-central cell, and synergid-egg are PAS-positive (Fig. 41). In a slightly younger megagametophyte the egg-central cell wall, the egg-synergid wall and the synergid-central cell wall nearest the lateral edge of the megagametophyte stain orthochromatically with crystal violet, while the more centripetal regions of these walls remain unstained (Fig. 40).

The common synergid-central cell wall of the older megagametophyte in figure 41, extends laterally from the edge of the megagametophyte and then chalazally forming what is termed the synergid hook. This synergid hook, located 20 um from the micropylar end of the synergid is also evident in the younger megagametophye in figure 40. Both of these young synergids were approximately 25 um long. Continued chalazal expansion of the synergid into the central cell results in a pronounced sigmoid synergid hook region in slightly older pre-anthesis megagametophytes (Figs. 43, 47), which is evident at both the light and electron microscope levels in older megagametophytes at anthesis (Figs. 78, 83), at post-anthesis (Figs. 101, 135) and is present in the persistent and degenerate synergid (Fig. 118, 119) following fertilization. In all of these older megagametophytes the distance from the synergid hook to the micropylar end of the synergid is approximately 20 um.

Similar to the synergid, the lateral extension of the young egg cell (Fig. 40) followed by a chalazal expansion of the egg into the central cell produces an egg hook region (Fig. 41). The egg hook is

also evident in mature megagametophytes at anthesis (Fig. 78, 83), at post-anthesis, and is present in the zygote (Fig. 121). The common wall between the antipodals and the central cell produces an antipodal hook region (Fig. 43) which remains rudimentary due to the absence of cell expansion by the antipodal cells during the later stages of megagametogenesis.

At the ultrastructural level, the common cell wall between the synergid and egg, extending from the lateral wall of the young cellular megagametophyte toward the central cell, is of relatively even thickness, while the more centripetal regions of the wall are of variable thickness and have a beaded appearance (Fig. 42). In this centripetal region the wall often appears discontinuous and difficult to discern. Strands of both egg and synergid ER follow the contours of the common cell wall with some cisternae appressed to the egg and synergid plasma membranes. Dictyosomes, active in vesicle production, are visible in the synergid cell cytoplasm. However, the number of dictyosomes present is appreciably less than in the older 4-nucleate stage of megagametophyte development (Fig. 31). Microtubules are present in the vacuolar region of the synergid, between the egg and synergid nuclei (Fig. 42).

In slightly older megagametophytes, the cell walls of the antipodals (Fig. 46), the synergids (Figs. 47, 48), and the egg (Fig.48) are more regular and the electron-transparent region between the common wall plasma membranes is wider. Plasmodesmata are a common occurrence. They are most abundant in the antipodal cells and traverse the cell walls between antipodal cells (Fig. 44, 46), between the antipodals and the central cell, and between the antipodals and the

nucellus (Fig. 46). Plasmodesmata also traverse the common walls between synergids (Fig.45), synergid and central cell (Fig. 47), egg and synergid, and the egg central cell particularly in the region of the egg hook (Fig. 78). Plasmodesmata were not observed between the inner integument and the egg, or between the inner integument and the synergid.

Cytologically the antipodals (Fig. 46), synergids (Figs. 47, 48), egg (Fig. 48) and central cell (Fig. 48, 51) of the young cellular megagametophyte are very similar. The similarity in the composition and distribution of organelles in the cells of the egg apparatus and the central cell in the young pre-anthesis megagametophyte is evident in figure 48. Small vacuoles are present in the young egg, synergid (Figs. 36, 41) and antipodal (Fig 38) cells. A distinctive feature of all megagametophyte cells at this stage of development is the pleiomorphic plastids that range in shape from spherical to elliptical to allantoid. The allantoid plastid is up to 6 um long by 0.5 um wide (Fig. 47, 51). Serial sections reveal that some of the spherical and elliptical plastids are allantoid plastids in transverse view. The plastid stroma is electron-opaque with weakly developed thylakoid lamellae and is generally free of starch. Like the plastids, the mitochondria of the young cellular megagametophyte range from spherical to elliptical to allantoid (Figs. 47, 48, 51). Mitochondrial cristae are well developed. Lipid bodies (Fig. 43), dictyosomes and short strands of ER are distributed throughout the cytoplasms of the egg, synergids, and antipodals (Figs. 46, 47, 48). The cytoplasm of the central cell occupies a thin band between the large central vacuole and the cells of the egg apparatus, the antipodals, and the

lateral edges of the megagametophyte (Fig.43). The greatest abundance of organelles occurs in the immediate vicinity of the two polar nuclei located in the micropylar and chalazal regions of the central cell (Figs. 43, 51). In older pre-anthesis megagametophytes, projections begin to form on the lateral wall of the megagametophyte central cell in the region of the synergid hook (Fig. 48). There are numerous dictyosomes, active in vesicle production, in the immediate vicinity of the developing wall projections.

Following the cellularization of the megagametophyte, the two polar nuclei migrate to the mid-region of the central cell. In figure 43 the micropylar polar nucleus lies immediately adjacent the chalazal tip of one of the synergids while the chalazal polar nucleus is located in the mid-chalazal region of the central cell. Figure 49 shows the spatial relationship of the chalazal polar nucleus to the antipodals. Microtubules parallel to the long axis of the central cell are positioned in the central cell cytoplasm lateral and adjacent to the chalazal polar nucleus (Figs. 50, 51). Spiral polysomes appear to be associated with the nuclear envelope (Fig. 51). There are no apparent microtubules associated with the micropylar polar nucleus. In figure 52 two juxtaposed polar nuclei are located in the centre of the vacuolate central cell cytoplasm, surrounded by PAS-positive starch grains.

Except for megagametophyte differences, the external and internal morphologies of the ovule at the earliest cellular stage of development (Fig. 34) areyvry almost identical to the ovule following the completion of the migration of the polar nuclei (Fig. 52).

II. MATURE OVULE

(A) Central Cell

The mature central cell, at anthesis, is devoid of the large central vacuoles characteristic of the coenocytic and early cellular stages of megagametophyte development. The central cell is composed of a heterogeneous cytoplasm extending from the egg apparatus to the antipodals (Fig. 53). A small vacuolate region remains at the chalazal end of the central cell adjacent to the antipodals (Figs. 53, 71).

A distinctive feature of the mature megagametophyte was the presence of wall projections associated with the lateral walls of the central cell, adjacent to the inner integument. A transverse section of the megagametophyte, in the mid-region of the egg apparatus, shows wall projections circumscribing the circumference of the central cell (Fig. 79). The wall projections extend, in the longitudinal plane, from the mid-region of the lateral central cell wall, opposite the polar nuclei (Figs. 63, 66), to the synergid and egg hook region of the central cell (Figs. 78, 101). The distribution of wall projections corresponds with the region of starch distribution in the integuments (Figs. 55, 56). The wall projections are difficult to distinguish at the level of the light microscope where they appear as an indistinct hazy layer adjacent to the lateral wall of the central cell (Figs. 55, 98). When stained with Calcofluor and viewed with epifluorescence optics under UV light, the wall projections exhibit a positive but weak fluorescense (Fig. 99). Ultrastructurally, the projections appear as branched pegs often showing a labyrinth appearance (Fig. 56). The tripartite plasma membrane of the central cell follows the contours of the wall projections (Fig. 58). The wall projections contain numerous

electron-opaque deposits embedded in a fibrillar matrix (Fig. 57). Occasionally, aggregations of tubules occur in regions of the wall projections corresponding to electron-opaque deposits (Fig. 58). Presumably these tubules were deposited or became entrapped during the synthesis of the wall projections. The electron-opaque deposits may represent remnants of degenerate tubules. An osmiophilic, electron-opaque layer occurs as a more or less continuous boundary between the central cell, including the wall projections, and the inner integument (Figs.56, 57, 58). This boundary is continuous with the electron-opaque cuticle of the inner integument epidermis in the chalazal regions of the ovule lateral to the antipodals and the chalazal nucellus (Fig. 77). There are gaps in the cuticular layer particularly in the micropylar region of the megagametophyte (Figs. 58, 60). A transverse section of the central cell, stained with the Thiery PA-TCH-SP method to localize total insoluble carbohydrate, resulted in an even distribution of silver proteinate over the wall projections (Fig. 59). The distribution of silver proteinate over the adjacent inner integument wall exhibits a fibrillar pattern.

Central cell dictyosomes, adjacent to regions of wall projection formation, show silver proteinate deposits in the vesicles being released from the maturing face (Fig. 61). Control sections in which water was substituted for periodic acid show no deposition of silver proteinate over the inner integument wall or the wall projections (Fig 60) or within the dictyosome vesicles (Fig. 62).

The two juxtaposed polar nuclei of the mature megagametophyte are typically located in the micropylar central cell cytoplasm, adjacent to the egg apparatus (Fig.55). At the ultrastructural level the polar

nuclei, just prior to anthesis, exhibit slight undulations in the nuclear envelope (Fig. 63). Mitochondria, small vacuoles, lipid bodies,

and long strands of ER lie between the two flat and appressed surfaces of the polar nuclei. Serial sectioning revealed that partial fusion of the two polar nuclei had occurred prior to anthesis, most probably shortly after nuclear migration during the young cellular stage of megagametophyte development (Fig. 52). The union consists of a number of narrow nuclear bridges where a continuity of nuclear envelopes and nucleoplasms has been established between the two polar nuclei (Fig. 64). Strands of RER, located between the appressed faces of the polar nuclei, are connected to the outer nuclear envelope. Connections between ER and the nuclear envelope of the non-appressed faces of the polar nuclei were much less frequent.

Following anthesis the polar nuclei appear more labile and contorted with numerous invaginations and evaginations of the nuclear envelope (Fig. 66). Wide cytoplasmic embayments, containing organelles, occur between the polar nuclei. OsFeCN staining shows the distribution of central cell ER. Following anthesis, the amount of internuclear ER increases (Fig. 66) and this internuclear ER remains attached to the outer membrane of the nuclear envelope (Fig. 65). Some of the internuclear ER is aggregated into a compact symmetrical array of tubular cisternae. Both surface and section views of the cisternae are present in figure 65, allowing a three dimensional interpretation of the aggregate. In surface view the tubular ER appears as stellately branched cisternae radiating around a circular perforation. In section view, the near perfect alignment of 22 of the stellate cisternae

results in a straight cylindrical channel between the flat tubular cisternae. The purpose of this symmetrical array of ER cisternae is unclear.

The polar nuclei of unfertilized megagametophytes never fuse to a form a single fusion nucleus, but remain interconnected by nuclear bridges and ER.

The remaining ER of the OsFeCN-stained central cell is distributed throughout the micropylar half of the cell from the chalazal region of the polar nuclei to the egg apparatus (Fig. 66). Much of the central cell ER is lamellate with spiral polysomes occurring on the flattened membrane surface of the cisternae (Fig. 70). Along the lateral wall of the central cell, multiple strands of the ER are associated with the central cell wall projections. Large numbers of branched ER cisternae are associated with the common egg-central cell wall (Fig. 67). The ER of the adjacent egg cell is not stained by the OsFeCN treatment. Both rough and smooth ER are present near the egg-central cell boundary (Fig. 68) and in some sections a definite continuity exists between the central cell plasma membrane, adjacent to the egg cell and the smooth tubular ER of the central cell. The tripartite plasma membranes of the egg and central cell are similar to the tripartite membrane of the ER cisternae.

Prior to anthesis, central cell plastids changed from the proplastid type, characteristic of the coenocytic and early cellular megagametophyte, to elliptical chloroplasts with stacked thylakoid lamellae (Fig. 63). The electron-transparent regions within the chloroplast stroma are presumed to be starch. There are PAS-positive grains within the plastids (Fig. 55) and chloroplasts within the

central cell are distributed primarily in the region of the polar nuclei (Figs. 55, 63, 66, 84) and the synergid hook region of the egg apparatus (Fig. 101).

Mitochondria are distributed throughout the central cell, but are most abundant in the synergid and egg hook regions of the central cell, adjacent to the wall projections (Figs. 69, 78, 79). Many of the mitochondria in the latter regions are pleiomorphic. The shape of the mitochondria is often amoeboid with portions of the organelle wrapping around pegs of wall projection material (Fig. 69). The tubular cristae are well developed and nucleoid regions containing fine stands of DNA are visible in the matrix (Fig. 57).

Lipid bodies are distributed throughout the central cell (Figs. 66, 67) and electron-opaque microbodies (Figs. 63, 67, 70), which were rare in the central cell at the young cellular stage of development, are abundant in the central cell cytoplasm at anthesis. In certain sections the unit membrane of the microbody is appressed to the edge of the lipid body (Fig. 70). The central cell in figure 70 was fixed by the OsFeCN method. The ER cisternae of the central cell are unstained while the cisternae of the dictyosomes contain electron-opaque deposits. The nucleoid regions of the mitochondria appear electron-transparent after OsFeCN fixation.

(B) Antipodal Cells

The three antipodal cells, at anthesis, are slightly smaller than they were following the initial cellularization of the megagametophyte (Fig 46) with the majority of the cell volume occupied by the nucleus (Figs. 71, 74). The shape of the antipodal cell is conical to obdeltoid and the three cells are in a triangular configuration at the

extreme chalazal end of the megagametophyte (Fig. 71). Because of the triangular arrangement, the antipodals share common walls with each other and with the central cell and the chalazal nucellus. The electron-transparent walls of the mature antipodals have a wrinkled appearance. Plasmodesmata are still common between antipodal cells and between the antipodal and central cells (Fig. 73), but were not observed between the antipodals and the nucellus. The common antipodal-central cell wall is somewhat irregular with numerous evaginations of wall material on both the central cell and antipodal cell side of the wall. When stained by Thiery PA-TCH-SP method, silver proteinate is distributed over the entire wall including the evaginated regions (Fig. 75). The small vesicles at the maturing face of the antipodal dictyosomes are free of silver proteinate deposits. The control section, in which water is substituted for periodic acid, is an adjacent serial section and shows no deposits of silver proteinate over the antipodal cell wall, evaginated regions, or antipodal dictyosome vesicles (Fig. 76).

To detect beta 1,4 glucans, the antipodal cells were stained with Calcofluor and viewed with fluorescence optics under UV light. All antipodal cell walls show an intense pale blue flourescence (Fig. 72).

OsFeCN staining reveals an increase in the amount of antipodal cell ER immediately prior to anthesis (Fig. 74). The ER of the adjacent central cell cytoplasm did not react to the OsFeCN stain. The ER of the antipodal cell is predominantly rough, while that of the adjacent central cell region is predominantly smooth (Fig. 73).

Mitochondria with tubular cristae and dictyosomes are distributed throughout the non-vacuolate antipodal cell cytoplasm (Fig. 74).

At anthesis, the plastids of the antipodals, unlike the adjacent central cell, maintain the proplastid morphology (Fig. 74). Except for the absence of the allantoid shape, the starchless proplastid of the mature antipodal is similar to the proplastid of the young cellular megagametophyte (Fig. 46).

The antipodals are ephemeral cells. Along with the chalazal nucellus (Fig. 104), the antipodals show signs of degeneration soon after anthesis. Figure 77 shows a portion of two antipodal cells that were fixed four hours after anthesis. Some of the ER has become dilated and there are ER-derived, double membrane-bound inclusions, similar to those in the prophase megasporocyte cell (Fig. 11), enclosing regions of antipodal cytoplasm, as well as plastids. Dictyosomes are rare in the degenerating antipodal cell.

(C) Egg Apparatus - Position

The egg apparatus is composed of three cells in a triangular arrangement, the egg and two synergids, each 40-45 um long at maturity (Figs. 78, 83, 84). The egg is pyriform and attached to the lateral megagametophyte wall approximately 10 um from the extreme micropylar end of the megagametophyte (Fig. 78). Since the cells of the egg apparatus are of approximately the same length, the chalazal portion of the egg extends beyond the chalazal portion of the synergids (Figs. 78, 83, 84, 98, 101). The contiguous wall between the egg and the lateral region of the megagametophyte extends for less than 10 um to the point where the common egg-central cell wall extends into the

central cell forming the egg hook. The distance from the egg hook to the extreme chalazal tip of the egg is between 30 and 35 um.

The synergids are pyriform to ovoid with the proximal portion of each synergid located in the extreme micropylar end of the megagametophyte (Figs. 78, 83, 84), adjacent to the inner integument micropyle (Figs. 101, 115). The contiguous wall between the synergid and the lateral region of the megagametophyte extends nearly 20 um, from the extreme micropylar end of the megagametophyte to a point where the common synergid-central cell wall extends into the central cell cytoplasm forming the synergid hook (Fig. 78, 83, 84). The distance from the synergid hook to the extreme chalazal tip of the synergid ranges from 20 to 25 um.

Figure 80, at the light microscope level and figure 79, at the ultrastructural level, represent transverse sections through the same egg apparatus at the level of the synergid nuclei, immediately chalazal to the synergid and egg hook regions of the megagametophyte (for a corresponding longitudinal orientation, see figure 78). In transverse view, each synergid is oblong to elliptical with a long axis of 20 um and a short axis of 10 um. The 12 o'clock - 6 o'clock axis in figure 80 is the adaxial-abaxial sagittal plane of the mature ovule. Thus, using the common wall between the two synergids as a reference line, the two synergids are situated in the megagametophyte at an angle of 45 degrees to the sagittal plane of the ovule. A portion of the egg is in the lower right quadrant of figure 80 which corresponds to the abaxial or funicular side of the megagametophyte. Figures 78 and 83 illustrate egg cells and figure 123 a zygote positioned on the abaxial side of the megagametophyte, nearest the

funiculus. Adaxially located eggs, on the side of the megagametophyte directed away from the funiculus also occur (Fig. 53, 104), illustrating the variation of position of the egg apparatus within the micropylar portion of the megagametophyte.

(D) Egg Apparatus - Cell Walls

There is a common cell wall between the two synergid cells, between the two synergids and the egg and between all three cells of the egg apparatus and the central cell. The morphology of the cell wall between contiguous cells of the mature egg apparatus, at anthesis, lacks the uniformity of the cell walls of the young egg apparatus shortly after the completion of megagametophyte cellularization (Fig. 48).

The common synergid-synergid wall is thickest in the micropylar region of the megagametophyte where it is contiguous with the digitate filiform apparatus of each synergid (Fig. 84, 86, 91, 92). A wall of similar morphology separates the egg from the central cell in the egg hook region, the synergid from the central cell in the synergid hook region, and each synergid from the egg in the micropylar regions of these cells (Fig. 78). These common walls consist of an electron-transparent region separated by two plasma membranes. The more chalazal region of the common egg-synergid and synergid-central cell wall is composed of, for the most part, two appressed plasma membranes (Fig. 69, 78, 97). At the level of the light microscope, common walls of the egg apparatus are PAS-positive (Fig.84). The reaction of the contiguous chalazal walls between the egg and synergids to the PAS stain is detectable but weak. Similarly, all walls of the egg apparatus show intercellular deposits of silver

proteinate when stained by the Thiery PA-TCH-SP method (Figs. 87, 89, 91, 95). Controls, where water was substituted for periodic acid, showed no deposition of silver proteinate in the intercellular cell wall regions (Fig. 88, 90, 92, 96).

The common wall between the egg and central cell, is unique within the mature megagametophyte. Beyond the egg hook region, the contiguous egg-central cell wall consists of expanded intercellular regions containing electron-opaque deposits surrounding a more fibrillar matrix (Fig. 78, 79, 101). The expanded regions of egg-central cell wall material are not continuous, but typically alternate with narrow regions consisting of two appressed plasma membranes (Fig. 68). The ultrastructural morphology of the electron-opaque region varies from diffuse (Fig. 69), to elliptical (Fig. 97), to regular deposits between parallel plasma membranes (Fig. 100). These electron-opaque deposits stain orthochromatically with crystal violet (Fig. 83). When stained by the Thiery PA-TCH-SP method, deposits of silver proteinate are found over the entire intercellular region of the common egg-central cell wall, including the regions of electron-opaque material (Fig. 95). Control sections in which water was substituted for silver proteinate, showed no silver proteinate deposits over the intercellular regions of the common egg-central cell wall (Fig. 96)

To detect beta-1,4-linked glucans, the cells of the egg apparatus were stained with Calcofluor and viewed under UV light. A weak, pale blue fluorescence could only be detected in the more micropylar regions of the egg apparatus including the common synergid-synergid wall, the common walls in the regions of the egg and synergid hook,

and in obliquely sectioned walls between the egg and synergids (Figs. 99, 115). There was no detectable fluorescence in the chalazal walls between the synergid and the egg or between the egg-central cell.

(E) Egg

At anthesis, the egg nucleus and the majority of the egg cytoplasm are located in the turbinate chalazal region of the cell (Figs. 83, 78) with the micropylar two-thirds of the cell occupied by vacuole (Fig. 104). Plastids are of the proplastid type with weakly developed thylakoid lamellae, an electron-opaque stroma and electron-transparent regions, presumed to be starch (Fig 97). Thiery PA-TCH-SP staining shows silver proteinate deposits over the electron-transparent region of the proplastid stroma (Fig. 95). The control section, where water is substituted for periodic acid, shows little deposition of silver proteinate over this region (Fig. 90). The plastids are located in the micropylar region of the egg (Fig. 78), in the middle region of the egg adjacent to the large central vacuole (Fig 78,79), but are most abundant in the perinuclear chalazal region of the egg cell (Fig. 78, 84). Mitochondria are somewhat more numerous than plastids but exhibit a similar distribution with the largest numbers of mitochondria being perinuclear (Figs. 78, 100). ER is not well developed in the mature egg with only a few short strands of ER cisternae present in the cytoplasm (Figs. 67, 97). At no stage of development did ER cisternae of the unfertilized egg react positively to OsFeCN staining. Lipid bodies are large, few in number, and mainly located within the large egg vacuole or in the micropylar region of the egg cell (Fig. 78). Dictyosomes are composed of 5-7 flattened cisternae that are relatively inactive in vesicle production

(Fig. 100). When stained by the Thiery PA-TCH-SP method, there are no silver proteinate deposits within the small vesicles of the dictyosome (Fig. 89) or in the dictyosome vesicles of the control where water was substituted for silver proteinate (Fig. 90).

(F) Synergids

The synergid nuclei, at anthesis (Figs. 78, 83, 84), are morphologically the same as in the young cellular megagametophyte (Fig. 47), though in a slightly more chalazal position. The synergid nuclei remain in close juxtaposition separated by a cell wall (Fig. 80). Except for the absence of the allantoid shape, the proplastids of the young synergid (Fig. 47) are similar to the proplastids of the mature synergid at anthesis (Figs. 78, 79). The distribution of plastids in the mature synergid is primarily perinuclear. Electron-transparent regions within some synergid proplastids (Fig. 79) are assumed to be starch. When stained by the Thiery PA-TCH-SP method a central region of silver proteinate deposition, surrounded by an electron-transparent region, is apparent (Fig. 87). The control section, in which water was substituted for periodic acid, is virtually free of silver proteinate deposits (Fig. 88).

Irregularly shaped vacuoles occur in the micropylar (Fig. 78), middle (Fig. 79), and extreme chalazal regions (Fig. 78) of the mature synergid. Vacuoles never become a predominant component of the mature synergid cell. Unlike the young synergid cell (Fig. 47), the amount of stored lipid is markedly reduced in the mature synergid while the number of microbodies present in the perinuclear cytoplasm has increased (Fig. 79). The microbodies do not appear to be associated with a particular organelle.

The mature synergid, when compared with the young synergid (Fig. 47), contains more mitochondria, RER, and dictyosomes (Fig. 78, 79, 82). The mitochondria are spherical to elliptical with well defined tubular cristae (Fig. 82) and are distributed throughout the mature synergid cell cytoplasm (Fig. 78).

There is an extensive network of RER from the micropylar to the mid-chalazal regions of the synergid cell. Strands of RER encircle the synergid nucleus (Fig. 78). Immediately chalazal to the nucleus, in a region adjacent to the common synergid-synergid cell wall, the RER exhibits an unusually regular arrangement of parallel cisternae intermixed with chloroplasts, mitochondria, and active dictyosomes (Figs. 79, 82). Smooth ER is also present but much less frequent. In comparison to the RER cisternae, those of the smooth ER are narrow but become increasingly dilated in certain regions forming irregular electron-transparent vacuoles (Fig. 82). Smooth ER cisternae are also frequently found appressed to the chalazal synergid plasma membrane of the common synergid-egg wall (Fig. 101) and to the plasma membrane of the common synergid-synergid wall (Fig. 82).

Dictyosomes, active in vesicle production, are a prominent component of the mature synergid cytoplasm (Figs. 78, 79, 82). The distribution of dictyosomes is from the micropylar to the chalazal end of the cell, with the greatest number occurring in the perinuclear region and to a lesser extent the micropylar region of the cell (Fig. 78). Each dictyosome is composed of 5-6 flattened cisternae with distinct forming (cis) and maturing (trans) faces (Fig. 81). The unit membrane of the individual cisterna is tripartite and there is an increase in the electron-opacity of the cisternae from the forming to

the maturing face of the dictyosome. Expanded vesicles with a tripartite unit membrane are associated with peripheral regions of the maturing face and exhibit a fibrillar content when stained with UA/Pb. Often there is a close spatial relationship between the forming face of the dictyosome and adjacent cisternae of ER (Fig. 82) with transition vesicles occurring between the two organelles (Fig. 81). At the level of the light microscope, dictyosomes are seen as small basiophilic discs when stained with crystal violet (Fig. 83).

Mature synergids, at anthesis, were stained by the Thiery PA-TCH-SP method. Dictyosomes from the micropylar (Figs. 91, 93) middle (Fig. 87) and chalazal (Fig. 89) regions of the synergid showed silver proteinate deposits within the vesicles at the maturing face of the organelle while the vesicles at the forming face of dictyosomes sectioned in the appropriate plane, showed an absence of silver proteinate deposits (Figs. 87, 89, 91). Controls, in which periodic acid was replaced by water, showed no silver proteinate deposition within any of the dictyosome vesicles (Figs. 88, 90, 92, 94).

The most distinctive feature of the micropylar end of the mature synergid is the filiform apparatus, an extensive labyrinth of wall material with digitate projections extending deep into the synergid cell cytoplasm (Figs. 85, 86). The filiform apparatus consists of a core of electron-opaque material surrounded by a peripheral electron-transparent zone adjacent to the synergid cell cytoplasm. The cytoplasm adjacent to the digitate projections contains mainly ER, mitochondria, and dictyosomes active in vesicle production (Figs. 86, 91). When stained by the Thiery PA-TCH-SP method, there are deposits of silver proteinate over the entire filiform apparatus, with the

central zone of the digitate wall staining more intensely than the peripheral zone immediately adjacent to the cytoplasm (Figs. 91, 93). A plasma membrane, which follows the contours of the digitate projections, is also stained by the Thiery method as are numerous vesicles being released from the maturing face of dictyosomes. Spherical bodies, similar to dictyosome vesicles in size, morphology, and Thiery staining intensity, appear to be fusing with the peripheral regions of the filiform apparatus (Fig. 93). Narrow, finger-like projections of the filiform apparatus extend deep into the central region of the synergid near the nucleus, and are stained positively by the Thiery PA-TCH-SP method (Fig. 87). Control sections, where periodic acid is replaced by water, show a virtual absence of silver proteinate over the entire filiform apparatus as well as the dictyosome vesicles, and the dictyosome-like vesicles fusing to the peripheral walls (Figs. 94).

At anthesis, the filiform apparatus is PAS-positive (Fig. 84), and shows an intense pale blue fluorescence when stained with Calcofluor and viewed with fluorescence optics under UV light (Figs. 99, 115). After cellulase extraction, the filiform apparatus, egg apparatus cell walls and the cell walls of the inner and outer integument no longer fluoresce when stained with calcoflour. When stained with alcian blue GX , the entire filiform apparatus, including the centrally located, narrow, finger-like projections, and a portion of the common synergid-synergid cell wall show a positive reaction for acidic polysaccharides (Fig. 85).

Both synergids, at anthesis, exhibit similar ultrastructural morphologies and UA/Pb staining characteristics (Fig. 79). At the

light microscope level, staining with cationic dyes such as crystal violet (Fig. 80) and aniline blue black for total protein (Fig. 84) reveals a similarity between synergid cytoplasms. One of the two synergids, from ovules fixed 24-36 hours after anthesis, shows a more intense basiophilia when stained with crystal violet (Figs. 98, 102). This intensely staining synergid is the incipient degenerate synergid. The second synergid remains intact for some time following anthesis and/or fertilization and is termed the persistent synergid. A fluorescence microscope examination of aniline blue stained stigma-style regions of the pistils from which these ovules were obtained, showed no evidence of pollen tube growth.

Figures 102 and 103 are light and electron micrographs of the same egg apparatus obtained from non-adjacent serial sections. The basiophilic, crystal violet stained synergid in figure 102 (the incipient degenerate synergid) shows a electron-opaque cytosol when stained with UA/Pb (Fig. 103). Organelles such as mitochondria, dictyosomes, and ER show no sign of degeneration.

When treated with OsFeCN, the ER and nuclear envelope of the persistent synergid stain positively while the ER and nuclear envelope of the incipient degenerate synergid show no reaction (Fig. 101). Only the micropylar half of the nuclear envelope and the ER between the nucleus and the filiform apparatus of the persistent synergid (Fig. 86) accumulate electron-opaque deposits.

During the early stages of synergid degeneration there is a marked hypertrophy of the ER network that encircles pockets of cytoplasmic ribosomes (Fig. 106). Bound ribosomes on the surfaces of the electron-opaque ER cisternae exhibit a distinctly beaded

appearance. Mitochondrial profiles are recognizable, though there has been a loss of mitochondrial membrane integrity. Dictyosome cisternae are no longer visible but enlarged vesicles similar to the dictyosome visicles of the intact synergid remain. The contents of these vesicles are fibrillar and a bounding membrane is no longer visible. The degenerate synergid collapses and shrinks markedly, particularly at the chalazal tip (Fig. 104, 105). Following the collapse of the cell, the electron-transparent wall in the hook region of the degenerate synergid takes on an irregular, wrinkled appearance (Fig. 105). The common boundary between the degenerate synergid and the egg (Fig. 105) is virtually the same as the boundary between the intact synergid and the egg at anthesis (Fig. 78) The micropylar portion of the degenerate synergid-egg wall is electron-transparent while the chalazal region at the junction of the degenerate synergid, egg, and central cell is devoid of electron-transparent wall material (Fig. 105), and is non-fluorescent when stained with Calcofluor and viewed with epifluorescence optics under UV light (Fig. 99).

At this post-anthesis stage of ovule development, the megagmetophyte consists of a central cell with two interconnected polar nuclei, three degenerate antipodals, a degenerating chalazal nucellus, and an egg apparatus composed of a vacuolate egg, a persistent synergid, and a degenerate synergid. Figure 104 is an overview of a fertile ovule at the post-anthesis stage of development (The persistent synergid, polar nuclei, and degenerate antipodals are out of the plane of section). At the extreme chalaza of the nucellus a persistent starch-storing region of nucellus does not degenerate but remains intact. This region is the incipient chalazal proliferating

tissue that undergoes further development during the early stages of embryogenesis.

III. FERTILIZED OVULE

(A) Pollen Tube: Stigma to Ovule

The portion of the pistil distal to the ovary is composed of a style and a stigma (Fig. 109). The stigmatic papillae are highly vacuolate, obovate cells with a central nucleus. Between the stigmatic papillae and the style is a narrow stigmatic zone of small isodiametric parenchyma cells. The central core of the style is occupied by the parenchymatous transmitting tissue, which extends through the style from the stigma to the replum of the ovary. Strands of vascular tissue, extending from the ovary to the base of the stigma, are located lateral to the transmitting tissue.

The stigmas of flowers 24 hours from anthesis were dusted with pollen from compatible plants. The pistils of these flowers were 6-7 mm long and the stigma of the pistil was near the level of the four longest stamens of the tetradynamous androecium (Fig. 116). The time from pollination to the initial germination of the pollen tube was between 3 and 3.5 hours. The more vigorous pollen tubes had already penetrated the narrow parenchyma zone of the stigma and entered the transmitting tissue at 5 hours after pollination. Figure 110 is a longitudinal view of the stigma and distal region of the style 5 hours after pollination. The fresh section was stained with aniline blue and viewed with epifluorescence optics under UV light. The callosic walls and plugs of the pollen tubes show a pale blue fluorescence that contrasts with the deep blue autofluorescence of the adjacent stigmatic, transmitting, and vascular tissues. The germinated pollen

tubes do not appear to penetrate the stigmatic papillae but grow along the lateral surface of the papillae before entering the narrow zone of stigmatic parenchyma tissue (Fig. 112). The most vigorous pollen tubes reach the mid-point of the style 6 hours after pollination.

The pollen tubes grow out of the cellular environment of the stylar transmitting tissue into the two loculi of the ovary. Within the ovary, the pollen tubes grow on the surface of the replum (Fig. 111) and first contact the ovule at the more proximal region of the funiculus. The tissue in figure 111 was stained with aniline blue and viewed with epifluorescence optics under blue light. The callosic walls and plugs of the pollen tubes fluoresce yellow in contrast with the red autofluorescence of chlorophyll within the ovule and replum plastids.

Figure 115 shows the outer and inner integument components of the ovule micropyle between the funiculus-outer integument boundary and the base of the synergid filiform apparatus. The pollen tubes grow along the funiculus to the junction of the funiculus and outer integument and enter the ovule by way of the curved outer integument micropyle (Fig. 113) before penetrating the relatively straight inner integument micropyle that terminates at the base of the synergid (Fig. 114). The earliest evidence for the entrance of pollen tubes into the outer integument micropyle occurred between 9.5 and 9.75 hours after pollination under continuous light at 22°C.

Figures 107 and 108 represent non-adjacent serial sections through an ovule fixed 9.5 hours after pollination. The pollen tube had penetrated the outer integument micropyle, but had yet to reach the inner integument micropyle. At this stage, the megagametophyte

consists of two interconnected polar nuclei in a non-vacuolate heterogeneous central cell cytoplasm, an intact persistent synergid, a degenerate synergid, and a vacuolate egg. The egg nucleus has migrated from the extreme chalazal tip location, characteristic of the unpollinated egg following anthesis, to the middle region of the egg cell, immediately adjacent to the common degenerate synergid-egg wall (Fig. 108).

(B). Degenerate Synergid: Pollen Tube Penetration and Discharge

The early stages of pollen tube penetration into the megagametophyte and the process of double fertilization were not observed in this study. The evidence presented here represents megagametophytes and zygotes from ovules that were fixed 18 and 24 hours after pollination. It is not possible to discriminate, purely on external morphology, the first ovules to be penetrated by a pollen tube (9-10 hours after pollination) from those penetrated by subsequent pollen tubes. For this reason the precise time of fertilization and the age of the zygote could not be determined.

The pollen tube first contacts the megagametophyte at the base of the filiform apparatus of the synergids (Fig. 117). The cells of the inner integument immediately adjacent to the pollen tube are intact and show no sign of degeneration. OsFeCN staining shows an aggregation of ER in the inner integument cells adjacent to the micropyle. The pollen tube does not always take the most direct route to the base of the degenerate synergid. Figure 119 shows a pollen tube that has grown laterally along the base of the persistent synergid before entering the degenerate synergid.

The pollen tube penetrates the degenerate synergid through the base of the filiform apparatus and grows chalazally within the degenerate synergid, following the contours of the common degenerate synergid-persistent synergid wall (Fig. 118). The walls of the pollen tube are electron-opaque in contrast to the electron-transparent common wall between the synergid cells and the filiform apparatus. The pollen tube cell wall is PAS-positive (Fig. 123) and exhibits a weak pale blue fluorescence when stained with Calcofluor and viewed with epifluorescence optics under UV light (Fig. 122). The portion of the pollen tube within the degenerate synergid appears collapsed following pollen tube discharge (Fig. 118) while those portions outside the degenerate synergid remain intact (Figs. 117, 119, 121). The majority of the pollen tube outside the degenerate synergid is filled with a flocculent material that is continuous with the pollen tube wall (Fig 117, 119). This thickened region forms a plug which exhibits a strong fluorescence when stained with aniline blue and viewed with epifluorescence optics under UV light (Fig. 114). The pollen tube grows to the mid-point of the degenerate synergid and discharges its contents by means of a terminal pore (Fig. 120, 121). The organelles of the penetrated degenerate synergid in the immediate vicinity of the terminal pore of the pollen tube show a lack of membrane integrity (Fig. 120). However, profiles of identifiable ER and mitochondria with long tubular cristae, similar to those seen in the unpenetrated degenerate synergid (Fig. 106) are apparent in the cytoplasm. It was not possible to ascertain whether these organelles originated from the pollen tube or the synergid. There are numerous spherical particles with an electron-transparent border around a fine granular,

electron-opaque core present in the synergid cytoplasm. These spherical particles are not present in the unpenetrated degenerate synergid (Figs. 105, 106) and extend from the discharge pore of the pollen tube to the chalazal tip of the degenerate synergid adjacent to the common boundary between the degenerate synergid, central cell, and zygote (Fig. 121). This region of the degenerate synergid corresponds to the region in the unfertilized egg apparatus where there is no definite electron-transparent wall separating the egg from the chalazal tip of the degenerate synergid (Figs. 78, 105). The cell wall between the degenerate synergid and the zygote, and the cell wall of the synergid hook are markedly thickened (Fig. 121). Numerous spherical particles are in close proximity to the thickened portions of the synergid wall (Fig. 130).

(C) Zygote: Cytoplasm

There are marked changes in the egg cell following fertilization. The large micropylar vacuole of the egg disappears and the length of the cell is reduced to between 30-35 um (Figs. 121, 123, 126). In contrast to the turbinate chalazal tip of the egg, the chalazal tip of the zygote assumes an ampulliform shape. The zygote nucleus, like that of the egg nucleus immediately prior to the arrival of the pollen tube (Fig. 108), occupies the the middle region of the cell and, in one zygote, the portion of the nucleus opposite the region of pollen tube discharge in the degenerate synergid showed a small elliptical island of nuclear material separated from the main nuclear body by a band of cytoplasm (Fig. 121). Serial sections revealed that the small island of nuclear material is an invagination connected to the main body of the nucleus by a narrow nuclear bridge (Fig. 130). The position of the

invagination relative to the region of pollen tube discharge in the degenerate synergid (Fig.121) suggests that the invagination may represent a late stage in nuclear fusion between the egg and sperm nucleus. A nucleolar organizing region is evident in the zygote nucleus (Fig. 130). The central cell of the megagametophyte in figure 121 contained two endosperm nuclei suggesting that triple fusion and the first mitotic division of the primary endosperm nucleus had occurred.

A small reniform, electron-opaque mitochondrion is appressed to the nuclear envelope of the outer invaginated portion of the zygote nucleus (Fig. 130). This reniform mitochondrion differs from the other spherical to elliptical mitochondria of the zygote which maintain the general morphology of those found in the egg (Fig. 78). Proplastids are distributed throughout the zygote (Fig. 121, 126, 130) and often contain starch deposits. OsFeCN staining shows the distribution of short strands of ER throughout the zygote (Fig. 126). The strands of ER are associated with ribosomes (Fig. 132) and the ER cisternae in surface view show the presence of spiral polysomes (Fig. 130). The number and size of lipid bodies within the zygote cell increase following fertilization (Fig. 126). Dictyosomes are mainly associated with the cell wall but are not highly active in vesicle production (Fig. 130).

(D) Zygote: Cell Wall

In comparison to the egg (Figs. 78, 105), the zygote wall is markedly thickened in the micropylar and lateral regions of the cell. The ampulliform chalazal tip of the zygote in figure 121 is relatively thin-walled and the electron-opaque deposits of the chalazal wall of

the egg (Fig. 78) are absent. The tip of the zygote is PAS-negative while the micropylar and lateral regions of the zygote in figure 121 are PAS-positive (Fig. 123) and fluoresce a pale blue when stained with Calcofluor and viewed with UV optics (Fig. 122). There is a progressively weaker fluorescence from the mid-chalazal region of the wall to the chalazal tip. A glancing section through the lateral wall of the ampulliform tip of the zygote shows the presence of numerous microtubules immediately adjacent to the cell wall (Fig.124). The majority of the microtubules were oriented with the long axis perpendicular to the long axis of the zygote (Fig. 125).

The zygote plasma membrane follows a relatively regular cell wall surface while on the central cell side, the cell wall surface is irregular (Fig. 132). In seeds fixed with OsFeCN, the common cell wall between the zygote and the central cell is electron-opaque and there are wide evaginated regions of wall material extending into the central cell cytoplasm (Figs. 126, 129). The evaginated regions on the central cell side of the common wall show a homogeneous electron-opacity while the adjacent thin regions of common wall exhibit a more granular electron-opacity. The region of the zygote wall between the homogeneous electron-opaque evagination and the zygote plasma membrane shows a similar granular electron-opacity. This narrow band of granular electron-opaque material probably represents the newly synthesized wall material deposited by the zygote following fertilization. The wide evaginated, homogeneous electron-opaque regions of the zygote wall stain orthochromatically with crystal violet (Fig. 127). When stained by the Thiery PA-TCH-SP method there is an even deposition of silver proteinate over the entire zygote wall

including the evaginated region (Fig. 128). The electron-transparent zone adjacent to the zygote plasma membrane probably represents a slight plasmolysis induced during tissue preparation. The ER cisternae and lipid droplets of the OsFeCN-fixed zygote show heavy deposition of silver proteinate as do the starch grains of the central cell chloroplasts. The control section, where water was substituted for periodic acid, show deposition of silver proteinate over the ER cisternae and lipid bodies, but none over the zygote cell wall or the starch grain of the central cell plastid (Fig. 129). The orthochromatic staining with crystal violet (Fig. 127) and homogeneous electron-opacity of the evaginations (Fig. 129) in the zygote-central cell wall correspond to characteristic orthochromatic staining (Fig. 83) and electron-opaque deposits found in the expanded intercellular regions (Fig. 78) of the egg-central cell wall in the mature megagametophyte at anthesis. Electron-transparent, membrane-bound evaginations of the zygote plasma membrane are occasionally seen at the chalazal tip of the zygote (Fig. 129). These evaginations generally contain membranous inclusions.

(E) Persistent Synergid

Following fertilization, the persistent synergid does not degenerate but remains an intact cell (Fig. 118). In some fertilized megagametophytes, the plasma membranes separating the persistent synergid and central cell disappear resulting in a mixing of persistent synergid and central cell cytoplasms. Figure 119 shows an incomplete common persistent synergid-central cell wall, containing plasmodesmata, extending from the edge of the megagametophyte into the central cell cytoplasm. Numerous central cell chloroplasts are

intermixed with synergid proplastids in the region of the persistent synergid filiform apparatus. The presence of central cell-like wall projections in the micropylar region of the persistent synergid between the common synergid-central cell wall and filiform apparatus is noteworthy.

(F) Central Cell

Following fertilization, chloroplasts are aggregrated in the micropylar and perinuclear regions of the central cell and are actively replicating at the two nucleate stage of endosperm development (Fig. 133). The chloroplasts show well developed thylakoid lamellae and numerous starch deposits within the stroma (Fig. 119, 133). There are numerous mitochondria, dictyosomes, lipid bodies, and microbodies present throughout the central cell cytoplasm which, except for the ER, is similar to the unfertilized central cell (Fig. 63). Much of the ER near the zygote is fragmented and has become dilated (Fig.131). Spiral polysomes are attached to the surface of the ER cisternae (Fig.132).

Following fertilization, the micropylar and mid-chalazal regions of the central cell become highly vacuolate (Fig. 123, 126, 127) with some of the enlarging vacuoles occurring in close proximity to the common zygote-central cell wall (Figs. 129, 131, 132). The large vacuole in figure 131, between the zygote cell wall and the central cell proplastid (of persistent synergid origin?) shows no apparent connections to either the central cell plasma membrane or to adjacent ER cisternae. However, in figure 132, a non-adjacent serial section, there is a definite continuity between the central cell plasma membrane and the bounding membrane of the central cell vacuole. In

addition, the narrow strand of rough ER sandwiched between the proplastid and the vacuole shows a continuity with the outer membrane of the vacuole.

IV. NON-FERTILE OVULE

Ovules remain viable and are capable of being fertilized for a period of approximately 72 hours following anthesis. At around 72 hours there is a rapid decline in ovule fertility. The pistil at this time has increased in length to 11-13 mm and petal abscission is commencing (Fig. 116).

In contrast to the mature fertile ovule (Fig. 104) the non-fertile ovule, 72 hours from anthesis, exhibits a large chalazal vacuole that occupies the majority of the megagametophyte (Fig. 134). The expansion of this vacuole is at the expense of the degenerate chalazal nucellus. The chalazal proliferating tissue remains intact. The egg apparatus, at this time, consists of two degenerate synergids and an intact egg (Figs. 135, 136). At the level of the light microscope, the cytoplasm of both synergids stains intensely with crystal violet (Fig. 136). There is no apparent ultrastructural difference between the two degenerate synergids (Fig. 135). The chalazal region of one of the synergids, adjacent to the egg, has become plasmolysed. Profiles of dilated ER, mitochondria, vesicles, and a nucleus are discernable in the degenerate synergid cytoplasm but the integrity of organelle membranes has been, with the exception of the mitochondrial cristae, lost (Fig. 139). There is a number of electron-opaque deposits associated with the nuclear envelope and the outer membrane of the mitochondria. Both synergids resemble the post-anthesis degenerate synergid of the mature megagametophyte prior

to fertilization (Fig. 106) except for the absence of ribosomes associated with the dilated ER. The filiform apparatus is PAS-positive, except for a subulate zone at the micropylar end of the two synergids (Fig. 136). Figure 135, which is an non-adjacent serial section to Figure 136, shows, at the ultrastructural level, no morphological or staining differences between the subulate zone and the rest of the filiform apparatus. When stained with Calcofluor and viewed with UV optics the entire filiform apparatus fluoresces a pale blue (Fig. 137) as do the micropylar portion of the common wall between the synergids and the wall in the region of the synergid hook. The chalazal region of the egg of the non-fertile ovule, like that of the fertile ovule (Fig. 99), is non-fluorescent (Fig. 137).

The egg of the non-fertile ovule shows little sign of degeneration (Fig. 135, 136) or structural modification as compared to the egg at anthesis (Fig. 78). The cytoplasms are similar with regard to the types and distributions of organelles, however, as in the zygote, there is a marked increase in lipid bodies (Fig. 135). The common wall between the egg and the central cell is similar to that of the egg at anthesis (Fig. 78). There is, however, a dilation of the electron-transparent expanded cell wall and a corresponding irregular undulation of the plasma membranes except in the region of the electron-opaque deposits (Fig. 138). Here, the plasma membranes are straight and tightly appressed to the more regular electron-opaque region of the wall. These electron-opaque deposits, like the egg at anthesis (Fig. 83) stain orthochromatically with crystal violet (Fig. 136).

Except for the large chalazal vacuole, the central cell of the non-fertile ovule (Fig. 140, 141) is similar to the central cell following anthesis (Fig. 66). The two polar nuclei remain labile, contorted, and interconnected by nuclear bridges and the type and distribution of organelles remains for the most part unchanged (Fig.140). A notable difference however, is the dilation of ER cisternae, particularly in the wide cytoplasmic embayments between the polar nuclei. Throughout the polar nuclear region of the central cell the dilated ER appears to be sequestering cytoplasm and organelles.

The chloroplasts maintain the stacked thylakoids characteristic of plastids active in photosynthesis, but starch grains, present in the chloroplasts of the unfertilized central cell at anthesis (Fig. 55, 63), and in the central cell following fertilization (Figs. 129, 133), are conspicuously absent from the central cell of the non-fertile ovule (Fig. 141). In addition, PAS-positive starch grains present in the integument region lateral to the central cell wall projections, the egg apparatus (Fig. 84) and the zygote (Fig. 121, 123) have disappeared from the non-fertile ovule 72 hours after anthesis (Fig. 136). The egg and central cell of older ovules soon degenerate, followed by a general yellowing and eventual degeneration of the integumentary tissue.

LEGEND

NOTE: the arrowhead adjacent to the figure number represents, where applicable, the direction of the micropyle.

Figure 1. Light micrograph of a young ovary in cross-section. The ovule primordium (OP) is trizonate. Zone 1 (protodermal layer) and Zone 2 (subdermal layer) divide anticlinally; Zone 3 exhibits anticlinal, periclinal, and oblique divisions. Two replum primordia (RP) are situated between the ovule primordia. CV. x480.

Figure 2. Light micrograph of an ovule primordium at the time of integument intitiation. The three zones (1,2,3) of the ovule primordium that contribute to the formation of the nucellus (N), chalaza (C), and funiculus (F) are clearly visible. The inner integument initial is formed by an oblique divison of a protodermal cell (unlabelled arrow) on the adaxial (Ad) side of the ovule adjacent to the replum (R). The future region of outer integument (OI) initiation, on the adaxial side of the ovule primordium, and inner integument (II) initiation, on the abaxial (Ab) side of the ovule primordium, are also visible. PAS/ABB. x1090.

Figure 3. Light micrograph of an ovule showing a primary parietal cell (PP) and a primary sporogenous cell (PSp), nucellus (Nu) and funiculus (F). The cytoplasms of the two cells are intensly stained by cationic dyes and regions of basiophilic heterochromatin (H) are visible in the peripheral regions of the nucleus of the vacuolate (V) primary sporogenous cell. The dermal and subdermal initials of the outer integument (OI) are visible on the adaxial (Ad) side of the ovule. CV. x990.

Figure 4. Light micrograph of an ovary in cross section showing the centrally located, small, thin-walled cells (unlabelled arrow) of the replum (R) and an ovule (Ov) at the archesporial cell stage of development. CV. x630

Figure 5. Light micrograph of an ovule showing a hypodermal archesporial cell (Ac), nucellus (Nu), chalaza (C), and funiculus (F). The large nucleus of the archesporial cell contains a prominent basiophilic nucleolus and peripheral heterochromatin (H). The wedge-shaped inner integument initials (unlabelled arrows) as well as the dermal and subdermal initials of the outer integument (OI) are visible on the adaxial (Ad) and abaxial (Ab) side of the ovule. CV. x1070.

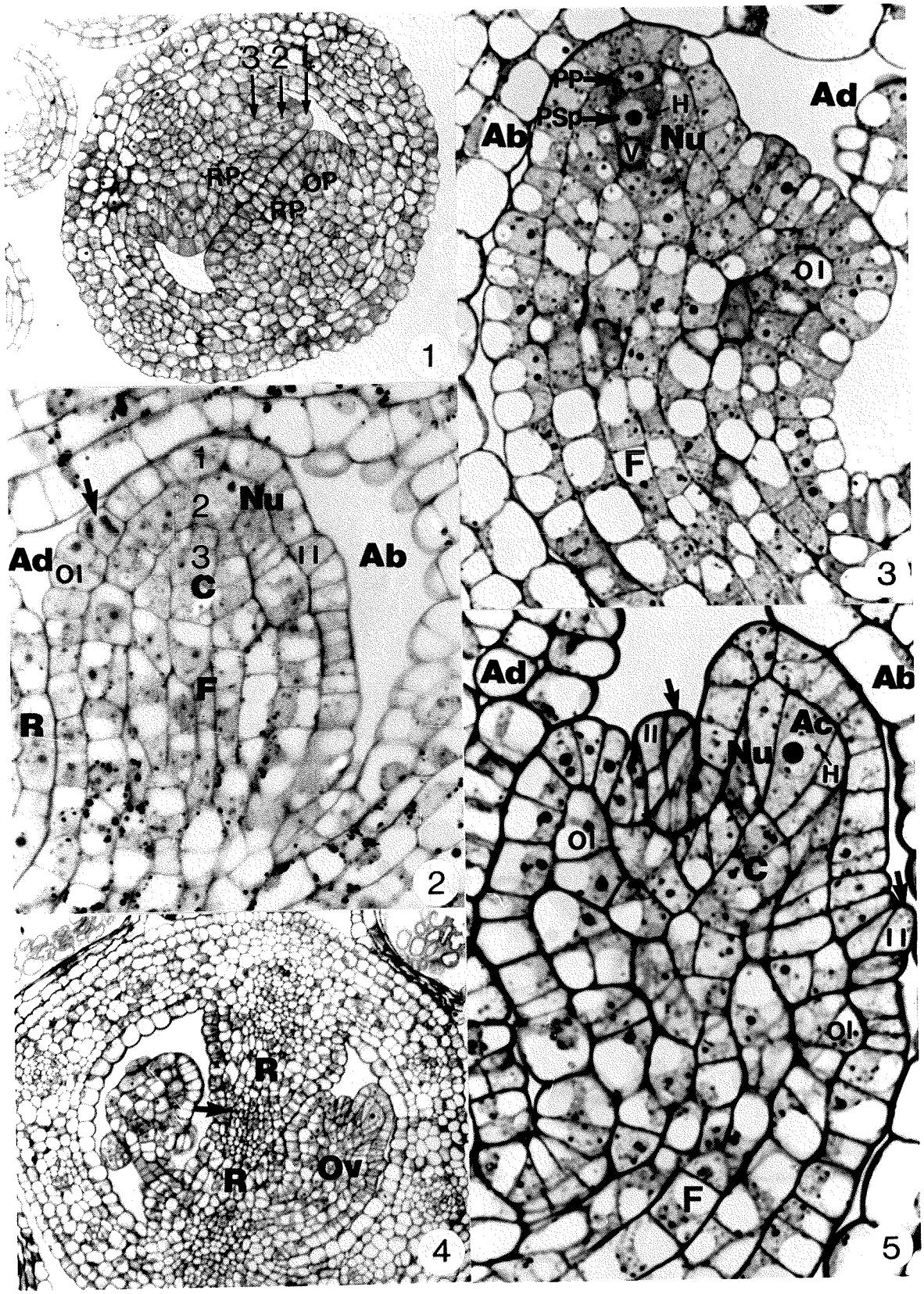
3 2 1
RP
OP
RP
1
pp
PSp
H
V
Nu
Ad
Ab
Ol
F
3
1
2
Nu
3
C
Ad
Ol
II
Ab
F
R
2
R
R
Ov
4
Ad
Ab
II
Ac
Nu
H
Ol
C
II
Ol
F
5

Figure 6. Electron micrograph of the chalazal region of a primary sporogenous cell (PSp). The large nucleus of the primary sporogenous cell exhibits nuclear pores (arrowheads), a prominent electron-opaque granular nucleolus (NL) and peripheral electron-opaque heterochromatin (H). The vacuolate (V) cytoplasm contains inactive dictyosomes, short stands of ER, ER-derived microbodies (Mb), and lipid bodies (L). The starch containing proplastids (P) and spherical mitochondria (M) are similar to those found in the adjacent nucellus (Nu). OsFeCN. UA/Pb. x11,300.

Figure 7. Light micrograph of an ovule showing a hypodermal megasporocyte cell (Ms) in mid-prophase of meiosis I, the nucellus (Nu), chalaza (C), and funiculus (F). The nucleoplasm of the megasporocyte is non-basiophilic and contains nucleoli (NL) and synaptonemal chromosomal complexes (arrowheads). The cytoplasm of the megasporocyte is less intensely stained with cationic dyes as compared to the adjacent nucellus. The wedge-shaped inner integument initials (unlabelled arrows) are seen on the adaxial (Ad) and abaxial (Ab) sides of the ovule. The dermal and subdermal initials of the outer integument (OI) are seen on the adaxial side of the ovule, proximal to the inner integument (II). x1070.

Figure 8. Light micrograph of an ovule showing a primary parietal cell (PP) and an enlarged megasporocyte cell (Ms). The region between the megasporocyte and the point of insertion of the inner integuments (II), the chalaza (C), is the expanded chalazal nucellus (CN). Bifacial divisions of the wedge-shaped apical initial (arrow) give rise to a two-layered inner integument. GMA. TB. x1070.

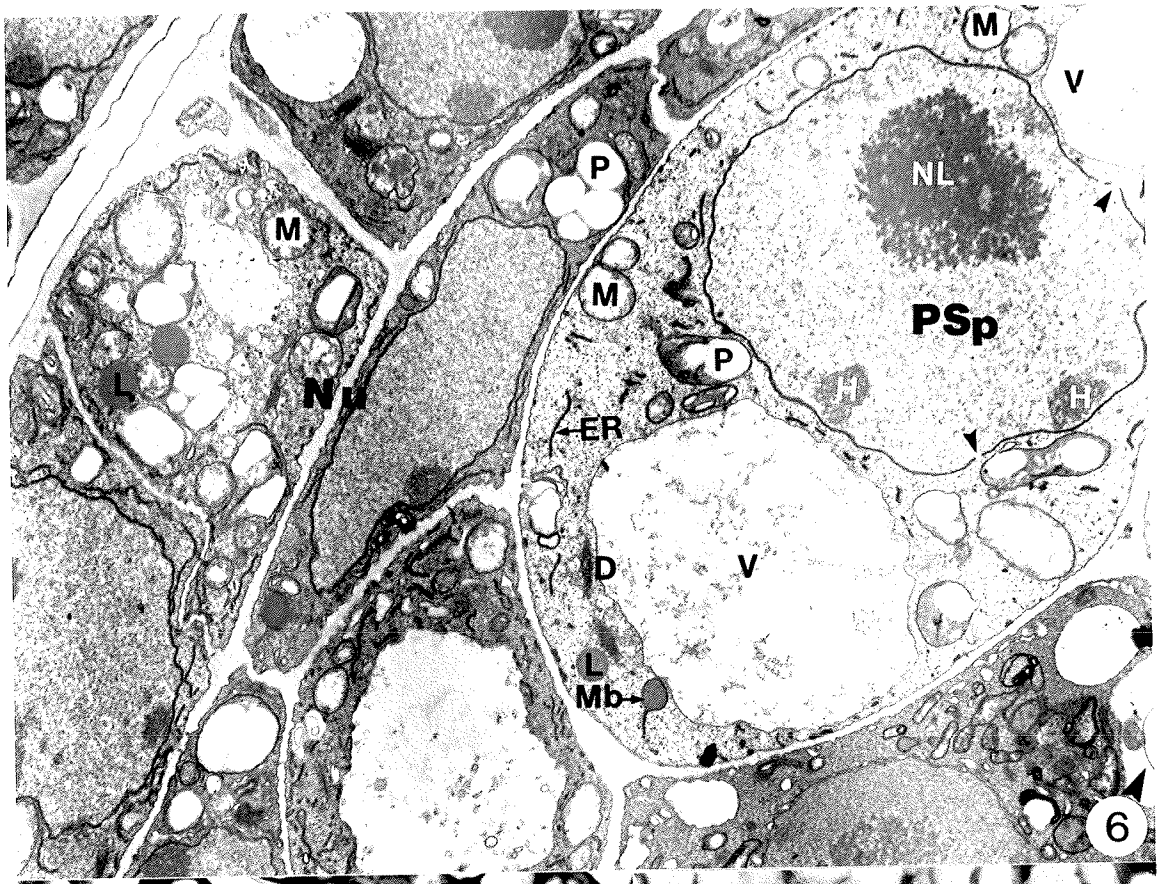
M
V
NL
P
M
PSp
M
P
L
Nu
H
H
ER
D
V
L
Mb
6

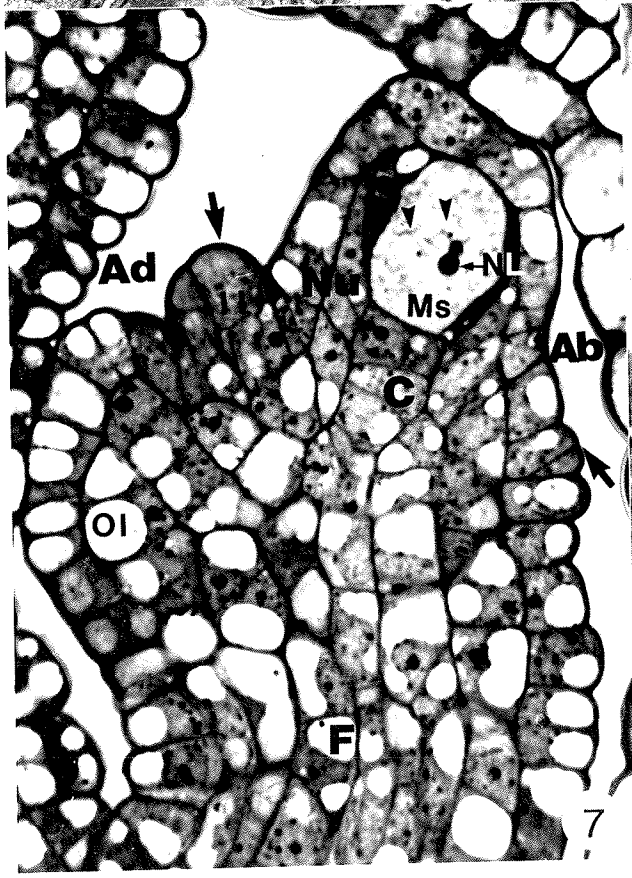
Ad
Nu
NL
Ms
Ab
C
Ol
F
7

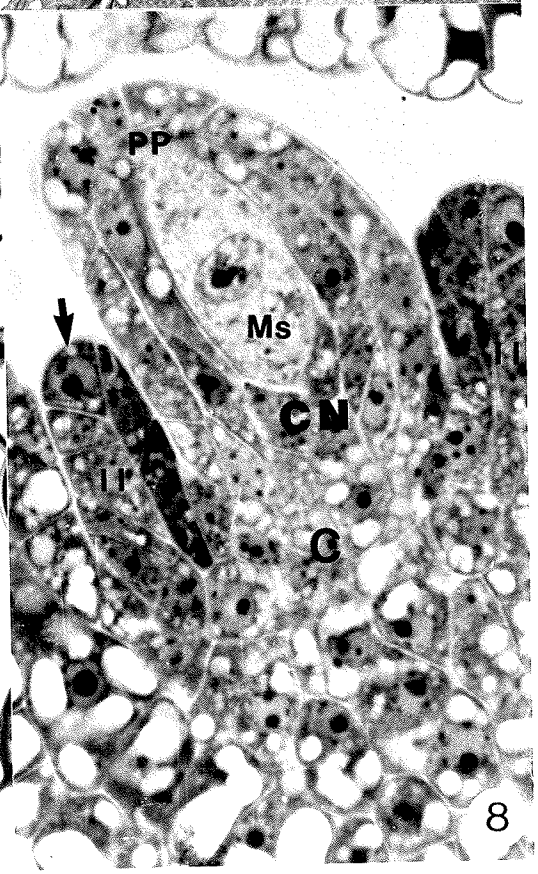
PP
Ms
CN
C
8

Figure 9. Electron micrograph of the micropylar tip of the nucellus (Nu) showing a primary parietal cell (PP) and a megasporocyte cell (Ms) in mid-prophase of meiosis I. The cytoplasm of the megasporocyte, as compared to the adjacent nucellus, is more electron-transparent and contains smaller, rod-shaped mitochondria (M). In contrast the mitochondria of the primary parietal cell and adjacent nucellus are large and spherical. A double membrane bound inclusion (dmi) is located in the micropylar region of the cell. The electron-transparent regions of megasporocyte cell wall (arrowheads) may represent deposits of callose. UA/Pb. x5,800.

Figure 10. Electron micrograph of the chalazal end of a primary sporogenous cell (PSp) showing plasmodesmata connections (pd) with the chalazal nucellus. The mitochondria (M) of the primary sporogenous cell are typically spherical with a size range of 1-2 um. UA/Pb. x19,000.

Figure 11. Electron micrograph of part of a megasporocyte cell (Ms) showing a multiple membrane bound inclusion (mmi) composed of four unit membranes. Note the reduced number of ribosomes in the multiple membrane bound inclusion as compared to the surrounding cytoplasm and the small (1.0 X 0.5 um) rod-shaped mitochondrion (M). UA/Pb. x26,000.

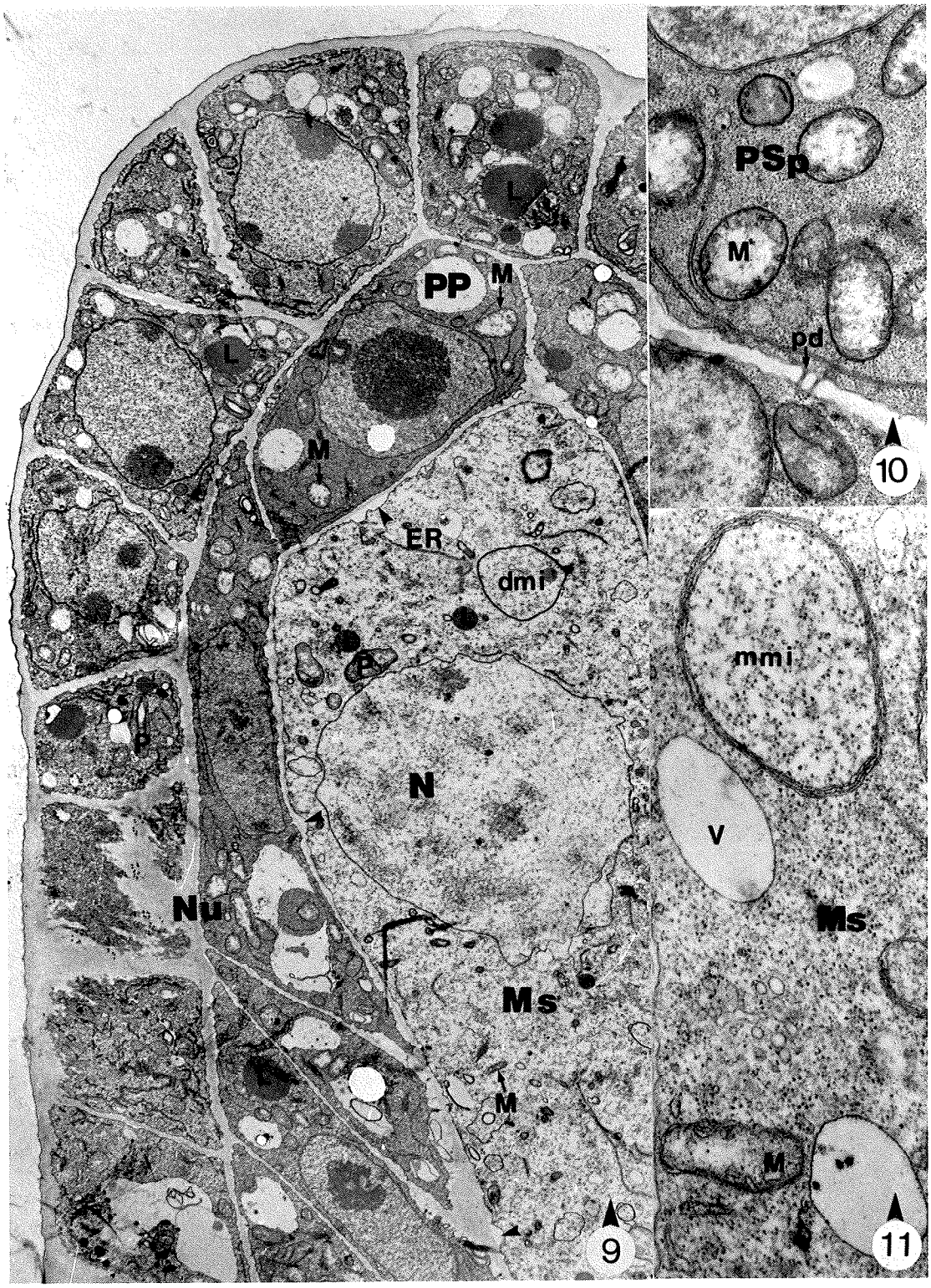
PSp
M
pd
10
L
PP
M
L
M
ER
dmi
P
P
N
Nu
Ms
M
9
mmi
V
Ms
M
11

Figure 12. Electron micrograph of the chalazal end of a megasporocyte (Ms) in mid-prophase of meiosis I showing a cytoplasm containing proplastids (P) without starch, lipid bodies (L), dictyosomes (D), ER, and multiple membrane bound inclusions (mmi). The mitochondria (M) appear condensed and rod-shaped. Occasional plasmodesmata (pd) traverse the cell wall between the megasporocyte and the chalazal nucellus. Within the nucleus (N) there is synaptonemal chromosome complex (unlabelled arrow) adjacent to a region of dilated nuclear envelope (ne) containing electron-opaque, membrane bound inclusions (arrowheads). OsFeCN. UA/Pb. x6,100.

Figure 13. Light micrograph of the chalazal dyad cell (CD) following the completion of meiosis I. The micropylar dyad cell (arrowhead) has degenerated. The majority of the micropylar dyad cell is out of the plane of section. GMA. TB. x1,070.

Figure 14. Light micrograph of the products of meiosis - the triad. The second meiotic division of the chalazal dyad cell is unequal producing a large chalazal functional megaspore (FM) and a smaller non-functional megaspore (NM). Both cells contain large basiophilic nucleoli. The micropylar dyad cell (MD) has degenerated and the adjacent hypodermal tissue of the nucellus (Nu) has enlarged. CV. x1,280.

Figure 15. Light micrograph of the products of meiosis - the triad. Fresh, whole mount of the ovule stained with aniline blue and viewed with epifluorescence optics under UV light. The cell walls between the functional megaspore (FM) and the non-functional megaspore (NM) and between the non-functional megaspore and the micropylar dyad cell (MD) fluoresce a pale blue in contrast to the surrounding nucellus. x1,070.

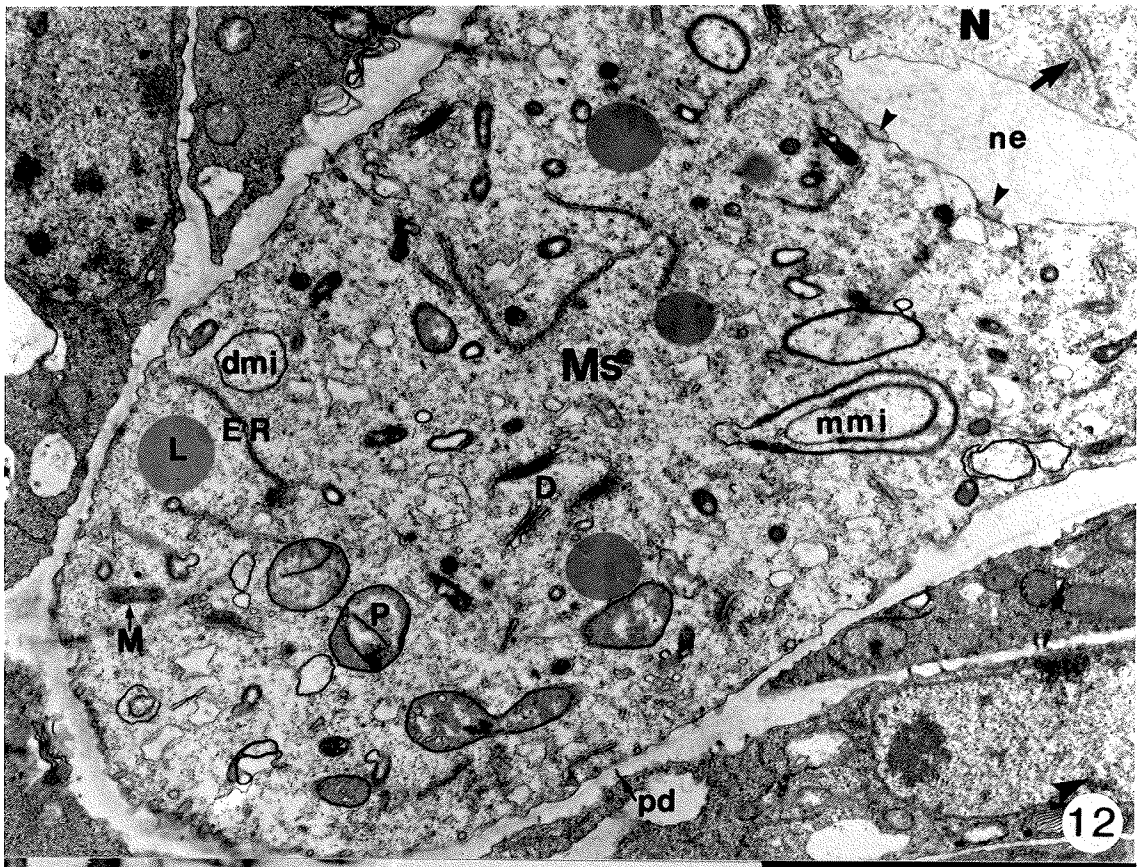
N
ne
dmi
Ms
mmi
L
ER
D
M
P
pd
12


Nu
CD
13

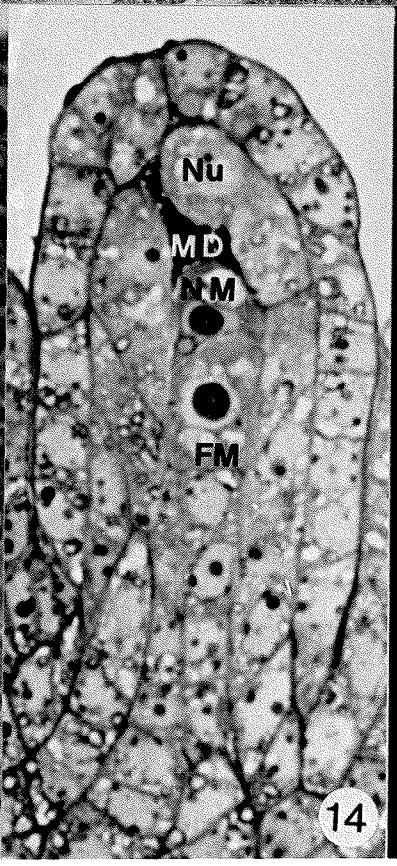
Nu
MD
NM
FM
14

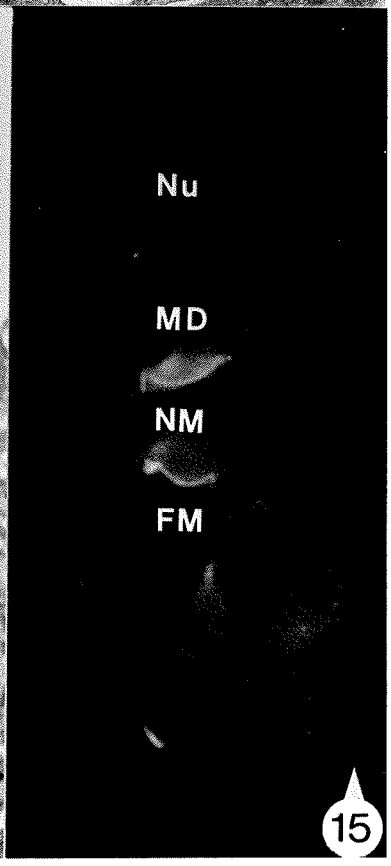
Nu
MD
NM
FM
15

Figure 16. Light micrograph of an older functional megaspore (FM). The older functional megaspore assumes an obdeltoid shape and retains the prominent basiophilic nucleolus seen in the young functional megaspore following completion of meiosis. The chalazal hypodermal cells remain intact. GMA. TB. x700.

Figure 17. Electron micrograph of a functional megaspore (FM). The cytoplasm of the functional megaspore, as compared with the prophase megasporoctye (Fig. 12), is richer in ribosomes but sparcer in cytoplasmic organelles. The plastids (P) are fewer in number and are relatively undifferentiated with an electron-transparent, starch-free stroma. The mitochondria (M) are small (0.5 - 1.0 um), spherical and exhibit an electron-transparent matrix with poorly developed cristae. The mitochondria of the adjacent nucellus (Nu) are similar to those found in the nucellus prior to the onset of meiosis (Figs. 6, 9). Short strands of ER are mainly associated with the peripheral regions of the functional megaspore adjacent to the cell wall. UA/Pb. x7,600.

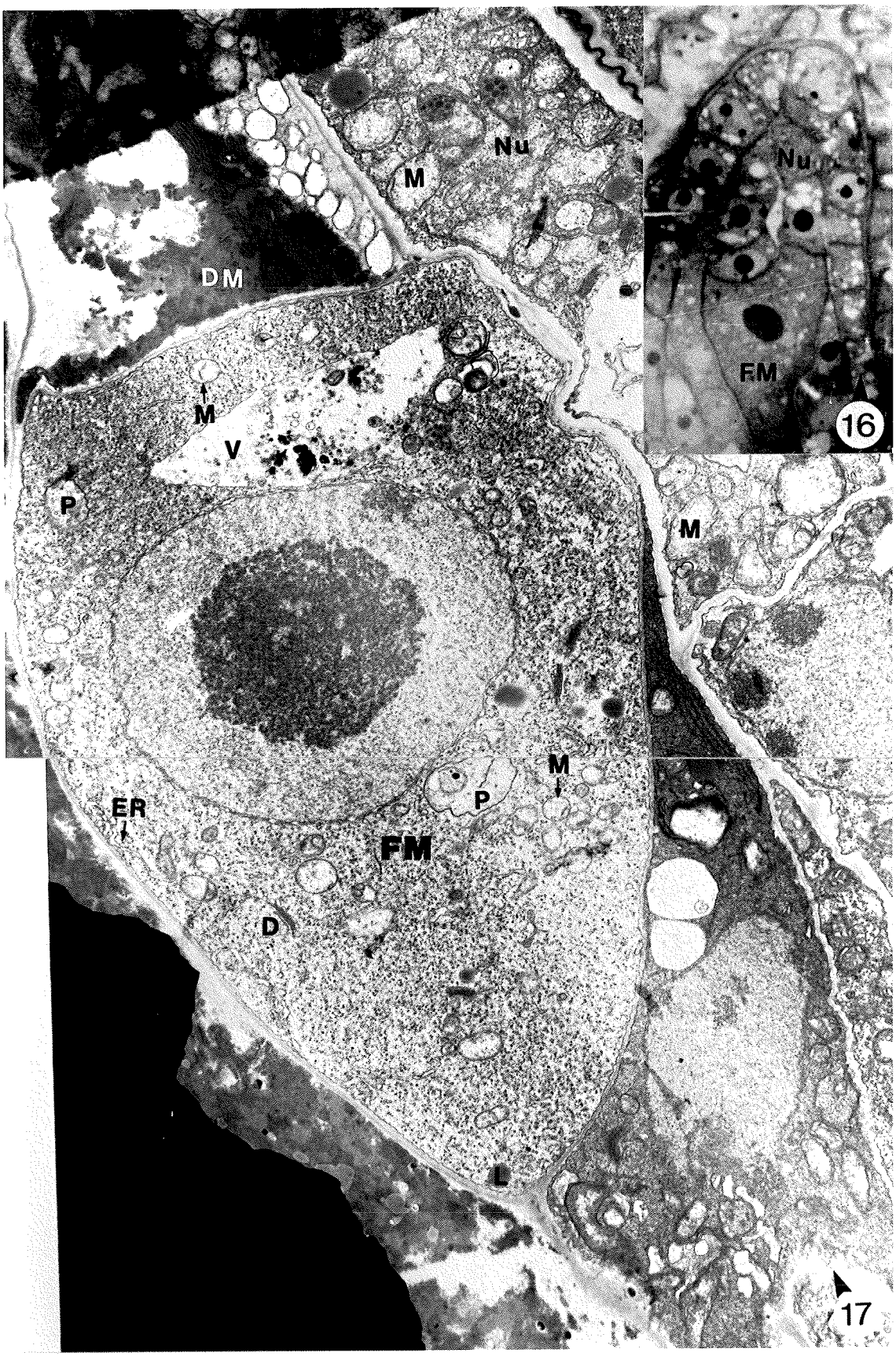
Nu
M
DM
M
V
P
Nu
FM
16
M
M
P
ER
FM
D
L
17

Figure 18. Light micrograph of an ovule at the functional megaspore stage of development showing the nucellus (Nu), chalaza (C), raphe (Ra), funiculus (F), outer integument (OI), and inner integument (II). The adaxial (Ad) side of the outer integument, including the region of outer integument contiguous with raphe (small arrowheads), exhibits the greatest growth of all integumentary tissues, and coupled with the arrested growth of the outer integument on the abaxial (Ab) side, produces an asymmetric curvature in the ovule. This, coupled with the greater growth of the funiculus on the abaxial side (large arrowheads) as compared to the adaxial side, results in a sigmoid ovule. By this stage of development the nucellus is nearly enveloped by the integuments. CV. x250.

Figure 19. Light micrograph of a possibly diplosporous, 2-nucleate megagametophyte. The megagametophyte (Mg) occupies a hypodermal position in the apical region of the nucellus. The development of the inner (II) and outer (OI) integuments is comparable to that at the 4-nucleate stage of megagametophyte development (Fig. 26). CV. x430.

Figure 20. Light micrograph of an older 2-nucleate megagametophyte derived from two non-adjacent serial sections. The appearance of a large central vacuole (V) between the two nuclei (N) coincides with the micropylar expansion of the megagametophyte. The lateral crescent-shaped region (CR) is the remnant of the degenerate megapores (arrows) and lateral hypodermal nucellus (arrowhead). At this stage of development the nucellar epidermis (Nu Ep) is still intact. CV. x850.

Figure 21. Light micrograph of a young obdeltoid 2-nucleate megagametophyte. The two juxtaposed nuclei (N) are flanked by small parietal vacuoles. Micropylar to the megagametophyte are two non-functional megaspores (arrows) that have degenerated, the lateral hypodermal nucellus (arrowhead), and the enlarged micropylar hypodermal nucellar tissue (Nu). The inner integuments (II) have completely enveloped the nucellus, forming the inner integument component of the micropyle (Mi). CV. x800.


Ad
Ol
Il
Nu
C
Ol
Ab
Ra
R
F
18
Ol
Pf
Mg
II
CN
19
Nu Ep
II
CR
V
N
20
Mi
Nu
II
II
V
N
N
21

Figure 22. Electron micrograph of a young 2-nucleate megagametopohyte. Each of the two juxtaposed nuclei (N) exhibits wide nuclear pores (small arrowheads) and are circumscribed by starch-free plastids (P) and mitochondria (M). The number of mitochondria and plastids is greater than at the functional megaspore stage (Fig. 17). There is evidence of plastid replication (large arrowhead). The internuclear region contains short strands of ER, lipid bodies (L) and the occasional dictyosome (D). There is a small vacuole (V) in the chalazal cytoplasm. UA/Pb. x5,200.

Figure 23. Electron micrograph of the internuclear region of a young 2-nucleate megagametophyte. There are numerous microtubules (arrowheads) between the two nuclei (N), oriented parallel to the long axis of the cell. Some of the microtubules appear to be associated with dictyosome (D) vesicles (arrow). The mitochondria (M) appear similar to those of the functional megaspore (Fig. 17). UA/Pb. x21,700.

Figure 24. Electron micrograph of a possibly diplosporous, hypodermal 2-nucleate megagametophyte in the extreme micropylar region of the nucellus (Nu). Vacuoles (V) appear to be coalescing between the two nuclei (N). The numbers and distribution of plastids (P) and mitochondria (M) are similar to the 2-nucleate megagametophyte in figure 22. There is a high content of lipid bodies (L). Some lipid bodies appear to be associated with vacuoles (arrowhead). UA/Pb. x5,900.

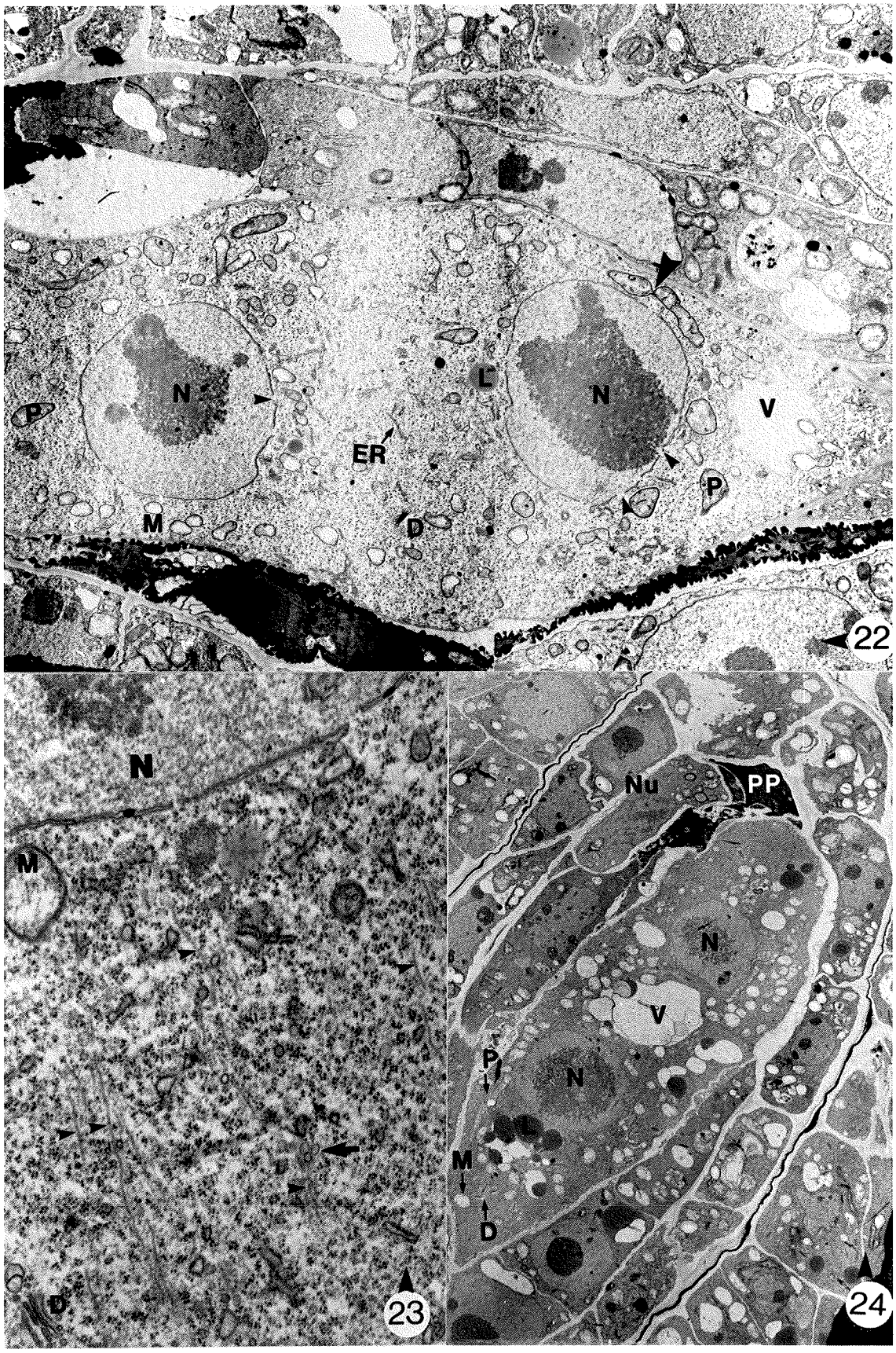
N
P
ER
L
N
V
P
M
D
22
N
M
D
23
Nu
PP
N
V
P
N
M
D
24

Figure 25. Electron micrograph of a young 4-nucleate megagametophyte. Two of the four nuclei (N) are separated by a large central vacuole. The micropylar and lateral nucellar epidermis (Nu Ep) has degenerated and the lateral crescent shaped region (CR) of degenerate megaspores and lateral hypodermal nucellus is evident. The outer tangential wall of the inner integument (II) possesses a relatively thick, osmiophilic electon-opaque cuticle (Cu). Thin anticlinal walls of the lateral inner integument epidermis (arrowheads) suggests the occurrence of anticlinal cell divisions within this tissue concurrent with the expansion of the megagametophyte. There is an accumulation of starch (St) in the micropylar and lateral integument cells. OSFeCN. UA/Pb. x2,400.

Figure 26. Light micrograph of an ovary showing a sagittal section through an ovule, including the raphe (Ra) and funiculus (F), at the 4-nucleate stage of megagametophyte development and a second ovule in a cross-section view. The central cells (arrowhead) of the replum (R) develop thick, PAS positive, unlignified cell walls. Between these cells and the lateral vascular bundle (Vb) of the ovary is a region of parenchyma cells containing PAS positive starch (St). The proximal region of the inner integument (II) has become 3-4 layered (unlabelled arrow), an inner integument basal body (Bb) has begun to develop, and PAS positive starch (St) accumulates in the region of the inner integument lateral to the 4-nucleate megagametophyte (Mg). By this stage of development the outer integument (OI) component of the micropyle (Mi) has been formed. The ovule (Ov), in the adjacent loculus of the ovary, represents a cross-section through the inner and outer integuments at the micropylar region of the ovule. PAS/CV. x280.

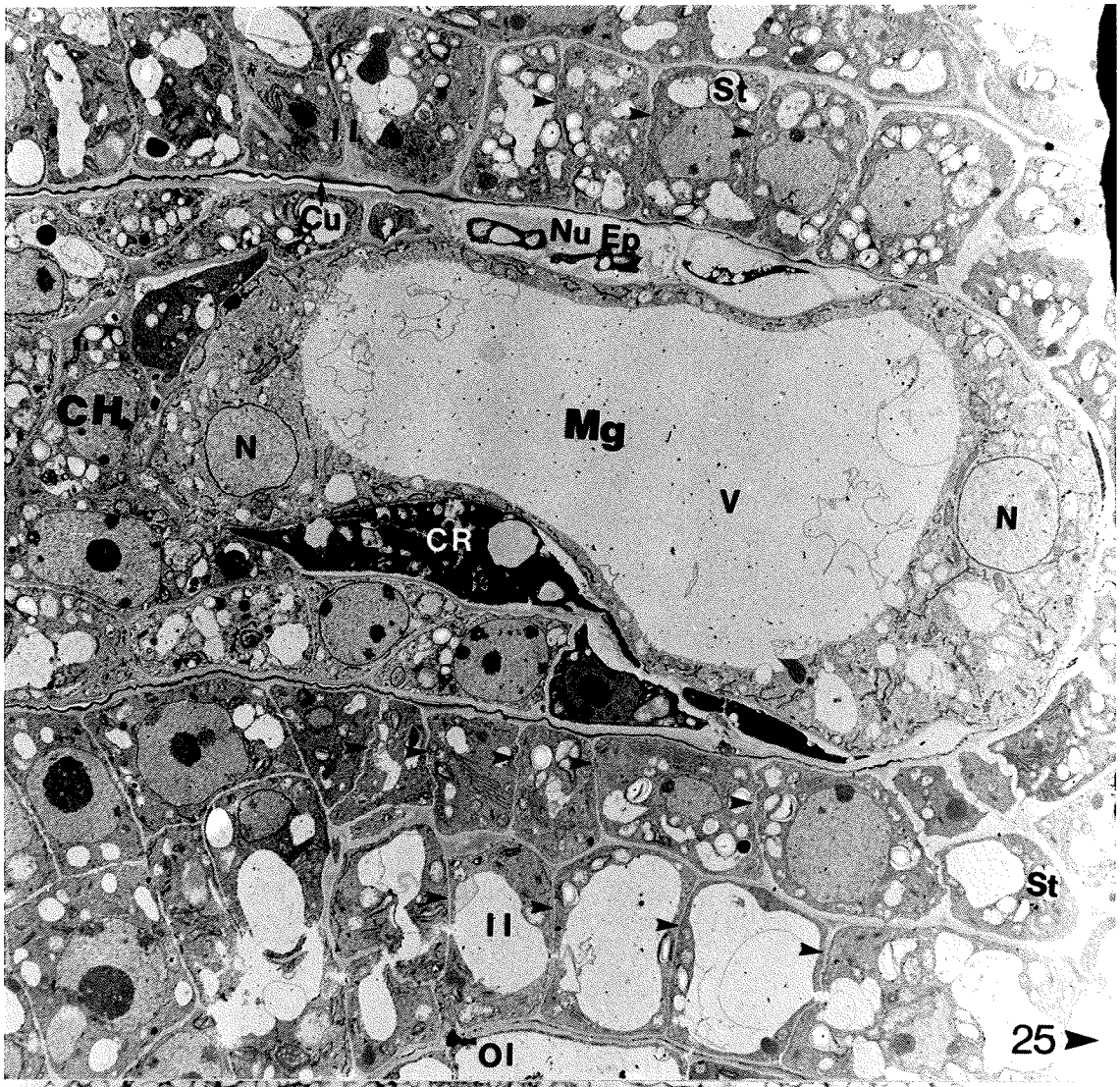
St
Il
Cu
Nu
Ep
CHL
N
Mg
V
CR
N
St
Il
Ol
25

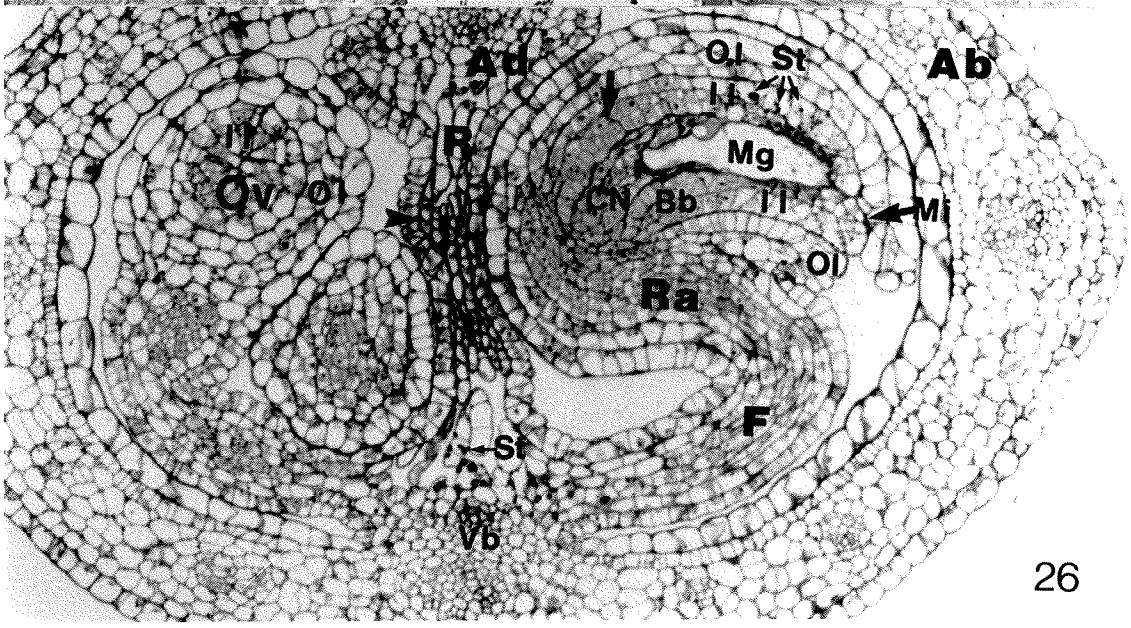
Ad
Ol
St
Ab
Il
R
Mg
Il
Ov
Ol
CN
Bb
Il
Mi
Ol
Ra
F
St
Vb

26

Figure 27. Electron micrograph of the micropylar region of a young 4-nucleate megagametophyte. Short strands of ER are distributed throughout the megagametophyte and there are ER connections (small arrowhead) to the nuclear envelope of one of the two juxtaposed nuclei (N). Plastids (P) are generally free of starch and are primarily located in the vicinity of the nuclei. Mitochondria (M) are distributed throughout the megagametophyte. They have well defined cristae, similar to the mitochondria (M) of the inner integument (II) and they show evidence of replication (large arrowhead). Dictyosomes (D), active in vesicle production, appear to be confined to the regions adjacent to the megagametophyte wall. OsFeCN. UA/Pb. x10,400.

Figure 28. Electron micrograph showing an overview of an older 4-nucleate megagametophyte (Mg). The sister nuclei (N) at the chalazal (C) end of the megagametophyte have been separated by a vacuole (V) and lipid bodies have accumulated in the adjacent cytoplasm. Certain cells of the inner integument epidermis (II Ep) in the micropylar region of the ovule, adjacent to the megagametophyte, have divided periclinally (arrow). UA/Pb. x1,760.


M
II
V
M
D
N
P
N
ER
V
ER
D
NuEp
27

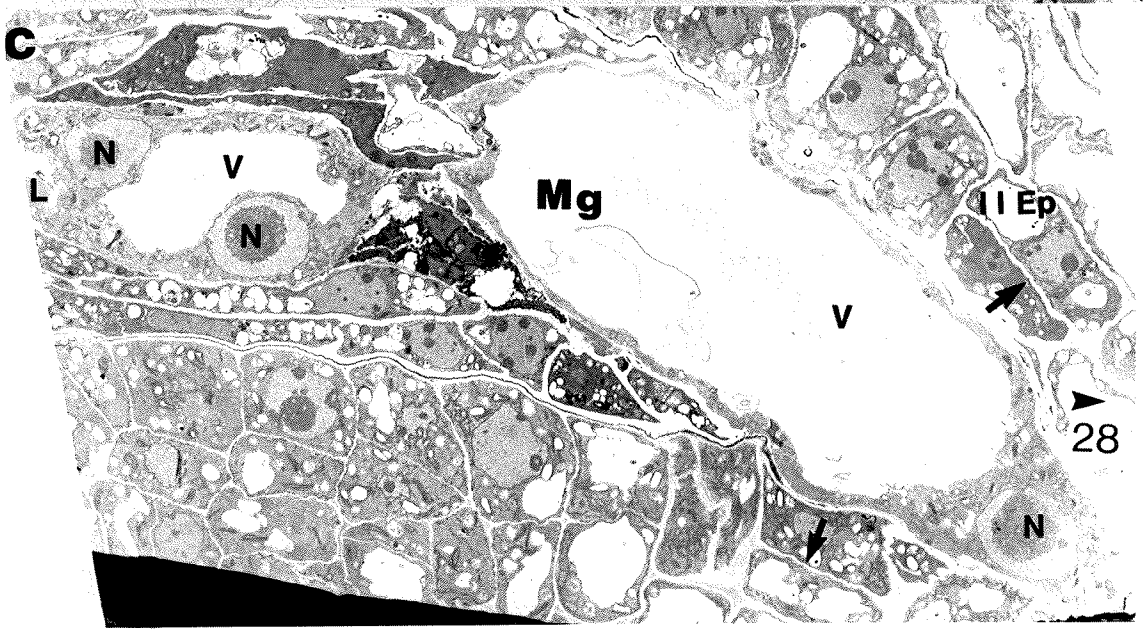
C
N
V
L
N
Mg
II Ep
V
28
N

Figure 29. Electron micrograph of the micropylar region of an older 4-nucleate megagametophyte. The cytoplasm is similar to that of the younger 4-nucleate megagametophyte with regard to the numbers and distribution of ER, mitochondria (M), and plastids (P). However, there is a marked increase in dictyosomes (D) and lipid bodies (L). An electron-opaque cuticle (Cu) is present between the inner integument and the megagametophyte. A cell of the inner integument epidermis (II Ep) has divided periclinally. The inner derivative, adjacent to the megagametophyte, is more electron-opaque. UA/Pb. x5,300.

Figure 30. Electron micrograph of the lateral region of an older 4-nucleate megagametophyte. Helical polysomes (arrowheads) and dictyosomes (D) active in vesicle production are present in the peripheral cytoplasm. Some of the dictyosome vesicles appear to be fusing with the megagametophyte wall (MgW). The electron-opaque cuticle layer (Cu) is discontinuous. UA/Pb. x39,600.

Figure 31. Electron micrograph of the micropylar region of an older 4-nucleate megagametophyte. Numerous dictyosomes (D), active in vesicle (Dv) production, are present in the cytoplasm. UA/Pb. x19,600.


L
D
L
II Ep
D
Cu
ER
N
M
P
29

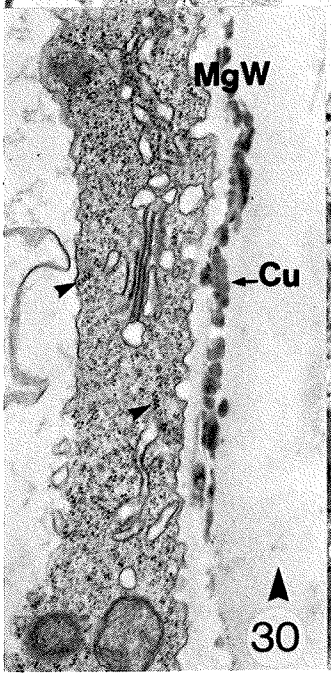
MgW
Cu
30

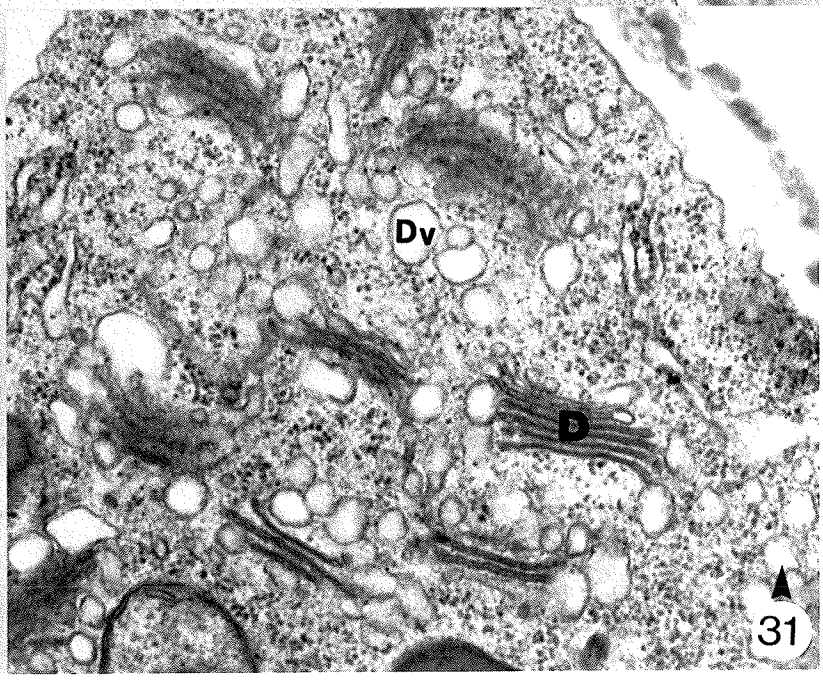
Dv
D
31

Figure 32. Electron micrograph of the chalazal region of an older 4-nucleate megagametophyte. Plasmodesmata (pd) traverse the wall between the chalazal nucellus (CN) and the megagametophyte (Mg). A membrane-bound vesicle containing tubular inclusions (Ti) lies adjacent to the megagametophyte wall. UA/Pb. x4,720.

Figure 33. Electron micrograph of the chalazal region of an older 4-nucleate megagametophyte (Mg). The section is serial to the section in figure 32. The plasma membrane (pm) of the megagametophyte wall appears continuous with the bounding membrane of the vesicle containing the tubular inclusions (Ti). Dictyosomes (D), active in vesicle production, are present in the chalazal cytoplasm of the megagametophyte. UA/Pb. x4,720.

Figures 34 to 37 represent non-adjacent serial sections through the young 8-nucleate megagametophyte of the ovule in figure 34.

Figure 34. Light micrograph of an ovule showing a young 8-nucleate megagametophyte (Mg), the outer (OI) and inner (II) integuments, the inner integument basal body (Bb), the chalazal nucellus (CN), the raphe (Ra), and the outer integument portion of the micropyle (Mi). Two juxtaposed antipodal nuclei (A) are present in the chalazal region, a synergid nucleus (S) is present in micropylar region, and two polar nuclei (PN) are present in the central region of the megagametophyte. CV. x500.

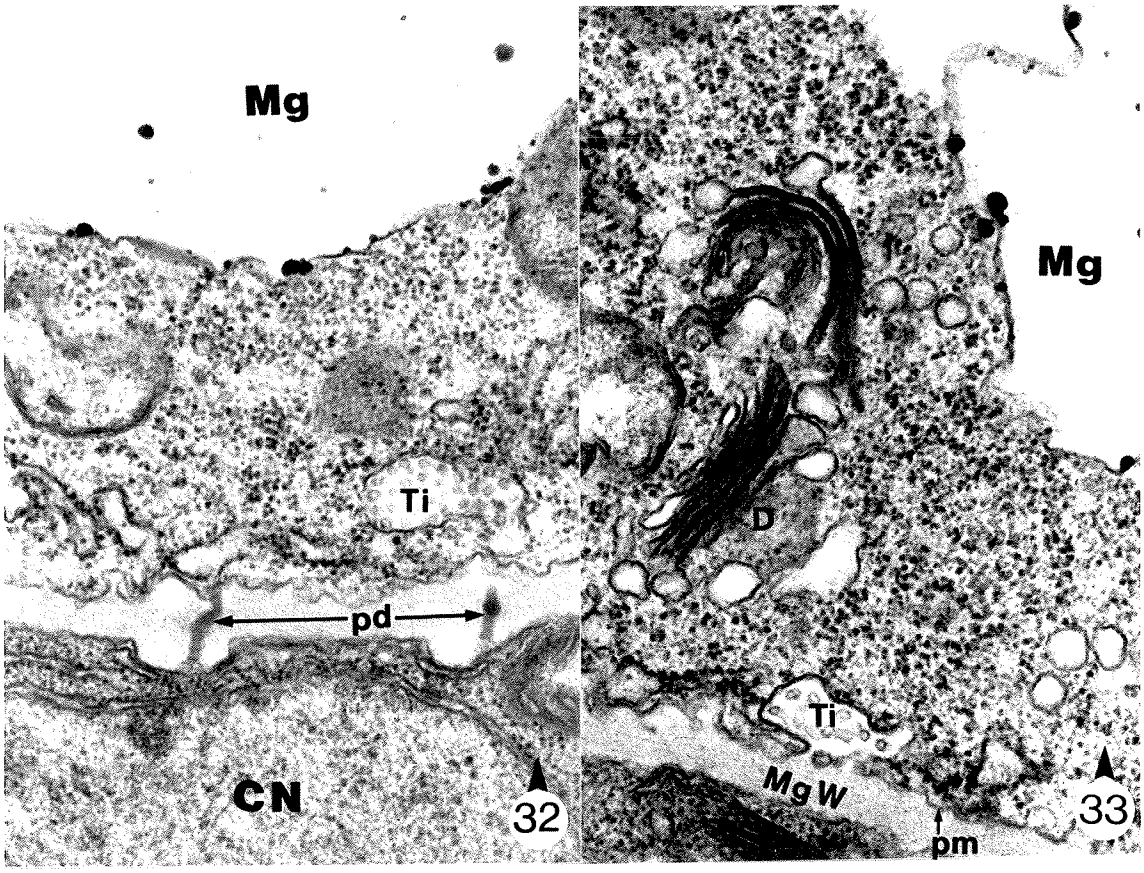

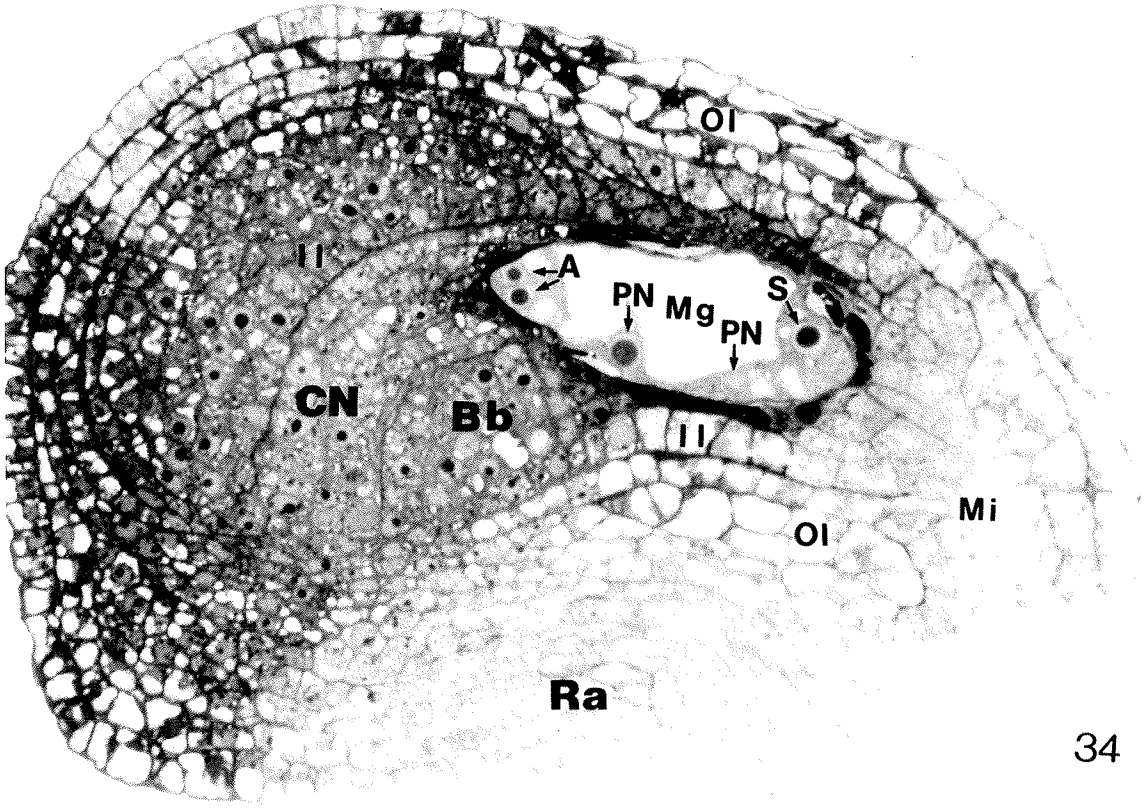

34

Figure 35. Light micrograph of the 8-nucleate megagametophyte showing two polar nuclei (PN) in the lateral region of the central cell (CC) cytoplasm and a chalazal antipodal nucleus (A) that is micropylar to the two antipodal nuclei shown in figures 34 and 38. CV. x750.

Figure 36. Light micrograph of the 8-nucleate megagametophyte showing a portion of the vacuolate synergid (S) and the adjacent egg nucleus (E) surrounded by perinuclear plastids (P). A faint boundary (arrowhead) appears to separate the synergid from the egg and from the central cell. CV. x750.

Figure 37. Light micrograph of the 8-nucleate megagametophyte showing the nucleus of the synergid (S) in figure 36. CV. x750.

Figure 38. Light micrograph of the 8-nucleate megagametophyte in figure 34, counter-stained with PAS. Two juxtaposed antipodal nuclei (A) are present in the chalazal region, a synergid nucleus (S) is present in the micropylar region, and two polar nuclei (PN) are present in the central cell (CC) region of the megagametophyte. The megagametophyte appears to be free-nuclear. The integument starch (St) is PAS positive. PAS/CV. x750.

Figure 39. Light micrograph of the 8-nucleate megagametophyte in figure 38, viewed with differential interference contrast optics. A definite partitioning of the antipodal and egg apparatus cytoplasms is evident, suggesting the presence of a cell wall. A common wall (large arrowhead) separates the juxtaposed antipodal nuclei (A) and a convexly curved wall (small arrowhead) separates the antipodals from the central cell (CC). The antipodals at this early stage of development are approximately 15 um long. The cell wall (unlabelled arrows) separating the synergid from the central cell is convexly curved and extends from the lateral to the central to micropylar end of the megagametophyte. The point of attachment of the common synergid-central cell wall to the lateral edge of the megagametophyte is approximately 20 um from the extreme micropylar end of the synergid cell (between large arrows). x800.

Figure 40. Light micrograph of a young egg apparatus showing an egg (E) and a synergid (S). The egg-central cell wall, the egg-synergid wall and the synergid-central cell wall nearest the lateral edge of the megagametophyte stain orthochromatically with crystal violet (arrowheads), while the more centripetal regions of these walls remain unstained. The synergid-central cell wall extending from the lateral megagametophyte wall shows the initial formation of the synergid hook (Sh). CV. x1,260.

Figure 41. Light micrograph of a young egg apparatus. In a slightly older egg apparatus to that in figure 40, the common cell walls of the synergid-central cell, egg-central cell, and synergid-egg are PAS positive. The egg (E) and synergid (S) cells have expanded chalazally into the central cell (CC), accentuating the synergid hook (Sh) and egg hook (Eh) regions. PAS/CV. x1,270.

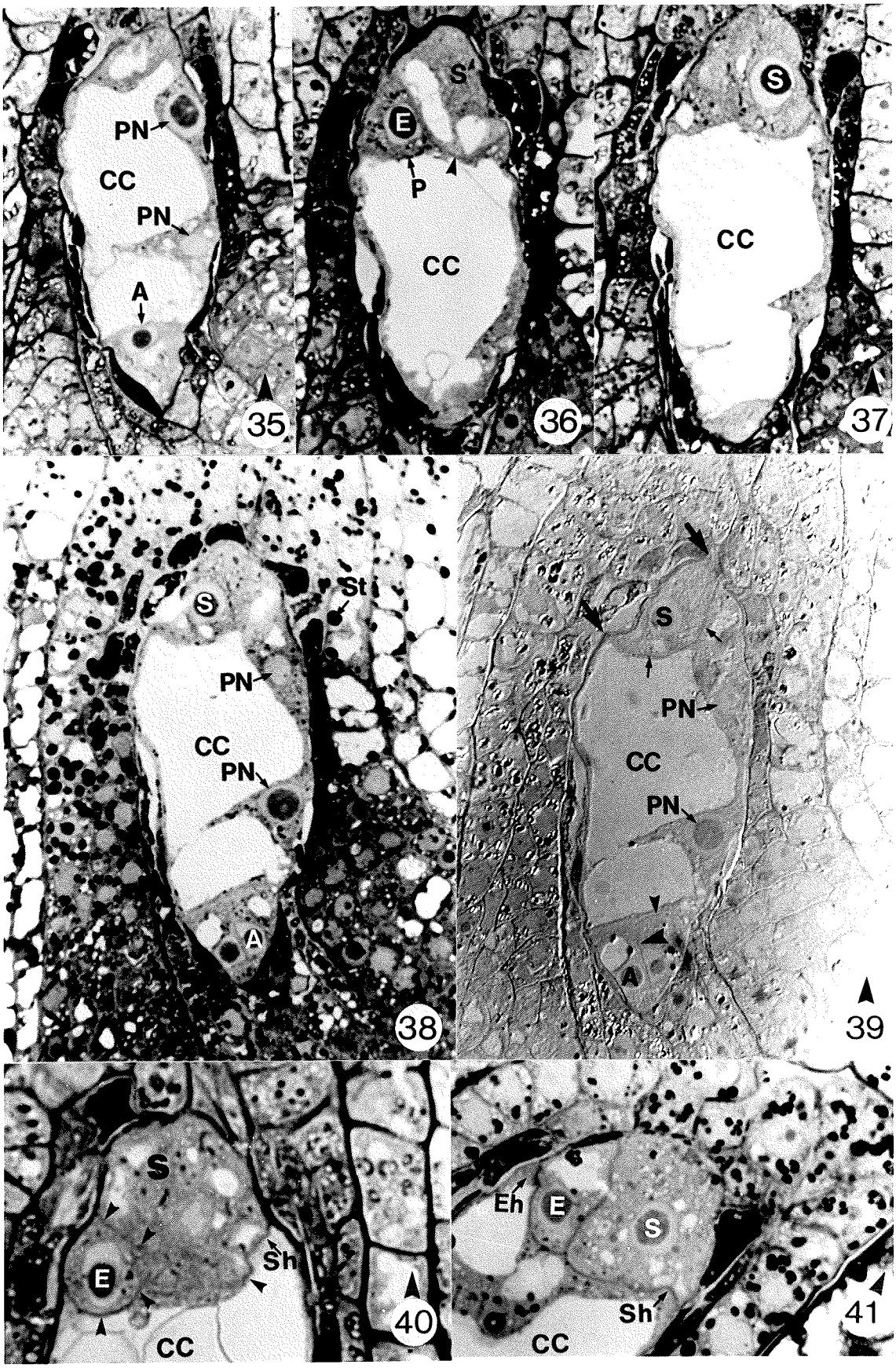
PN
CC
PN
A
35
S
E
P
CC
36
S
CC
37
S
St
PN
CC
PN
A
38
S
PN
CC
PN
A
39
S
E
Sh
CC
40
Eh
E
S
Sh
CC
41

Figure 42. Electron micrograph of a young egg apparatus. The common cell wall between the synergid (S) and egg (E), extending from the lateral wall (MgW) of the young cellular megagametophyte toward the central cell (CC), is of relatively even thickness (large arrowhead), while the more centripetal regions of the wall are of variable thickness and have a beaded appearance (small arrowheads). In this centripetal region, the wall often appears discontinuous and difficult to discern. Strands of both egg and synergid ER follow the contours of the common cell wall with some cisternae appressed to the plasma membranes (pm) of the egg and synergid. Dictyosomes (D), active in vesicle production, are visible in the synergid cell cytoplasm. Microtubules (mt) are present in the vacuole region of the synergid, between the egg and synergid nuclei (N). UA/Pb. x20,000.

Figure 43. Electron micrograph of a young 8-nucleate megagametophyte showing two synergids (S), two antipodals (A), and the edges of two polar nuclei (PN). The cytoplasm of the central cell (CC) occupies a thin band between the large central vacuole (V) and the cells of the egg apparatus, the antipodals, and the lateral edges of the megagametophyte. One of the synergids exhibits a distinctly sigmoid synergid hook (Sh). Lipid bodies (L) are present in the synergids, antipodals, and the central cell and there is starch (St) in the lateral and micropylar regions of the integuments. The epidermal cells of the inner integument, adjacent to the egg apparatus, have undergone periclinal divisions (unlabelled arrows). UA/Pb. x1,900.

Figure 44. Electron micrograph showing a surface view of the common cell wall (cw) between two antipodal cells (A). There are numerous plasmodesmata (pd) traversing the cell wall. UA/Pb. x45,400.

Figure 45. Electron micrograph of common cell wall between two young juxtaposed synergid (S) nuclei (N). Plasmodesmata (pd) interconnect the cytoplasms of the two cells and there are cisternae of ER in close proximity to the cell wall (cw) and plasmodesmata. UA/Pb. x45,400.

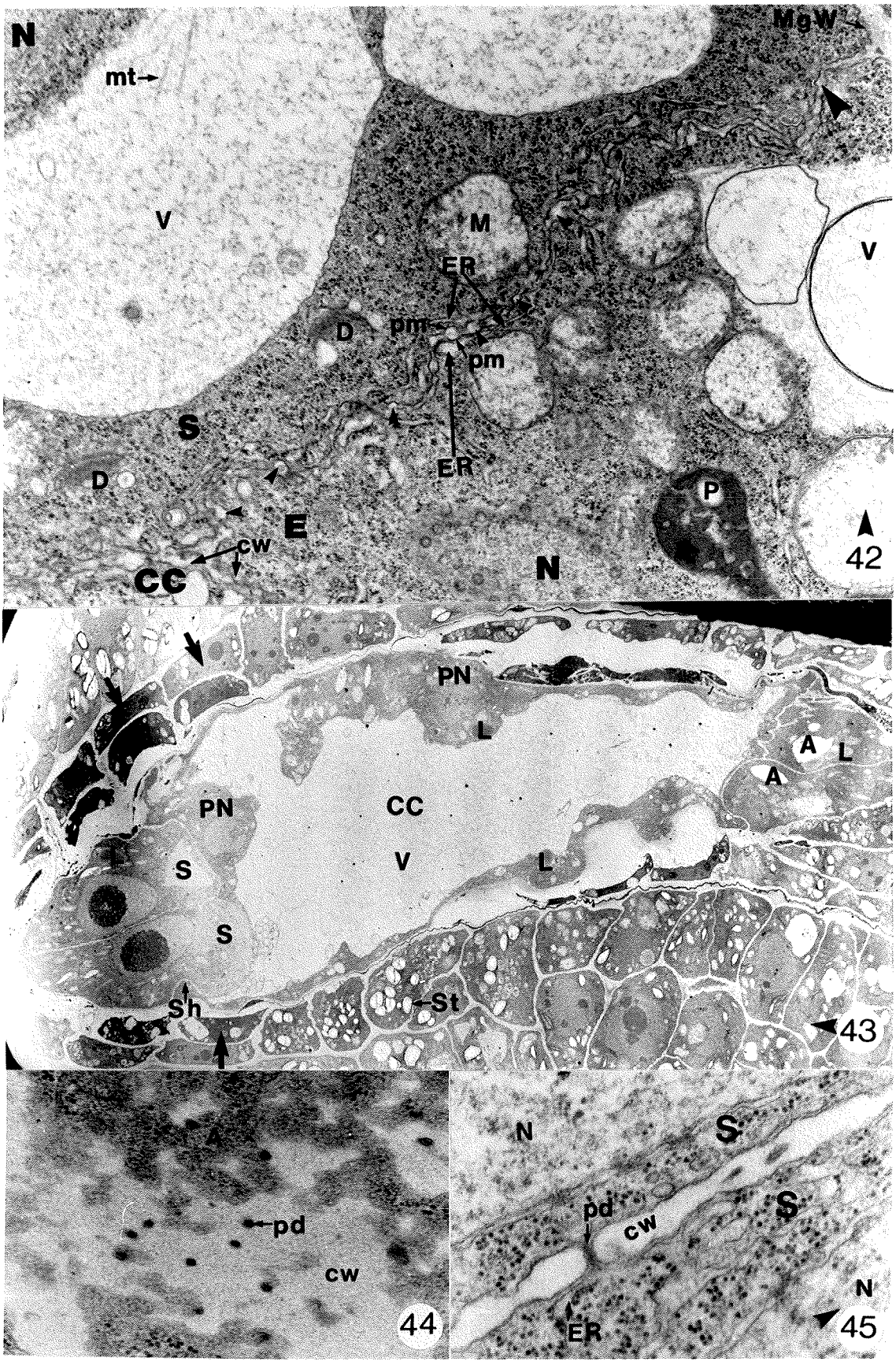
N
mt
MgW
V
M
ER
D
pm
pm
V
S
ER
D
P
E
cw
CC
N
42
PN
L
A
L
A
PN
CC
V
L
S
S
Sh
St
43
pd
cw
44
N
S
pd
cw
S
N
ER
45

Figure 46. Electron micrograph of two young antipodal cells (A). The cell walls (cw) between the antipodal cells, between the antipodals and the central cell (CC), and between the antipodals and the chalazal nucellus are electron-transparent and traversed by plasmodesmata (pd). Lipid bodies (L) are common in both the antipodal and central cell cytoplasms. The young antipodals contain mitochondria (M), plastids (P), dictyosomes (D), and ER. UA/Pd. x5,300.

Figure 47. Electron micrograph of two young synergid cells (S). The cell walls (cw) between the synergid cells, and between the synergid and central cell (CC) are electron-transparent with plasmodestmata (pd) traversing the wall between the synergid and the central cell. Continued expansion of the synergid into the central cell results in a sigmoid synergid hook (Sh). The synergids contain lipid bodies (L), ER, and dictyosomes (D) and distinctive allantoid plastids (P) and mitochondria (M). UA/Pb. x6,500.


D
CC
L
cw
A
pd
pd
P
M
E
R
A
L
CN
pd
46
PN
D
S
CC
P
pd
ER
cw
D
M
S
Sh
L
47

Figure 48. Electron micrograph of the chalazal portion of a young egg apparatus. The cytoplasms of the young egg (E), synergids (S), and the central cell are very similar with respect to organelle frequencies and morphologies. The allantoid plastids (P) are free of starch and the elliptical to allantoid mitochondria (M) exhibit well developed tubular cristae. Strands of ER permeate the cytoplasms. Dictyosomes (D) are common in all three cells. Wall projections (Wp) are beginning to form along the lateral central cell wall in the vicinity of the egg apparatus. There are numerous dictyosomes, active in vesicle production, in close proximity to developing wall projections. All the cell walls (cw) of the young egg apparatus are similar in terms of thickness and electron-transparency. UA/Pb. x10,300.

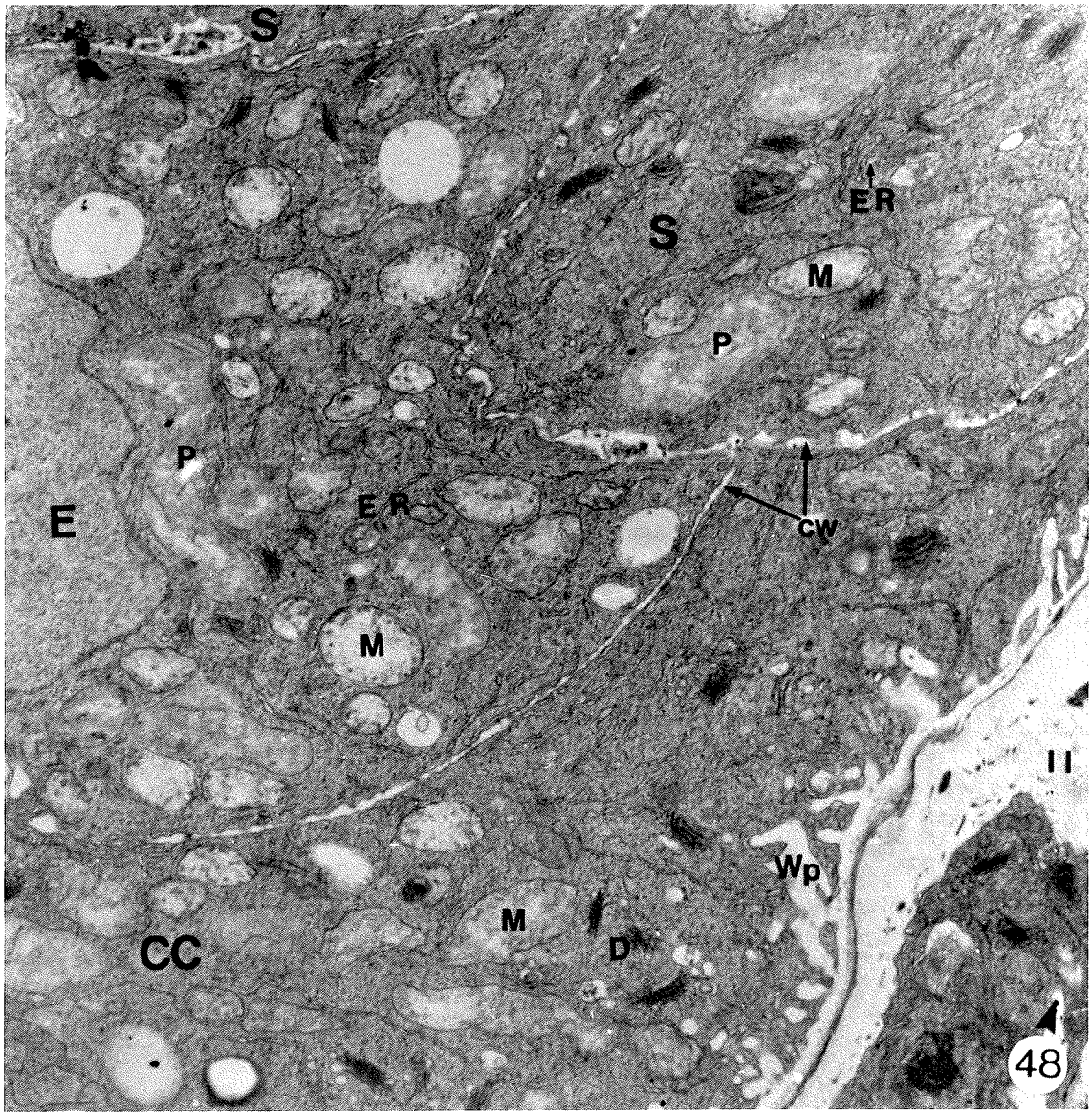
S
S
ER
M
P
P
E
ER
CW
M
II
Wp
M
D
CC
48

Figure 49. Electron micrograph of the chalazal region of a young cellular megagametophyte showing the spatial relationship between the chalazal polar nucleus (PN) and the antipodals (A). UA/Pb. x2,900.

Figure 50. Electron micrograph of the central cell cytoplasm, between the central cell vacuole and the chalazal polar nucleus (PN). There are numerous microtubules (arrowheads) with there long axes parallel to the long axis of the central cell positioned in the central cell cytoplasm lateral and adjacent to the chalazal polar nucleus. UA/Pb. x7,900.

Figure 51. Electron micrograph of the chalazal polar nucleus (PN). The perinuclear cytoplasm consists of dictyosomes (D), branched tubular smooth ER, and allantoid shaped mitochondria (M) and plastids (P). Microtubules (mt) are positioned on either side of the polar nucleus (PN). There are spiral polysomes (arrowhead) associated with the nuclear envelope which is also perforated by nuclear pores (unlabelled arrows). UA/Pb. x14,400.

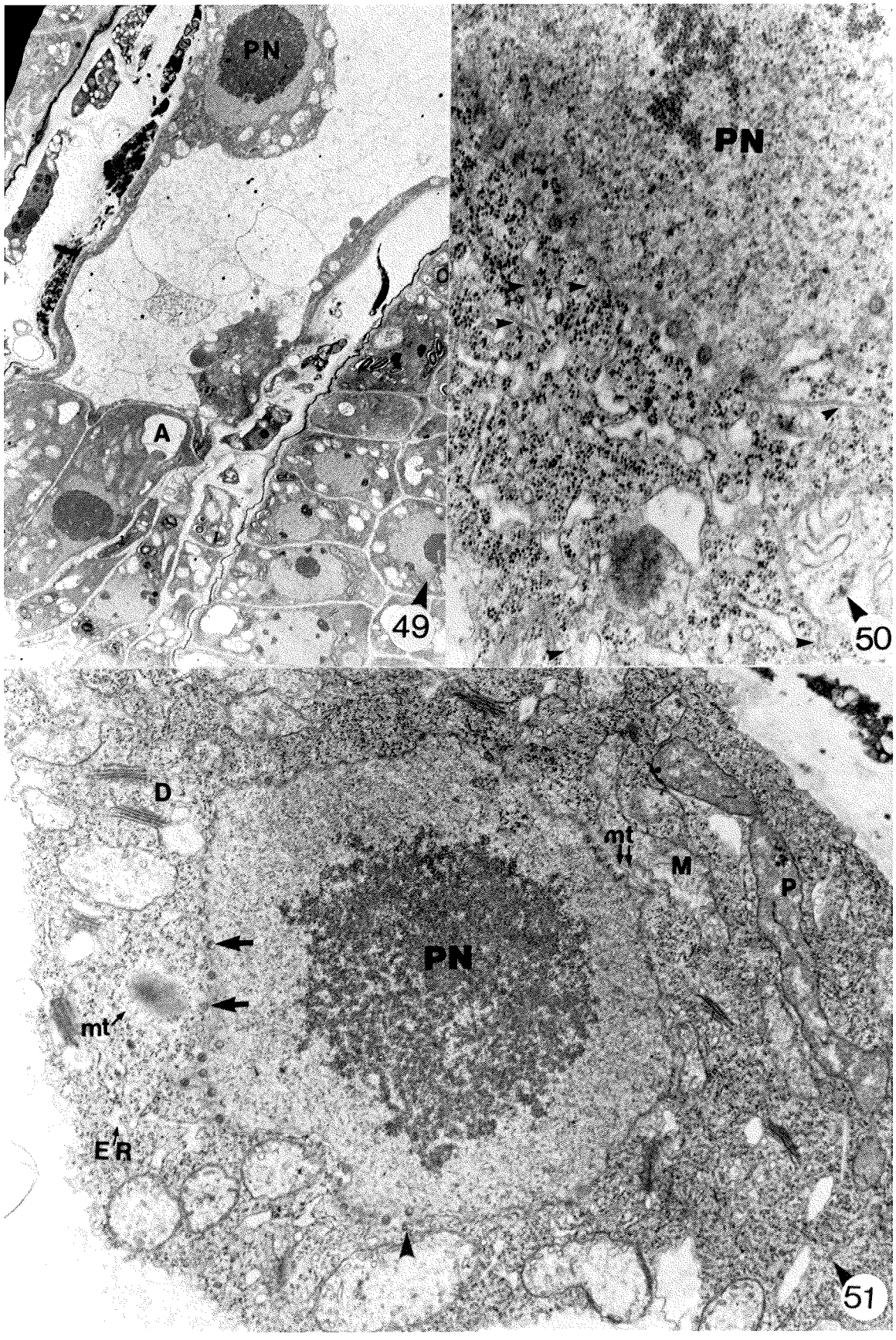
PN
PN
A
49
50
D
mt
M
P
PN
mt
ER
51

Figure 52. Light micrograph of an ovule showing a young cellular megagametophyte following the migration of the polar nuclei (PN). The two polar nuclei are appressed in the vacuolate central cell cytoplasm and surrounded by plastids containing PAS positive starch (St). Starch is common in the micropylar regions of both the inner (II) and outer (OI) integuments and in the proximal region of the funiculus (F). The inner integument basal body (Bb) and a portion of the chalazal nucellus are visible. A single synergid (S) and two antipodals (A) are also visible in the micropylar and chalazal regions of the megagametophyte. PAS/CV. x400.

Figure 53. Light micrograph showing an overview of the mature ovule at anthesis. The micrograph is derived from two non-adjacent serial sections. The proximal region of the outer integument (OI) is four-layered at anthesis. The inner integument basal body (Bb) has expanded into the chalazal nucellus (CN) and the cells of the inner integument, bordering the chalazal nucellus show a marked radial expansion. The micropylar regions of the integuments are rich in starch (St). The antipodals (A) are basiophilic and the central cell containing the polar nuclei (PN) has lost the large central vacuole. A mature synergid (S) and the egg (E) are visible in the micropylar region of megagametophyte. PAS/CV. x400.

Figure 54. Light micrograph of the raphe (Ra) region of a mature ovule at anthesis. Mature tracheary elements of xylem (xy) and sieve elements of phloem (Ph) terminate in the raphe region of the ovule at the base of the chalazal nucellus (CN). The base of the chalazal nucellus, which will form the future chalazal proliferating tissue, contains starch as does the vacuolate, subepidermal parenchyma of the raphe (arrowheads) between the proximal region of the outer integument and the funiculus . PAS/CV. x500.

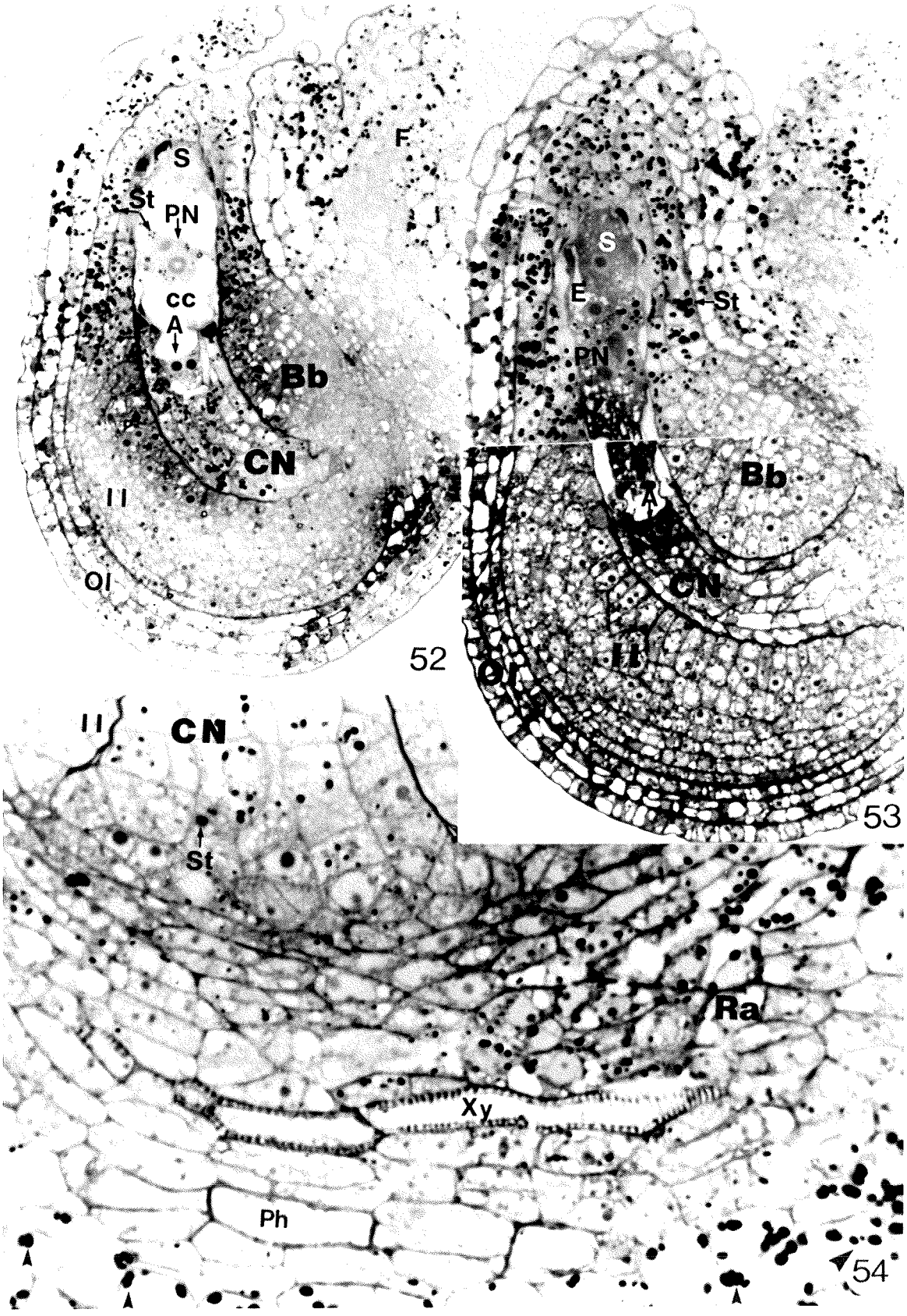
S
St
PN
cc
A
F
I
Bb
CN
II
Ol
52
S
E
St
PN
Bb
A
CN
II
Ol
53
II
CN
St
Ra
Xy
Ph
54

Figures 55-57. Mature central cell at anthesis

Figure 55. Light micrograph of the mature central cell. The polar nuclei (PN) are tightly appressed and surrounded by starch (St) containing plastids. The inner (II) and outer (OI) integuments contain starch to the level of the polar nuclei which corresponds to the distribution of central cell wall projections. The central cell wall projections appear as a hazy band (arrowheads) along the inner integument-central cell boundary. A transparent, crescent-shaped region (CR) is present in the chalazal region of the central cell. The cytoplasm of the central cell stains more intensely for protein than the adjacent cells of the inner integument. PAS/ABB. x1,150.

Figure 56. Electron micrograph of the boundary between the central cell and the inner integument at the level of the polar nuclei. Central cell wall projections (Wp) exhibit a labyrinth appearance. The distribution of wall projections coincides with the distribution of integument starch (St). Plastids (P) and mitochondria (M) in close proximity to the wall projections are present in the central cell. An electron-opaque cuticle (Cu) separates the inner integument (II) from the central cell (CC) UA/Pb. x6,700.

Figure 57. Electron micrograph of the central cell wall projections. Central cell mitochondria (M), containing fibrils of DNA in the nucleoid region (unlabelled arrow), adjacent to the wall projections (Wp) containing electron-opaque deposits. The cuticle (Cu) is continuous. UA/Pb. x42,000.

Figure 58. Electron micrograph of the central cell wall projections. A tripartite plasma membrane (pm) follows the contours of the wall projections (Wp). There are aggregations of tubular inclusions (Ti) between the discontinuous cuticle and the wall projections. UA/Pb. x42,000.

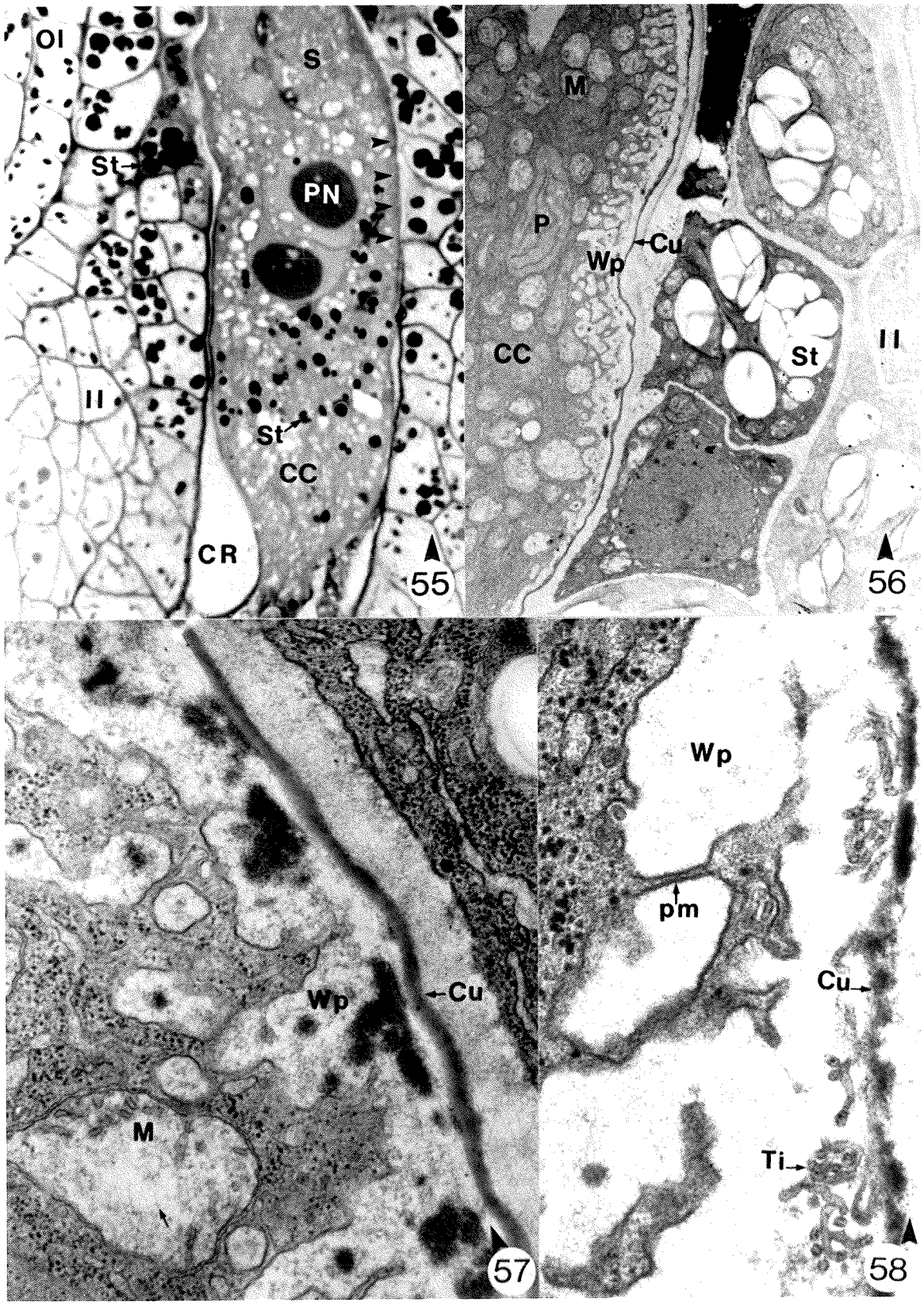
Ol
S
St
PN
II
St
CC
CR
55
M
P
Wp
Cu
CC
St
II
56
Wp
Cu
M
57
Wp
pm
Cu
Ti
58

Figures 59-63. Mature central cell at anthesis.

Figure 59. Electron micrograph of the central cell wall projections - Thiery test. There are deposits of silver proteinate over the wall projections (Wp) and the inner integument (II) wall. PA-TCH-SP. x26,900.

Figure 60. Electron micrograph of the central cell wall projections - Thiery control. There are no deposits of silver proteinate over the wall projections (Wp) or the inner integument (II) wall. H_2O-TCH-SP. x26,900.

Figure 61. Electron micrograph of dictyosomes adjacent to the central cell wall projections - Thiery test. There are deposits of silver proteinate within the vesicles (small arrowheads) being released from the maturing face (mf) of the dictyosome (D). Some of these vesicles (large arrowheads) appear to be fusing with the megagametophyte wall (MgW) and contributing to the formation of the wall projections (Wp). PA-TCH-SP. x50,600.

Figure 62. Electron micrograph of dictyosomes adjacent to the central cell wall projections - Thiery control. There are no deposits of silver proteinate within the dictyosome (D) vesicles (arrowheads). H_2O-TCH-SP. x50,600.

Figure 63. Electron micrograph of the polar nuclei and adjacent central cell cytoplasm. Mitochondria (M), ER, and lipid bodies (L) become entrapped between the two appressed faces of the polar nuclei (PN). Chloroplasts (P) with starch deposits (St), small vacuoles (V), and microbodies (Mb) occur in the central cell (CC) cytoplasm adjacent to the polar nuclei and wall projections (Wp). UA/Pb. x8,500.

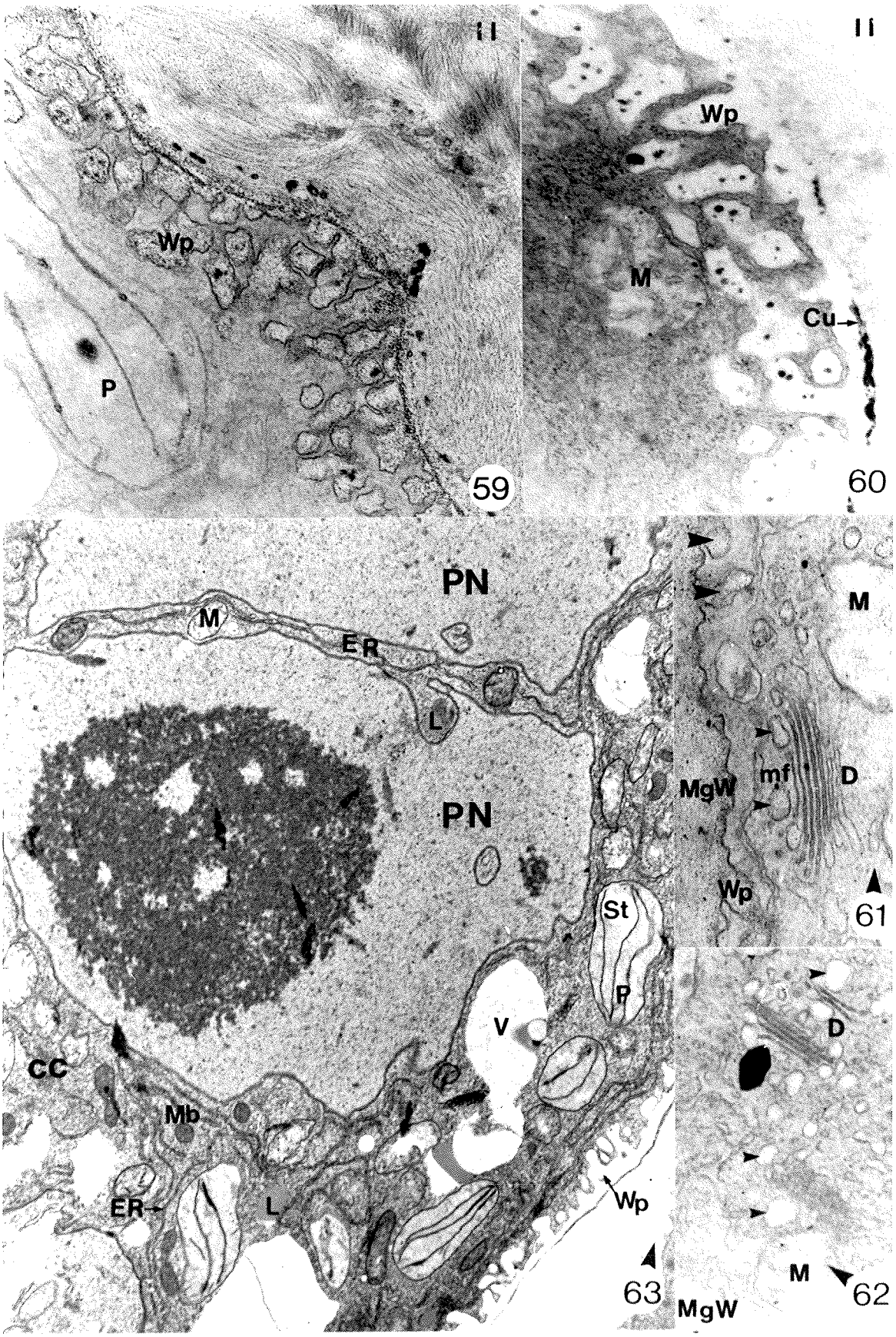
Wp
P
59
Wp
M
Cu
60
PN
M
ER
L
PN
St
P
V
CC
Mb
ER
L
Wp
63
M
MgW
mf
D
Wp
61
D
M
62
MgW

Figure 64. Electron micrograph showing the partial fusion of the two polar nuclei prior to anthesis. The nuclear envelopes (ne) of the two polar nuclei (PN) unite forming a narrow nuclear bridge (nb). Strands of RER are connected to the nuclear envelope. UA/Pb. x35,300.

Figure 65. Electron micrograph of an aggregation of ER in the cytoplasmic embayments between the post anthesis polar nuclei (PN). In surface view the tubular ER appears as stellately branched cisternae (large arrowhead) radiating around a circular perforation. In sectional view the alignment of the stellate cisternae results in a straight cylindrical channel (unlabelled arrow) between the flat tubular cisternae (small arrowhead). The are nuclear pores (np) in the nuclear envelope (ne). OsFeCN. UA/Pb. x15,700.

Figure 66. Electron micrograph of a post-anthesis central cell. The polar nuclei (PN) appear labile with wide cytoplasmic embayments (large arrowhead) containing organelles and a symmetrical aggregation of ER (small arrowhead) shown in more detail in figure 65. ER is distributed throughout the micropylar portion of the central cell (CC) and is associated with the wall projections (Wp) and the egg-central cell boundary (unlabelled arrow). There are chloroplasts (P), mitochondria (M), dictyosomes (D), and lipid bodies (L) throughout the central cell. OsFeCN. UA/Pb. x6,300.

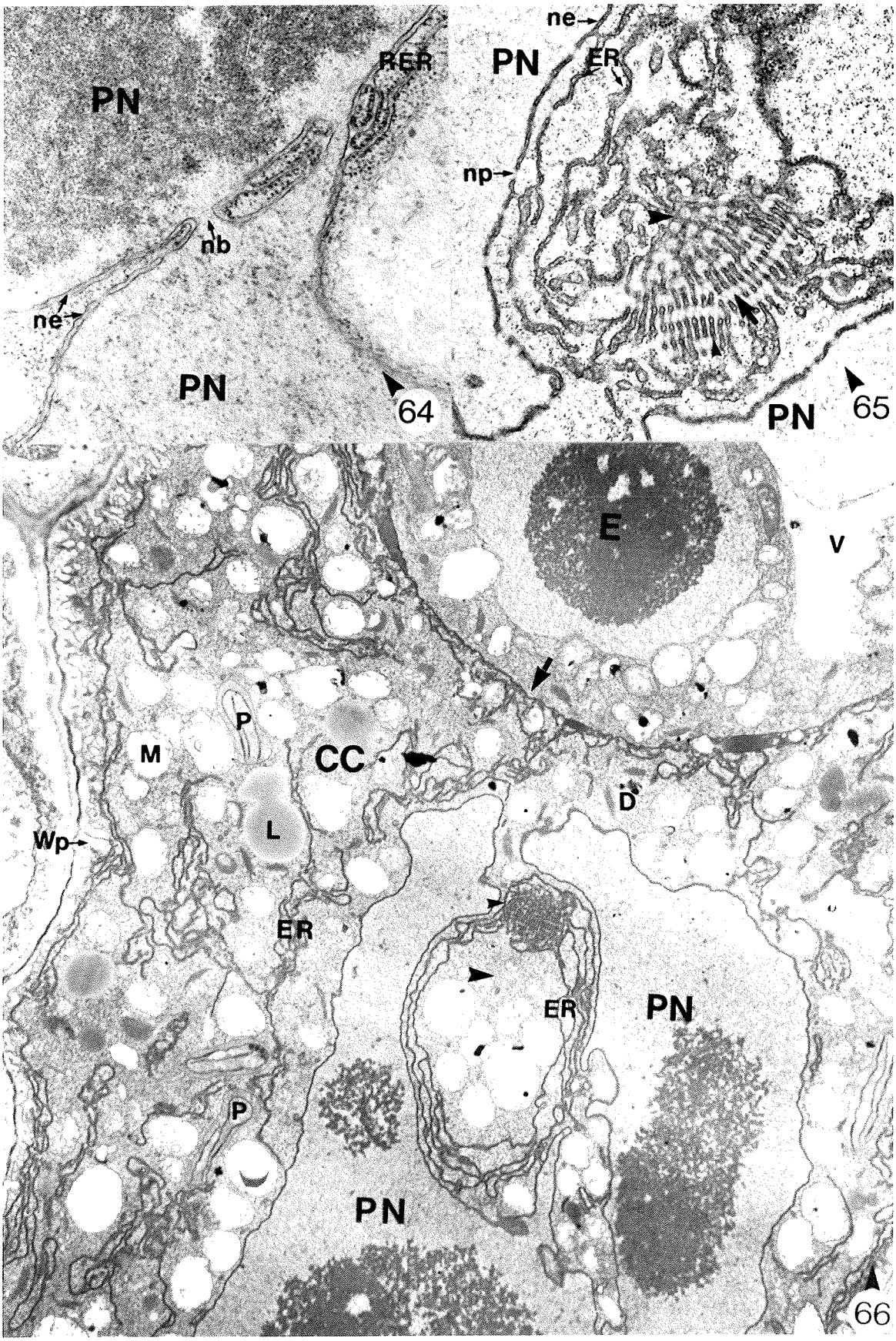
PN
RER
nb
ne
PN
64
ne
PN
ER
np
PN
65
E
V
P
M
CC
D
L
Wp
ER
ER
PN
P
PN
66

Figure 67. Electron micrograph of the chalazal boundary between the egg (E) and central cell (CC). Portions of branched central cell ER, containing electron-opaque deposits, are associated with the common egg-central cell wall (arrowheads) that is also stained by the OsFeCN method. The egg contains short strands of ER that are not stained by OsFeCN. OsFeCN. UA/Pb. x23,000.

Figure 68. Electron micrograph of the chalazal boundary between the egg (E) and central cell (CC). This boundary consists of regions of expanded cell wall (ecw) that alternate with narrower regions of cell wall between the tripartite plasma membranes (pm) of the egg and central cell. There is continuity between the tubular smooth ER (arrowhead) and the plasma membrane of the central cell. Note the similarity between the tripartite plasma membranes of the egg and central cell and the tripartite membrane of the ER cisternae (unlabelled arrow). UA/Pb. x42,400.

Figure 69. Electron micrograph of a cross-section through the megagametophyte in the mid-region of the egg apparatus. Some of the central cell mitochondria (M) are amoeboid shaped with portions of the organelle wrapped around pegs of wall projections (Wp). The cell wall (cw) between the egg and central cell contains diffuse deposits of electron-opaque material (unlabelled arrows). UA/Pb. x14,800.

Figure 70. Electron micrograph of the post-anthesis central cell cytoplasm. There are numerous spiral polysomes (large arrowhead) associated with the surface of lamellate ER cisternae and there is a close association between the lipid bodies and microbodies of the central cell. Following OsFeCN fixation the nucleoid regions of the mitochondria appear electron-transparent (small arrowhead). The dictyosome (D) cisternae contain electron-opaque deposits while the cisternae of the ER are unstained. Compare with figure 67, also fixed by the OsFeCN method. OsFeCN. UA/Pb. x17,200.

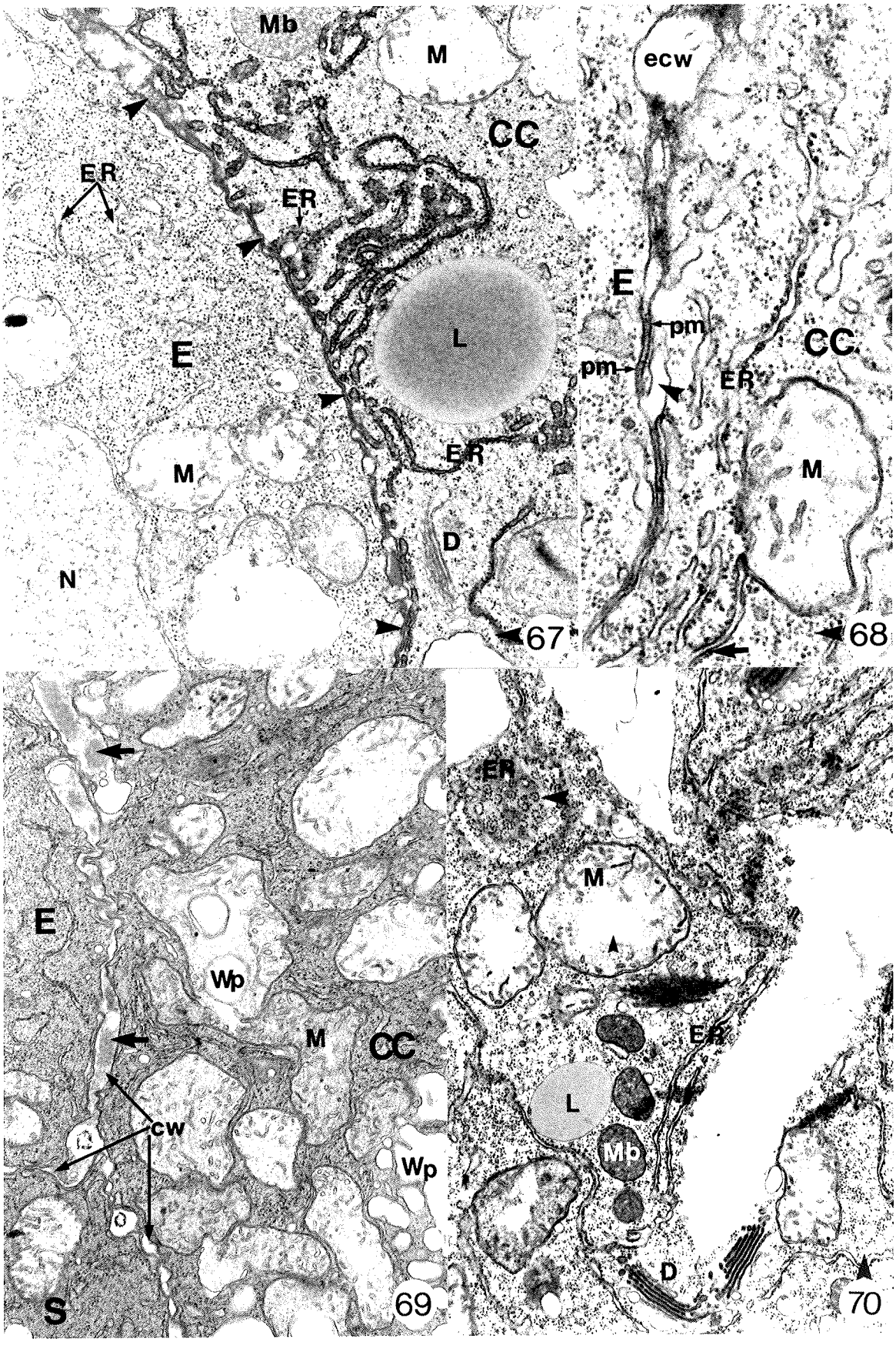
Mb
M
CC
ER
ER
E
L
ER
M
D
N
67
ecw
E
pm
pm
CC
ER
M
68
E
Wp
M
CC
cw
Wp
S
69
ER
M
ER
L
Mb
D
70

Figures 71-74. Mature antipodal cells at anthesis

Figure 71. Electron micrograph showing an overview of two of three antipodal cells (A) situated in the extreme chalazal region of the megagametophyte. A wrinkled electron-transparent cell wall separates the antipodal cells from one another and from the central cell (CC). The only vacuolated region in the mature central cell is in the extreme chalazal region, adjacent to the antipodals. OsFeCN. UA/Pb. x3,600.

Figure 72. Epifluorescence light micrograph of mature antipodals. Antipodal cell walls (cw) are strongly fluorescent when stained with Calcofluor and viewed under UV light. x400.

Figure 73. Electron micrograph of the cell wall between the antipodal and central cells. The electron-transparent cell wall between the antipodals and the central cell is evaginated (arrowhead) and contains numerous plasmodesmata (pd). Antipodal cell ER is predominantly rough while that of the adjacent central cell is predominantly smooth. UA/Pb. x45,000.

Figure 74. Electron micrograph of two mature antipodal cells. Strands of ER encircle the antipodal cell nucleus. Proplastids (P) , mitochondria (M) and dictyosomes (D) are present, but the majority of cell volume is occupied by nucleus. OsFeCN. UA/Pb. x10,300.

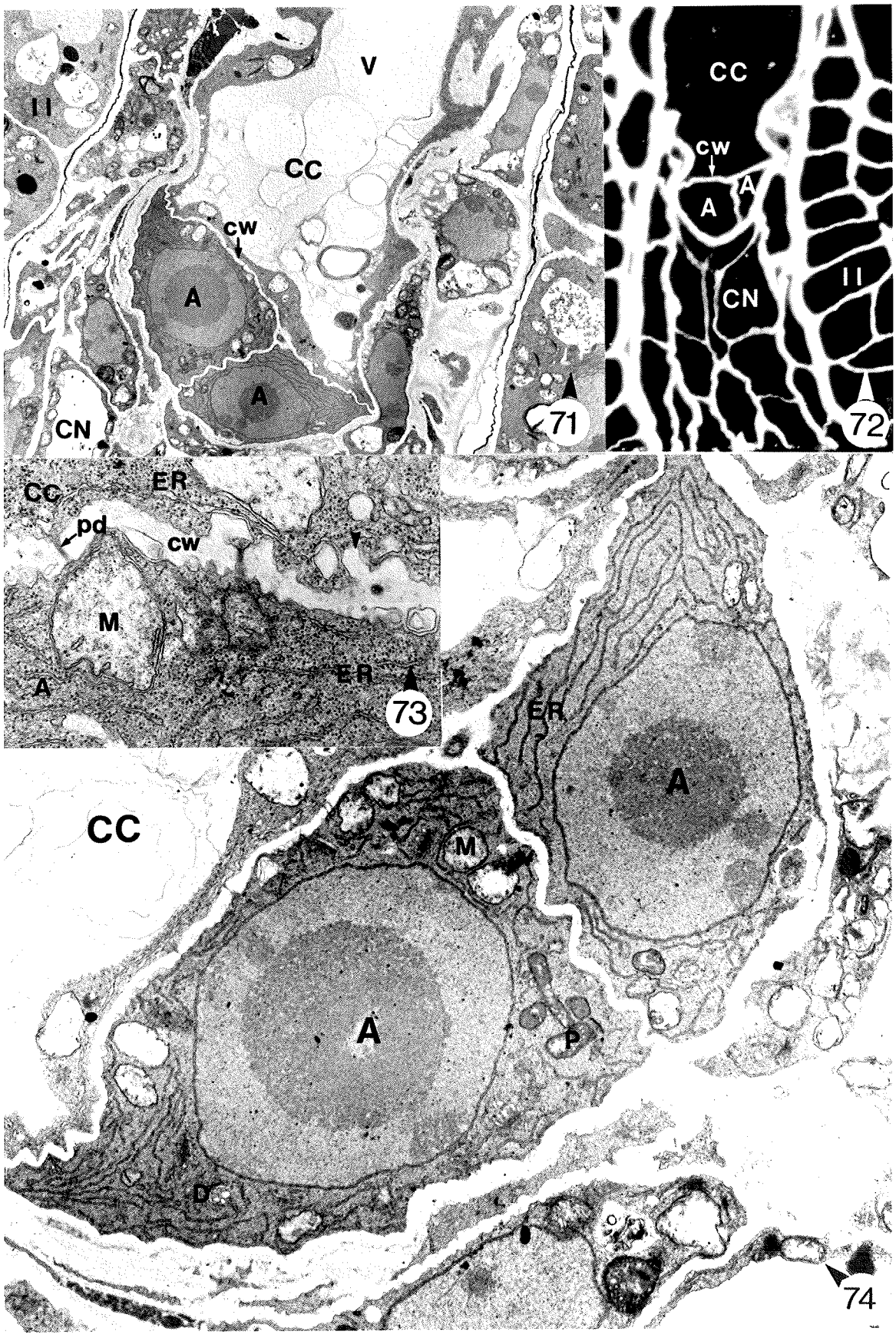
II
V
CC
cw
A
A
CN
71
CC
cw
A
A
CN
II
72
CC
ER
pd
cw
M
A
ER
73
ER
A
CC
M
A
P
D
74

Figures 75-77. Mature antipodal cells.

Figure 75. Electron micrograph of the cell wall between the antipodal and central cells -Thiery test. There are deposits of silver proteinate over the common cell wall, including the evaginated regions (arrowhead), between the antipodals and the central cell. There are no deposits of silver proteinate in the dictyosome vesicles (Dv) of the antipodal cell. PA-TCH-SP. x29,300.

Figure 76. Electron micrograph of the cell wall between the antipodal and central cells - Thiery control. There are no deposits of silver proteinate over the common cell wall, including the evaginated regions (arrowhead), between the antipodals and the central cell. There are no deposits of silver proteinate in the dictyosome vesicles (Dv) of the antipodal cell. H_2O-TCH-SP. x29,900.

Figure 77. Electron micrograph of a mature antipodal cell 4 h post-anthesis. The ER has become dilated (DER) and there are ER-derived double membrane-bound inclusions (dmi) enclosing regions of antipodal cell cytoplasm. An electron-opaque cuticle (cu) is present on the outer wall of the inner integument (II) epidermis. UA/Pb. x9,000.

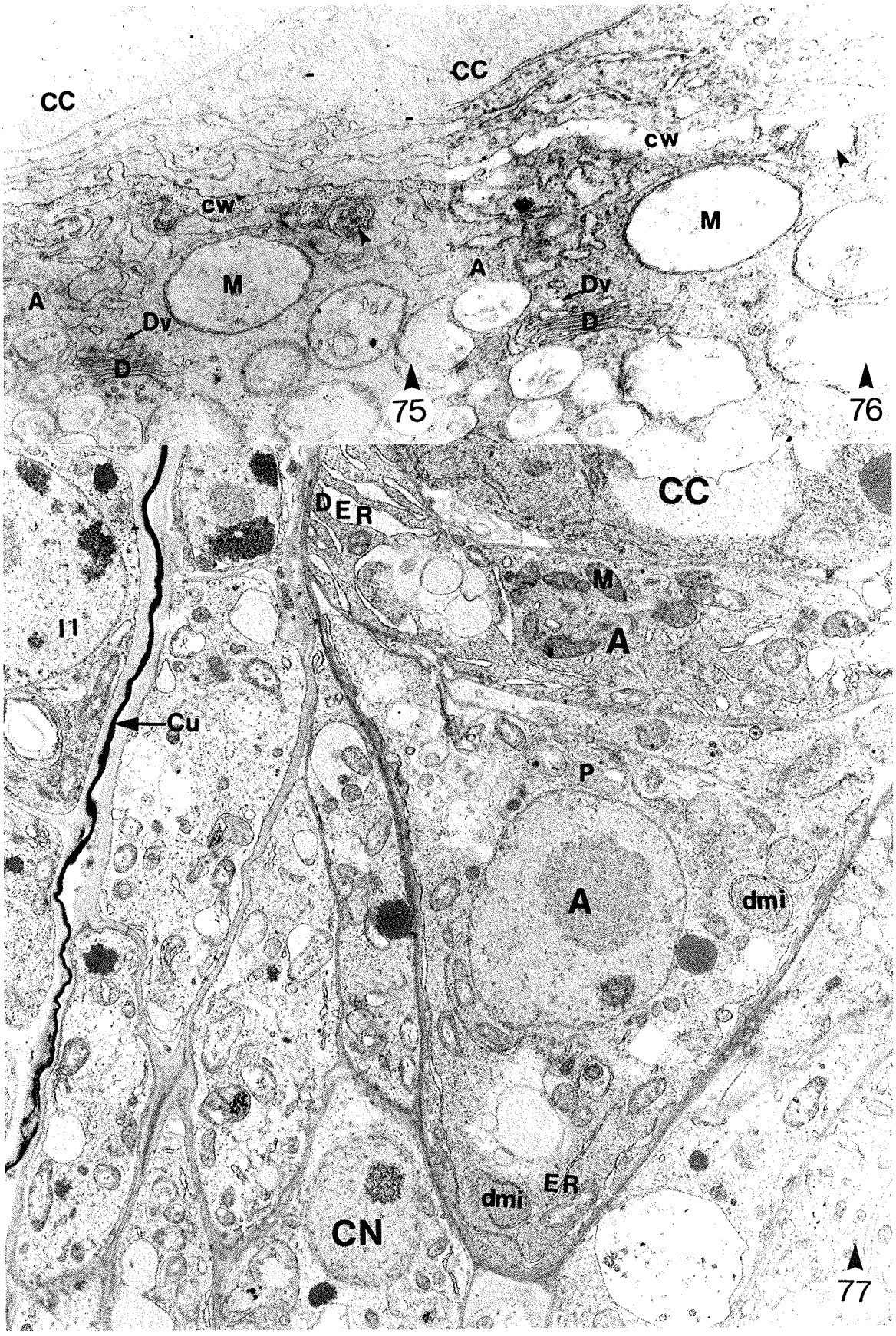
CC
cw
M
A
Dv
D
75
CC
cw
M
A
Dv
D
76
CC
DER
M
A
II
Cu
P
A
dmi
dmi
ER
CN
77

Figure 78. Electron micrograph of the mature egg apparatus at anthesis. The cell walls (cw) in the micropylar region of the egg apparatus, between the egg and the central cell, between the synergid and the egg, and between the synergid and the central cell, consist of an electron-transparent region traversed by plasmodesmata (pd). The wall between the chalazal region of the synergid and the egg consists of two appressed plasma membranes (small arrowheads) as does the wall between the synergid and the central cell (Large arrowheads). The chalazal wall between the egg and central cell consists of electron-transparent expanded regions of cell wall (ecw) alternating with deposits of electron-opaque material (unlabelled arrow). Plastids (P) and mitochondria (M) are found in the chalazal, middle and perinuclear regions of the egg and synergid. The synergid cell is rich in RER and dictyosomes (D). UA/Pb. x7,700.

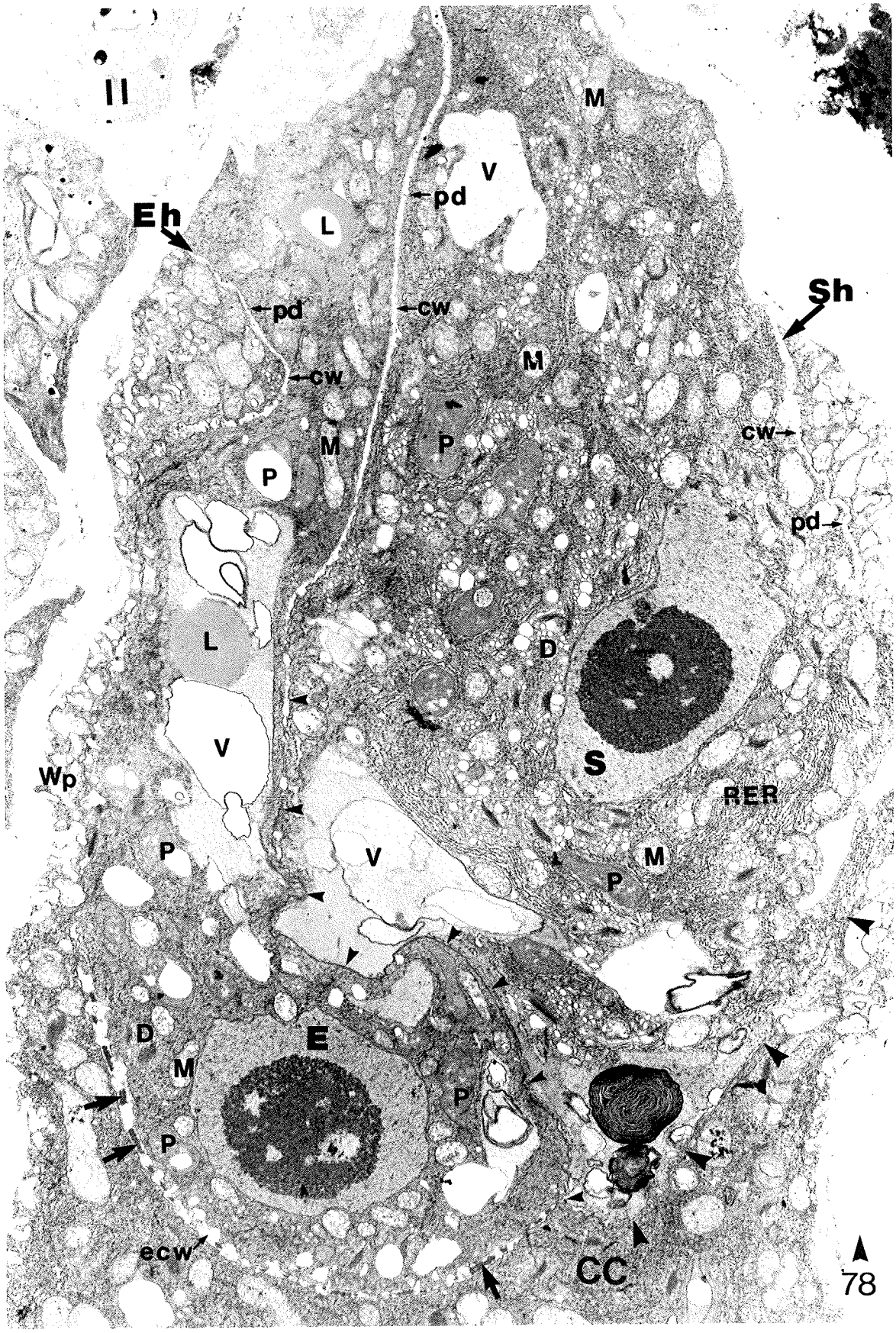
II
M
V
pd
Eh
L
Sh
pd
cw
cw
M
M
P
P
cw
pd
L
D
S
V
Wp
RER
P
V
M
P
D
E
M
P
P
ecw
CC
78

Figure 79. Electron micrograph showing a cross-section through the mid-region of a mature egg apparatus at anthesis. Thin electron-transparent cell walls (cw) separate the two synergid cells (S), the synergid and the central cell (CC), and the synergid and the vacuolate egg (E)(arrowheads). The cell wall between the egg and the central cell is wider and contains electron-opaque deposits (unlabelled arrows). Wall projections (Wp) circumscribe the central cell. The synergid cells contain plastids (P), lipids (L) , microbodies (Mb), small vacuoles (V) and are particularly rich in mitochondria (M), dictyosomes (D), and RER. The egg contains plastids and mitochondria and a prominent central vacuole (V). UA/Pb. x7,100.

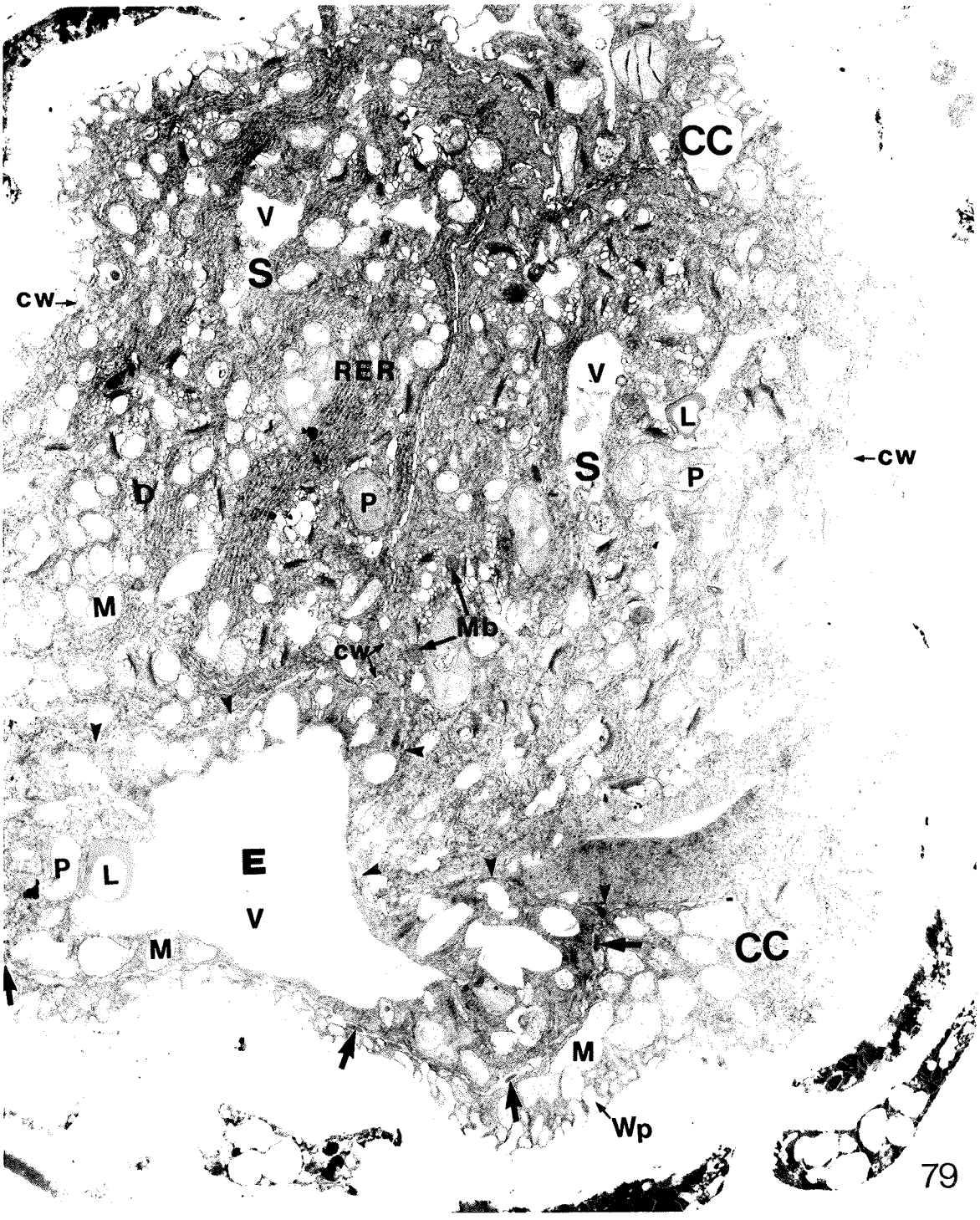
CC
V
S
cw
RER
V
L
S
P
cw
P
M
Mb
cw
P
L
E
V
M
CC
M
Wp

Figure 80. Light micrograph showing a cross-section through the mid-region of a mature egg apparatus at anthesis. The two juxtaposed synergid (S) nuclei (N) are separated by a cell wall that stains metachromatic pink with crystal violet. The 12 o'clock - 6 o'clock axis is the adaxial-abaxial sagittal plane of the mature ovule. A portion of the egg (E) is visible in the lower right quadrant. CV. x1,150.

Figure 81. Electron micrograph of a synergid dictyosome at anthesis. The dictyosome is composed of 6 flattened cisternae with a distinct forming face (ff) and a maturing face (mf) that is active in the production of vesicles (Dv). The cisternae and the vesicles are bounded by a tripartite membrane (unlabelled arrows). There are transition vesicles (arrowheads) between the ER and the dictyosome. UA/Pb. x80,800.

Figure 82. Electron micrograph showing a cross-section through the mid-region of the synergids (S), chalazal to the synergid nuclei. There is an abundance of parallel RER cisternae interspersed with mitochondria (M) with tubular cristae, and dictyosomes (D) active in vesicle production (small arrowheads). Some of the dictyosome-derived vesicles appear to have fused into larger vesicles (large arrowhead). Cisternae of smooth ER periodically become dilated (DER) forming irregular shaped vacuoles. ER cisternae (unlabelled arrows) are tightly appressed to the synergid cell wall (cw). UA/Pb. x18,100.

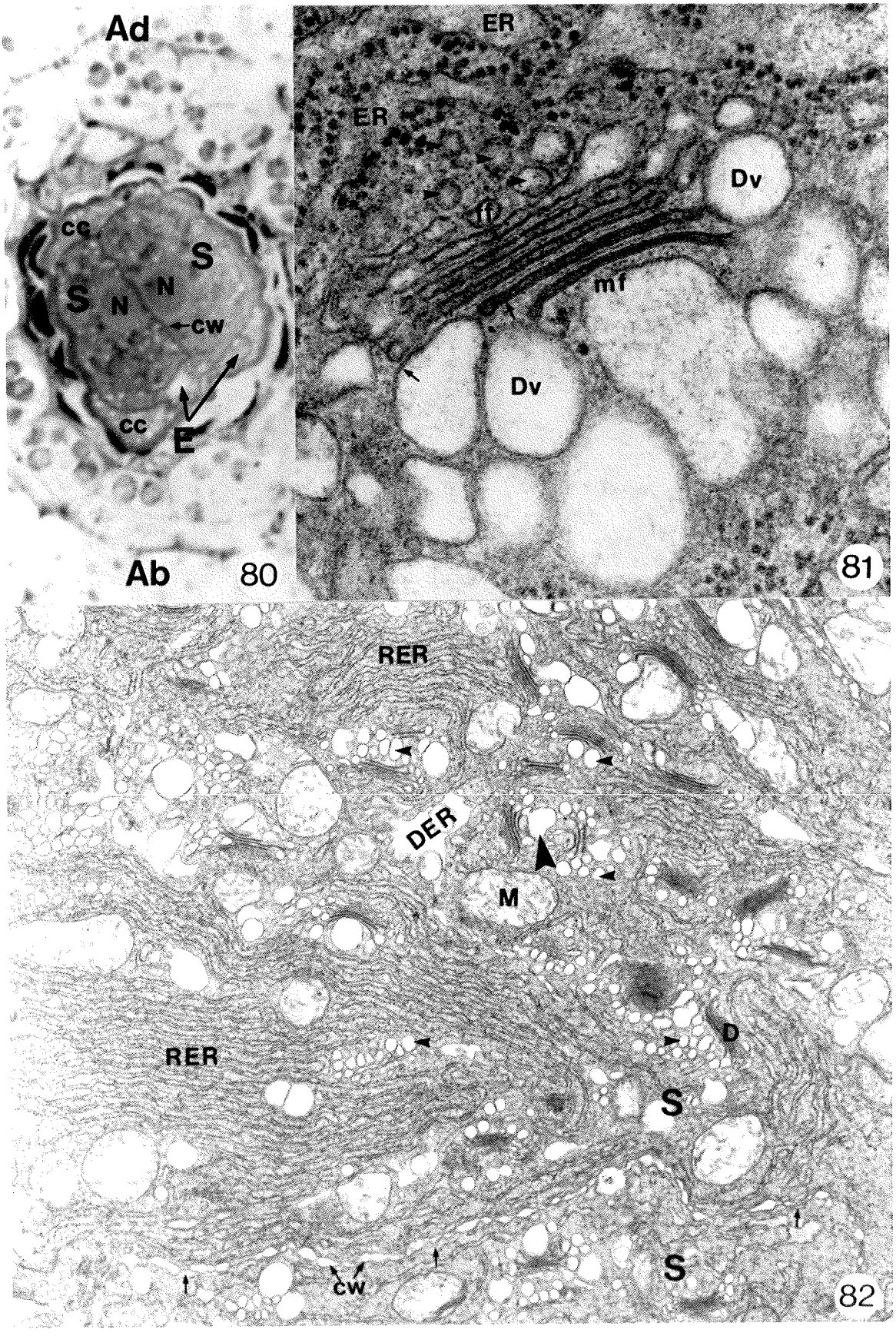
Ad
cc
S
N
S
N
cw
cc
E
Ab
80
ER
ER
Dv
ff
mf
Dv
81
RER
DER
M
RER
D
S
S
cw
82

Figures 83-85. Light micrographs of the egg apparatus at anthesis.

Figure 83. The synergid cell contains a large number of dictyosomes (D) that appear as basiophilic discs when stained with crystal violet. The electron-opaque deposits of the egg-central cell wall stain orthochromatically with crystal violet (unlabelled arrows). The filiform apparatus (Fa), synergid hook (Sh), and egg hook (Eh) regions are evident. PAS/CV. x1,100.

Figure 84. The filiform apparatus (Fa), and the micropylar walls of the egg apparatus between the two synergid cells, in the region of the synergid hook (Sh) and the chalazal wall between the egg and central cell are PAS poitive. The cell wall separating the chalazal region of the synergid from the egg and the chalazal region of the synergid from the central cell yield a faint PAS positive reaction (arrowheads). There are PAS positive starch deposits in the egg, synergid, central cell, and integuments. The egg, synergid, and central cell cytoplasms and the nucleoli stain a light blue with ABB. PAS/ABB. x980.

Figure 85. The cell wall (cw) between the two synergids (S) and the filiform apparatus (Fa), including the finger-like projections that extend deep into the synergid cell (arrowheads), stain positively for acidic polysaccharides. Alcian blue. x1,100.

Figure 86. Electron micrograph of the micropylar region of the persistent synergid (PS) and the incipient degenerate synergid (DS). The filiform apparatus (Fa) consists of an electron-opaque core (large arrowhead) surrounded by an outer electron-transparent region (small arrowhead). Finger-like electron transparent projections of the filiform apparatus (unlabelled arrows) extend into the chalazal region of the synergid. Plasmodesmata (pd) traverse the wall between the two synergids. There are electron-opaque deposits in the micropylar ER of the persistent synergid which are absent from the ER of the degenerate synergid. OsFeCN. UA/Pb. x9,400.

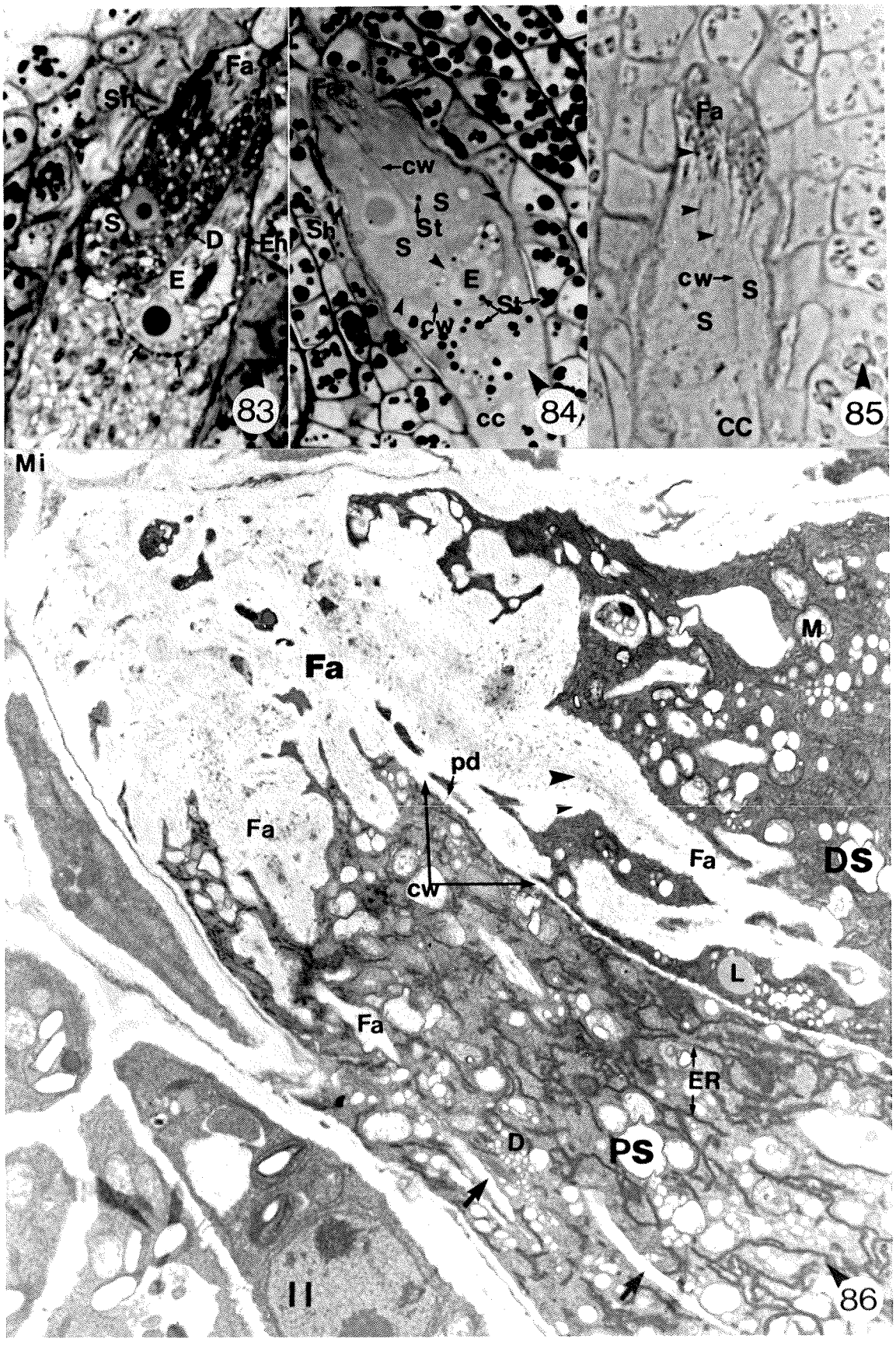
Fa
Sh
S
D
Eh
E
83
Fa
cw
S
Sh
St
S
E
St
cw
cc
84
Fa
cw
S
S
CC
85
Mi
Fa
M
pd
Fa
cw
Fa
DS
L
Fa
ER
D
PS
II
86

Figure 87. Electron micrograph of the mid-region of the two synergids (S) adjacent to the nucleus (N) - Thiery test. There are silver proteinate deposits over the common synergid-synergid cell wall (cw), over plastid (P) starch, over the finger-like projection of the filiform apparatus (Fa), and over the dictyosome vesicles (unlabelled arrows) being released from the maturing face (mf) of the dictyosome. The dictyosome vesicles (arrowheads) at the forming face (ff) are free of silver proteinate deposits. PA-TCH-SP. x26,200.

Figure 88. Electron micrograph of the mid-region of the two synergids (S) adjacent to the nuclei (N) - Thiery control. There are no silver proteinate deposits over the common synergid-synergid cell wall (cw), over the plastid (P) starch, or within the dictyosome vesicles (arrowheads). H_2O-TCH-SP. x27,200.

Figure 89. Electron micrograph of the chalazal region of the synergid (S), adjacent to the egg (E) - Thiery test. There are deposits of silver proteinate over the undulating cell wall (cw) between the synergid and the egg and over the dictyosome vesicles (large unlabelled arrow) being released from the maturing face (mf) of a synergid dictyosome. The vesicles at the forming face (ff) of the synergid dictyosome and the vesicles at the maturing face (small unlabelled arrows) of the egg dictyosome are free of silver proteinate deposits. Strands of synergid ER are closely appressed to the undulating cell wall. PA-TCH-SP. x27,600.

Figure 90. Electron micrograph of the chalazal region of the synergid (S), adjacent to the egg (E) - Thiery control. There are no deposits of silver proteinate over the undulating cell wall (cw) between the synergid and the egg or over the dictyosome vesicles (arrowheads) being released from the maturing face (mf) of a synergid dictyosome. The vesicles at the maturing face (small unlabelled arrow) of the egg dictyosome are free of silver proteinate deposits. H_2O-TCH-SP. x25,600.

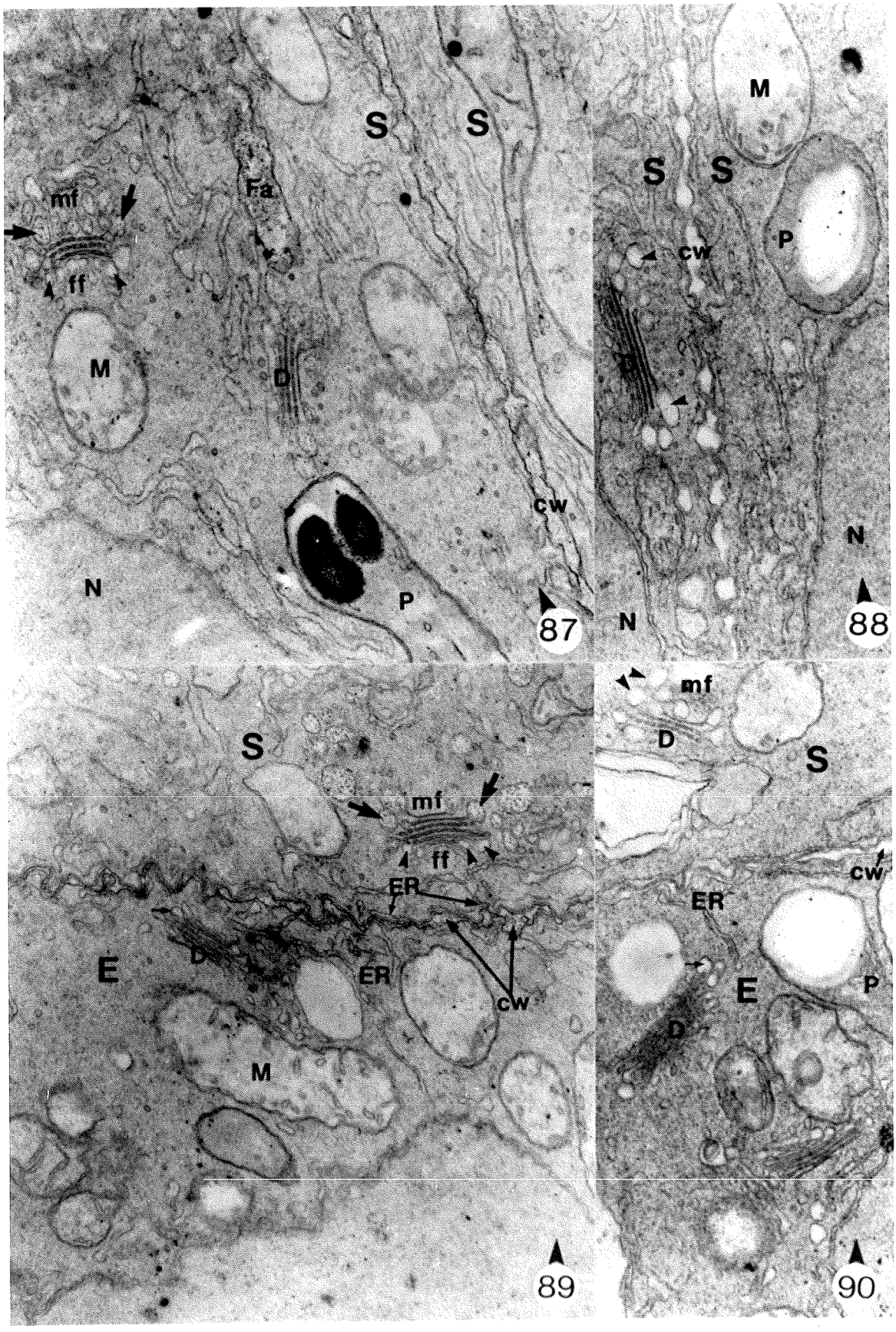
S
S
mf
Fa
ff
M
D
cw
N
P
87
M
S
S
P
cw
N
N
88
S
mf
ff
ER
D
E
ER
cw
M
89
mf
D
S
cw
ER
E
P
D
90

Figure 91. Electron micrograph of the micropylar region of the two synergids (S) - Thiery test. There are silver proteinate deposits over the common synergid-synergid cell wall (cw), over the filiform apparatus (Fa), and over the dictyosome vesicles (unlabelled arrows) being released from the maturing face (mf) of the dictyosome. The dictyosome vesicles (arrowheads) at the forming face (ff) are free of silver proteinate deposits. The plasma membrane (pm) follows the contours of the filiform apparatus. PA-TCH-SP. x16,000.

Figure 92. Electron micrograph of the micropylar region of the two synergids (S) - Thiery control. There are no silver proteinate deposits over the common synergid-synergid cell wall (cw) or within the dictyosome vesicles (arrowheads). H_2O-TCH-SP. x22,000.

Figure 93. Electron micrograph of the filiform apparatus (Fa) - Thiery test. There are deposits of silver proteinate over the entire filiform apparatus and within the vesicles (Dv) being released from the dictyosome (D). Numerous dictyosome-like vesicles (small arrowheads) containing deposits of silver proteinate are in close proximity to the filiform apparatus where there is an apparent fusion of the vesicles (large arrowheads). PA-TCH-SP. x35,300.

Figure 94. Electron micrograph of the filiform apparatus (Fa) - Thiery control. There is a virtual absence of silver proteinate over the entire filiform apparatus as well as the dictyosome vesicles, and the dictyosome-like vesicles (arrowhead) fusing to the peripheral walls. H_2O-TCH-SP. x26,400.

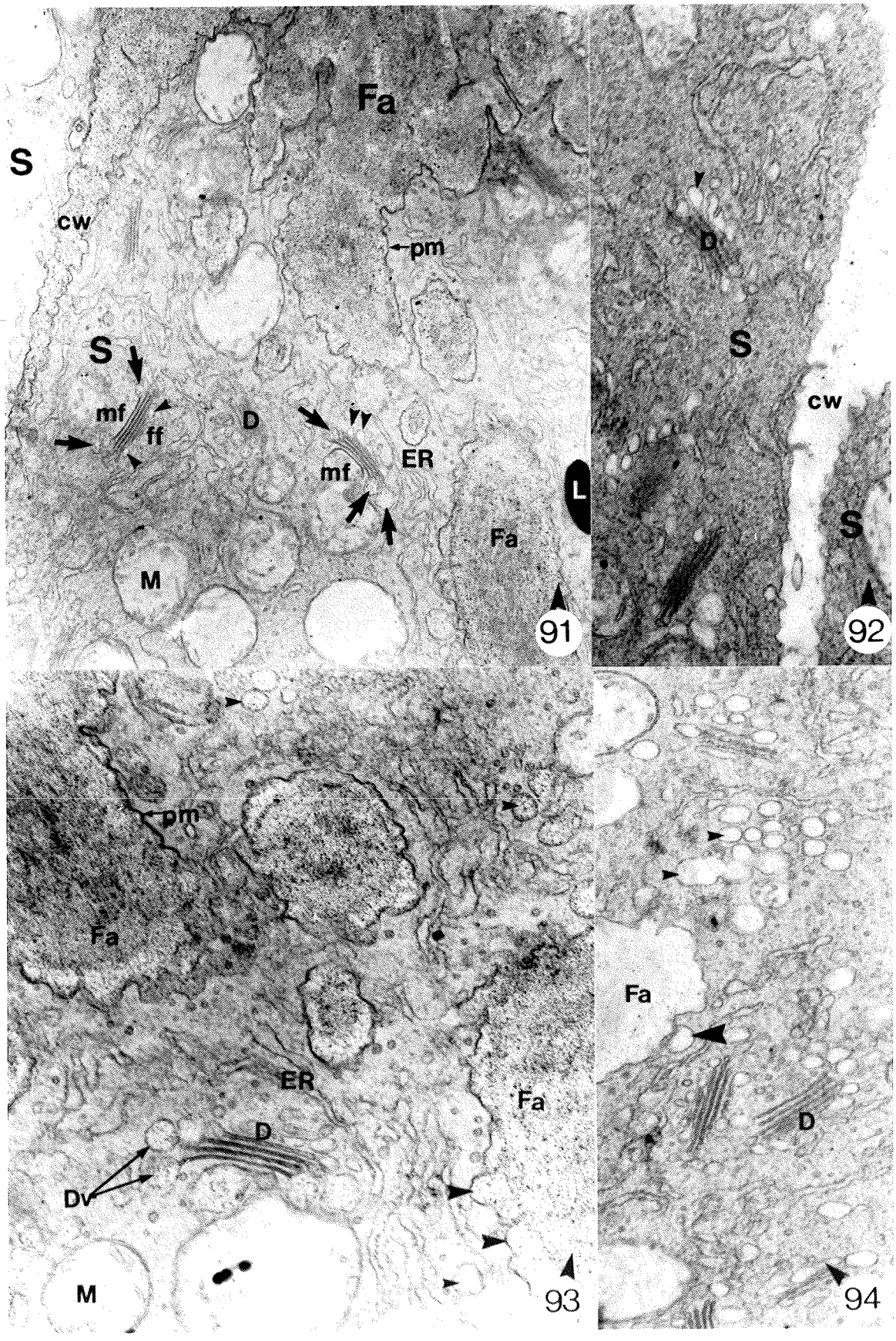
Fa
S
cw
pm
S
mf
ff
D
mf
ER
L
Fa
M
91
D
S
cw
S
92
pm
Fa
ER
Fa
D
Dv
M
93
Fa
D
94

Figure 95. Electron micrograph of the common cell wall between the egg (E) and central cell (CC) - Thiery test. There are deposits of silver proteinate over the expanded region of cell wall (ecw), over the region of electron-opaque deposits (unlabelled arrow), and the narrow zone of common cell wall (Arrowhead). There are also deposits of silver proteinate over the plastid (P) starch. PA-TCH-SP. x37,500.

Figure 96. Electron micrograph of the common cell wall between the egg (E) and central cell (CC) - Thiery control. There are no deposits of silver proteinate over the expanded region of cell wall (ecw), over the region of electron-opaque deposits (unlabelled arrow), or the narrow zone of common cell wall (Arrowhead). H_2O-TCH-SP. x36,000.

Figure 97. Electron micrograph of the chalazal tip of the egg (E) and synergids (S) showing a portion of the central cell (CC) polar nucleus (PN). The common cell wall between the egg and central cell contains elliptical deposits of electron-opaque material (unlabelled arrows). The egg contains perinuclear mitochondria (M) and plastids (P) with electron-transparent deposits of starch. The chalazal boundary between the egg and synergid consists of two appressed plasma membranes (pm) with strands of synergid smooth ER (SER) tightly appressed to the synergid plasma membrane. OsFeCN. UA/Pb. x10,300.

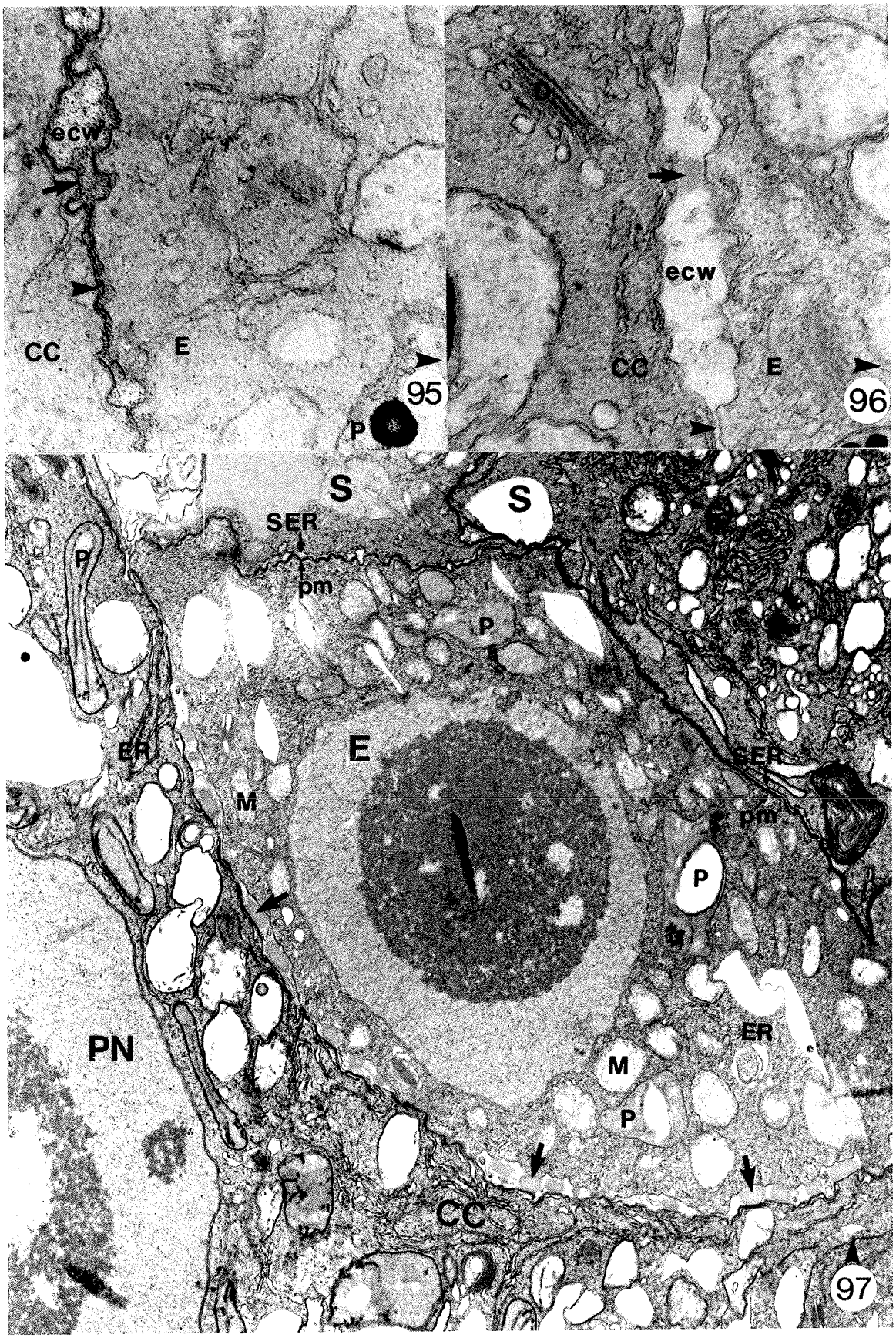
ecw
CC
E
95
P
ecw
CC
E
96
S
S
SER
pm
P
P
ER
E
M
SER
pm
P
PN
ER
M
P
CC
97

Figures 98 and 99. Two light micrographs of the same egg apparatus fixed 24 h after anthesis. Figure 98 was prepared for brightfield microscopy, Figure 99 was prepared for fluorescence microscopy. For comparative purposes, the two megagametophytes have been identically labelled.

Figure 98. Light micrograph of the egg apparatus, fixed 24 hours after anthesis, showing the persistent and incipient degenerate synergid and the egg. One of the two synergids, the incipient degenerate synergid (DS), shows a more intense basiophilia. The egg-central cell wall (large arrow) shows an intense orthochromatic staining reaction, while the cell wall between the persistent synergid and the egg (open arrow) is lightly stained. The micropylar portion of the filiform apparatus (Fa) is lightly stained, while the finger-like projections, extending into the synergid cytoplasm, are intensely stained and difficult to distinguish from the background cytoplasm. The central cell (CC) wall projections appear as a hazy layer (small arrows) adjacent to the lateral wall of the central cell. PAS/CV. x1,000.

Figure 99. Epifluorescence light micrograph of the egg apparatus, fixed 24 hours after anthesis, showing the persistent (PS) and incipient degenerate synergid (DS) and the egg (E). The section was stained with Calcofluor and viewed under UV light. The filiform apparatus (Fa) is intensely fluorescent as are the finger-like projections that extend deep into synergid cytoplasm. The micropylar portion of the egg-central cell wall (large arrow) shows a weak fluorescence while the chalazal portions of the egg-central cell wall exhibit no fluorescence. The obliquely sectioned common wall between the persistent synergid and the egg (open arrow) is weakly fluorescent as is a portion of the wall between the egg and the degenerate synergid (large arrowhead). The chalazal region of the degenerate synergid-egg wall, near the junction of the degenerate synergid, egg, and central cell (small arrowhead) is non-fluorescent. The central cell (CC) wall projections (small arrows) are weakly fluorescent. Calcofluor. x1,000.

Figure 100. Electron micrograph of the chalazal boundary between the egg and the central cell. The egg nucleus (N) is circumscribed by plastids (P) and mitochondria (M). Egg dictyosomes (D) are composed of 5-7 flattened cisternae and are relatively inactive in vesicle production. There are regular deposits of electron-opaque material between the parallel plasma membranes (pm) of the egg and the central cell. OsFeCN. UA/Pb. x3,300.

Figure 101. Electron micrograph of the egg apparatus showing the incipient degenerate synergid, the persistent synergid, and the egg. The cytosol of the incipient degenerate synergid (DS) is more intensely stained than that of the adjacent persistent synergid (PS) or egg (E). The ER of the persistent synergid, from the nucleus to the filiform apparatus (arrowheads) is stained positively by OsFeCN and shows electron-opaque deposits within the cisternae. The chalazal ER of the persistent synergid, and the ER of the incipient degenerate synergid and the egg are unstained by OsFeCN procedure. OsFeCN. UA/Pb. x3,300.

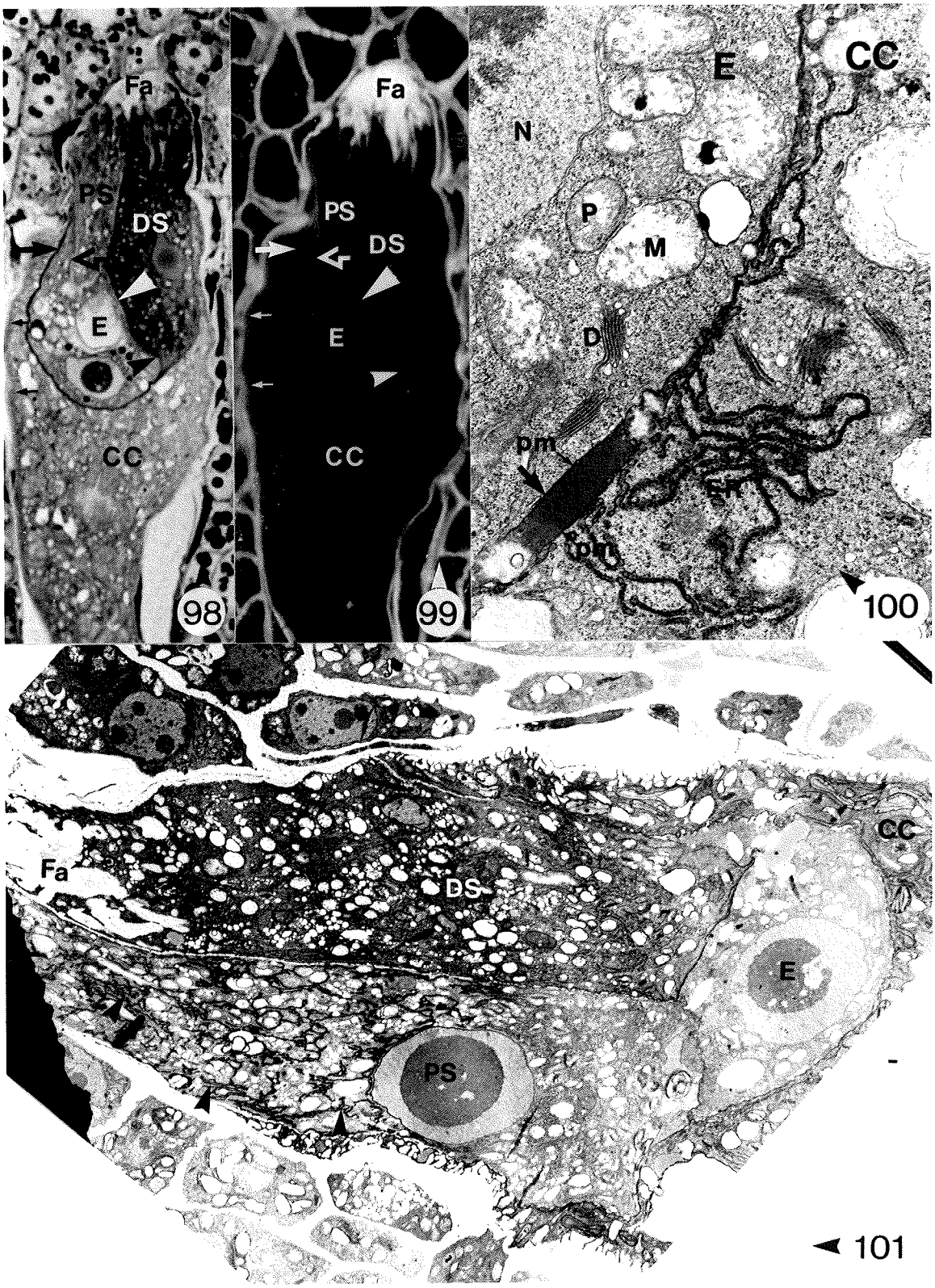
Fa
PS
DS
E
CC
98
Fa
PS
DS
E
CC
99
E
CC
N
P
M
D
pm
pm
ER
100
CC
Fa
DS
E
PS
101

Figures 102 and 103 are light and electron micrographs of the same egg apparatus obtained from non-adjacent serial sections.

Figure 102. Light micrograph of the egg apparatus of an ovule fixed 36 h after anthesis showing the egg (E) and incipient degenerate synergid (DS). The cytosol of the incipient degenerate synergid shows an intense basiophilia when stained with crystal violet. The outline of the cell would suggest the incipient degenerate synergid was turgid at the time of fixation. The adjacent egg and central cell (CC), including the polar nuclei (PN), exhibit a normal crystal violet staining pattern. CV. x1,000.

Figure 103. Electron micrograph of the egg apparatus of an ovule fixed 36 h after anthesis showing the egg (E) and incipient degenerate synergid. The cytosol of the incipient degenerate synergid (DS) shows an intense electron-opacity. The mitochondria (M), dictyosomes (D), and ER appear healthy and show no sign of degeneration. UA/Pb. x10,900.

Figure 104. Light micrograph showing an overview of a post-anthesis fertile ovule. At the micropylar end of the megagametophyte, there is a vacuolate egg with the egg nucleus (large arrowhead) occupying the extreme chalazal region of the cell. The degenerate synergid (DS) appears collapsed and shrunken, particularly at the chalazal tip (small arrowhead). The central cell (CC) cytoplasm appears heterogeneous, and remains non-vacuolate except for a small chalazal vacuole (V) adjacent to the degenerate antipodals (out of the plane of section). The cells of the chalazal nucellus (CN) have degenerated. At the extreme chalaza of the nucellus, is a persistent starch (St) storing region of nucellus, the chalazal proliferating tissue (cp). The inner integument basal body (Bb) has continued to expand following anthesis; however, the micropylar and lateral starch storing regions of the inner and outer integuments remain unchanged. PAS/CV. x370.

Figure 105. Electron micrograph of a post-anthesis egg apparatus showing the vacuolate egg (E) and degenerate synergid (DS). The degenerate synergid has collapsed and the thin electron-transparent wall in the synergid hook (Sh) region is irregular and wrinkled. The micropylar portion of the degenerate synergid-egg wall (small arrowheads) is electron-transparent while the chalazal region at the junction of the degenerate synergid, egg, and central cell (large arrowheads) is devoid of electron-transparent wall material. UA/Pb. x35,000.

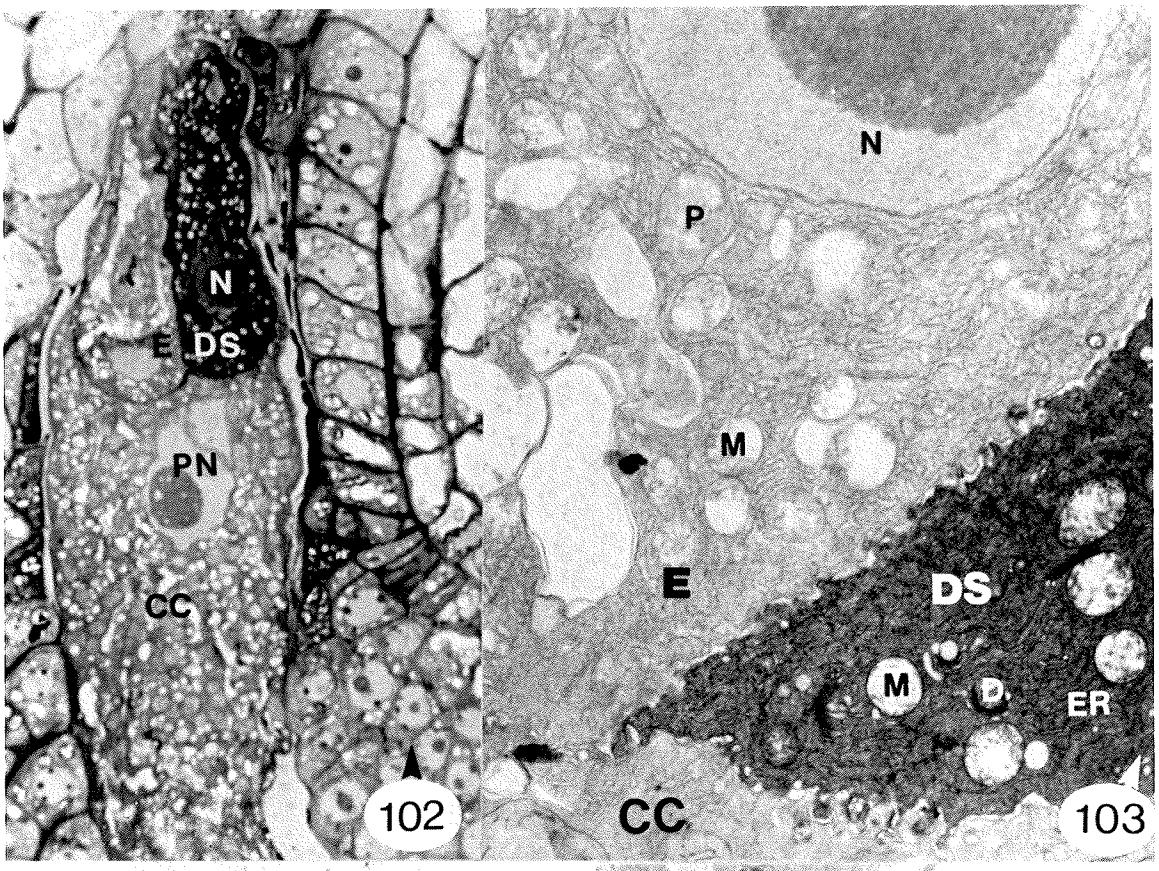
N
E
DS
PN
CC
102
N
P
M
E
DS
M
D
ER
CC
103

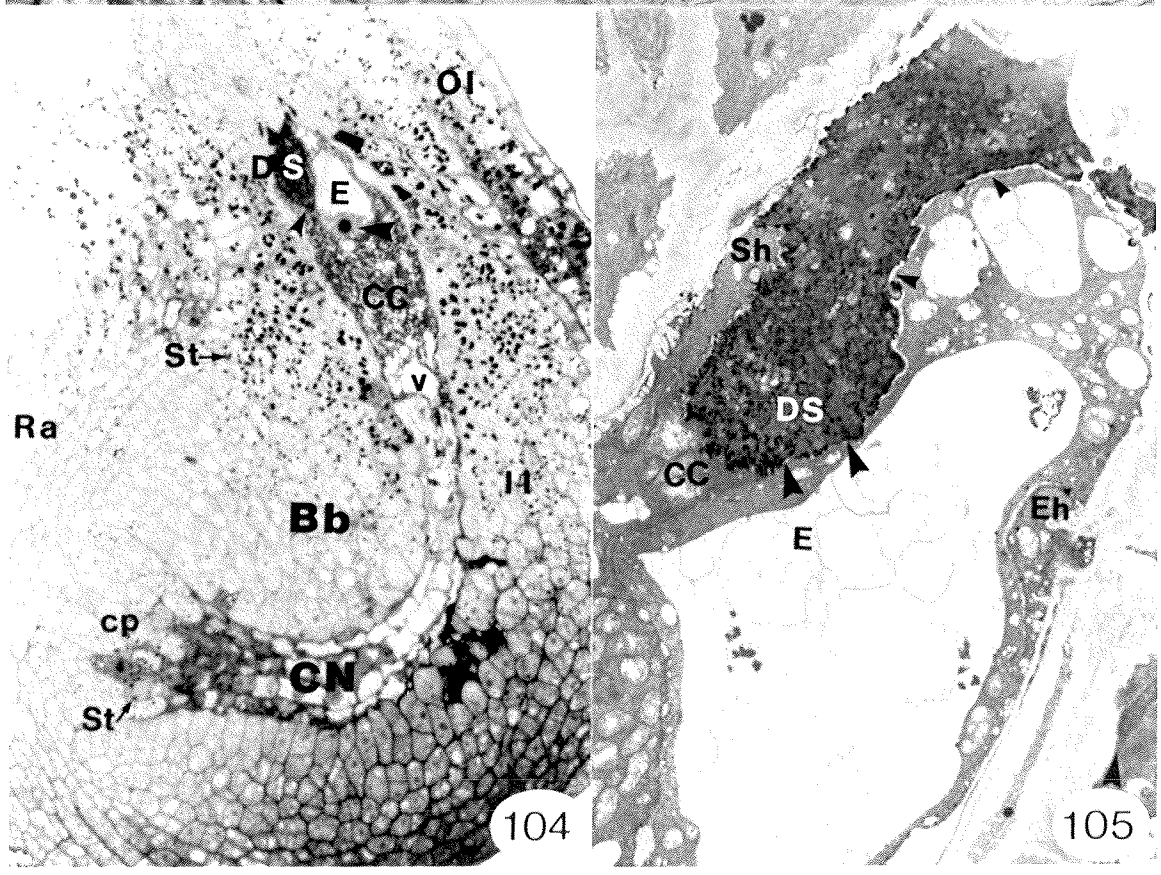
Ol
DS
E
CC
St
v
Ra
Il
Bb
cp
CN
St
104
Sh
DS
CC
E
Eh
105

Figure 106. Electron micrograph of the degenerate synergid cytoplasm. There is a marked hypertrophy of the ER network that encircles pockets of cytoplasmic ribosomes (small arrows). Bound ribosomes (large arrows) on the surfaces of the electron-opaque ER cisternae exhibit a distinct beaded appearance. Mitochondrial (M) profiles are recognizable, though there has been a loss of mitochondrial membrane integrity. Dictyosome cisternae are no longer visible but enlarged vesicles (arrowhead) similar to the dictyosome vesicles of the intact synergid remain. The contents of these vesicles are fibrillar and a bounding membrane is no longer visible. UA/Pb. x25,700.

Figures 107 and 108 represent non-adjacent serial sections through an ovule fixed 9.5 h after pollination. The pollen tube had penetrated the outer integument micropyle, but had yet to reach the inner integument micropyle.

Figure 107. Light micrograph of the micropylar portion of the megagametophyte 9.5 h after pollination. The megagametophyte consists of two interconnected polar nuclei (PN) in a non-vacuolate heterogeneous central cell (CC) cytoplasm, an intact persistent synergid (PS), a degenerate synergid (DS), and a vacuolate egg (E). PAS/CV. x950.

Figure 108. Light micrograph of the micropylar portion of the megagametophyte 9.5 h after pollination. The megagametophyte consists of two interconnected polar nuclei (PN) in a non-vacuolate heterogeneous central cell (CC) cytoplasm, an intact persistent synergid (PS), a degenerate synergid (DS), and a vacuolate egg (E). The egg nucleus (N) has migrated from the extreme chalazal tip location, characteristic of the unpollinated egg following anthesis, to the middle region of the egg cell, immediately adjacent to the common degenerate synergid-egg wall. PAS/CV. x950.

Figure 109. Light micrograph of the stigma and style. The stigmatic papillae (small arrowheads) are highly vacuolate, obovate cells with a central nucleus. Between the stigmatic papillae and the style is a narrow stigmatic zone (large arrowheads) of small isodiametric parenchyma cells. The central core of the style is occupied by the parenchymatous transmitting tissue (large arrow). Strands of vascular tissue are located lateral to the transmitting tissue (small arrow). CV. x230.

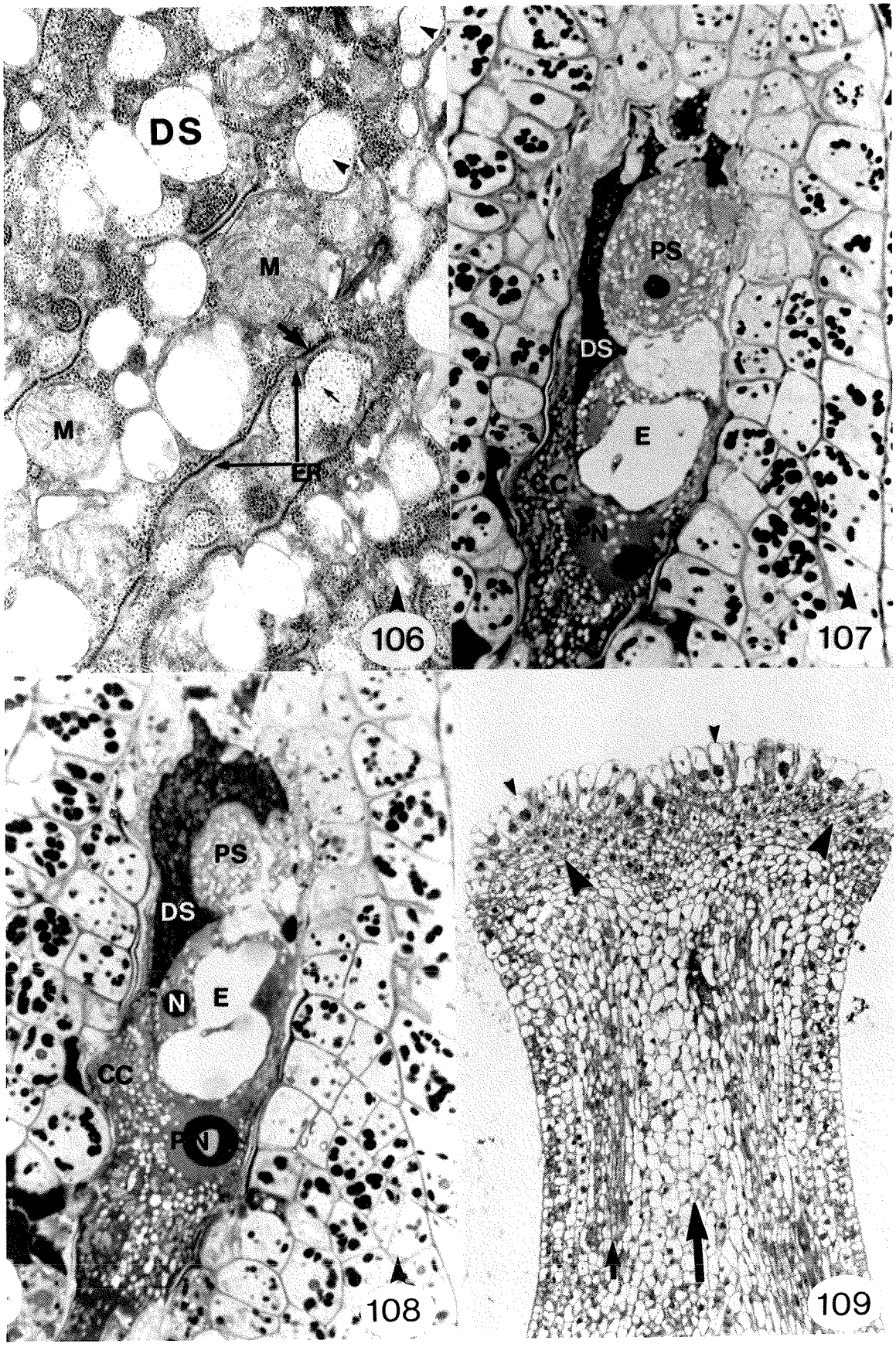
DS
M
M
ER
106
PS
DS
E
CC
N
107
PS
DS
N
E
CC
P
108
109

Figure 110. Epifluorescence light micrograph of stigma and style 5 h after pollination. The fresh section was stained with aniline blue and viewed under UV light. The callosic walls and plugs of the pollen tubes show a pale blue fluorescence that contrasts with the deep blue autofluorescence of the adjacent stigmatic, transmitting, and vascular tissues. Aniline blue. x270.

Figure 111. Epifluorescence light micrograph of an ovule attached to the replum of the ovary 15 h after pollination. The fresh tissue was stained with aniline blue and viewed under blue light. The callosic walls and plugs of the pollen tubes (Pt) fluoresce yellow in contrast with the red autofluorescence of chlorophyll within the ovule (Ov) and replum (R) plastids. The longitudinal axis of the mature ovule is parallel to the longitudinal axis of the ovary with the micropyle directed toward the stigmatic end of the pistil. The pollen tubes grow along the surface of the replum and first contact the ovule at the more proximal region of the funiculus (F) Aniline blue. x270.

Figure 112. Epifluorescence light micrograph of the stigma 5 h after pollination. The fresh section was stained with aniline blue and viewed under UV light. The germinated pollen tubes (Pt) do not appear to penetrate the stigmatic papillae (arrowheads) but grow along the lateral surface of the papillae before entering the narrow zone of stigmatic parenchyma tissue. The non-fluorescent pollen grain (arrow) is visible adjacent to the papillae. Aniline blue. x1,100.

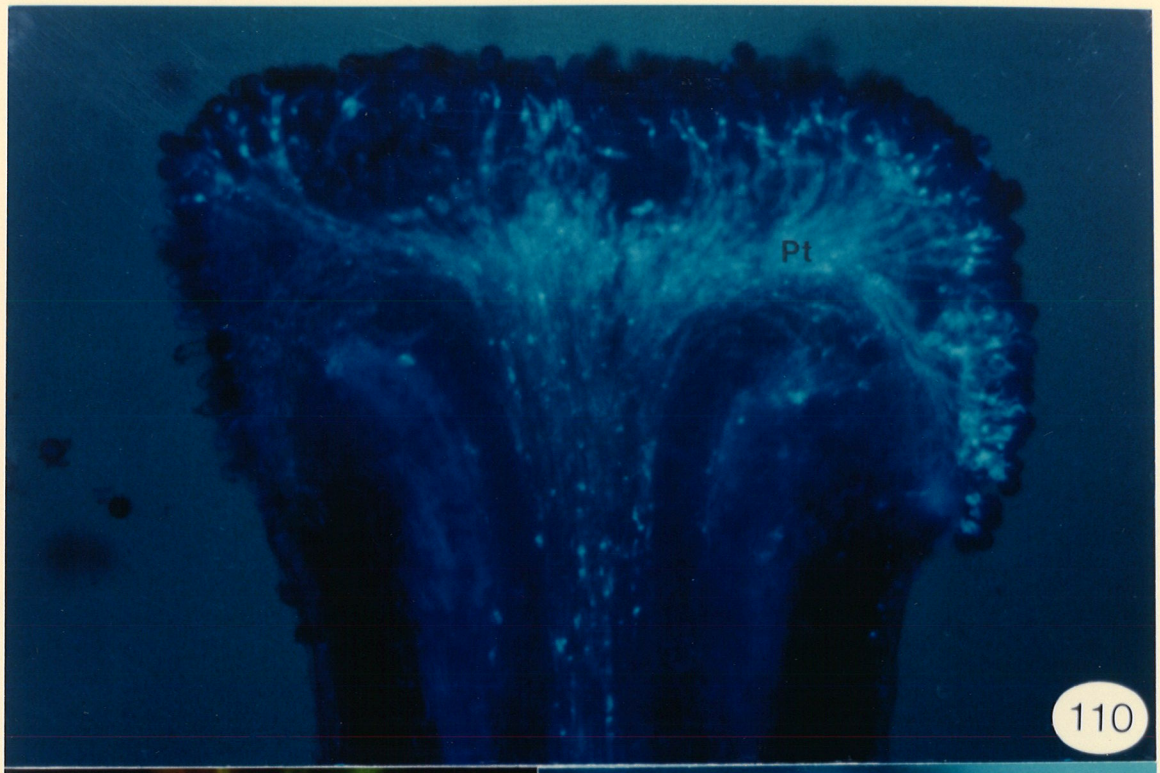
Pt
110

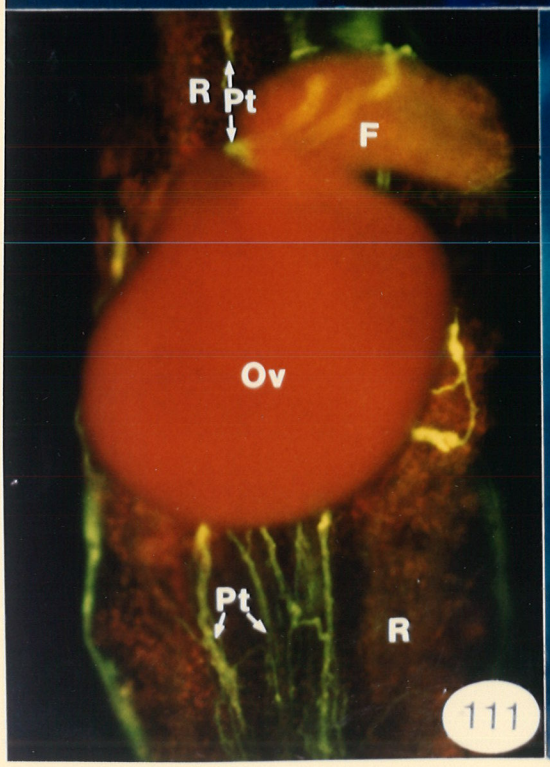
R
Pt
F
Ov
Pt
R
111

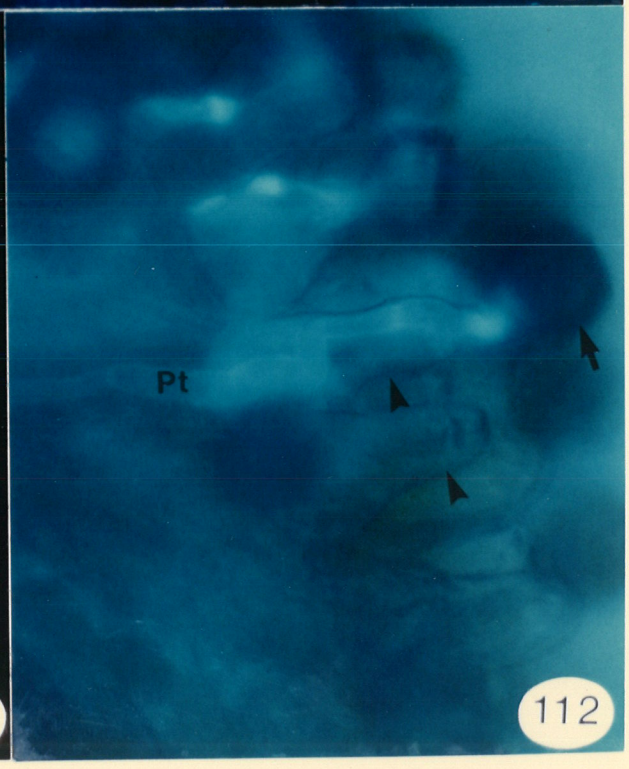
Pt
112

Figure 113. Epifluorescence light micrograph of an ovule 15 h after pollination. The fresh tissue was stained with aniline blue and viewed under UV light. The pollen tube (Pt) grew along the funiculus (F) to the junction of the funiculus and the outer integument (OI) and entered the ovule by way of the curved outer integument micropyle (Mi). The autofluorescent vascular tissue (arrow) extends from the funiculus and terminates in the raphe (Ra) region of the ovule. Aniline blue. x550.

Figure 114. Epifluorescence light micrograph of the micropylar end of the ovule 24 h after pollination. The fixed tissue was stained with aniline blue and viewed under UV light. The pollen tube grew along the inner integument (II) micropyle (Mi) to the base of the synergid (S). A thickened plug of what is presumed to be callose (unlabelled arrow) is present in the region of the pollen tube wall adjacent to the synergid. A more proximal portion of the pollen tube is visible near the tip of the outer integument (OI). Aniline blue. x1,100.

Figure 115. Epifluorescence light micrograph of the ovule at anthesis showing the synergids (S) and the inner (II) and outer (OI) integument components of the micropyle. The section was stained with Calcofluor and viewed under UV light. The course of the micropyle is indicated by unlabelled arrows (for orientation see fig. 26). The filiform apparatus of the synergid shows a strong pale blue fluorescence. The micropylar cell walls (cw) of the synergids are weakly fluorescent. Calcofluor. x1,100.

Figure 116. Light macrograph of the racemose inflourescence of Brassica campestris. The pistil of the flower, 24 h after anthesis (small arrow), was 6-7 mm long and the stigma of the pistil was near the level of the four longest stamens of the tetradynamous androecium. The pistil of the flower, 72 h after anthesis (large arrow), was 11-13 mm long and petal abscission was commencing. x1.2.

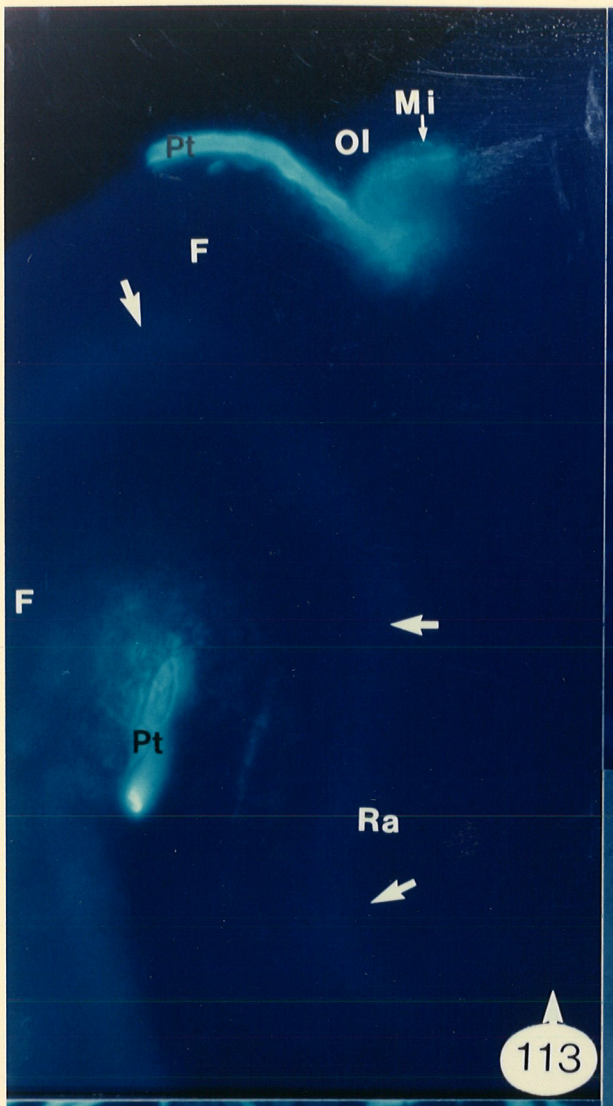
Mi
Pt
Ol
F
F
Pt
Ra
113

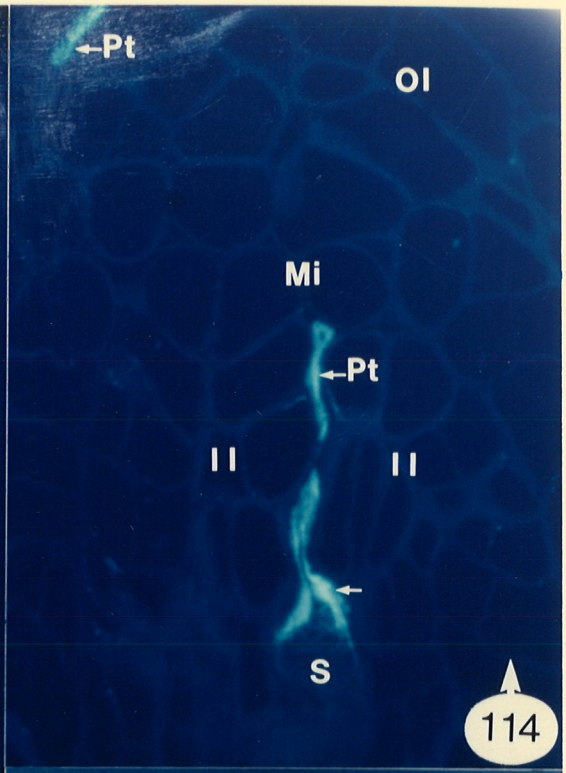
Pt
Ol
Mi
Pt
II
II
S
114

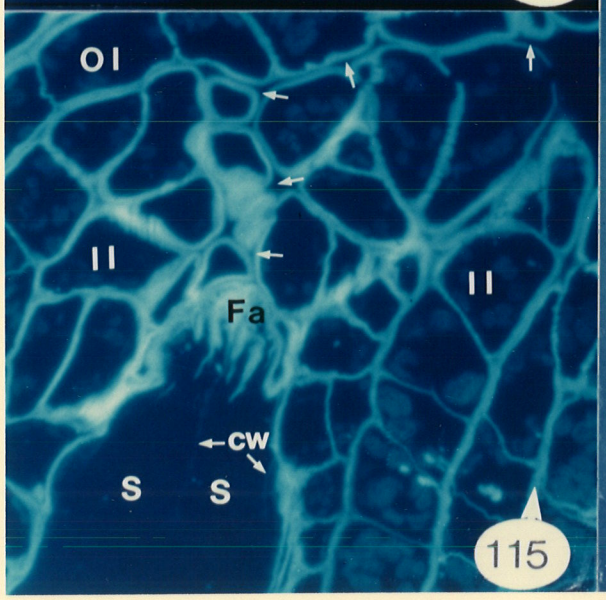
Ol
II
II
Fa
CW
S
S
115


116

Figure 117. Electron micrograph of a portion of the pollen tube at the base of the filiform apparatus. The pollen tube first contacts the megagametophyte at the base of the filiform apparatus (Fa) of the synergids. The cells of the inner integument micropyle immediately adjacent to the pollen tube are intact and show no sign of degeneration. OsFeCN staining shows an aggregation of ER in the inner integument cells adjacent to the micropyle. OsFeCN. UA/Pb. x1,120.

Figure 118. Electron micrograph of the egg apparatus 24 h after pollination showing the degenerate synergid (DS), persistent synergid (PS) and the base of the zygote (Z). The pollen tube (Pt) penetrates the degenerate synergid (DS) through the base of the filiform apparatus (Fa) and grows chalazally within the degenerate synergid, following the contours of the common degenerate synergid-persistent synergid wall (arrowheads). The walls of the pollen tube are electron-opaque in contrast to the electron-transparent common wall between the synergid cells and the filiform apparatus. The synergid-central cell wall in the region of the synergid hook (Sh) is thicker than that of the unpenetrated degenerate synergid (Fig. 105). The persistent synergid remains intact following zygote formation. UA/Pb. x4,800.

Figure 119. Electron micrograph of the pollen tube at the base of the degenerate synergid and the persistent synergid. The pollen tube had grown laterally along the base of the persistent synergid (PS) before entering the degenerate synergid (DS). There is an incomplete common persistent synergid-central cell wall (cw), containing plasmodesmata (pd), extending from the edge of the megagametophyte at the synergid hook (Sh) into the central cell cytoplasm. Numerous central cell chloroplasts (small arrowheads) are intermixed with synergid proplastids (large arrowheads) in the region of the persistent synergid filiform apparatus (Fa). Note the presence of wall projections (wp) in the micropylar region of the persistent synergid between the common synergid-central cell wall and filiform apparatus. UA/Pb. x4,500.

Figure 120. Electron micrograph of the tip of the pollen tube within the degenerate synergid. The pollen tube (Pt) discharges its contents by means of a terminal pore (large arrowheads). The organelles of the penetrated degenerate synergid (DS) in the immediate vicinity of the terminal pore of the pollen tube show a lack of membrane integrity. Profiles of identifiable ER and mitochondria (M) with long tubular cristae, similar to those seen in the unpenetrated degenerate synergid are apparent in the cytoplasm. There are numerous spherical particles with an electron-transparent border around a fine granular electron-opaque core (small arrowheads) present in the synergid cytoplasm adjacent to the discharge pore. UA/Pb. x35,000.

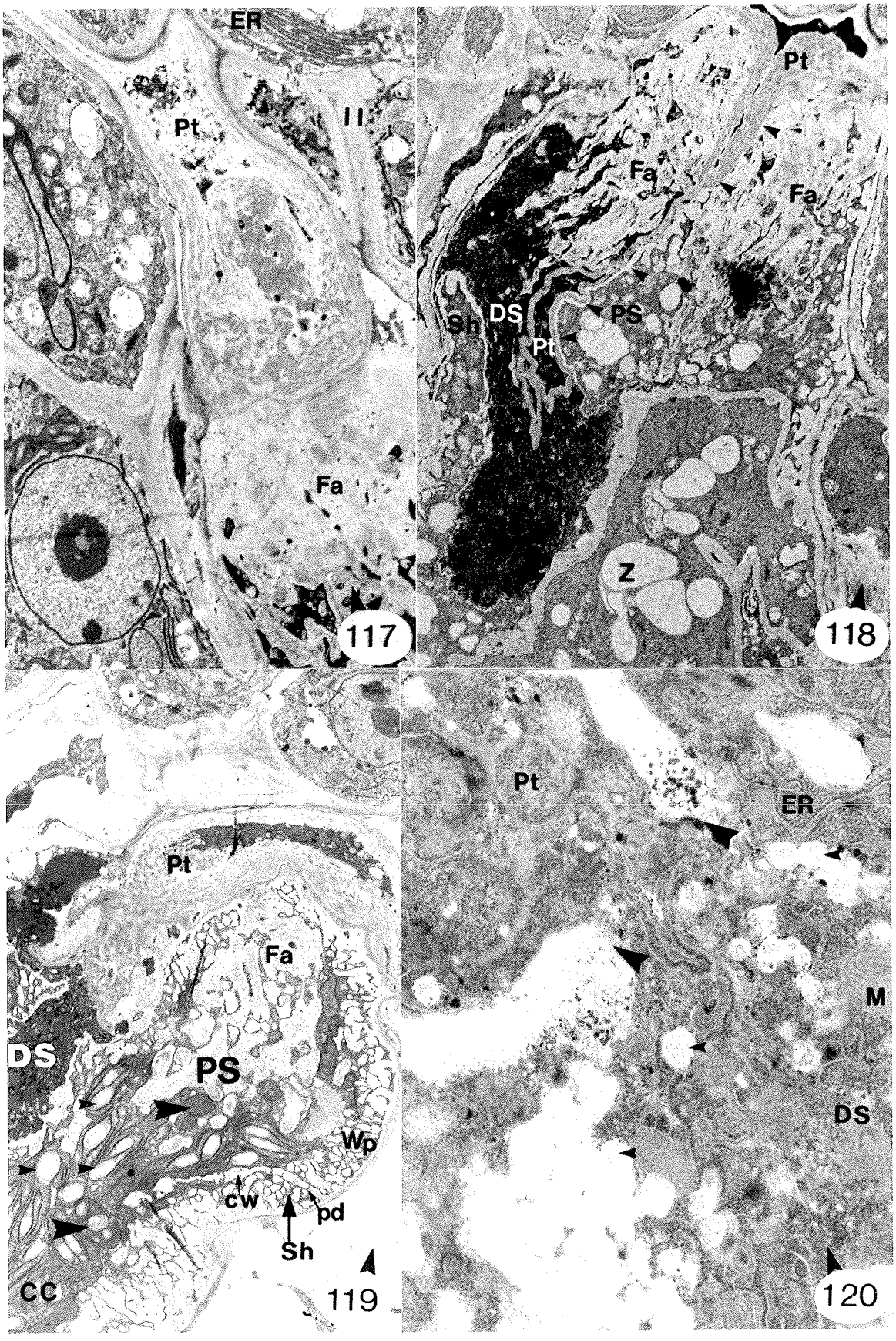
ER
Pt
II
Fa
117
Pt
Fa
Fa
Sh
DS
PS
Pt
Z
118
Pt
Fa
DS
PS
Wp
cw
pd
Sh
CC
119
Pt
ER
M
DS
120

Figure 121. Electron micrograph of a zygote, degenerate synergid, and pollen tube 24 h after pollination. A portion of the pollen tube is at the base of the filiform apparatus (Fa) while the tip of the pollen tube showing the discharge pore is in the mid-region of the degenerate synergid (DS) at the level of the synergid hook (Sh). A zone of spherical discharge particles (unlabelled arrows) extends from the discharge pore of the pollen tube to the chalazal tip of the degenerate synergid adjacent to the common degenerate synergid, central cell (CC), zygote (Z) boundary. The chalazal cell wall (cw) between the zygote and the degenerate synergid (in the region of pollen tube discharge) and the cell wall (cw) of the synergid hook are markedly thickened. The zygote (Z) lacks the prominent micropylar vacuole of the egg. The zygote nucleus occupies the centre of the cell. In the region of the nucleus opposite the region of pollen tube discharge in the degenerate synergid there is a small elliptical island of nuclear material (arrowhead) separated from the main body of the nucleus by a narrow band of cytoplasm. The zygote cytoplasm contains an abundance of proplastids (P), lipid bodies (L), and small vacuoles (V). The cell wall of the zygote is electron-transparent. The wall is thicker at the base where the cell is attached to the inner integument (II), in the region of the egg (zygote) hook (Eh) and in the region adjacent to the degenerate synergid. The wall is relatively thin in the region of chalazal ampulliform tip. A small portion of the persistent synergid (PS) containing wall projections (Wp) is visible near the base of the zygote. UA/Pb. x3,800.

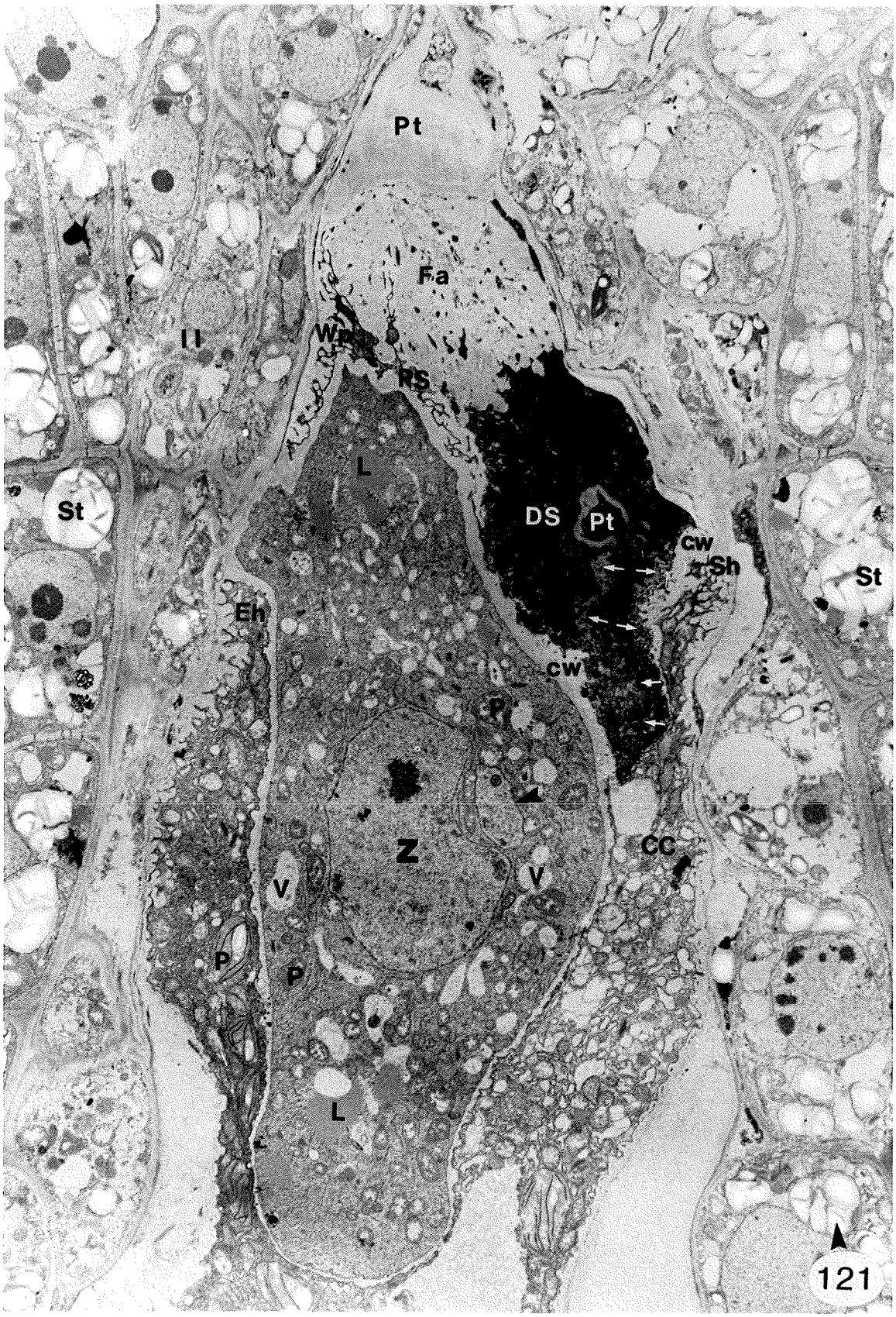
Pt
Fa
II
WP
RS
L
St
DS
Pt
cw
Sh
St
Eh
cw
P
Z
CC
V
V
P
P
L
121

Figures 122 and 123 are non-adjacent serial sections of the zygote cell in figure 121.

Figure 122. Epifluorescence light micrograph of the zygote and a portion of the pollen tube. The section was stained with Calcofluor and viewed under UV light. The micropylar and lateral walls (unlabelled arrows) of the zygote (Z) and the pollen tube (Pt) within the degenerate synergid (DS) fluoresce a pale blue while the ampulliform tip of the zygote and the walls of the degenerate synergid are non-flourescent. Calcofluor. x950.

Figure 123. Light micrograph of the zygote and a portion of the pollen tube. The micropylar and lateral walls (unlabelled arrows) of the zygote (Z) and the pollen tube (Pt) within the degenerate synergid (DS) are PAS-positive. The large starch (St) grains of the micropylar inner integument are PAS-positive. The ampulliform tip of the zygote is PAS-negative. PAS/CV. x950.

Figure 124. Electron micrograph of a glancing section through the lateral wall of the ampulliform tip of the zygote. There are numerous microtubules (arrowheads) in the zygote (Z) cytoplasm adjacent to the cell wall (cw). UA/Pb. x15,000.

Figure 125. Electron micrograph of the microtubules adjacent to the lateral wall in the ampulliform tip of the zygote. The majority of microtubules (arrowheads) were oriented with the long axis perpendicular to the long axis of the zygote. UA/Pb. x68,000.

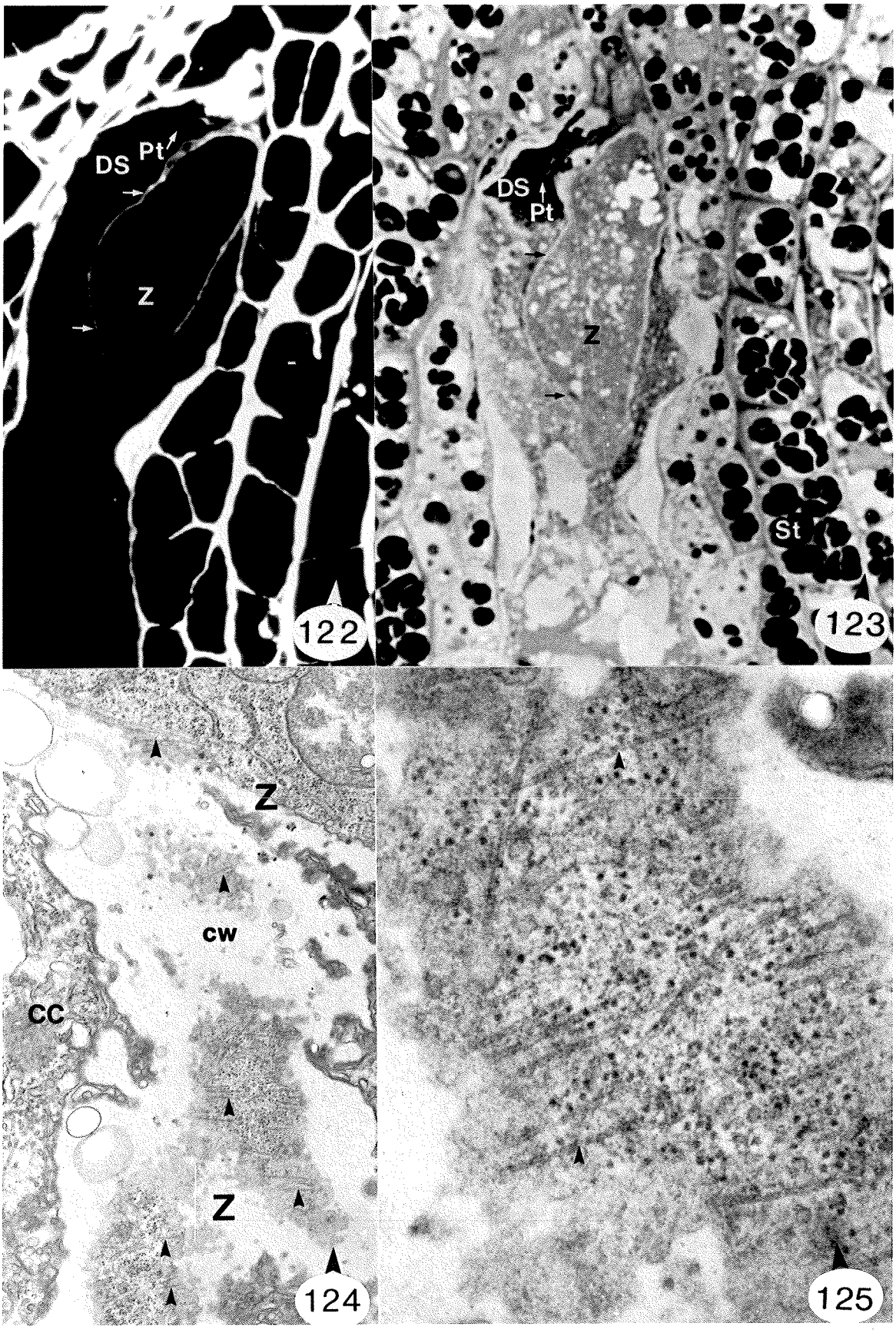
DS
Pt
Z
122
DS
Pt
Z
St
123
Z
cw
CC
Z
124
125

Figure 126. Electron micrograph of a zygote fixed by the OsFeCN method 18 h after pollination. The shape of the zygote is essentially the same as the zygote in figure 121. The cell walls are electron-opaque and the ampulliform tip shows thick evaginated regions of cell wall (between arrowheads). The ER cisternae of the zygote are positively stained by the OsFeCN method. The ER consists of short strands distributed throughout the cytoplasm. There is a marked increase in the amount of lipid (L) within the zygote. Both the central cell chloroplasts (P) and the zygote proplastids (P) contain starch. An endosperm nucleus (EN) is visible in the vacuolate central cell cytoplasm. OsFeCN without UA/Pb. x4,000.

Figure 127. Light micrograph of the zygote in figure 126. The lipid bodies of the zygote and central cell are stained by crystal violet. The evaginated regions of cell wall at the ampulliform tip of the zygote stain orthochromatically with crystal violet (arrow). One of two endosperm nuclei (EN) is visible in the vacuolate (V) central cell cytoplasm. CV. x1,500.

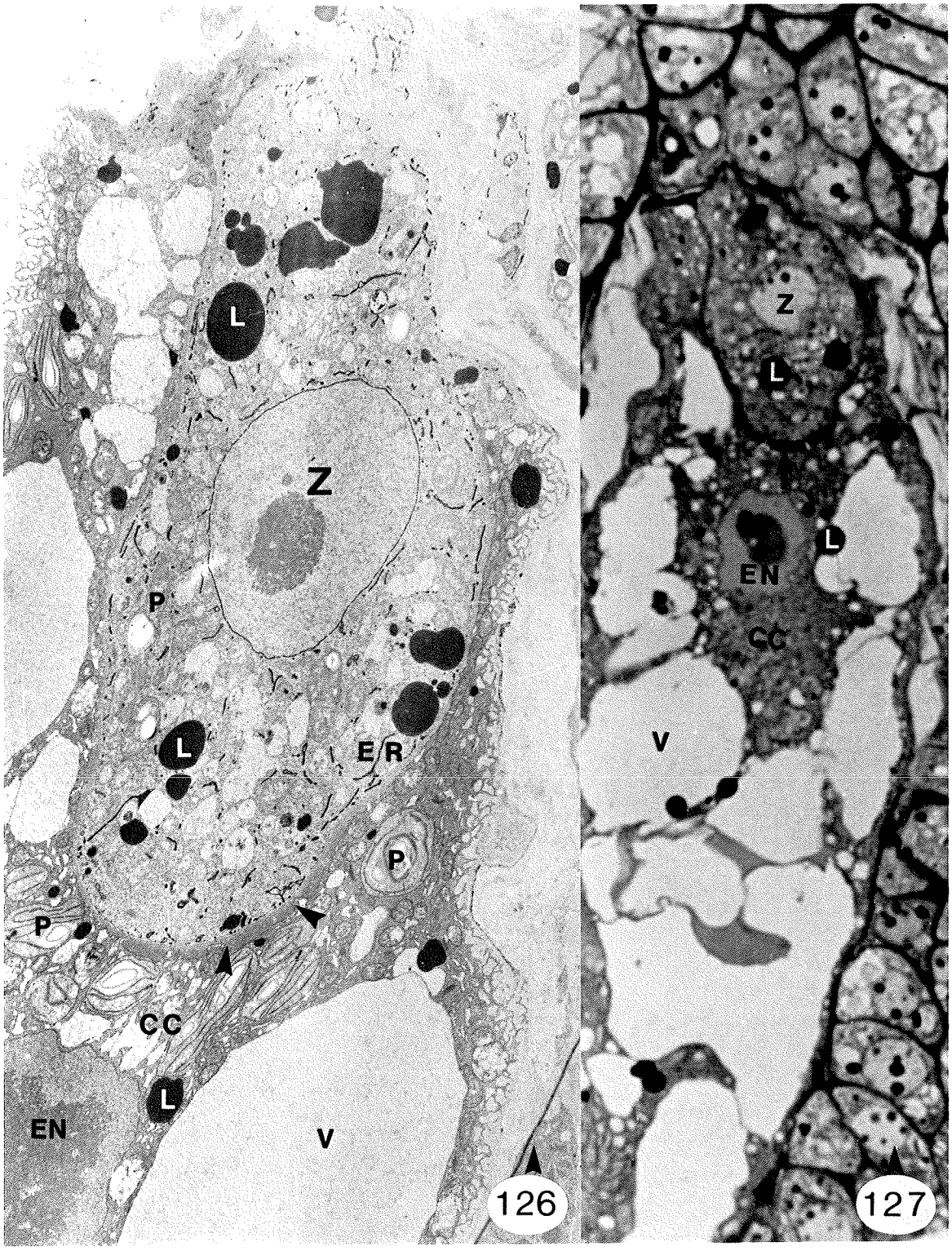
L
Z
P
L
ER
P
P
CC
L
EN
V
126
Z
L
L
EN
CC
V
127

Figure 128. Electron micrograph of the chalazal wall of the zygote in figure 126 - Thiery test. There is an even deposition of silver proteinate over the entire zygote cell wall (cw) including the evaginated region (between arrowheads). The electron-transparent zone adjacent to the zygote plasma membrane (pm) probably represents a slight plasmolysis induced during tissue preparation. The ER cisternae and lipid bodies (L) of the OsFeCN fixed zygote show heavy deposition of silver proteinate as do the starch grains of the central cell (CC) chloroplasts (P). OsFeCN. PA-TCH-SP. x34,000.

Figure 129. Electron micrograph of the chalazal wall of the zygote in figure 126 - Thiery control. There is a deposition of silver proteinate over the ER cisternae and lipid bodies (L), but none over the zygote cell wall (cw) or the starch grain of the central cell (CC) plastid (P). The evaginated regions on the central cell side of the common wall (between large arrowheads) show a homogeneous electron-opacity while the adjacent thin regions (small arrowheads) of common wall exhibit a more granular electron-opacity. The region of the zygote wall between the homogeneous electron-opaque evagination and the zygote plasma membrane (pm) shows a similar granular electron-opacity (arrows). OsFeCN. H_2O-TCH-SP. x20,100.

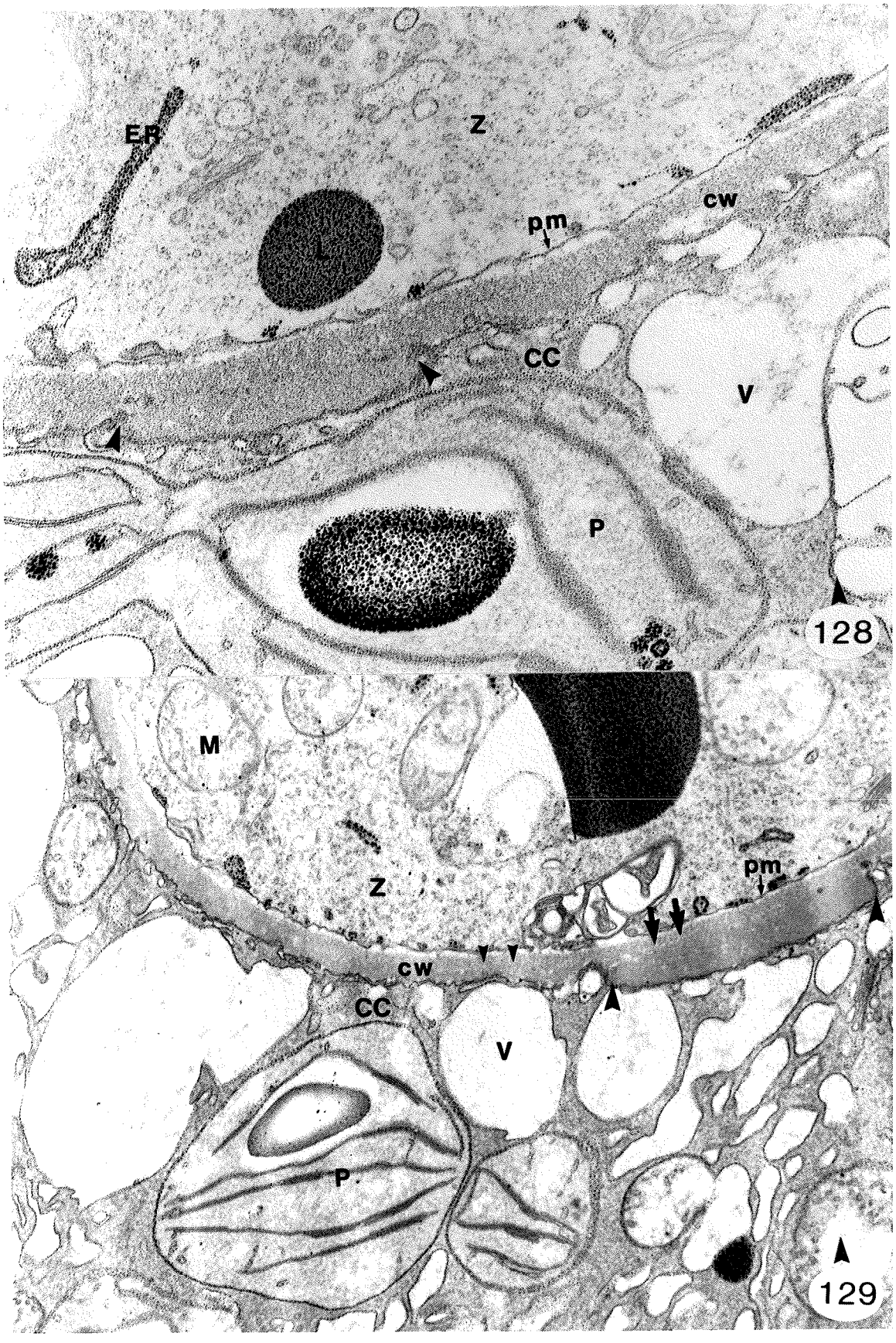
ER
Z
pm
cw
CC
V
P
128
M
Z
pm
cw
CC
V
P
129

Figure 130. Electron micrograph of a non-adjacent serial section of the zygote in figure 121. The small island of nuclear material is connected to the main body of the zygote (Z) nucleus (N) by a narrow nuclear bridge (nb). A small reniform mitochondrion (large arrow) is appressed to the nuclear envelope of the outer invaginated portion of the nucleus. Proplastids (P), mitochondria (M), and small vacuoles (V) encircle the zygote nucleus. Dictyosomes (D) are mainly associated with the cell wall but do not appear to be active in vesicle production. Short strands of ER are located throughout the cytoplasm. There are spiral polysomes (arrowhead) associated with the surface of the ER cisternae. Numerous spherical particles of pollen tube origin (small arrows) appear to be associated with thickened cell wall (cw) between the zygote and the degenerate synergid (DS). UA/Pb. x8,000.

Figures 131 and 132 are non-adjacent serial sections of the boundary between the zygote, degenerate synergid, and central cell.

Figure 131. Electron micrograph of the boundary between the zygote (Z), degenerate synergid (DS) and central cell (CC). The central cell cytoplasm contains a large vacuole (V) between the zygote and the central cell proplastid (P). This vacuole shows no continuity with the central cell plasma membrane (pm) or with the ER of the central cell. The central cell ER cisternae are fragmented and dilated. UA/Pb. x14,600.

Figure 132. Electron micrograph of the boundary between the zygote (Z), degenerate synergid (DS) and central cell (CC). There is a definite continuity between the central cell plasma membrane (pm) and the bounding membrane of the central cell vacuole (V). The narrow strand of rough ER sandwiched between the proplastid (P) and the vacuole (V) shows a continuity with the outer membrane of the vacuole. UA/Pb. x14,600.

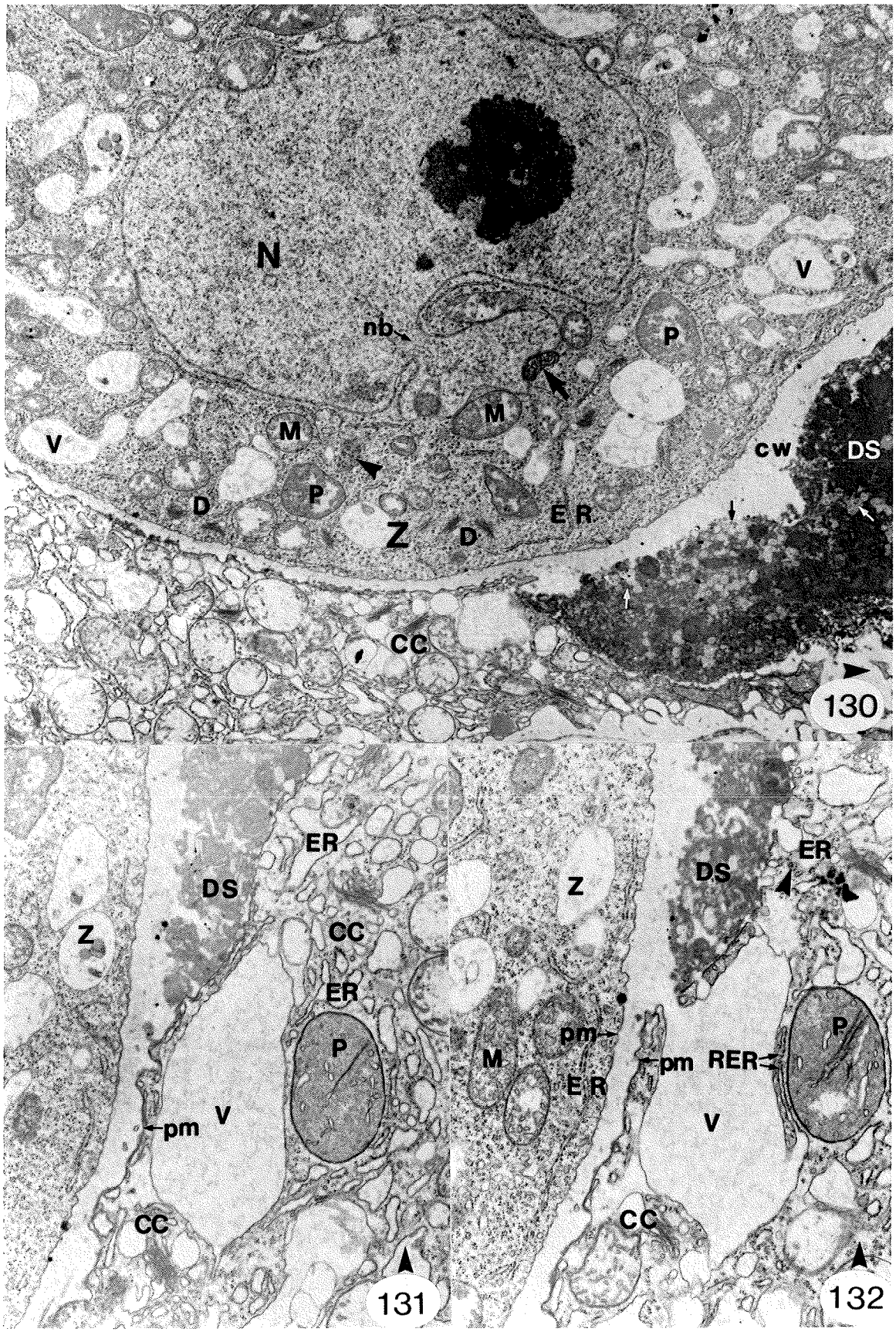
N
V
nb
P
M
M
V
cw
DS
D
P
Z
D
ER
CC
130
ER
DS
Z
DS
ER
Z
CC
ER
P
pm
M
pm
RER
P
E R
V
pm
V
CC
CC
131
132

Figure 133. Electron micrograph of the central cell cytoplasm following double fertilization. Chloroplasts (P) adjacent to an endosperm nucleus (EN) are actively replicating. The chloroplasts show well developed thylakoid lamellae and starch (St) deposits within the stroma. There are numerous mitochondria (M), dictyosomes (D), lipid bodies (L), and microbodies (Mb) present throughout the central cell (CC) cytoplasm. x10,700.

Figure 134. Light micrograph of a non-fertile ovule 72 h after anthesis. The egg apparatus consists of the vacuolate egg (E) and two degenerate synergids (S). The central cell contains two appressed polar nuclei (PN) adjacent to the egg apparatus. There is a large central cell vacuole (V) that expands at the expense of the degenerate chalazal nucellus (CN). The chalazal proliferating tissue (cp), between the raphe (Ra) and the chalazal nucellus is intact. The inner integument basal body (Bb) has expanded into the central cell vacuole. CV. x300.

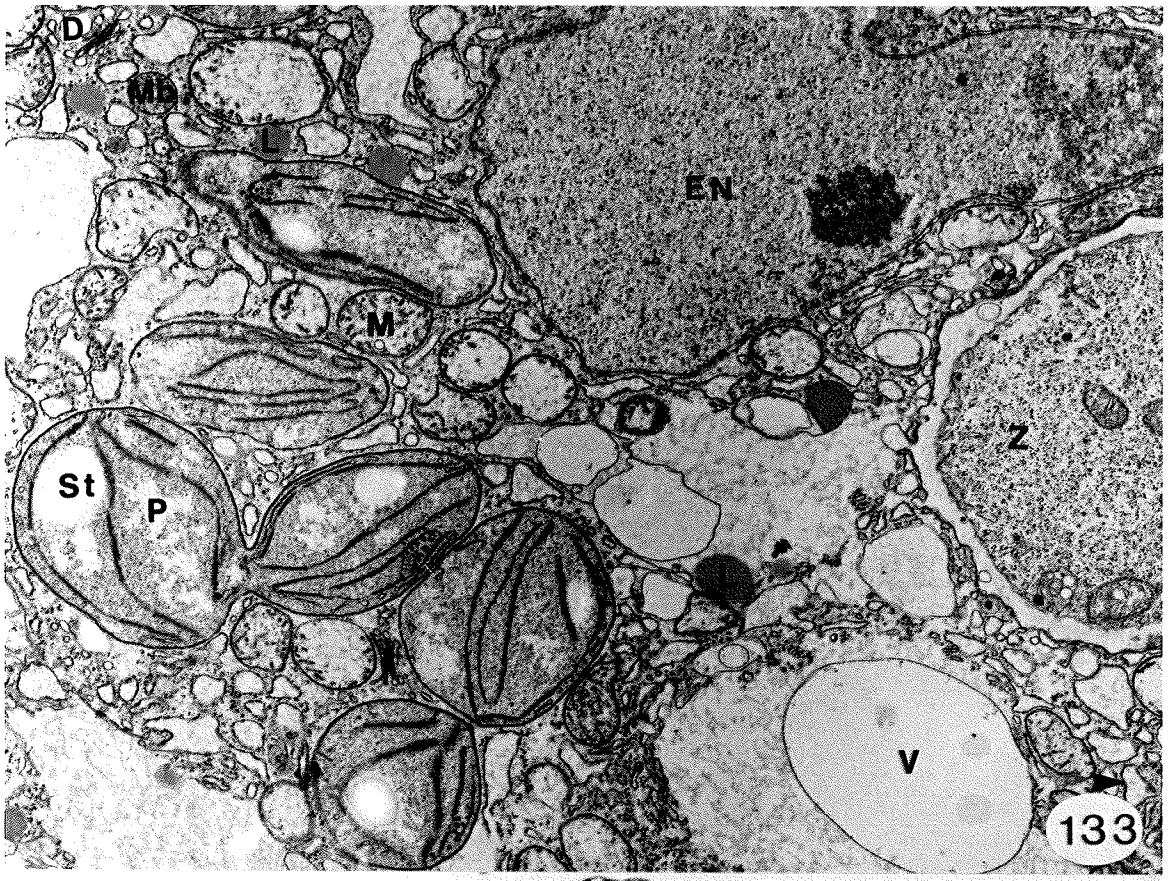
D
Mb
L
EN
M
St
P
Z
V
133

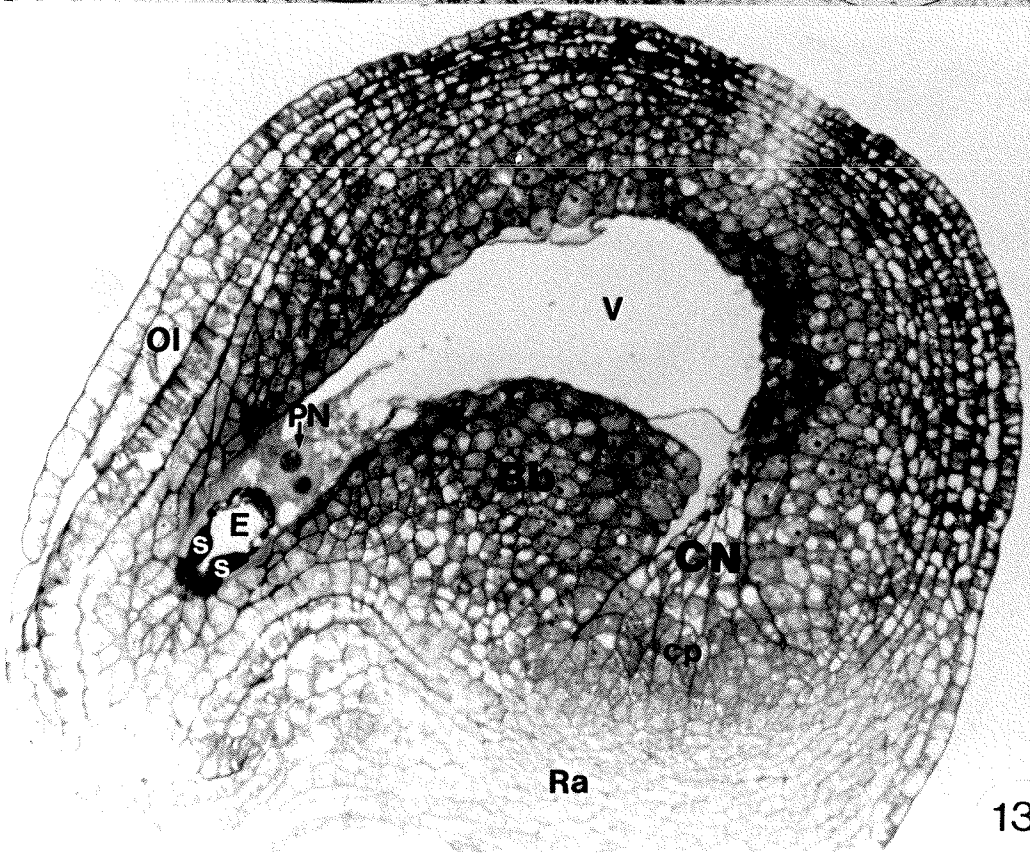
V
Ol
PN
Pb
E
S
S
CN
cp
Ra
134

Figure 135. Electron micrograph of a non-fertile egg apparatus 72 h after anthesis. The cytoplasm at the egg (E) appears healthy and consists of organelles typical of the egg cell at anthesis. The nucleus (N) is in the extreme chalazal position within the egg and is circumscribed by mitochondria (M) and plastids (P). Dictyosomes (D) are present in the chalazal cytoplasm. There has been a marked increase in lipid bodies (L) and there are numerous small vacuoles (V) in the chalazal region in addition to the typical large micropylar vacuole. The common chalazal wall between the egg and central cell (CC) consists of regions of expanded cell wall (ecw) containing electron-opaque deposits (unlabelled arrow) and narrower regions of wall consisting of appressed plasma membranes (large arrowhead). Both synergids (S) have degenerated and in one, the chalazal cytoplasm, adjacent to the egg has become plasmolysed (medium arrowheads). The filiform apparatus (Fa) is similar to that of the egg at anthesis. The PAS-negative subulate zone of the filiform apparatus shown in figure 136 is slightly more electron-transparent (small arrowheads), but not distinctly different from the surrounding wall material of the filiform apparatus. UA/Pb. x3,600.

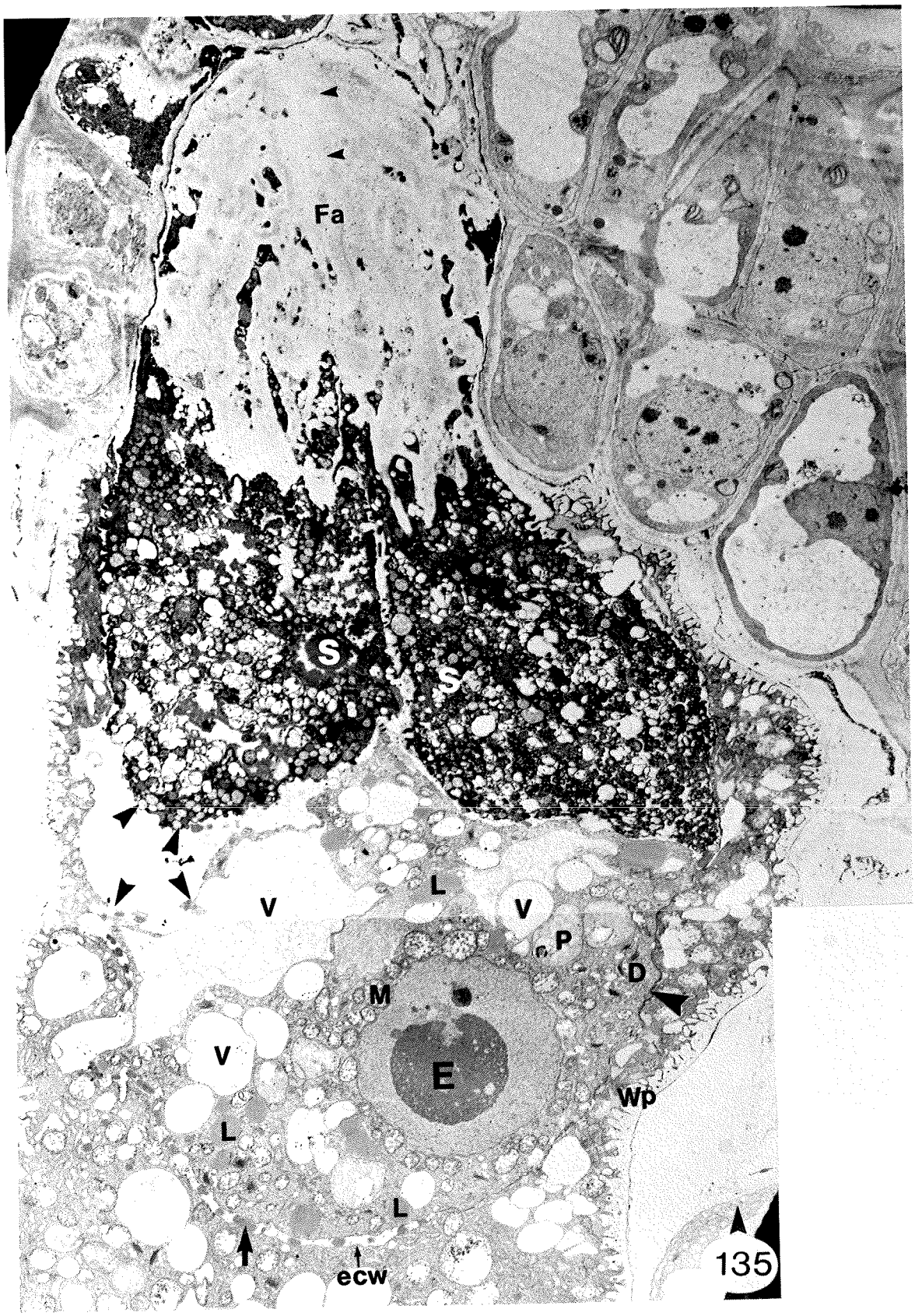
Fa
S
S
V
L
V
P
D
M
V
E
Wp
L
L
ecw
135

Figure 136. Light micrograph of a non-fertile egg apparatus 72 h after anthesis. The section is a non-adjacent serial section to the egg apparatus in figure 136. The vacuolate egg contains plastids (P) with PAS-positive starch grains and the electron-opaque deposits of the egg-central cell wall stain orthochromatically with crystal violet (unlabelled arrow). The majority of the filiform apparatus (Fa) is PAS positive except for a subulate zone (arrowhead) in the micropylar region. Starch (St) is noticeably absent from the micropylar and lateral regions of the integuments adjacent to the egg apparatus. PAS/CV. x900.

Figure 137. Epifluorescence light micrograph of a non-fertile egg apparatus 72 h after anthesis. The section was stained with Calcofluor and viewed with UV light. The pattern of fluorescence is the same as in the egg apparatus at anthesis and following anthesis (Fig. 99, 115). The filiform apparatus (Fa) shows a strong fluorescence. The micropylar wall (unlabelled arrow) separating the synergids (S) and the walls in the region of the synergid hook (Sh) are weakly flourescent. The chalazal walls of the synergids and the egg are non-fluorescent. Calcofluor. x1,100.

Figure 138. Electron micrograph of the chalazal egg-central cell wall from a non-fertile egg apparatus 72 h after anthesis. The expanded cell wall regions (arrowheads) appear labile and dilated. In the region of the electron-opaque wall material (arrow) the plasma membranes (pm) of the egg (E) and central cell (CC) are straight and tightly appressed to the electron-opaque deposit. The dictyosomes (D) of the 72 h egg appear more active in vesicle production than the egg at anthesis (Fig. 100). The mitochondria (M) are intact with well defined cristae. UA/Pb. x25,800.

Figure 139. Electron micrograph of a degenerate synergid from a non-fertile egg apparatus 72 h after anthesis. Profiles of dilated ER, mitochondria (M), vesicles (arrowhead), and a nucleus (N) are discernable. Except for the mitochondrial cristae the integrity of organelle membranes has been lost with numerous electron-opaque deposits associated with the nuclear (N) envelope and the outer membrane of the mitochondria. Both synergids resemble the post-anthesis degenerate synergid of the mature megagametophyte prior to fertilization (Fig. 106) except for the absence of ribosomes associated with the dilated ER. UA/Pb. x7,600.

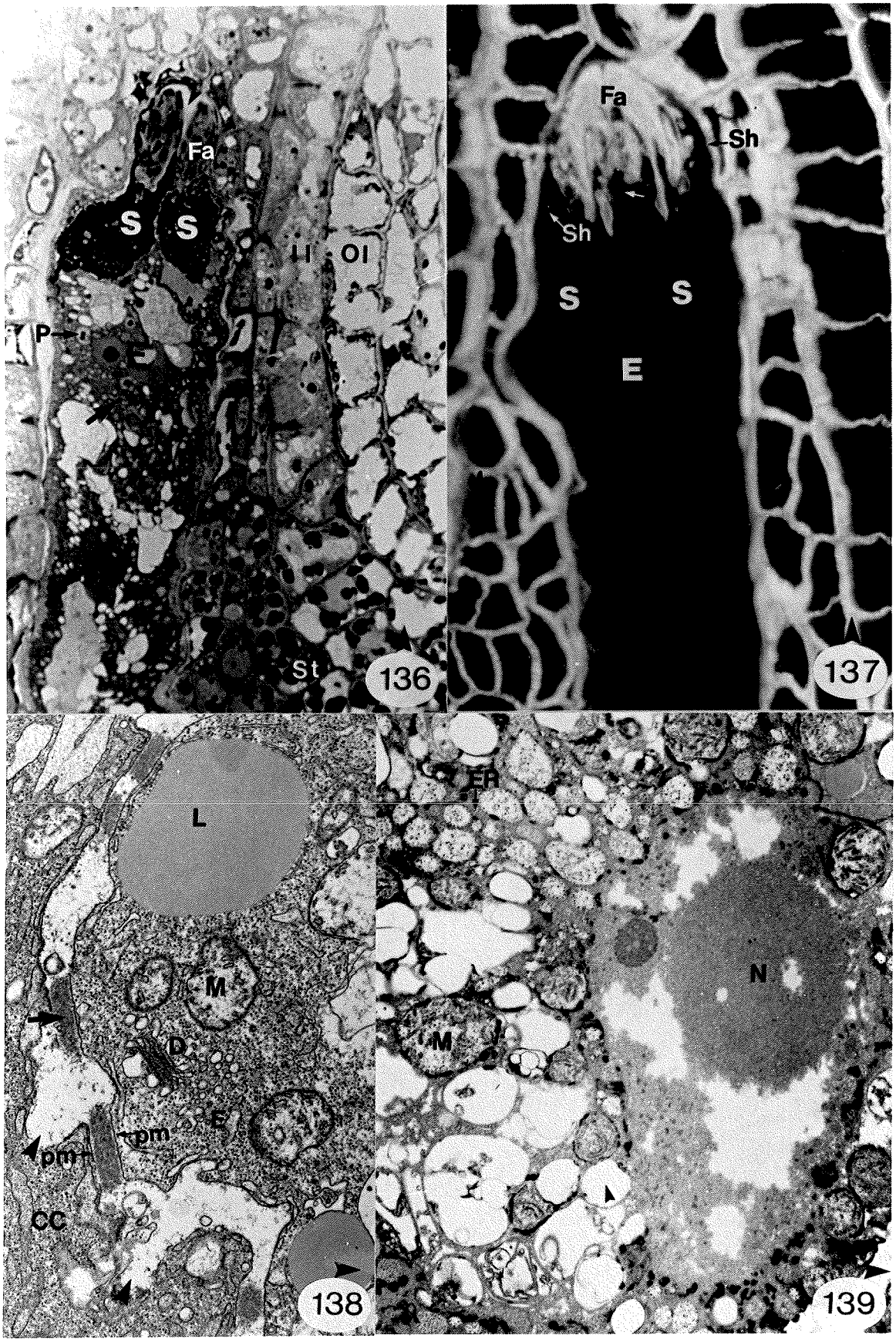
Fa
S
S
II
OI
P
St
136
Fa
Sh
Sh
S
S
E
137
L
M
D
E
pm
pm
CC
138
ER
N
M
139

Figure 140. Electron micrograph of the polar nuclei from a non-fertile ovule 72 h after anthesis. The polar nuclei (PN) are interconnected by nuclear bridges (nb) and there are mitochondria (M), ER, and lipid bodies (L) entrapped in the cytoplasmic embayments between the nuclei. The ER is highly branched and dilated. There are plastids (P) and dictyosomes (D) in the perinuclear regions. UA/Pb. x7,900.

Figure 141. Electron micrograph of the central cell cytoplasm from a non-fertile ovule 72 h after anthesis. The chloroplasts (P) possess well defined, stacked thylakoid lamellae. Starch is notably absent from the chloroplasts. Microbodies (Mb) and dictyosomes (D) active in vesicle production are present in the central cell cytoplasm. The extensive network of branched smooth ER (SER) appears to be sequestering cytoplasm and organelles. UA/Pb. x20,000.

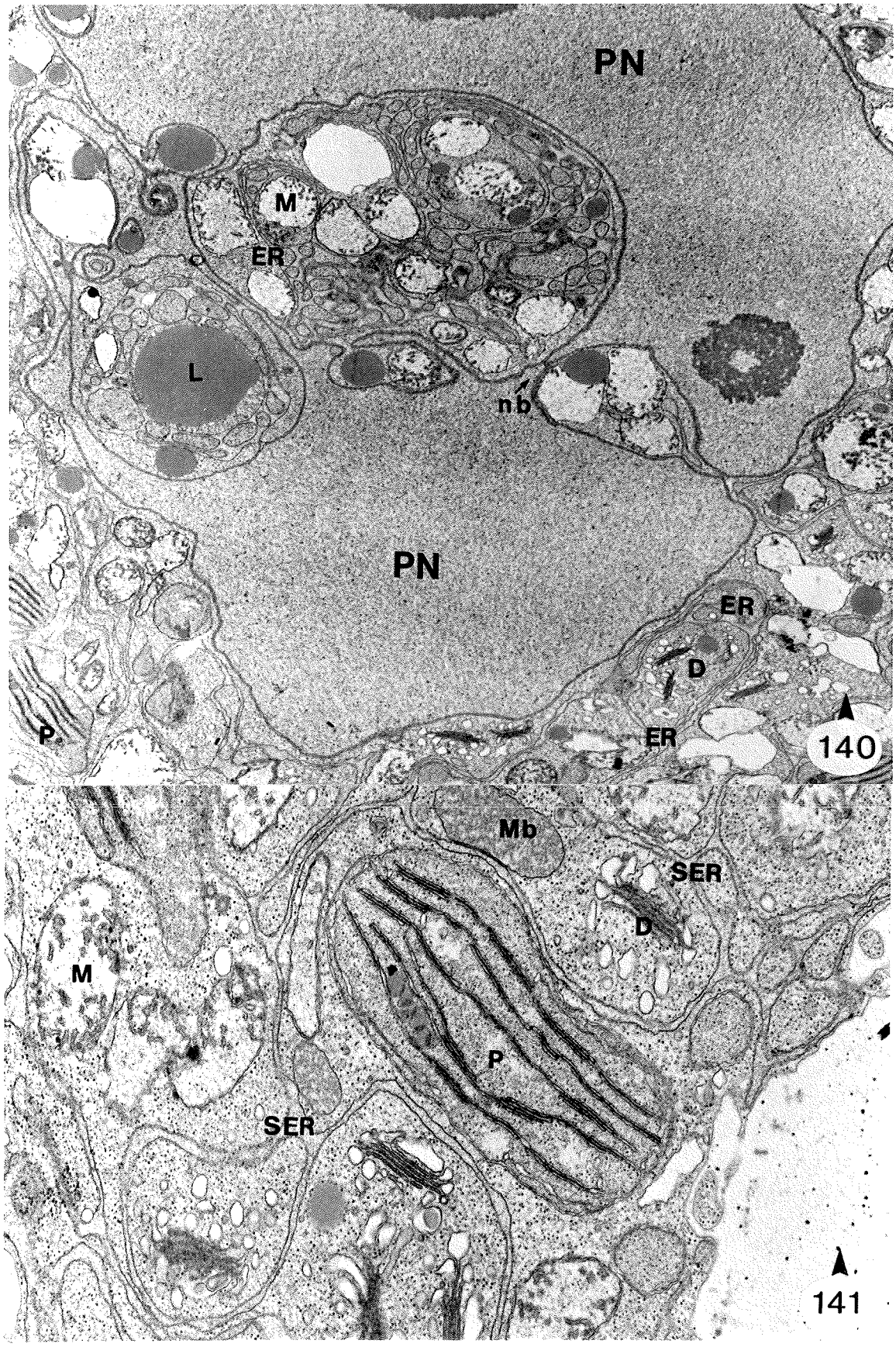
PN
M
ER
L
n.b
PN
ER
D
P
ER
140
Mb
SER
D
M
P
SER
141

DISCUSSION

There have been relatively few studies on the origin and development of angiosperm integuments. Maheshwari (1950) in an extensive review of the early literature on angiosperm embryology discusses the integuments primarily with reference to plant systematics. Unfortunately our knowledge of integument ontogeny still remains rather rudimentary (see the review by Bouman 1984). The most detailed account was by Roth (1957) on Capsella, a member of the family Cruciferae. The camera lucida drawings show that, unlike Brassica campestris, both the inner and outer integuments of Capsella are of dermal origin and remain, for the most part, two layered during the course of ovule development. Bouman (1975), in a study of integument initiation in the Cruciferae, described for the first time the subdermal origin of the outer integument in Brassica. Bouman also reported a partly subdermal origin for the outer integument of another member of the Cruciferae, Lunaria. In Lunaria the abaxial portion of the outer integument is of dermal origin while the portion of the outer integument on the adaxial side of the ovule is of subdermal origin. The transition region between the dermal and the subdermal modes of outer integument initiation was not discussed and micrographs substantiating this mode of outer integument ontogeny in the Cruciferae were not provided. The present study concurs with Bouman (1975) as to the subdermal origin of the outer integument of Brassica. Subsequent development of the integuments in the formation of the inverted campylotropous ovule in Brassica campestris is in agreement with the interpretations of Roth (1957) for Capsella. The report of

three modes of outer integument initiation within the Cruciferae illustrates a need for additional studies on integument development in the family.

The unequal division of the archesporial cell into a small primary parietal cell and a larger chalazal primary sporogenous cell, which differentiates into the megasporocyte cell, has been reported to occur in a number of the Cruciferae including Brassica campestris var.yellow sarson (Rathore and Singh 1968). In other Cruciferae, including Brassica oleracea, the archesporial cell is transformed directly into the megasporocyte cell (Thompson 1933, Davis 1966). Thus both tenuinucellate and crassinucellate ovules are represented in the Cruciferae (Davis 1966). The present study has reported for the first time the occurrence of both modes of development in the single Cruciferous species Brassica campestris.

With the onset of meiosis the megasporocyte cell enters a period of both cytoplasmic and nuclear change during the transition from the sporophyte to the gametophyte generation. At mid-prophase, following the formation of the synaptonemal chromosomal complex, the inner membrane of the nuclear envelope becomes dilated. This separation of the nuclear envelope coincides with the appearance of membrane-bound electron-opaque inclusions between the two membranes. The first question concerning the dilated envelope is whether its appearance is real or is an artifact. The present study cannot conclusively answer this question but can only point out the difficulty encountered in preserving the morphology of the megasporocyte cell without some degree of plasmolysis. There are a number of reports on the occurrence of a dilated nuclear envelope (often termed nuclear vacuoles or

nuclear blebs) during sporogenesis in vascular plants. Nuclear vacuoles with membrane-bound inclusions have been shown to occur in Zea (Russell 1979), Pteridium, Dryopteris, Marsilea, Pinus, and Lycopersicon (Scheffield et al. 1979), Gasteria (Willemse and De Boer-De Jeu, 1981), and Capsella (Schulz and Jensen 1981). The chemical compostion and possible function of the membrane-bound inclusions remain speculative. A concensus among a number of authors is that contents of the inclusion are of nuclear origin and are being eliminated from the nucleus and degraded in the cytoplasm during the transition from sporophyte to gametophyte (Dickinson and Heslop-Harrison 1977).

In the present study the intense staining of the primary sporogenous cell cytoplasm with cationic dyes would suggest an increase in metabolic activity. By mid-prophase, the staining intensity of the megasporocyte cytoplasm drops sharply. This decrease in basiophilia and electron-opacity of the megasporocyte is due in part to a reduced number of cytoplasmic ribosomes. A number of studies have shown a similar decrease of ribosomes in the prophase megasporocyte (Newcomb 1973a; Dickinson and Potter 1978; De Boer-de Jeu 1978; Russell 1979; Schulz and Jensen 1981; Medina et al. 1981) and microsporocyte (Rashid et al. 1982). Pritchard (1964), in a cytochemical study of megagametophyte development in Stellaria, noted the archesporial cell stained more intensely for RNA than the surrounding nucellar tissue, followed by a sharp decline in staining intensity by the end of meiosis I, followed by an increase in RNA staining at the beginning of megagametophyte development. There have been, to my knowledge, no biochemical studies on RNA levels in

prophase megasporocyte cells. However, a biochemical study of RNA and acid phosphatase levels in the microsporocytes of Cosmos (Knox et al. 1970) showed a 50% decline in RNA by the end of meiosis I with a corresponding increase in levels of acid phosphatase. Acid phosphatase was thought to be one of the major enzymes involved in the elimination of RNA from the cell (Knox et al. 1970).

There are currently two theories on the mechanism of ribosome elimination from the megasporocyte cell. Both involve double and multiple membrane-bound inclusions derived from RER cisternae. The theory of Dickinson and Heslop-Harrison (1977) is that a portion of the sporocyte ribosomes is encapsulated within the membrane-bound inclusions and in some manner isolated and protected from hydrolytic enzymes that eliminate the remainder of the cytoplasmic ribosome population. Thus a major portion of the RNA synthesized during the diploid phase is removed prior to gametophyte formation (Dickinson and Andrews 1977).

Schulz and Jensen (1981, 1986) in a study of megasporogenesis in Capsella present evidence for the encapsulation and elimination of ribosomes and organelles during meiosis by double and multiple membrane-bound autophagic vacuoles. These autophagic vacuoles arise from ER cisternae within the megasporocyte during pachytene of meiosis I and persist in the dyad, tetrad, functional megaspore, and 2-nucleate stage of megagametophyte development. The vacuoles contain acid phosphatase and function to eliminate the encapsulated portions of the cytoplasm. A similar view for the elimination of megasporocyte cytoplasm in Zea was made by Russell (1979), though the "lytic complex" described in the study consisted of both concentric multiple

membrane-bound inclusions derived from whorls of ER and single membrane-bound vacuoles derived from dilated ER.

Unfortunately the present study can neither refute nor support either of the theories. The type of membrane-bound inclusions in Brassica megasporocytes is identical to those described by Dickinson and Heslop-Harrison (1977); however in direct contrast to their results the present study found fewer ribosomes within the inclusion as compared to the adjacent cytoplasm. This observation would tend to support the autophagic vacuole concept proposed by Schulz and Jensen (1981, 1986).

The large nucleoli apparent in both chalazal megaspores at the level of the light microscope suggest an increase in nucleolar activity at the completion of meiosis. This nucleolar activity is perhaps an indicator of increased ribosome synthesis at the inception of the gametophyte phase of development, as is evident at the ultrastructural level in the older functional megaspore and young 2-nucleate megagametophyte of Brassica. An increase in functional megaspore ribosomes has been reported in a number of angiosperms (Newcomb 1973a; Dickinson and Potter 1978; Russell 1979; Medina et al. 1981; and Schulz and Jensen 1986).

The completion of meiosis in Brassica results in either a tetrad of megaspores or, more commonly, a triad of two megaspores derived from the chalazal dyad cell and the micropylar dyad cell that has not undergone the second meiotic division. Failure of the micropylar dyad to divide has been reported to occur in a number of angiosperms (Davis 1966) but the first account of it occurring in the Cruciferae (Dentaria) was made recently by Spooner (1984). Spooner

made no reference to formation of typical meiotic tetrads and implied that triads were the common product of female meiosis in Dentaria. Schulz and Jensen (1986) noted periodic abnormal, cell wall formation in the micropylar dyad cell of Capsella following completion of meiosis II.

In the mid-propahse megasporocyte of Brassica, there is a polar distribution of cytoplasmic organelles with the major portion of the plastids and constricted mitochondria being found in the chalazal cytoplasm. The reduction in size of the mitochondria and a corresponding increase in the electron-opacity of the matrix has also been reported in the tetrasporic genus Lilium (Dickinson and Heslop-Harrison 1977) and two monosporic genera, Gasteria (Willemse and Franssen-Verheijen 1978) and Capsella (Schulz and Jensen 1981, 1986). The apparent activity of dictyosomes in the megasporocyte cytoplasm of Brassica may relate to the incipient formation of cell walls during meiotic cytokinesis as was suggested by Kennel and Horner (1985). There is also a polarity of meiotic products in terms of cell size. The division of the chalazal dyad cell is unequal with the functional megaspore being larger than the non-functional sister megaspore. Whether the cytoplasmic polarity exhibited by the megasporocyte is carried into the dyad, triad, or tetrad cannot be answered at this time due to the absence of ultrastructural information on these stages of development. At the light microscope level the two cells are cytologically similar. Stewart and Gifford (1967) showed a chalazal polarity following meiosis I in the gymnosperm Ginkgo. The majority of mitochondria and chloroplasts segregated into the chalazal dyad cell that is destined to produce the

functional megaspore. A similar distribution in organelles was reported in Gasteria (Willemse and Bednara 1979). Woodcock and Bell (1968) found that in Myosurus the distribution of organelles following meiosis was random. Russell (1979) found that in Zea the megasporocyte showed a chalazal polarity of organelles but this polarity was not carried through to the dyad and tetrad stages of development as there was no apparent difference in the distribution of organelles in the post-meiotic cells. Recently Kennel and Horner (1985) showed a chalazal polarity of organelles at mid-prophase of meiosis I. The absence of ultrastructural observations made it impossible for them to identify or follow the fate of these organelles through to the completion of meiosis.

With the exception of the double membrane-bound inclusions which have disappeared following meiosis, the cytoplasm of the functional megaspore of Brassica possesses the full complement of cytoplasmic organelles found in the megasporocyte. However, the number of organelles have been radically reduced and the chloroplasts and mitochondria appear more electron-transparent than at the megasporocyte stage of development. This dedifferentiation of chloroplasts and mitochondria has been shown to occur in Myosurus (Woodcock and Bell 1968), Lilium (Dickinson and Potter 1978), Pisum (Medina et al. 1981) and the elimination of a number of these organelles during meiosis by autophagic vacuoles has been suggested by Schulz and Jensen (1986). Early studies on megasporogenesis in angiosperms postulated the total elimination of plastids and mitochondria during meiosis (Bell and Muhlethaler 1964; Israel and Sagawa 1964; Bell et al. 1966; Bell and Woodcock 1968) and their "de

novo" synthesis from blebs of the nuclear envelope (Bell 1972), a concept that has not gained wide acceptance. In Brassica both plastids and mitochondria survive meiosis, but in reduced numbers, and are present as progenitors of these organelles for the new megagametophyte geneneration. It would appear from the literature that there is considerable variation in the behavior, distribution and ultimate fate of cytoplasmic organelles during meiosis. The presence of chloroplasts in the megagametophyte of Brassica campestris concurs with the genetic studies on female cytoplasmic inheritance, via chloroplast DNA, of resistance to the herbicide atrazine (Machado and Bandeen 1982).

The strong aniline blue fluorescence of the newly formed cross walls between cells of the triad may indicate the presence of a callose-like substance. The absolute specificity of the fluorochrome in aniline blue for callose has been questioned by Smith and McCully (1978), who indicate that unidentified compounds other than callose may also bind the fluorochrome.

The encasement of microsporocyte cells by callose and its subsequent deposition between microspores is a common feature of microsporogenesis in angiosperms (Bhandari 1984). Heslop-Harrison and Mackenzie (1967), in a study on the uptake of radioactive thymidine into the anther of Lilium, showed that the tracer was readily incorporated into the microsporocytes prior to the onset of meiosis, but was excluded from the meiotic cells from mid-prophase through to the separation of the microspores from the tetrad. The exclusion of the thymidine correlates with the deposition of callose. These authors suggest that callose acts as a barrier to certain macromolecules and serves to isolate the developing microspores from the surrounding

diploid tissue. This isolation allows the autonomous development of the microgametophyte generation.

The isolation of the haploid phase from the diploid phase does not occur in Brassica. The megasporocyte cell wall is virtually free of callose deposits which is in contrast to the total encasement of the megasporocyte cell by callose in Oenothera (Rodkiewicz 1970), Zea (Russell 1979), and Capsella (Schulz 1981). Following meiosis in Brassica the deposition of callose is such that the cells of the triad are isolated from one another but not from the surrounding sporophyte tissue. In fact the functional megaspore is in a favored position to receive metabolites and hormonal stimuli/inhibitors from the parent sporophyte via the funiculus of the ovule. A similar distribution of callose has been found in a number of post-meiotic monosporic Polygonum-type angiosperms (Russell 1979; Schulz and Jensen 1981, 1986; Kennel and Horner 1985). In the monosporic Oenothera-type, where the three chalazal megaspores degenerate and the micropylar megaspore forms the megagametophyte, the distribution of callose is similar to the Polygonum-type except it is the micropylar functional megaspore that is free of callose desposits (Rodkiewicz 1970, Jalouzot 1978). In the tetrasporic type, where the entire original megasporocyte cell functions in megagametophyte development, there are no deposits of callose during meiosis (Kapil and Bhatnagar 1981). It would appear that the function of callose during megasporogenesis is to isolate the non-functional megaspores and to ensure that only the functional megaspore participates in megagametophyte development.

Following meiosis the functional megaspore enlarges and assumes an obdeltoid shape. A thick electron-transparent, PAS-negative lateral

wall, traversed by microvillus-like membranous extensions, as seen in the functional megaspore of Capsella (Schulz and Jensen 1986), was not observed Brassica. The enlarged functional megaspore contains few vacuoles. Vacuole formation does not occur until after the first mitotic division within the functional megaspore. The early 2-nucleate stage of megagametophyte development is characterized by perinuclear plastids that are actively dividing. The numbers of mitochondria are also greater but the internal structure of the organelle remains simple. Numerous small vacuoles, the origin of which could not be determined, occur in the peripheral cytoplasm. It is assumed that the fusion of these small peripheral vacuoles contributes to the large central vacuole that forms between the two nuclei. As this vacuole increases in size the megagametophyte expands in a micropylar direction at the expense of the degenerate megaspores and the enlarged hypodermal nucellar cells. The expansion of the 2-nucleate megagametophyte does not occur until such time as the inner and outer integuments have completely enveloped the nucellus. The lateral resistance that the integuments impose on the nucellus may be important in determining the micropylar direction of megagametophyte expansion.

Lintilhac (1974) proposed a biophysical model for the ovule of Gossypium in which the externally imposed tectonic stress of the integuments and nucellus may play a role in the development of the megagametophyte. However, the radial pattern of perpendicular walls merging at the centre of the functional megaspore and megagametophyte and forming a region of null stress in the well developed

crassinucellate ovule of Gossypium (Lintilhac 1974) does not occur in Brassica.

The micropylar expansion of the megagametopyte coincides with anticlinal divisions within the inner integument, lateral to the megagametophyte. This intercalary growth of the integuments during the early 4-nucleate stage continues to maturity and is a clear example of coordinated growth between different parts of the ovule. A similar coordination of integument and megagametophyte growth has been reported for Oryzopis by Maze et al. (1970). In Oryzopis the initial growth of the integument is apical, followed by divisions in the basal regions of the integument at the 4-nucleate stage.

During the coenocytic phase of megagametogenesis in Brassica there is a progressive increase in the numbers of plastids, mitochondria, and dictyosomes suggesting a corresponding increase in megagametophyte metabolism. These results concur with those of Godineau (1973) for Crepis. In contrast, Russell (1979) reports a temporary increase in the number of megagametophyte organelles during the 2-nucleate phase in Zea followed by their elimination through the reactivition of the "lytic complex" at the 4-nucleate stage of development. By the 8-nucleate stage of development the autophagic complex was incorporated into the central vacuole at which time he suggests that activity of the lytic complex ceases. A lytic complex such as described by Russell was not observed in Brassica. There were however, numerous examples of organelles associated with the poorly fixed remains of the tonoplast of the expanding megagametophyte central vacuole. Under these fixation conditions, implying an autophagic function to the megagmetophyte vacuole of Brassica would

be, at best, tenuous. Matile (1975) suggests that autophagy and the turnover of cellular proteins is a major function of the plant vacuole. Recent biochemical evidence has confirmed an autophagic function for the vacuole of the alga Chara (Moriyasu and Tazawa 1986).

In Gasteria, Willemse and Franssen-Verheijen (1978) report that the maximum number of organelles is attained at the functional megaspore stage of development, prior to the first nuclear division of the megagametophyte and prior to vacuolation of the megagametophyte. Except for an increase in polysomes at the 4-nucleate stage of development, as was also observed in Brassica, the numbers of organelles remained constant during megagametogenesis in Gasteria. Clearly the limited number of ultrastructural studies on the coenocytic phase of megagametogenesis has failed to provide a consensus as to the behavior of megagametophyte organelles during this phase of megagametophyte development.

In Brassica there appears to be a flux of energy reserves during megasporogenesis and megagametogenesis. During megasporogenesis, the number of lipid bodies increased followed by a decrease at the end of meiosis. Similarly lipids increased during the 2-nucleate phase and were absent from the early 4-nucleate megagametophyte. At the late 4-nucleate stage of development, prior to the formation of cell walls, the numbers of lipid bodies in the megagametophyte once again increased. It would seem that the appearance of these lipid reserves is correlated with periods of impending metabolic activity associated with megasporogenesis, megagametophyte expansion, and the incipient cellularization of the megagametophyte. Starch is never a major energy reserve within the coenocytic megagametophyte. The micropylar region

of the integuments becomes a sink for carbohydrate commencing at the 4-nucleate stage of development but the megagametopyte plastids remain starch-free from the functional megaspore stage until shortly after the migration of the polar nuclei following cellularization of the megagametophyte. Concurrently with megagametophyte expansion during the 4-nucleate stage of development in Brassica the number of dictyosomes associated with the lateral wall of the megagametophyte increases. These dictyosomes appeared active in vesicle production and there was evidence for the subsequent fusion of dictyosome vesicles with the expanding lateral wall of the megagametophyte. This would seem reasonable in light of the requirement for additional wall material during the expansion phase of the megagametophyte. A similar conclusion was reached by Newcomb (1973a) for Helianthus.

The transition from the coenocytic to the cellular phase of the megagametophyte has long eluded plant embryologists. There are two basic theories dealing with the mechanism of cell wall formation in the angiosperm megagametophyte. One theory envisions the encapsulation of the synergid, antipodal, and egg nuclei and cytoplasms by what is termed free wall formation. According to the theory, free wall formation occurs independently of karyokinesis and does not involve microtubules. The cell walls are initiated at the wall of the megagametophyte as pegs of wall material that expand centripetally into the megagametophyte cytoplasm. Evidence supporting the free wall theory as it pertains to the formation of the egg, synergid, and antipodal cell walls is lacking. Wilms (1981a) reported that the cell walls separating the antipodal cells of Spinacia formed from the

periphery of the megagametophyte to the centre. However, Wilms failed to provide evidence in the form of micrographs to support this claim.

Most of the literature in support of the free wall theory is derived from studies on endosperm formation in Helianthus (Newcomb 1973a), Stellaria (Newcomb and Fowke 1973), Haemanthus (Newcomb 1978), and Triticum (Morrison and O'Brien 1976). Fineran et al. (1982) have challenged the free wall theory and provide convincing evidence that the initial endosperm cell walls in Triticum involve typical phragmoplasts and that these cell walls are derived from centifugally growing cell plates. Each parietal endosperm nucleus becomes enclosed within an open ended alveolus derived from four circular phragmoplasts oriented perpendicular to one another and to the lateral wall of the central cell. The centrifugally expanding phragmoplasts eventually fuse with one another and with the lateral wall of the central cell, while that portion of the phragmoplast opposite the lateral central cell wall continues to expand centripetally into the central cell.

Cass et al. (1985) in a study on cell wall formation in the megagametophyte of Hordeum have provided the first ultrastructural evidence for the formation of cell walls around the antipodal and egg apparatus nuclei in the angiosperm megagametophyte. Cell wall formation in the megagametophyte of Hordeum was shown to involve elongated cell plates associated with clusters of microtubules. The young cell walls of the megagametophyte have a beaded appearance and the authors suggest that the beaded cell walls are derived from dictyosome vesicles. They further speculate that the formation of these cell plates may be associated with centrifugally expanding phragmosplasts, similar to those described by Fineran et al. (1982)

for the endosperm of Triticum. In a recent publication, Cass et al. (1986) suggest that the four nuclei at the micropylar end of the megagametophyte of Hordeum are separated by two cell plates. A vertical cell plate separates the sister synergid nuclei and an initially horizontal cell plate separates the egg and polar nuclei. The horizontal cell plate expands centrifugally with one edge contacting the megagametophyte wall while the opposing edge of the horizontal plate branches. One branch grows in a micropylar direction and separates the egg nucleus from the two synergid nuclei. Chalazal growth of the vertical wall between the synergids eventually contacts and fuses with the horizontal plate. The horizontal plate forms the chalazal wall of all three cells.

The earliest cell wall of the egg apparatus viewed at the ultrastructural level in Brassica consists of beads of wall material that are similar to those described by Cass et al. (1985). Histochemically, the differentiation of the cell walls of Brassica appears to occur in a centripetal direction, but whether or not these walls were derived from centrifugally growing phragmoplasts or from centripetally growing free walls independent of a phragmoplast cannot be answered at this time.

The cell walls of the young egg apparatus show a strong PAS-positive reaction and consist of a relatively wide electron-transparent space between two plasma membranes. The initial chalazal expansion of the two synergids and the egg into the central cell produces curved cell walls and results in the formation of the synergid and egg hook cell wall regions. Continued expansion of the chalazal half of the egg apparatus results in a marked thinning of the

common cell walls with periodic pockets of expanded electron-transparent material. The cell walls remain PAS-positive. The micropylar walls of the mature egg apparatus and the chalazal egg-central cell wall show a strong PAS reaction while the thinner walls of the egg apparatus (ie. the common chalazal wall between the synergid and the egg and the common chalazal wall between the synergid and the central cell) show a weak PAS-positive reaction that is barely visible at the level of the light microscope. The chalazal expansion of the cells of the egg apparatus results in the egg and synergids doubling in length from approximately 20 um to approximately 40-45 um. The electron-opaque deposits and expanded electron-transparent regions of the extreme chalazal egg-central cell wall are formed after elongation of the egg apparatus. Even with the thinning of the chalazal cell walls between the synergid and the egg and between the synergid and the central cell during the expansion phase of the egg apparatus, there would be a need for additional plasma membrane and cell wall material. The source of the additional plasma membrane and wall material could not be determined. Dictyosomes, adjacent to the cell walls of the egg apparatus, were present in the young and mature egg, synergid, and central cells. There was, however, no direct evidence of dictyosome-derived vesicles contributing to the formation of the expanding cell walls. The close proximity of ER to the plasma membranes of the egg and synergid and the evidence showing a direct continuity of central cell ER and the plasma membrane on the central cell side of the egg suggests the possible involvement of ER cisternae in the deposition of cell wall material in the egg apparatus. The involvement of ER in the synthesis and deposition of cell wall

material has been previously suggested by Unzelman and Healy (1974), Singh and Mogensen (1975), Schulz and Jensen (1977), and by Mogensen and Suthar (1979).

As would be expected, all of the cell walls of egg apparatus were stained positively by the Thiery test. The positive staining of the cell walls by both the Thiery test and the PAS reaction suggests the presence of polysaccharides with vicinal hydroxyl groups in the cell walls of the egg apparatus. Positive staining with alcian blue for acid polysaccharides would suggest that some of these PAS-Thiery-positive compounds are a matrix of alpha 1-4 polyuronides. The weak but positive reaction of the micropylar cell walls of the egg apparatus with Calcofluor suggests the additional presence of beta 1-4 glucans in these regions. The absence of a Calcofluor-positive reaction after cellulase digestion would suggest that the beta 1-4 glucan in the micropylar cell walls of the egg apparatus is cellulose.

In a recent review, Willemse and van Went (1984) report that cell walls are absent in the chalazal half of the egg apparatus in the majority of angiosperms that have been surveyed. Exceptions, in which the egg apparatus is encased entirely by a PAS-positive wall, have been reported in Capsella (Schulz and Jensen 1968a, 1968b), Epidendrum (Cocucci and Jensen (1969a), Papaver (Olson and Cass 1981), Ornithogalum (Tilton 1981), and Scilla (Bhandari and Sachdeva 1983). Folsom and Peterson (1984) have shown the chalazal walls of the synergids and egg of Glycine to be Thiery-positive. They presumed, based on the positive Thiery test, that the chalazal cells walls of the egg apparatus contained cellulose, and further suggested that the wall material was derived from dictyosome vesicles. Bhandari and

Sachdeva (1983) also state, based on the positive PAS reaction, that the chalazal walls of the egg apparatus contain cellulose. It should be noted, however, that both the PAS and Thiery tests will give a positive reaction with a variety of polysaccaride and non-polysaccharide compounds and that neither test is specific for cellulose. The role of dictyosomes in the formation of a cellulosic cell wall, as was suggested by Folsom and Peterson (1984), is not supported by the recent literature. There is convincing evidence that the plasma membrane is the site of cellulose synthesis in plant cells (Herth 1985).

The young antipodals of Brassica, situated in the extreme chalazal region of the megagametophyte, are morphologically similar to the egg apparatus at the same period of development. The young antipodal cells are vacuolate and appear turgid with the convex common antipodal-central cell wall expanding into the central cell. Both the chalazal and micropylar cell walls of the antipodals are Thiery-positive and intensely fluorescent following Calcofluor staining. The positive reaction with Calcofluor suggests the presence of cellulose in the antipodal cell wall. The antipodal cell walls of Capsella (Schulz and Jensen 1971), Papaver (Olson and Cass 1981), and Scilla (Bhandari and Sachdeva 1983) have been shown to be PAS-positive.

During maturation of the megagametophyte of Brassica the antipodal cells do not show an increase in size. Prior to anthesis there is a slight reduction in cell size and an apparent loss of turgor. The common antipodal-central cell wall becomes concave and the mature cell walls of the antipodal cells are often wrinkled. The

majority of the mature antipodal cell is occupied by the nucleus and the cytoplasm does not have an abundance of proplastids, mitochondria, and dictyosomes. The high lipid content of the young antipodals may reflect the requirement for energy molecules that are used during the early phases of antipodal differentiation or these compounds may be shunted into the central cell which maintains a high concentration of lipids throughout megagametophyte development. Yu and Chao (1979) report a high concentration of lipid in the young antipodal cells of Paspalum and the subsequent disappearance of lipid from the antipodal cells at maturity. The mature antipodals of Brassica are not a sink for energy reserve compounds. The mature antipodals are devoid of lipid reserves and the proplastids do not contain starch. In Stipa (Maze and Lin 1975) the mature antipodals are rich in lipids and may function in the transfer of lipids into the megagametophyte.

The mature antipodal of Brassica possesses a moderate amount of ER. Immediately following anthesis, the three antipodal cells degenerate. There is evidence for the formation of ER-derived double membrane-bound inclusions in the antipodal cell prior to degeneration. These inclusions may have an autophagic function and play a role in the degradation of the antipodal cell cytoplasm.

The pre-anthesis antipodals may represent a symplastic route for the flow of nutrients from the vascular trace that terminates in the chalaza-raphe region of the ovule, through the chalazal nucellus, and into the central cell of the megagametophyte. There are abundant plasmodesmata between antipodal cells, between the antipodals and the central cell, and to a lesser degree, between the chalazal nucellus and the antipodal cells. The presence of plasmodesmata linking the

sporophytic and gametophytic tissues of the angiosperm ovule has also been reported for Capsella (Schulz and Jensen 1971), Helianthus (Newcomb 1973a), and Spinacia (Wilms 1981a).

The antipodals of a number of angiosperms have been shown to be potentially active in the transport of nutrients prior to and following anthesis. In Papaver (Olson and Cass 1981), Scilla (Bhandari and Sachdeva 1983), and in Aconitum (Bohdanowicz and Turala-Szybowska 1985), the antipodal cells enlarge following anthesis and develop wall projections of the transfer cell type (Gunning and Pate 1969). These persistent antipodals are rich in plastids, mitochondria, and dictyosomes and appear to play a role in the transport of nutrients into the megagametophyte following fertilization. Commonly, in grasses, the three antipodal cells undergo a series of mitotic divisions to form a chalazal aggregation of antipodal tissue. In Zea (Diboll and Larson 1966) and in Hordeum (Cass et al. 1986) the antipodal cells adjacent to the chalazal nucellus develop wall ingrowths and in Zea all the antipodal cells possess a cytoplasm that appears to be synthetically active.

Wall ingrowths have also been shown to occur in angiosperms that possess ephemeral, but synthetically active antipodal cells (Newcomb 1973a, Wilms 1981a). Wall ingrowths, of the transfer cell type, are not found in the antipodal cells of Brassica. The ephemeral antipodals of Brassica are similar to the antipodals of Capsella (Schulz and Jensen 1971). In both genera, the antipodals and chalazal nucellus degenerate shortly after anthesis. Schulz and Jensen (1971) report that the chalazal proliferating tissue of Capsella is synthetically active and may play a major role in transferring

nutrients to the megagametophyte during the early phase of embryo development. In Capsella, the nucellar chalazal proliferating tissue begins to degenerate at the octant stage of embryo development, at which time membrane-bound inclusions, similar to those of the degenerating antipodal cells of Brassica, become prevalent in the cytoplasm. The appearance of starch in the chalazal proliferating tissue of Brassica would imply that the tissue is a sink for carbohydrates. The possible post-fertilization nutritional role of the chalazal proliferating tissue in Brassica will be the subject of future research.

The central cell is the largest cell of the the megagametophyte and plays an important role in the post-fertilization development of endosperm tissue. In most angiosperms the mature central cell is a highly vacuolate binucleate cell containing two polar nuclei and a thin layer of parietal cytoplasm adjacent to the egg apparatus, antipodals, and lateral walls of the megagametophyte (Willemse and van Went 1984). It would appear that Brassica campestris is somewhat unique in that the large central cell vacuole, characteristic of the coenocytic and early cellular phases of development, disappears, leaving a small central cell vacuole in the extreme chalazal region of the cell adjacent to the antipodals. Prior to the disappearance of the central cell vacuole, and shortly after the completion of cell wall formation around the nuclei of the antipodals and egg apparatus, the chalazal polar nucleus begins to migrate in a micropylar direction. Microtubules parallel to the long axis of the central cell are closely associated with the chalazal polar nucleus. It is not possible, in a static image, to ascertain the role of these microtubules in Brassica

campestris. During elongation of the apical cells in the caulonema of the moss Funaria, the nuclei are seen to migrate in an apical direction (Schmiedel and Schnepf 1980). Ultrastructural studies have shown that the migrating nuclei of Funaria are encased by microtubules in a manner similar to that exhibited by the chalazal polar nucleus of Brassica. In Funaria, microtubules are thought to play a role in nuclear movement. There are numerous other reports in the literature that implicate microtubules in the movement of nuclei and other cytoplasmic organelles (Gunning and Hardham 1982). Recent reports have implicated microtubule-associated ATPases in the directional movement of organelles in a giant freshwater amoeba (Schliwa 1984, Koonce and Schliwa 1986). Whether a similar system is involved in the movement of the polar nuclei within the central cell is unknown at this time. It should be noted that microtubules were not associated with the micropylar polar nucleus in the central cell of Brassica. The eventual fusion of polar nuclei takes place in the mid-micropylar end of the central cell suggesting that the micropylar polar nucleus must move in a chalazal direction prior to nuclear fusion. If one of the roles of microtubules is in the directional movement of organelles one would assume the incipient formation of microtubules around the micropylar polar nucleus. The other alternative that has been postulated by McKerracher and Heath (1985) is that microtubules that ensheath the hyphal nuclei of Basidiobolus have a purely structural role in positioning the nucleus in the cytoplasm. The position of the chalazal polar nucleus and associated microtubules near the middle of the central cell at the time of fixation and the lack of microtubules around the micropylar polar nucleus, suggests that a stabilizing

function of these central cell microtubules is a possible alternative explanation for their presence in the central cell cytoplasm.

The fusion of the polar nuclei within the central cell of Brassica, the involvement of ER and the formation of polar bridges appears to be similar to that initially described by Jensen (1964). Subsequent reports have confirmed the presence of nuclear bridges between partially fused polar nuclei in Capsella (Schulz and Jensen 1973), Petunia (Went 1970b), Stipa (Maze and Lin 1975), Spinacia (Wilms 1981b) and Glycine (Folsom and Peterson 1984). In Capsella (Schulz and Jensen 1973) and in Lepidium (Prasad 1975), both members of the Cruciferae, the polar nuclei were reported to merge completely forming a single fusion nucleus prior to double fertilization. In Brassica, a fusion nucleus was never observed and the two polar nuclei remained attached by the nuclear bridges and common, uniting strands of ER throughout the development of the unfertilized central cell, including the central cell of the non-fertile ovule, 72 h after anthesis.

The central cell, prior to the migration and fusion of the polar nuclei, contains numerous plastids of the proplastid type. Following nuclear fusion the plastids of the central cell begin to accumulate starch and by anthesis the plastids have enlarged and developed a well defined system of thylakoid lamellae. The control of plastid development in the megagametophyte of Brassica must reside in the central cell itself, assuming all plastids of the megagametophyte are of comparable ages and are subject to the same physical stimuli (eg.light). The plastids of the egg, synergids, and antipodals remain as proplastids throughout the development of the megagametophyte while

those of the central cell differentiate into chloroplasts. The only other report of the occurrence of choloroplasts in the central cell of an angiosperm ovule was in Capsella (Schulz and Jensen 1973). In addition to chloroplast starch, in the central cell of Brassica before and after fertilization, there is also an abundance of lipid bodies and microbodies present in the central cell over the same developmental time period. The frequent close association of central cell lipid and microbodies suggests that the latter are glyoxysomes that function in the glyoxylate cycle (Huang et al. 1983).

A distinctive feature of the mature central cell of Brassica is the development of wall projections along the lateral wall of the central cell from its mid-region, opposite the polar nuclei, to the micropylar end of the central cell, adjacent to the synergid and egg hook region. The plasma membrane of the central cell follows the contours of wall projections suggesting a transfer cell function as described by Gunning and Pate (1969). In Brassica there are numerous mitochondria in close proximity to the wall projections which could conceivably provide the energy for membrane-associated active transport of solutes in or out of the megagametophyte. Transfer cells may well be an important means of transport into the megagametophyte in light of the absence of plasmodesmata connecting the sporophyte and gametophyte phases in the micropylar region of the ovule. Preliminary attempts to localize, at the ultracytochemical level, membrane-associated phosphatase activity in the central cell wall projections of Brassica have been unsuccessful.

Wall projections have been reported to occur in the unfertilized central cell of Linum (Vasart and Vasart 1966), Helianthus (Newcomb

and Steeves 1971, Newcomb 1973a), Stellaria (Newcomb and Fowke 1973), Euphorbia (Gori 1977), and Glycine (Folsom and Peterson 1984). In Capsella, wall projections are absent from the central cell prior to fertilization (Schulz and Jensen 1973), but develop on the lateral walls of the central cell, on the central cell side wall of the suspensor (Schulz and Jensen 1974), and on the extreme chalazal walls of the central cell following fertilization. Tilton et al. (1984), contrary to the report of Folsom and Peterson (1984), describe the formation of central cell wall projections in Glycine as occurring between fertilization and the first divisions of the zygote, coinciding with the degeneration of the adjacent nucellar tissues. Mogensen and Suthar (1979) report the occurrence of wall projections on the central cell side of the synergids of Nicotiana.

Newcomb and Steeves (1971) reported the close proximity of dictyosomes to the developing wall projections and implicated dictyosomes and dictyosome vesicles in the formation of the central cell wall projections. In Brassica, as in Glycine (Folsom and Peterson 1984), the central cell wall projections are Thiery-positive. In Brassica, vesicles being released from the maturing face of dictyosomes in close proximity to the developing wall projections are Thiery-positive. Thiery-positive, dictyosome-like vesicles appear to be fused with the lateral central cell wall and contribute to the formation of the central cell wall projections. Tubular inclusions, associated with the central cell wall projections, appear to be membranous in nature and similar to what Marchant and Robards (1968) term paramural bodies. Whether the inclusions are lomasomes or plasmalemmasomes (Marchant and Robards 1968) is unknown at this time

since the origin of the tubular inclusions could not be determined. Paramural bodies have been reported associated with the phloem transfer cells of Hieracium (Peterson and Yeung 1975) and leaf epidermal transfer cells in Zostera (Barnabas et al. 1982). The function of paramural bodies is speculative. They have been implicated in the actual formation of cell wall projections and in providing increased membrane surface area for the active transport of solutes. Paramural bodies have also been assigned a secretory function (Roland 1973). The tubular inclusions in the central cell wall projections of Brassica are transitory. The numerous electron-opaque deposits, that are also a characteristic feature of the central cell wall projections, may represent the degenerative remains of the tubular inclusions.

The distribution of central cell wall projections of Brassica corresponds with the micropylar region of starch distribution in the integuments. The first appearance of micropylar integument starch occurs during the 4-nucleate stage of megagametophyte development and becomes a prominent feature of the micropylar integuments in the mature ovule prior to fertilization. One can speculate that the integuments are an initial, but temporary, sink for carbohydrate being transported into the ovule via the funicular vascular trace. Portions of the starch may be mobilized as sugars and transported into the megagametophyte by the transfer cell activity of the central cell wall projections. The proximity of long strands of central cell smooth ER in the immediate vicinity of the wall projections and the presumed interconnection of this ER with the ER in close proximity to the egg apparatus could provide a direct transportation route for sugars and

other solutes into the micropylar region of the megagametophyte. ER has a close association with transfer cell wall projections in cells that are active in absorption and secretion (Gunning and Pate 1974). It has been known for over twenty years that the ER of the mammalian liver is active in the transport of soluble carbohydrate (Porter 1963) and it is conceivable that a soluble carbohydrate ER transport system may be operating in the central cell of the ovule. The presence of spiral polysomes associated with the surfaces of the ER cisternae suggests that much of the lamellate central cell ER is active in protein synthesis prior to and following fertilization.

In the majority of angiosperms, the egg has been shown to be a polarized cell. The micropylar region of the cell typically contains a large vacuole with the nucleus and the majority of organelles in the cytologically inactive chalazal cytoplasm (Willemse and van Went 1984). In Gossypium (Jensen 1965b) and Papaver (Olson and Cass 1981), the polarity of the egg is reversed with the majority of the egg cytoplasm, including the nucleus, in the micropylar region of the cell while the chalazal region is occupied by a large vacuole. The young egg of Brassica, following cellularization, is cytologically similar to the young synergids, antipodals and central cell. Small vacuoles are present in the cytoplasm along with allantoid, starchless, proplastids. Mitochondria, dictyosomes, and ER are distributed throughout the cell. In the mature egg, the nucleus is in the extreme chalazal region of the cell. During the maturation of the egg a large micropylar vacuole develops. The majority of plastids, mitochondria, and dictyosomes in the mature egg are perinuclear, though some of these organelles are present throughout the egg cell cytoplasm. The

mature egg appears to be a sink for carbohydrate and the proplastids typically contain starch. ER is sparse and the dictyosomes of the mature egg are not active in vesicle production. The small vesicles at the maturing face of the egg dictyosomes are Thiery-negative. The cytology of the mature egg cell of Brassica is similar to Gossypium (Jensen 1965b), Capsella (Schulz and Jensen 1968b), Petunia (Went 1970c), Helianthus (Newcomb 1973a), Nicotiana (Mogensen and Suthar 1979) and Spinacia (Wilms 1981a). In all of the aforementioned genera, with the exception of Helianthus (Newcomb 1973a) in which the egg was considered to be metabolically active, the cytology of the egg was indicative of an inactive cell. Between the extremes, as evidenced by the organelle-poor mature antipodals and the organelle-rich mature synergids of Brassica, it is difficult to judge the metabolic activity of a cell based on morphology alone.

In all angiosperms studied to date, the mature synergids appear to be metabolically active. The synergids are typically rich in mitochondria, plastids, ER, and dictyosomes, though the distribution of these organelles varies in different species (for a review see Willemse and van Went 1984). In addition, a micropylar filiform apparatus is a characteristic feature of the synergid. In Plumbago, where synergids are lacking, the egg cell has been shown to possess a filiform apparatus (Cass and Karas 1974).

The filiform apparatus of Brassica is stained positively by the Thiery, PAS, and Alcian blue histochemical tests suggesting the presence of substances with vicinal hydroxyl groups, and acidic polysaccharides. A strong fluorescence following Calcofluor staining suggests the presence of beta 1-4 glucans. The absence of Calcofluor

induced fluorescence following cellulase extraction suggests that the beta 1-4 glucan present in the filiform apparatus is cellulose. Chao (1971) suggested that the PAS-positive material in the filiform apparatus of Paspalum was hemicellulose derived from the breakdown of synergid starch (Yu and Chao 1979). Jensen (1963) identified pectins and suggested the probable presence of cellulose as the major chemical components of the filiform apparatus of Gossypium. Newcomb (1973a) reported the occurrence of active dictyosomes in the immediate vicinity of the filiform apparatus of Helianthus and suggested the possible involvement of dictyosomes in its formation. The release of Thiery-positive vesicles from the maturing face of dictyosomes in the immediate vicinity of the filiform apparatus of Brassica and the fusion of Thiery-positive dictyosome-like vesicles with the peripheral edge of the expanding filiform apparatus provides convincing histochemical evidence for involvement of dictyosomes in the formation of the filiform apparatus. The absence of silver proteinate in the vesicles at the forming face of the dictyosome would suggest that the glycosyl transferases responsible for the polymerization of the polysaccharide are associated with the dictyosome vesicle and are active in the transition phase between the forming and maturing faces of the dictyosome. The close association of the synergid ER and dictyosomes in Brassica and the occurrence of intervening transition vesicles between the two organelles lends support for the application to plant cells of the endomembrane concept as proposed by Morre and Mollenhauer (1974). The formulation of this concept was based on evidence from animal systems. The ER was seen as the site of synthesis of protein and lipid bound for the plasma membrane and extracellular

environment. These compounds would be transported to the forming face of the dictyosome cisternae by transition vesicles, while at the maturing face the secretory vesicles destined for plasma membrane would be released. The movement of membrane from ER to dictyosome to plasma membrane was termed membrane flow. Robinson and Kristen (1982) maintain that the ER-dictyosome connection is not common in higher plant cells and is restricted to those plant tissues, such as the ligules of Isoetes (Kristen 1980), that are primarily involved in the secretion of proteins. They further contend that the primary function of the dictyosome in the majority of plant cells, unlike those of animals, is carbohydrate secretion. Robinson (1980) maintains that transition vesicles are rare between the ER and dictyosomes of higher plant cells. There appears to be clear evidence in Brassica synergids to support the application of the endomembrane concept to the carbohydrate secreting system of a plant. The Thiery-positive substance in the dictyosome vesicles at the maturing face could be a glycoprotein, or a pure carbohydrate with the ER possibly supplying the glycosyl transferases required for their polymerization. There is considerable evidence that pectic and hemicellulosic substances, and glycoproteins are incorporated into the wall of a variety of plant cells by exocytosis involving dictyosome vesicles (Chrispeels 1976).

The filiform apparatus in angiosperm synergids varies from a simple vase-shaped micropylar thickening of the common synergid wall as seen in Petunia (Went 1970a), Helianthus (Newcomb 1973a), and Nicotiana (Mogensen and Suthur 1979) to a highly digitate elaboration of cell wall material as seen in Gossypium (Jensen 1965a), Zea (Diboll and Larson 1966), Capsella (Schulz and Jensen 1968a), Hordeum (Cass

and Jensen 1970), Stipa (Maze and Lin 1975), Spinacia (Wilms 1981a), Scilla (Bhandari and Sachdeva 1983) and Glycine (Folsom and Peterson 1984). In Brassica the filiform apparatus is of the digitate type which greatly extends the surface area of the plasma membrane. Synergids of the type found in Brassica are considered transfer cells (Gunning and Pate 1969). Jensen (1965a) was the first to suggest an absorption function for the synergid based on the presence of a filiform apparatus, numerous mitochondria in the immediate vicinity of the filiform apparatus which would provide the energy for the active transport of solutes, an elaborate network of ER that would function as an internal transport system, active dictyosomes, and the plasmodesmatal connections between the cells of the egg apparatus and the central cell which would provide the symplastic route through the megagametophyte. A similar absorption function has been attributed to the synergids of Capsella (Schulz and Jensen 1968a), Stipa (Maze and Lin 1975), Spinacia (Wilms 1981a), and Glycine (Folsom and Peterson 1984). The absence of an extended area of plasma membrane in the filiform apparatuses of Helianthus (Newcomb 1973a), Quercus (Mogensen 1972) and Petunia (Went 1970a) suggests that these cells do not function as transfer cells (sensu Gunning and Pate 1969).

Went (1970a) considered that the primary function of the synergid of Petunia was the secretion of a chemotropic substance into the micropyle for the attraction of the pollen tube. The synergids of Petunia, like those of Brassica, are in direct contact with the micropyle. Newcomb (1973a) speculated that the synergids of Helianthus may secrete a chemotropic substance that is stored in the filiform apparatus. In Spinacia, where there is an extensive region of nucellar

tissue between the synergids and the micropyle, Wilms (1981b) suggests that the synergids function in the secretion of digestive enzymes for the dissolution of the middle lamellae of the nucellar tissue prior to the arrival of the pollen tube. In Agave (Tilton and Mogensen 1979) and Ornithogalum (Tilton 1981) the synergids are suspected of secreting chemotropic substances into the nucellar cap. Chao (1971, 1977) identified a PAS-positive substance in the micropyle of Paspalum and suggested that the substance may function in guiding the pollen tube to the megagametophyte. These authors suggest that both the synergids and the epidermal cells lining the micropyle, are involved in the production of the mucopolysaccharides. Coe (1954) fed radioactive carbon dioxide to plants of Zephyranthes and studied, via autoradiography, the distribution of labelled carbon in the ovule. A gradient of silver grains occurred between the synergids and the micropyle with a maximum concentration over the synergids. Coe suggested that the labelled compounds were chemotropic substances secreted by the synergids. Mascarenhas and Machlis (1964) found an increasing gradient of calcium ions from the stigma to the placenta and provided evidence that calcium was involved in chemotropism in Antirrhinum. Jensen (1965a) found a high concentration of ash in the synergid vacuole of Gossypium following the microincineration of freeze-dried ovules and suggested that the ash may represent an accumulation of calcium that is released from the vacuole during degeneration of the synergid and may have a chemotropic function in attracting the pollen tube to the egg apparatus. However, calcium alone has proven to be chemotropically inactive in a number of angiosperms (Rosen 1971). Mascarenhas (1966) reported a decrease in

calcium from the placenta to the ovule in Antirrhinum and suggested that other factors must be involved in guiding the pollen tube to the ovule. Glenk (1971) speculates that the chemotropic substance in angiosperms is probably a mixture of different organic and inorganic substances. In Brassica, dictyosomes active in the release of Thiery-positive vesicles were not only located in the vicinity of the filiform apparatus but were distributed throughout the synergid. It is possible that some of these vesicles contained a chemotropic substance, perhaps originating in the ER, that is secreted by the synergid into the micropylar region of the ovule. Perhaps dictyosome vesicles, that appear to fuse with the filiform apparatus contain substances in addition to cell wall material. In contrast, the elaborate ER and active dictyosomes in the middle and chalazal regions of the synergids of Brassica may function in repackaging metabolites absorbed by the synergid and transferring these new compounds to the egg and central cell as was originally suggested by Jensen (1965a). It is likely that the synergids could have multiple functions and may be involved in both secretion and absorption. The accumulation of starch in the synergid proplastids and the presence of lipid bodies suggest that the synergid does absorb and store nutrients. The role of the synergid filiform apparatus as an expanded membrane surface for active transport has not been substantiated by cytochemical studies. Mogensen (1981) failed to localize membrane associated phosphatase activity in the filiform apparatus of Saintpaulia. In a similar study on Nicotiana ovules, Mogensen (1985) failed to detect phosphatase activity in the membranes of the wall projections associated with the central cell side of the synergids. Clearly cytochemical studies must be undertaken

to determine if megagametophyte transfer cells (filiform apparatus and central cell wall projections) are involved in the active uptake and/or secretion of solutes.

Another function of the synergid is to receive the pollen tube. In all species of angiosperms that have been studied using modern techniques of light and electron microscopy, the pollen tube has been shown to enter one of the synergids by way of the filiform apparatus (Willemse and van Went 1984). In Brassica one of the synergids degenerates shortly after anthesis and it is this degenerate synergid that receives the pollen tube. Rathore and Singh (1968) reported that the pollen tube bypassed the synergid of Brassica campestris and discharged two male gametes into the central cell of the megagametophyte. On examination of their camera lucida drawings it would appear that what Rathore and Singh refer to as a pollen tube located adjacent to the egg, is in fact the degenerate synergid. Degeneration of one of the synergids prior to the arrival of the pollen tube but after germination of the pollen tube on the stigma, has been shown to occur in Gossypium (Jensen and Fisher 1968), Quercus (Mogensen 1972), Stipa (Maze and Lin 1975), Proboscidea (Mogensen 1978b), Nicotiana (Mogensen 1979), Spinacia (Wilms 1981b). Cass and Jensen (1970) also report the degeneration of one of the synergids of Hordeum irrespective of whether pollination has occurred or not. Jensen et al. (1977) reported that in cultured ovules of Gossypium the early degeneration of one of the synergids and the persistence of the other synergid was independent of pollination suggesting that one of the synergids is preprogrammed for eventual degeneration. The results obtained in the present study suggest that the post-anthesis

degeneration of one of the synergids of Brassica is independent of pollination. Whether the prior degeneration of one of the synergids is a requirement for successful double fertilization is unknown at this time. In Capsella (Schulz and Jensen 1968a), Petunia (Went 1970a) Papaver (Olson and Cass 1981), and perhaps Helianthus (Newcomb 1973b) both synergids remain intact until one is penetrated by the pollen tube. Pre-anthesis bud pollination of the normally sporophytically self-incompatible Brassica campestris is known to result in the production of fertile seeds (Hinata and Nishio 1980). It would be of interest to examine the interaction between the pollen tube and the synergids in a pre-anthesis ovule of Brassica that would normally contain two healthy synergids.

The pathway of the pollen tube in Brassica campestris, following germination of the pollen grain on the stigma, is through the stylar transmitting tissue to the replum of the ovary and into an ovule by way of the funiculus and the micropyle. The time required for the most vigorous growing pollen tube to reach the ovule was approximately 9.5 h. The pathway described in the present study concurs with the report of Vandendries (1909) for various members of the Cruciferae. There was no evidence of the pollen tube growing through the vascular bundles of the style, ovary, and funiculus (mesogamy) as has been reported to occur invariably in a Brassica oleracea hybrid (Mackiewicz 1973) or through the replum as has been reported for Dentaria (Spooner 1984), also a member of the Cruciferae. Times between pollination and fertilization in earlier studies of Brassica vary from 20 h (Mackiewicz 1973), to 48 h (Iwasaki 1975) to 3 days (Rathore and Singh 1968).

Prior to the pollen tube entering the inner integument micropyle, the chalazally located egg nucleus migrates to the middle region of the egg cell, opposite the common chalazal wall between the degenerate synergid, egg, and central cell. To my knowledge this is the first report of the micropylar migration of the egg nucleus prior to fertilization and would suggest some form of communication between the egg and pollen tube. The pollen tube enters the degenerate synergid through the filiform apparatus and grows along the common synergid wall before discharging its contents via a terminal pore. Included in the pollen tube discharge are numerous spherical particles with electron-opaque cores. Similar particles were initially observed in the growing pollen tubes of Lilium (Rosen et al. 1964) and subsequently in the degenerate synergid of Gossypium (Jensen and Fisher 1968), Capsella (Schulz 1968a), Stipa (Maze and Lin 1975), Proboscidea (Mogensen 1978b), Nicotiana (Mogensen and Suthar 1979), and Spinacia (Wilms 1981b) after penetration by the pollen tube. The principal polysaccharide component was determined by Wounde et al. (1971) to be galacturonic acid. The pectic nature of the spheres has subsequently been confirmed by Heslop-Harrison and Heslop-Harrison (1982). They provide wall material for the growing pollen tube. In Brassica the polysaccharide spheres extend from the discharge pore of the pollen tube to the intersection of the common wall between the zygote, degenerate synergid, and central cell. The cell wall between the degenerate synergid and the zygote, and the cell wall between the degenerate synergid and the central cell, in the region of pollen tube discharge, become markedly thickened following penetration of the pollen tube. There are aggregations of pollen tube polysaccharide

spheres in the immediate vicinity of the thickened walls and a number of the spheres appear to be fusing to the cell wall. There has been one previous report of the fusion of pollen tube polysaccharide spheres with the degenerate synergid wall in Nicotiana (Mogensen and Suthar 1979).

The trajectory of the pollen tube discharge suggests that the transfer of sperm to the egg and central cell would occur at the junction of the egg, degenerate synergid, and central cell. The egg nucleus, following migration to the centre of the egg cell, and the two polar nuclei, in the adjacent central cell cytoplasm, would be in a position that would provide the shortest possible route for the participation of the two sperm cells in the process of double fertilization. There is a strong possibility that the two sperm cells would be discharged from the pollen tube as a unit in close association with the vegetative nucleus of the pollen grain. Recent ultrastructural studies on the mature tricellular pollen of Brassica campestris (McConchie et al. 1985) and Brassica oleracea (Dumas et al. 1984) have shown a close association between the two sperm cells and the vegetative nucleus forming what has been termed the "male germ unit". In both species each sperm cell nucleus is encased by a plasma membrane that is appressed to the plasma membrane of the second sperm cell which is, in turn, closely associated with the vegetative nucleus by means of a tail-like extension of the second sperm plasma membrane. The cytoplasm of each sperm cell contains mitochondria, but is devoid of plastids.

Russell (1983) has proposed a mechanism, substantiated by electron micrographs, for the transfer of sperm cells to the egg and

central cell of Plumbago. It should be noted, however, that the mechanism proposed by Russell can not be applied to all angiosperms since there are no synergid cells in Plumbago. In Plumbago the pollen tube penetrates the filiform apparatus of the egg, continues growing chalazally through the PAS-positive wall, between the egg and central cell plasma membranes, and discharges the vegetative nucleus and two sperm cells into the chalazal wall region between the egg and central cell. According to Russell, the prior dispersion of the egg-central cell wall material permits the direct apposition of sperm, egg, and central cell plasma membranes which subsequently fuse. The dissolution of the fusion membranes results in the transmission of one sperm nucleus and its associated mitochondria and chloroplasts into the egg cell and the other sperm nucleus and its associated mitochondria into the central cell. If a similar mechanism of gamete transfer occurs in Brassica, the small mitochondrion appressed to the nuclear envelope of the zygote nuclear evagination in Brassica campestris could perhaps be of sperm cell origin.

The transfer of the two sperm cells from the degenerate synergid to the egg and central cell has not been observed in angiosperms (Went and Willemse 1984). Went (1970b) and Jensen (1974) have proposed a mechanism of sperm cell transfer involving the dissolution of the degenerate synergid plasma membrane thus providing direct access for the two sperm cells to the plasma membranes of the egg and central cell. It should be noted that in the majority of angiosperms there is an apparent absence of cell wall material in the chalazal region of the egg apparatus. The van Went-Jensen hypothesis for the actual transfer of the gametes is essentially the same as was described by

Russell (1983) for Plumbago. The hypothesis proposes that the plasma membrane of one of the sperm cells would unite with the egg plasma membrane and subsequently deposit its nucleus and cytoplasm into the egg cell. The same plasma membrane interaction would occur between the second sperm cell and the central cell.

The applicability of the van Went-Jensen hypothesis to those angiosperms in which the entire egg apparatus is enclosed by a PAS-positive wall, Capsella (Schulz and Jensen 1968a, 1968b), Epidendrum (Coccuci and Jensen (1969a), Papaver (Olson and Cass 1981), Ornithogalum (Tilton 1981), and Scilla (Bhandari and Sachdeva 1983), has been questioned by a number of authors since a supposed cellulosic cell wall would be a barrier to direct access of the sperm to the egg and central cell plasma membranes (Went and Willemse 1984). Schulz and Jensen (1968a) have shown the formation of a pore in the electron-transparent, PAS-positive wall between the egg and degenerate synergid of Capsella, and it is through this pore that the sperm is supposedly transferred to the egg. In Brassica the micropylar and chalazal regions of the egg apparatus are PAS and Thiery-positive. However, it is only the micropylar cell walls of the egg apparatus that are Calcofluor-positive suggesting the presence of cellulose microfibrils in these regions. The chalazal boundary between the incipient degenerate synergid, egg, and central cell is Calcofluor-negative suggesting the absence of cellulose in this region. It is entirely possible that the PAS-Thiery-positive material between the plasma membranes of the egg, synergid, and central cell is an amorphous material that would not pose a barrier to the transfer of the two sperm cells to the egg and central cell of Brassica. Is there

a requirement for the dissolution of the chalazal egg-central cell wall in Plumbago, prior to the discharge of gametes? It should be emphasized that a PAS-Thiery-positive wall does not confirm the presence of cellulose and that the proposed barrier to gamete transfer in the egg apparatuses of a number of angiosperms is based on inconclusive histochemical evidence.

Following fertilization, the egg of Brassica undergoes a marked change. The large micropylar vacuole disappears and the zygote cell becomes appreciably smaller than the egg. Zygote shrinkage has been observed in Gossypium (Jensen 1968), Hibiscus (Ashley 1972), and Nicotiana (Mogensen and Suthar 1979). The purpose of the shrinkage of the zygote is unknown but it may involve the reorganization of cytoplasm prior to the onset of embryogenesis. The shrinkage may be caused by an abrupt loss of turgor. In a typical vacuolate plant cell this would result in plasmolysis. The region of electron-transparent expanded cell wall material between the chalazal region of the egg and central cell does not appear to exhibit any rigidity. The region is PAS-Thiery-positive but reacts negatively when stained with Calcofluor suggesting the absence of cellulose. In the 72 h non-fertile ovule this region of egg-central cell wall was dilated and appeared labile. A sudden shrinkage of the egg cell after fertilization could result in a wider separation of the egg and central cell plasma membranes; in effect, a plasmolysis of the zygote. In the region of the electron-opaque deposits in the common chalazal wall between the egg and the central cell, the plasma membranes of the egg and central cell are straight, parallel and tightly appressed to the periphery of the electron-opaque region. The electron-opaque material between the egg

and central cell may have an adhesive function, preventing plasmolysis during shrinkage of the zygote, and function in a manner analogous to the spot desmosomes that occur in the intercellular space between the plasma membranes of certain animal cells (Staehelin and Hull 1978). Spot desmosomes hold animal epithelial cells together. Similar electron-opaque deposits have been reported between the egg and central cell of Capsella (Schulz and Jensen 1968b), Plumbago (Russell 1983) and Glycine (Folsom and Peterson 1984). Russell speculates that the deposits may stabilize the egg during the period of gamete transfer in Plumbago.

The loss of the vacuole and the shrinkage of the zygote may relate to the onset of the plasmic growth phase (Street and Opik 1975) of the meristematic zygote cell. The zygote shows an increase in plastids, mitochondria, and dictyosomes. The ER remains short stranded but shows a positive reaction to OsFeCN staining. In contrast, throughout its development, the unfertilized egg never exhibited a positive reaction to OsFeCN staining. In addition there is a marked increase in spiral polysomes on the surface of the zygote ER cisternae suggesting an increase in protein synthesis. There is a marked increase in lipid reserves within the zygote cell following fertilization which may relate to the energy requirements of early embryogenesis. An increase in lipid seems to be a developmental phenomenon unrelated to the process of fertilization since the non-fertile egg, 72 h after anthesis, also exhibited a similar increase in lipid over that found in the egg shortly after anthesis.

Fertilization appears to be the stimulus for cell wall synthesis in the zygote. There is a deposition of new cell wall material in the

micropylar and lateral regions of the zygote. These regions are PAS-positive and fluoresce a pale blue when stained with Calcofluor. The positive results with Calcofluor staining suggest that cellulose deposition has occurred in the lateral regions of the zygote that were Calcofluor-negative, and presumably free of cellulose prior to fertilization. The initial expansion of the zygote is apical, forming an ampulliform tip. There is a progressively weaker Calcofluor-induced fluorescence from the mid-chalazal region of the zygote wall to the extreme chalazal tip where the zygote wall is non-fluorescent following Calcofluor staining. The lateral-ampulliform tip region of the zygote wall, exhibiting the weak but positive Calcofluor fluorescence, also exhibits an abundance of cell wall-associated microtubules with the long axis of the majority of the microtubules perpendicular to the long axis of the zygote. Cortical microtubules have been shown in numerous studies over the last 20 years to lie parallel with recently formed cellulose microfibrils, and they appear from the available evidence to be responsible for the control of microfibril orientation in the cell (Robinson and Quader 1982). How this control is achieved is unclear. What has become clear over the last 5 years is that microtubules themselves are not directly involved in the polymerization and assembly of cellulose microfibrils at the plasma membrane (Herth 1985).

The time of cellulose deposition within the cell walls of the megagametophyte of Brassica is variable. In the antipodal cells, the deposition of cellulose appears to occur early in antipodal cell wall development and is independent of fertilization events. On the other hand the chalazal cell walls of the egg cell, 72 h after anthesis,

remain non-cellulosic and exhibit the same histochemical staining characteristics as the unfertilized egg cell immediately following anthesis. It would appear that the lack of cellulose synthesis in the chalazal region of the egg apparatus is related to the potential barrier a cellulosic cell wall would impose on gamete transfer and that the stimulus for cellulose synthesis in the egg is triggered by fertilization.

Following double fertilization, the central cell becomes highly vacuolate. The evidence in Brassica is that the vacuoles, at least in the micropylar region of the central cell, are derived from the dilation of ER. The involvement of ER in vacuole formation has been reported in a number of plant cells (Matile 1975). By the 2-nucleate stage of endosperm development, the perinuclear starch-rich chloroplasts of the central cell are seen to be actively replicating, and the central cell contains numerous lipid bodies, microbodies, and dictyosomes. A similar endosperm cytoplasm has been described for Capsella (Schulz and Jensen 1974) except for a decrease in lipid reserves and chloroplast starch. It should be noted that the loss of starch and a decrease in lipid reserve were characteristic features of the non-fertile ovule of Brassica, 72 h after fertilization. If, as in Capsella, there is a loss of starch and lipid from the older fertilized central cell of Brassica, this would indicate that the mobilization of energy reserves in the central cell is not under the control of the double fertilization stimulus.

In all of the fertilized ovules observed in this study, the persistent synergid showed no indication of degeneration and would appear to remain metabolically active for a period of time following

fertilization as is evidenced by the formation of wall ingrowths of the transfer cell type along its lateral walls, micropylar to the synergid hook. Periodically, in a fertilized ovule, a portion of the cell wall separating the persistent synergid and central cell disappeared resulting in an apparent mixing of synergid and central cell cytoplasms. Schulz and Jensen (1968a) reported a similar post-fertilization mixing of the persistent synergid and central cell cytoplasms of Capsella. Newcomb (1973b) reported that the persistent synergid of Helianthus remained viable well into the heart stage of embryo development and may play a role in the transfer of nutrients into the developing embryo. The presence of wall ingrowths of the transfer cell type, suggests a similar role for the persistent synergid of Brassica.

There is indirect evidence in Brassica that the persistent synergid may be important in directing the growth of the pollen tube to the egg apparatus. In the 72 h non-fertile ovule, the egg and central cell would appear to be cytologically similar to the egg and central cell of the fertile ovule at anthesis. The notable difference in these ovules as compared to those at anthesis and shortly after anthesis is the degeneration of both synergids. If the normal degenerate synergid alone was responsible for somehow directing the growth of the pollen tube, one would expect the presence of pollen tubes in these ovules, irrespective of the ensuing viability of the zygote/embryo in the absence of a persistent synergid. It is interesting to note that the ER in the micropylar one-half of the persistent synergid stained positively with OsFeCN. Though the precise mechanism of OsFeCN staining is unknown, it can be assumed that there

is a chemical difference between the substances within the persistent synergid ER cisternae as compared to the unstained ER of the degenerate synergid and egg. Perhaps the persistent synergid has a role in the production of a chemotropic agent. In Brassica campestris approximately 65 % of the ovules in a silique develop into mature seeds. The present study has revealed, on a number of occasions in ovules collected at anthesis, the apparent precocious degeneration of both synergids in an otherwise healthy ovule. Preliminary results indicate that these ovules, like the non-fertile ovules 72 h from anthesis, will not attract pollen tubes. This further implies that both synergids are important in the production of mature fertile seeds, an observation that will be the subject of further research.

LITERATURE CITED

Ahuja, J.R., and P.N. Bhaduri. 1956. The embryology of Brassica campestris L. var toria Duth. Phytomorphology 6:63-67.

Ashley, T. 1972. Zygote shrinkage and subsequent development in some Hibiscus hybrids. Planta 108:303-317.

Barnabas, A.D., V. Butler, and T.D. Steinke. 1982. Zostera capensis Setchell: III. Some aspects of wall ingrowth development in leaf blade epidermal cells. Protoplasma 110:87-94.

Bell, P.R. 1972. Nucleocytoplasmic interaction in the eggs of Pteridium aquilinum maturing in the presence of thiouracil. J. Cell Sci. 11:739-755.

_____, and K. Muhlethaler. 1964. The degeneration and reappearance of mitochondria in the egg cells of a plant. J. Cell Biol. 20:235-248.

_____, A. Frey-Wyssling, and K. Muhlethaler. 1966. Evidence for the discontinuity of plastids in the sexual reproduction of a plant. J. Ultrastruct. Res. 15:108-121.

Bhandari, N.N. 1984. The microsporangium. In Embryology of the angiosperms. Edited by B.M. Johri. pp.53-121. Springer-Verlag, Berlin. New York. Tokyo.

_____, and A. Sachdeva. 1983. Some aspects of organization and histochemistry of the embryo sac of Scilla sibirica Sato. Protoplasma 116:170-178.

Bohdanowicz, J., and K. Turala-Szybowska. 1985. Ultrastructure of endopolyploid antipodals in Aconitum vulparia Rchb. I. Antipodals in the mature embryo sac. Protoplasma 127:163-170.

Bouman, F. 1975. Integument initiation and testa development in some Cruciferae. Bot. J. Linn. Soc. 70:213-229.

_____. 1984. The ovule. In Embryology of angiosperms. Edited by B.M. Johri. pp.123-157. Springer-Verlag, Berlin. New york. Tokyo.

Bruijin de, W.C. and P. Breejen. 1975. Glycogen, its chemistry and morphological appearance in the electron microscope. II. The complex formed in the selective contrast staining of glycogen. J. Histochem. 7:205-229.

Cass, D.D. 1972. Occurrence and development of a filiform apparatus in the egg of Plumbago capensis. Amer. J. Bot. 59:279-283.

_____, and W.A. Jensen. 1970. Fertilization in Barley. Amer. J. Bot. 57:62-70.

_____, and I. Karas. 1974. Ultrastructural organization of the egg of Plumbago zeylanica. Protoplasma 81:49-62.

_____, D.J. Peteya, and B.L. Robertson. 1985. Megagametophyte development in Hordeum vulgare. 1. Early megagametogenesis and the nature of cell wall formation. Can. J. Bot. 63:2164-2171.

_____, _____, _____. 1986. Megagametophyte development in Hordeum vulgare. 2. Later stages of wall development and morphological aspects of megagametophyte cell differentiation. Can. J. Bot. 64:2327-2336.

Chao, C.Y. 1971. A periodic acid-Schiff's substance related to directional growth of the pollen tube into the embryo sac in Paspalum longifolium. Amer. J. Bot. 58:649-654.

_____. 1977. Further cytological studies of a periodic acid-Schiff's substance in the ovules of Paspalum orbiculare and P. longifolium. Amer. J. Bot. 64:922-930.

Chrispeels, M.J. 1976. Biosynthesis, intracellular transport, and secretion of extracellular molecules. Ann. Rev. Plant Physiol. 27:19-38.

Cocucci, A.E., and W.A. Jensen 1969a. Orchid embryology: The mature megagametophyte of Epidendrum scutella. Kurtziana 5:23-38.

_____, and _____. 1969b. Orchid embryology: Megagametophyte of Epidendrum scutella following fertilization. Amer. J. Bot. 56:629-640.

Coe, G.E. 1954. Distribution of carbon-14 in ovules of Zephyranthes drummondi. Bot. Gaz. 115:342-346.

Davis, G.L. 1966. Systematic embryology of the angiosperms. John Wiley and Sons. New York.

De Boer-de Jeu, M.J. 1978. Ultrastructural aspects of megasporogenesis and initiation of megagametogenesis in Lilium. Actual. Bot. 125:175-181.

Diboll, A.G., and D.A. Larson. 1966. An electron microscope study of the mature megagametophyte in Zea mays. Amer. J. Bot. 53:391-402.

Dickinson, H.G., and L. Andrews. 1977. The role of membrane bound cytoplasmic inclusions during gametogenesis in Lilium longiflorum Thunb. Planta 134:229-240.

Dickinson, H.G., and J. Heslop-Harrison. 1977. Ribosomes, membranes and organelles during meiosis in angiosperms. Phil. Trans. R. Soc. Lond. B. 277:327-342.

Dickinson, H.G., and U. Potter. 1978. Cytoplasmic changes accompanying the female meiosis in Lilium longiflorum Thunb. J. Cell Sci. 29:147-169.

Dumas, C., R.B. Knox, and T. Gaude. 1984. The mature viable tricellular pollen grain of Brassica: sperm cell characteristics. Protoplasma 124:168-174.

Feder, N., and T.P. O'Brien. 1968. Plant microtechnique: some principles and new methods. Amer. J. Bot. 55:123-142.

Fineran, B.A., D.J.C. Wild, and M. Engerfeld. 1982. Initial wall formation in the endosperm of wheat, Triticum aestivum: a reevaluation. Can. J. Bot. 60:1776-1795.

Fisher, D.B. 1968. Protein staining of ribboned epon sections for light microscopy. Histochemie 16:92-96.

Folsom M.W., and C.M. Peterson. 1984. Ultrastructural aspects of the mature embryo sac of soybean, Glycine max (L.) Merr. Bot. Gaz. 145:1-10.

Forbes, M.S., B.A. Plantholt, and N. Sperelakis. 1977. Cytochemical staining procedures selective for sarcotubular systems of muscle: modifications and applications. J. Ultrastruct. Res. 60:306-327.

Fulcher, R.G., and S.I. Wong. 1980. Inside cereals - a fluorescence microchemical view. In Cereals for food and bevereges - recent progress in cereal chemistry. Edited by G.E. Inglett and L. Munch. pp.1-26. Academic Press, N.Y.

Gerhardt, P., R.G.E. Murray, R.N. Costilow, W.A. Wood, N.R. Krieg, G.B. Phillips. 1981. Manual of Methods for General Bacteriology. p.26. American Society for Microbiology, Washington, D.C.

Gleck H.O. 1971. Can calcium ions act as a chemotropic factor in Oenothera fertilization. In Pollen: Development and physiology. Edited by J. Heslop-Harrison. pp. 255-261. Butterworth. London.

Godineau, J.C. 1973. Les sac embryonnaire des angiosperms. Morphogenese et infrastructure. Bull. Soc. Bot. Fr. 122:25-54.

Gori, P. 1977. Wall ingrowths in the embryo sac of Euphorbia helioscopia. Israel J. Bot. 26:202-208.

Gunning B.E.S., and J. S. Pate. 1969. "Transfer cells." Plant cells with wall ingrowths, specialized in relation to short distance transport of solutes - their occurrence, structure, and development. Protoplasma 68:107-133.

_____, and _____. 1974. Transfer cells. In Dynamic aspects of plant ultrastructure. Edited by A.W. Robards. pp. 441-480. McGraw-Hill. London.

_____, and A.R. Hardham. 1982. Microtubules. Ann. Rev. Plant Physiol. 33:651-698.

Hale, A.J. 1957. The histochemistry of polysaccarides. Int. Rev. Cytol. 6:193-263.

Hepler, P.K. 1980. Membranes in the mitotic apparatus of barley cells. J. Cell Biol. 21:490-499.

_____.1981. The structure of the endoplasmic reticulum revealed by osmium tetroxide-potassium ferricyanide staining. Eur. J. Cell Biol. 26:102-110.

_____.1982. Endoplasmic reticulum in the formation of the cell plate and plasmodesmata. Protoplasma 111:121-133.

Herth, W. 1985. Plant cell wall formation. In Botanical microscopy. Edited by A.W. Robards. pp.285-310. Oxford University Press. Oxford, New York, Tokyo.

_____, and E. Schnepf. 1980. The fluorochrome, Calcofluor white, binds oriented structural polysaccharide fibrils. Protoplasma 105:129-133.

Heslop-Harrison, J., and A. McKenzie. 1967. Autoradiography of soluble (2-carbon 14)-thymidine derivatives during meiosis and microsporogenesis in Lilium anthers. J. Cell. Sci. 2:387-400.

_____, and Y. Heslop-Harrison. 1982. The growth of the grass pollen tube: 1. Characteristics of the polysaccharide particles (P-particles) associated with apical growth. Protoplasma 112:71-80.

Hickey, E.L., and M.D. Coffey. 1978. A cytochemical investigation of the host-parisite interface in Pisum sativum infected by the Downey Mildew fungus Peronospora pisi. Protoplasma 97:201-220.

Hinata, K., and T. Nishio. 1980. Self-incompatibility in Crucifers. In Brassica crops and wild allies - biology and breeding. Edited by S. Tsunoda, K. Hinata, and C. Gomez-Campo. pp. 223-234. Japan Scientific Press. Tokyo.

Huang, A.H.C., T.N. Trelease, and T.S. Moore. 1983. Plant peroxisomes. Academic press. New York. London.

Hughes, J. and M.E. McCully. 1975. The use of an optical brightener in the study of plant structure. Stain Technol. 50:319-329.

Israel, H.W., and Y. Sagawa. 1964. Post-pollination ovule development in Dendrobium orchids. II. Fine structure of the nucellar and archesporial phases. Caryologia 17:301-316.

_____ and _____. 1965. Post-pollination ovule development in Dendrobium orchids. III. Fine structure of meiotic prophase I. Caryologia 18:15-34.

Iwasaki, F. 1975. Histochemical observations on embryo development in Brassica varieties. Jap. J. Breed. 25:46-51.

Jalouzot, M.F. 1978. Differentiation des elements de la tetrade femelle chez Oenothera erythrosepala. Actual. Bot. 125:167-170.

Jensen, W.A. 1962. Botanical histochemistry. Freeman, San Francisco.

_____. 1964. Observations on the fusion of nuclei in plants. J. Cell Biol. 23:669-672.

_____. 1965a. The ultrastructure and histochemistry of the synergids of cotton. Amer. J. Bot. 52:238-256.

_____. 1965b. The ultrastructure and composition of the egg and central cell of cotton. Amer. J. Bot. 52:781-797.

_____. 1968. Cotton embryogenesis: The zygote. Planta 79:346-366.

_____. 1974. Reproduction in flowering plants. In Dynamic aspects of plant ultrastructure. Edited by A.W. Robards. pp. 481-503. McGraw-Hill. London.

_____, and D.B. Fisher. 1967. Cotton embryogenesis: Double fertilization. Phytomorpholgy 17:261-269.

_____, and D.B. Fisher. 1968. Cotton embryogenesis: The entrance and discharge of the pollen tube in the embryo sac. Planta 78:158-183.

_____, P. Schulz, and M.E. Ashton. 1977. An ultrastructural study of early endosperm development and synergid changes in unfertilized cotton ovules. Planta 133:179-189.

Johri, B.M. 1984. Embryology of Angiosperms. Springer-Verlag. Berlin. New York. Tokyo.

Kapil, R.N., and A.K. Bhatnagar. 1981. Ultrastructure and biology of female gametophyte in flowering plants. Int. Rev. Cytol. 70:291-341.

Kennell, J.C., and H.T. Horner. 1985. Megasporogenesis and megagametogenesis in soybean, Glycine max. Amer. J. Bot. 72:1553-1564.

Knox, R.B., H.G. Dickinson, and J. Heslop-Harrison. 1970. Cytochemical observations on changes in RNA content and acid phosphatase activity during the meiotic prophase in the anther of Cosmos bipinnatus Cav. Acta Bot. Neerl. 19:1-6.

Koonce, M.P., and M. Schliwa. 1986. Reactivation of organelle movements along the cytoskeletal framework of a giant freshwater amoeba. J. Cell Sci. 103:605-612.

Kristen, U. 1980. Endoplasmic reticulum - dictyosome interconnections in ligule cells of Isoetes lacustris. Eur. J. Cell Biol. 23:16-21.

Lane, B.P., and D.L. Europa. 1965. Differential staining of ultrathin sections of epon-embedded tissues for light microscopy. J. Histochem. Cytochem. 13:579-582.

Lintilhac, P.M. 1974. Differentiation, organogenesis, and the tectonics of cell wall orientation. II. Separation of stresses in a two-dimensional model. Amer. J. Bot. 61:135-140.

Machado, V.S., and J.D. Bandeen. 1982. Genetic analysis of chloroplast atrazine resistance in Brassica campestris. Weed Sci. 30:281-285.

MacKiewicz, T. 1973. Fertilization, endosperm and embryo development in Brassica oleracea var. capitata L. X B. oleracea var. acephala DC. hybrid - as compared with the parental forms. Genetica Polonica 14:11-18.

Maheshwari, P. 1950. An introduction to the embryology of the angiosperms. McGraw-Hill, New York.

_____. 1963. Recent advances in the embryology of angiosperms. Catholic Press. Ranchi, India.

Marchant, R., and A.W. Robards. 1968. Membrane systems associated with the plasmalemma of plant cells. Ann. Bot. 32:457-471.

Mascarenhas, J.P. 1966. The distribution of ionic calcium in the tissues of the gynoecium of Antirrhinum majus. Protoplasma 62:53-58.

_____, and L. Machlis. 1964. Chemotropic response of the pollen Antirrhinum majus to calcium. Pl. Physiol. Lancaster. 39:70-77.

Matile, P. 1975. The lytic compartment of plant cells. Wien-New york: Springer.

Maze, J., L.R. Bohm, and L.E. Mehlenbacher Jr. 1970. Embryo sac and early ovule development in Oryzospis miliacea and Stipa tortilis. Can. J. Bot. 48:27-41.

_____, and S. Lin. 1975. A study of the mature megagametophyte of Stipa elmeri Can. J. Bot. 53:2958-2977.

McConchie, C.A., S.Jobson, and R.B. Knox. 1985. Computer-assisted reconstruction of the male germ unit in pollen of Brassica campestris. Protoplasma 127:57-63.

McCully, M.E. 1970. The histological localization of the structural polysaccharides of seaweeds. Annals N.Y. Acad. Sci. 175:702-711.

McKerracher, L.J., and I.B. Heath. 1985. Microtubules around migrating nuclei in conventionally-fixed and freeze-substituted cells. Protoplasma 125:162-172.

Medina, F.J. 1980. The occurrence of two different processes of cytoplasmic vacuolation in the megaspore formation in peas. Electron Microscopy 2:238-239.

_____, M.C. Risueno, and M.I. Rodriguez-Garcia. 1981. Evolution of cytoplasmic organelles during female meiosis in Pisum sativum L. Planta 151:214-225.

Mogensen, H.L. 1972. Fine structure and composition of the egg apparatus before and after fertilization in Quercus gambelii. The functional ovule. Amer. J. Bot. 59:931-941.

_____. 1978a. Synergids of Proboscidea louisianica (Martineaceae) before fertilization. Phytomorphology 28:1114-122.

_____. 1978b. Pollen tube-synergid interactions in Proboscidea louisianica (Martineaceae). Amer. J. Bot. 65:953-964.

_____. 1981. Ultracytochemical localization of adenosine triphosphatase in the ovules of Saintpaulia ionantha (Gesneriaceae) and its relation to synergid function and embryo sac nutrition. Amer. J. Bot. 68:183-194.

_____. 1985. Ultracytochemical localization of plasma membrane-associated phosphotase activity in developing tobacco seeds. Amer. J. Bot. 72:741-754.

_____, and H.K. Suthar. 1979. Ultrastructure of the egg apparatus of Nicotiana tabacum (Solanaceae) before and after fertilization. Bot. Gaz. 140:168-179.

Moriyasu, Y., and M. Tazawa. 1986. Plant vacuole degrades exogenous protiens. Protoplasma 130:214-215.

Morre, D.J., and H.H. Mollenhauer. 1974. The endomembrane concept: a functional integration of endoplasmic reticulum and golgi apparatus. In Dynamic aspects of plant ultrastructure. Edited by A.W. Robards. pp. 84-137. McGraw-Hill. London.

Morrison, I.N., and T.P. O'Brien. 1976. Cytokinesis in the developing wheat grain; division with and without a phragmoplast. Planta 130:57-67.

Newcomb, W. 1973a. The development of the embryo sac of sunflower Helianthus annuus before fertilization. Can. J. Bot. 51:863-878.

_____. 1973b. The development of the embryo sac of sunflower Helianthus annuus after fertilization. Can. J. Bot. 51:879-890.

_____. 1978. The development of cells in the coenocytic endosperm of the African blood lily Haemanthus katharinae. Can. J. Bot. 56:483-501.

_____, and L.C. Fowke. 1973. The fine structure of the change from the free nuclear to the cellular condition in the endosperm of chickweed Stellaria media. Bot. Gaz. 134: 134:236-241.

_____, and T.A. Steeves. 1971. Helianthus annuus embryogenesis: embryo sac wall projections before and after fertilization. Bot. Gaz. 132:367-371.

Norstog, K. 1972. Early development of the barley embryo: Fine structure. Amer. J. Bot. 59:123-132.

O'Brien, T.P., N. Feder, and M.E. McCully. 1964. Polychromatic staining of plant cell walls by Toluidine blue O. Protoplasma 59:368-373.

_____, and M.E. McCully. 1981. The study of plant structure. Principles and selected methods. Termarcarphi Pty. Ltd., Melbourne Australia.

Olson, A.R., and D.D. Cass. 1981. Changes in megagametophyte structure in Papaver nudicaule L. (Papaveraceae) following in vitro placental pollination. Amer. J. Bot. 68:1333-1341.

Orr, A.R. 1978. Inflorescence development in Brassica campestris L. Amer. J. Bot. 65:466-470.

Pearson, O.H. 1933. The life-history of Brassica oleracea. Bot. Gaz. 94:535-550.

Peterson, R.L., and E.C. Yeung. 1975. Ontogeny of phloem transfer cells in Hieracium floribundum. Can. J. Bot. 53:2745-2758.

Porter, K. R. 1963. Diversity at the subcellular level and its signifigance. In The nature of biological diversity. Edited by J.M. Allen. McGraw-Hill. London.

Prasad, K. 1975. Development and organization of gametophytes in certain species of Cruciferae. Acta Bot. Indica 3:147-154.

Pritchard, H.N. 1964. A cytochemical study of embryo sac development in Stellaria media. Amer. J. Bot. 51:371-378.

Rashid, A., A.W. Siddiqui, and J. Reinert. 1982. Subcellular aspects of differentiation of microspore mother cells of Nicotiana tabacum. Protoplasma 113:80-84.

Rathore, R.K.S., and R.P. Singh. 1968. Embryological studies in Brassica campestris L. var yellow sarson Prain. J. Ind. Bot. Soc. 67:341-349.

Reynolds, E.S. 1963. The use of lead citrate at high pH as an electron opaque stain in electron microscopy. J. Cell Biol. 17:208.

Robinson, D.G. 1980. Dictyosome-endoplasmic reticulum associations in higher plant cells? A serial section analysis. Eur. J. Cell Biol. 23:22-26.

_____, and U. Kristen. 1982. Membrane flow via the Golgi apparatus of higher plant cells. Int. Rev. Cytol. 77:89-127.

_____, and H. Quadar. 1982. The microtubule-microfibril syndrome. In The cytoskeleton in plant growth and development. Edited by C.W. Lloyd. pp. 109-126. Academic Press. London.

Rodkiewicz B. 1970. Callose in cell wall during megasporogenesis in angiosperms. Planta 93:39-47.

Roland, J.C. 1973. The relationship between the plasmalemma and the plant cell wall. Int. Rev. Cytol. 36:45-92.

_____. 1978. General preparation and staining of thin sections. In Electron microscopy and cytochemistry of plant cells. Edited by J.L. Hall. pp. 1-62. Elsevier/North-Holland Biomedical Press, Amsterdam.

Rosen, W.G. 1971. Pistil-pollen tube interactions in Lilium. In Pollen: Development and physiology. Edited by J. Heslop-Harrison. pp. 239-254. Butterworth. London.

_____, W.V. Dashek, and K.A. Siegesmund. 1964. Fine structure and cytochemistry of Lilium pollen tubes. Amer. J. Bot. 51:61-71.

Roth, I. 1957. Die histogenese der integumente von Capsella bursa-pastoris und ihre morphologische bedeutung. Flora 145:212-235.

Russell, S.D. 1979. Fine structure of the megagametophyte of Zea mays. Can. J. Bot. 57:1093-1110.

_____. 1983. Fertilization in Plumbago zeylanica: gametic fusion and fate of the male cytoplasm. Amer. J. Bot. 70:416-434.

Scheffield, E., A.H. Cawood, P.R. Bell, and H.G. Dickinson. 1979. The development of nuclear vacuoles during meiosis in plants. Planta 146:597-601.

Schliwa, M. 1984. Mechanisms of intracellular organelle transport. In Cell and muscle motility. Vol. 5. The cytoskeleton. Edited by J. W. Shay. pp. 1-66. Plenum press. New York and London.

Schmiedel, G., and E. Schnepf. 1980. Polarity and growth of the caulonema tip cells of the moss Funaria hygrometrica. Planta 147:405-413.

Schnepf, E., G. Deichgraber, and W. Herth. 1982. Development of cell wall appendages in Acanthosphaera zachariasi (Chlorococcales): Kinetics, site of cellulose synthesis and microfibril assembly, and barb formation. Protoplasma 110:203-214.

Schulz, P., and W.A. Jensen. 1971. Capsella embryogenesis: the chalazal proliferating tissue. J. Cell Sci. 8:201-227.

_____, and _____. 1973. Capsella embryogenesis: the central cell. J. Cell Sci. 12:741-763.

_____, and _____. 1974. Capsella embryogenesis: the development of the free nuclear endosperm. Protoplasma 80:183-205

_____, and _____. 1977. Cotton embryogenesis: the early development of the free nuclear endosperm. Amer. J. Bot. 64:384-394.

_____, and _____. 1981. Pre-fertilization ovule development in Capsella: ultrastructure and ultracytochemical localization of acid phosphatase in the meiocyte. Protoplasma 107:85-107.

_____, and _____. 1986. Pre-fertilzation ovule development in Capsella: the dyad, tetrad, developing megaspore, and two-nucleate gametophyte. Can. J. Bot. 64:875-884.

Schulz, S.R. and W.A. Jensen. 1968a. Capsella embryogenesis: the synergids before and after fertilization. Amer. J. Bot. 55:541-552.

_____, and _____. 1968b. Capsella embryogenesis: the egg, zygote, and young embryo. Amer. J. Bot. 55:807-819.

Singh, A.P., and H.L. Mogensen. 1975. Fine structure of the zygote and early embryo in Quercus gambelii. Amer. J. Bot. 64:105-115.

Spooner, D.M. 1984. Reproductive features of Dentaria laciniata and D. diphylla (Cruciferae), and the implications in the taxonomy of the eastern North American Dentaria complex. Amer. J. Bot. 71:999-1005.

Spurr, A.R. 1969. A low-viscosity epoxy embedding medium for electron microscopy. J. Ultrastruct. Res. 26:31-43.

Smith, M.M., and M.E. McCully. 1978. A critical evaluation of the specificity of aniline blue induced fluorescence. Protoplasma 95:229-254.

Staehelin, L.A., and B.E. Hull. 1978. Junctions between living cells. Sci. Amer. 238:141-152.

Street, H.E., and H. Opik. 1975. The physiology of flowering plants (2nd ed.). Edward Arnold. London.

Stewart, K.D., and E.M. Gifford, Jr.1967. Ultrastructure of the developing megaspore mother cell of Ginkgo biloba. Amer. J. Bot. 54:375-383.

Sulbha, K. 1957. Embryology of Brassica juncea Czern. J. Indian Bot. Soc. 36:292-301.

Thiery, J.P. 1967. Mise en evidence des polysaccharides sur coupes fines en microscope electronique. J. Microsc. 5:31-43

Thompson, R.C. 1933. A morphological study of flower and seed development in cabbage. J. Agr. Res. 27:215-237.

Tilton, V.R. 1981. Ovule development in Ornithogalum caudatum (Liliaceae) with a review of selected papers on angiosperm reproduction. IV. Egg apparatus structure and function. New Phytol. 88:505-531.

_____, and L.H. Mogensen. 1979. Ultrastructural aspects of the ovule of Agave parryi before fertilization. Phytomorphology 29:338-350.

_____, L.W. Wilcox, and R.G. Palmer. 1984. Postfertilization wandlabrinthe formation and function in the central cell of soybean, Glycine max (L.) Merr. (Leguminosae). Bot. Gaz. 145:334-339.

Unzelman, J.M., and P.L. Healey. 1974. Development, structure and occurrence of secretory trichomes of Pharbitis. Protoplasma 80:285-303.

Vandendries, R. 1909. Contribution 1' ovule du development de 1'ovule dans les Cruciferae. La Cellule 412-459.

Vasart, B., and J. Vasart. 1966. Infrastructure du sac embryonnaire du Lin (Linum usitatissimum L.). Rev. Cytol. Biol. Veg. 24:251-266.

Went, J.L. van. 1970a. The ultrastructure of the synergids of Petunia. Acta Bot. Neerl. 19:121-132.

_____. 1970b. The ultrastructure of the fertilized embryo sac of Petunia. Acta Bot. Neerl. 19:468-480.

_____. 1970c. The ultrastructure of the egg and central cell of Petunia. Acta Bot. Neerl. 19:313-322.

_____, and M.T.M. Willemse. 1984. Fertilization. In Embryology of the angiosperms. Edited by B.M. Johri.pp. 273-317. Springer-Verlag, Berlin. New York. Tokyo.

White, D.L., J.E. Mazurkeiwicz, R.J. Barrnett. 1979. A chemical mechanism for tissue staining by osmium tetroxide-ferrocyanide mixtures. J. Histochem. Cytochem. 27:1084-1091.

Willemse. M.T.M., and M.A.W. Franssen-Verheijen. 1978. Cell organelle changes during megasporogenesis and megagametogenisis in Gasteria verrucosa (Mill.) Haw. Bull. Soc. Bot. Fr. 125:187-191.

_____, and J. Bednara. 1979. Polarity during megasporogenesis in Gasteria verrucosa. Phytomorphology 29:156-165.

_____, and M.J. De Boer-De Jeu. 1981. Megasporogenesis and early megagametogenesis. Acta Soc. Bot. Pol. 50:105-114.

_____, and J.L. Van Went. 1984. The female gametophyte. In Embryology of the angiosperms. Edited by B.M. Johri.pp. 159-196. Springer-Verlag, Berlin. New York. Tokyo.

Wilms, H.J. 1981a. Ultrastructure of the developing embryo sac of spinach. Acta Bot. Neerl. 30:75-99.

_____. 1981b. Pollen tube penetration and fertilization in spinach. Acta Bot. Neerl. 30:101-102.

Wood, P.J., and R.G. Fulcher. 1978. Interactions of some dyes with cereal beta glucans. Cereal Chem. 55:952-966.

Woodcock, C.L.F., and P.R. Bell. 1968. Features of the ultrastructure of the female gametophyte of Myosurus minimus. J. Ultrastruct. Res. 22:546-563.

Woude, W.J. van der, W.J. Morre, and C.E. Bracker. 1971. Isolation and characterization of secretory vesicles in germinated pollen of Lilium longiflorum. J. Cell Sci. 8:331-351.

Yu, S.H., and C.Y. Chao. 1979. Histochemical studies of ovary tissues during the embryo sac development in Paspalum longifolium Roxb. Caryologia 32:145-160.